Dissertation zur Erlangung des Doktorgrades
der Fakultät für Chemie und Pharmazie
der Ludwig-Maximilians-Universität München

Armed YB-1 dependent oncolytic adenoviruses for combined virotherapy and suicide gene therapy

Youlia Kostova
aus
Kardzhali, Bulgarien

2014

Erklärung

Diese Dissertation wurde im Sinne von § 7 der Promotionsordnung vom 28. November 2011 von Herrn Prof. Dr. Christian Plank betreut und von Herrn Prof. Dr. Ernst Wagner von der Fakultät für Chemie und Pharmazie vertreten.

Eidesstattliche Versicherung

Diese Dissertation wurde eigenständig und ohne unerlaubte Hilfe erarbeitet.

München, 08.08.2014

.....

Youlia Kostova

Dissertation eingereicht am: 11.08.2014

1. Gutachter: Prof. Dr. Ernst Wagner

2. Gutachter: Prof. Dr. Christian Plank

Mündliche Prüfung am: 27.01.2015

TABLE OF CONTENTS

1. INTRODUCTION

1.1. Glioblastoma multiforme

1.1.1. Pathology

Gliomas are a group of low-grade and high-grade brain tumours that originate from glia (from Greek for “glue”), the brain tissue providing support functions to neural cells [1]. The cells of origin for the development of gliomas are currently unknown. A major theory has been established that neural stem cells or neural progenitor cells undergo transformation events during development [2, 3]. Another hypothesis refers to the mutation-induced dedifferentiation of mature brain cells like astrocytes and oligodendrocytes as the origin of gliomas [4].

According to the World Health Organisation (WHO), gliomas are classified as grade I to IV. Grade I and II gliomas are generally benign, with low proliferative and infiltrative potential, whereas grade III and IV gliomas are characterised by a high proliferative activity, marked infiltration into surrounding tissue and a very low median survival rate [5, 6]. Grade III and IV malignant gliomas account for 80 % of all primary malignant tumours of the brain and the central nervous system (CNS) [7].

The most common malignant glioma subtype is grade IV astrocytoma, also known as glioblastoma multiforme (GBM) [6]. The high aggressiveness and recurrence rate of GBM characterise this glioma subtype as the most common deadly primary brain tumour [1, 8]. GBM represents 45.2 % of all primary malignant brain tumours and has an incidence rate of 3.19 per 100,000 inhabitants of the United States. Despite state-of-the-art therapy, less than 5 % of GBM patients survive within five years post diagnosis [7]. Currently there are over 150 ongoing clinical trials for GBM, including standard and alternative treatment [9].

1.1.2. Standard therapy

Conventional treatment of GBM comprises surgical intervention, radiotherapy and chemotherapy. While surgery and radiotherapy have proven only limited efficacy as monotherapies [8, 10, 11], the administration of the chemotherapeutic temozolomide (TMZ, Temodal®) is considered as the most important progress in malignant glioma therapy [6]. Median survival times of all patients with newly diagnosed GBM improved from 8.1 months in 2000–2003 to 9.7 months in 2005–2008 due to the introduction of TMZ [12]. TMZ is an orally available DNA-alkylating agent of the imidazotetrazine group. Under physiological conditions TMZ spontaneously decomposes to the active substance monomethyltriazene 5-(3-methyltriazen-1-yl)-imidazole-4-carboxamide (MTIC). MTIC further releases a highly reactive methyldiazonium cation that mediates the cytotoxic activity of TMZ mainly through methylation at the O^6 position of guanine residues in guanine-rich regions of the DNA [13, 14]. Although TMZ affects non-specifically rapidly dividing cells, the benefits of the drug are good oral

tolerance and efficient penetration of the blood-brain barrier [15] that renders TMZ an attractive therapeutic agent for GBM.

TMZ was established as the standard of care chemotherapy against malignant glioma and GBM after a study of Stupp et al. [6, 16]. In a randomised phase III clinical trial they demonstrated that the median survival of patients with newly diagnosed GBM significantly improved from 12.1 to 14.6 months by combined TMZ treatment and postoperative radiation, and the 2 year survival rates increased to 26 %, in comparison to radiation therapy alone. A follow-up clinical trial revealed a 10 % survival rate after 5 years with adjuvant TMZ treatment versus only 2 % with radiation therapy alone [17]. Recent clinical trials with GBM pointed out that concomitant and adjuvant TMZ treatment with radiation therapy was beneficial for survival outcome [18, 19].

1.1.3. Strategies for targeting cellular molecules

Because of the poor prognosis of GBM despite the application of state-of-the-art therapy, novel treatment approaches against cellular targets are being evolved in order to inhibit angiogenesis and tumour growth or to stimulate anti-tumour immune responses.

A promising therapeutic strategy to prevent angiogenesis of malignant glioma and thus to arrest neoplasm expansion is the human recombinant monoclonal antibody bevacizumab, which targets vascular endothelial growth factor (VEGF), a crucial mediator of tumour angiogenesis [20, 21]. Bevacizumab was approved in 2009 in the United States for the treatment of recurrent GBM based on encouraging response rates [22-24] and led to improved median survival in combination with protracted TMZ [25] and radiotherapy [26].

Further cellular targets for GBM therapy are cell surface growth factor receptors and signalling molecules. Overexpression of epidermal growth factor receptor (EGFR) is common in about 40 % of the GBM cases [27]. However, it was shown that small-molecule EGFR inhibitors such as gefitinib and erlotinib could not prolong survival of GBM patients in clinical trials substantially [28, 29].

Several approaches to target aberrant signalling pathways in GBM through inhibition of effector molecules have been investigated. Attractive molecular targets are the mammalian target of rapamycin (mTOR) from the phosphatidylinositide 3-kinase/protein kinase B/mTOR (PI3K/Akt/mTOR) pathway [30-32] or protein kinase C (PKC) [33-35].

Targeting the immune system has been considered a promising future experimental modality for treatment of cancer, including malignant gliomas. A panel of approaches are being currently investigated in clinical trials for GBM, including immunotherapy with cytokines, dendritic cells and autologous stimulated lymphocytes, as well as tumour- or peptide-based vaccines [9].

1.2. Limitations of current glioma therapy

1.2.1. Defence mechanisms of GBM against therapies

Despite recent survival prolongation of GBM patients by combined TMZ treatment and radiotherapy, and despite the development of novel approaches for molecular targeting, the long-term benefit of current therapy for GBM remains debatable. A critical factor hampering the eradication of GBM is the highly invasive and dispersive nature of GBM cells, leading to dissemination of the tumour and thus making complete resection impossible [36, 37]. The immune privilege of the CNS facilitates the immune evasion of tumour cells and thus contributes to the immunological ignorance towards GBM antigens [38, 39]. These factors limit the efficacy of immunotherapies. The variability of molecular aberrations and dysregulated signalling pathways within GBM cases, but also within tumours in general, is a considerable obstacle for the development of sustained targeted therapies. Moreover, combinations of targeted molecular drugs result in additive toxicity and drug efficacy is diminished due to insufficient penetration into the tumour tissue [1]. Finally, the presence of a self-renewable $CD133^+$ tumour stem-like cell population that is resistant to chemo- and radiotherapy, is another major challenge contributing to tumour recurrence and dismal long-term survival prognosis [40].

1.2.2. Mechanisms of drug resistance

1.2.2.1. Resistance to alkylating agents

Drug-resistance in glioma can often arise from aberrant DNA repair mechanisms [41]. The most thoroughly explored DNA repair protein in GBM, associated with poor prognosis and drug-resistance, is mediated by the enzyme O^6-methylguanine-DNA methyltransferase (MGMT). MGMT is capable of removing the O^6-methylguanine adducts formed by alkylating agents and high level of the enzyme reduces the efficacy of these agents [42]. Hegi et al. showed that *MGMT* promoter hypermethylation, which was detected in 40-50 % of GBM cases, prevents *MGMT* gene expression and is associated with better response to the alkylating drug TMZ and radiation, resulting in longer survival [43]. In contrast, overexpression of MGMT due to unmethylated promoter was associated with resistance to alkylating drugs in clinical trials [44, 45]. To circumvent resistance to alkylating agents resulting from *MGMT* overexpression, therapeutic approaches using the inhibitor of MGMT O^6-benzylguanine (O^6-BG) were investigated in combination with alkylating agents as nitrosoureas or TMZ, however with limited success [46-48].

1.2.2.2. Multidrug resistance

Many tumours can become resistant not only to the specific cytostatic drug applied as a current therapy, but also to other agents. This cross-resistance is also called multidrug resistance and is caused by multiple mechanisms [49]. The first identified factor mediating multidrug resistance is overexpression of the multidrug resistance 1 (*MDR1*) gene that encodes for the MDR1/P-

glycoprotein (P-gp) or ABCB1, a member of the adenosine triphosphate (ATP)-binding cassette (ABC) transporter family [50]. ABC-transporters mediate a drug efflux that leads to decrease in cellular accumulation of cytostatic compounds [49]. Multidrug-resistant cells become insensitive not only to structurally unrelated cytostatic drugs such as anthracyclines, vinca alkaloids, and taxanes, but also to other compounds such as antiviral drugs and antibiotics, which are transported by P-gp [50]. The classical P-gp-mediated as well as alternative mechanisms of multidrug resistance have been extensively studied in different cancer cell lines with an established multidrug-resistant phenotype [51-53]. However, it has still to be investigated if alternative therapeutic compounds or gene therapy approaches using specific prodrugs for example, are also hampered by multidrug resistance mediated by P-gp.

Promising tools to circumvent the above described limitations for a successful therapy of GBM are alternative tumour-targeting approaches as suicide gene therapy and oncolytic virotherapy. Oncolytic viruses have the ability to replicate in and selectively kill tumour cells. To increase their killing potential, oncolytic viruses can be equipped with suicide genes that mediate cytotoxicity as a part of a suicide gene system. Suicide gene therapy and oncolytic virotherapy have already demonstrated their efficacy in tumour eradication, as described in the following.

1.3. Suicide gene therapy

Suicide gene therapy, also termed gene-directed enzyme prodrug therapy, describes the delivery of a gene that encodes an enzyme, which is able to convert a non-toxic prodrug into a metabolite that exerts cytotoxic effects in target cells. Prodrugs are inert compounds that can be transformed into toxins by suicide gene-encoded enzymes specific for certain tissue or overexpressed in tumours as a result of gene delivery [54]. Prodrug-mediated suicide gene systems are therefore convenient tools for the application in cancer therapy. Due to its minimal toxicity in healthy tissue, suicide gene therapy is designed to address the limitations of conventional chemotherapy, such as severe adverse effects and lack of specificity.

1.3.1. HSV1-TK/GCV suicide system

The most extensively studied suicide gene strategy in cancer therapy is the Herpes simplex virus 1 thymidine kinase (*HSV1-TK*) gene in combination with the prodrug Ganciclovir (GCV) [55]. The HSV1-TK enzyme is a homodimer with a subunit molecular mass of 45 kDa [56] and is responsible for the phosphorylation of its natural substrate deoxythymidine to deoxythymidine triphosphate, which is incorporated into nascent DNA of HSV1 [57]. Thus, HSV1-TK is involved in the reactivation of HSV1 from ganglionic neurons during the latent stage of its life-cycle [58]. HSV1-TK exhibits a broad

specificity to other nucleosides, such as deoxycytidine, deoxythymidylate and various pyrimidine and guanosine analogues [56]. Of them, the guanosine analogue GCV is metabolised by HSV1-TK with a 1000-fold higher efficiency compared to mammalian thymidine kinases [59] and this property provides the basis for the application of GCV in combination with the suicide gene HSV1-TK for cancer gene therapy [57]. Moreover, HSV1-TK exhibits better catalytic properties for GCV than for Acyclovir (ACV), a GCV-related guanosine analogue [60, 61]. The prodrug GCV is initially phosphorylated by HSV1-TK to GCV-monophosphate, which is further phosphorylated to GCV-di- and -triphosphate by cellular enzymes, such as guanylate kinase and nucleoside diphosphokinase [56, 62, 63]. The toxic metabolite GCV-triphosphate competes with deoxyguanosine triphosphate for the incorporation into nascent DNA of dividing cells and inhibits the cellular DNA polymerase, causing double strand destabilisation that leads to abrogation of DNA synthesis and subsequently to cell death [61, 62, 64] (figure 1.1). In addition, GCV exerts potent anti-viral activity against viruses of the herpesvirus family [65] and against hepatitis B virus variants [66].

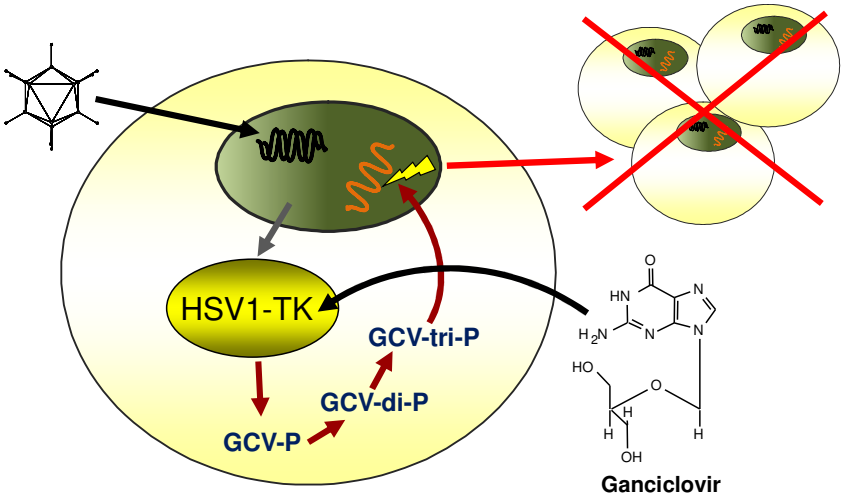

Figure 1.1: Mode of action of the HSV1-TK/GCV suicide system. After transfection or viral transduction of target cells with *HSV1-TK*-bearing vectors, the HSV1-TK enzyme is expressed and translocated to the cytoplasm. HSV1-TK phosphorylates its specific prodrug Ganciclovir (GCV) to GCV-monophosphate (-P), which is further phosphorylated to GCV-di-P and GCV-tri-P by cellular kinases. The toxic metabolite GCV-tri-P incorporates into the DNA of dividing cells, causing double strand destabilisation, and inhibits the cellular DNA polymerase, resulting in termination of DNA synthesis and cell death.

It has been suggested that the mode of cell death elicited by the HSV1-TK/GCV system in tumours involves both apoptotic [67-70] and non-apoptotic mechanisms [71, 72], depending on the tumour cell type. The regulation of the mitochondrial death pathway by B cell lymphoma-2 (Bcl-2) family proteins was suggested as the most probable mechanism of HSV1-TK/GCV-mediated apoptotic death [68-70]. Death of some tumour cell lines after HSV1-TK/GCV activation can also be caused by

apoptosis in the G1 phase of the cell cycle combined with late apoptotic or necrotic sub-G1 DNA fragmentation [73].

1.3.2. Bystander effect

The efficacy of the HSV1-TK/GCV suicide gene system is greatly facilitated by the so called bystander effect. The principle of the bystander effect was first demonstrated in a mosaic co-culture of untransfected and HSV1-TK transfected cells, in which the untransfected cells, surrounded by transfected cells, became sensitive to GCV [55]. This finding showed the existence of a bystander effect that contributes to the eradication of neighbouring non-HSV1-TK-borne cells, even if there is only a small subpopulation of HSV1-TK-bearing cells. Considering the low transduction efficiency of some gene delivery vehicles for HSV1-TK, the bystander effect is essential for successful tumour eradication by prodrug-mediated suicide systems. The basic principle of the bystander effect is the transport of GCV-monophosphate, GCV-diphosphate and GCV-triphosphate into adjacent cells, where GCV-monophosphate and GCV-diphosphate are further phosphorylated by cellular kinases and accumulated GCV-triphosphate directly leads to cytotoxicity [74, 75] (figure 1.2). It has been shown that, when only 10 % of cell culture had been transduced to express HSV1-TK, the treatment with GCV could result in 100 % cell killing. Corresponding *in vivo* tumour models, including glioma, also confirmed that treatment with GCV induced a complete tumour regression, when 10-50 % of the cell population was HSV1-TK positive [76-80].

One main drawback of the HSV1-TK/GCV system is that, in contrast to the prodrug, the phosphorylated GCV metabolites are highly charged and thus unable to passively diffuse throughout the cellular lipid membranes and into neighbouring cells [57, 75]. Therefore, the transfer of phosphorylated GCV between HSV1-TK positive cells and neighbouring cells was shown to be accomplished through direct intercellular contact, mediated by gap junctions [81-83]. Another mechanism for a local bystander effect might be the phagocytosis of apoptotic bodies, generated from HSV1-TK-modified cells, by adjacent unmodified tumour cells [77].

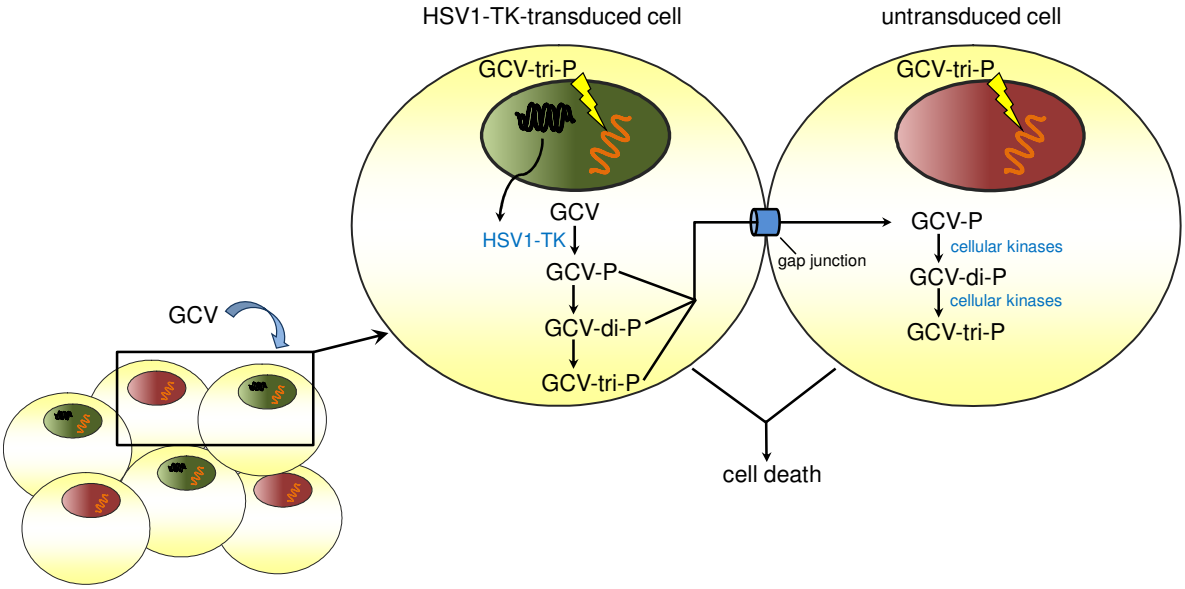

Figure 1.2: Basic principle of the HSV1-TK/GCV-mediated bystander effect. In a population of HSV1-TK-transduced and untransduced cells, the metabolites GCV-P, GCV-di-P and GCV-tri-P produced by HSV1-TK and cellular enzymes in HSV1-TK-transduced cells, are transported to neighbouring untransduced cells through gap junctions. GCV-P and GCV-di-P are phosphorylated to GCV-tri-P by kinases of the untransduced cells. Finally, accumulated GCV-tri-P induces cytotoxicity in both HSV1-TK-transduced and untransduced cells [75].

1.3.3. HSV1-TK isoforms

Considering that the Michaelis constant (K_m) value of HSV1-TK for GCV is about 100-fold higher than its K_m value for deoxythymidine [61, 84], the enzyme has a higher affinity for deoxythymidine and therefore, both molecules compete for the active site of HSV1-TK. Because of this competition, high clinically relevant doses of GCV are needed to be applied, but they often cause undesirable side effects in patients [54, 56]. In order to overcome unspecific toxicity mediated by GCV, novel mutant variants of HSV1-TK with improved specificity towards GCV have been developed and already used in preclinical investigations [85-88].

The most extensively studied mutant is the HSV1-TK variant sr39TK, derived by semi-random sequence mutagenesis of amino acid residues within the putative active site of the enzyme [86]. Among seven HSV1-TK variants, HSV1-sr39TK was identified as the most sensitive to GCV. This mutant contains five amino acid substitutions (table 1.1) that confer a 43-fold greater sensitivity to GCV as well as a 20-fold increased sensitivity to ACV than the wild-type HSV1-TK and better efficiency in tumour ablation than the wild-type enzyme [85, 86]. The observed low half maximal inhibitory concentration (IC_{50}) of 0.017 µM for GCV with HSV1-sr39TK enabled a drastic reduction of the prodrug dose applied *in vitro* and favoured a 10-fold lower GCV concentration to efficiently inhibit the growth of HSV1-sr39TK-expressing glioma xenograft models in comparison to GCV with wild-type

HSV1-TK [86]. HSV1-sr39TK in combination with GCV was shown to be more efficient in *in vitro* and *in vivo* studies against metastatic prostate cancer [89], as well as against various tumour cell lines [90], compared to wild-type HSV1-TK or other variants.

Table 1.1: Deduced amino acid sequence of the HSV1-TK semi-random mutant sr39TK. Mutated residues conferring increased sensitivity towards GCV and/or ACV are displayed [86].

	Amino acid residues 159-161 and 168-169				
HSV1-TK (wt)	L	I	F	A	L
sr39TK (mutant)	I	F	L	F	M

A: Alanine; F: Phenylalanine; I: Isoleucine; L: Leucine; M: Methionine

1.3.4. Clinical application of HSV1-TK/GCV gene therapy for cancer

The success of the HSV1-TK/GCV suicide system in preclinical studies encouraged the conduction of several clinical trials towards various tumour types. Beneficial for the therapeutic outcome in cancer are the minimal adverse effects of the suicide gene system, due to the preferential killing of rapidly dividing cells such as tumour cells, but not of normal tissue [56]. Clinical phase I/II trials towards various cancer types, including ovarian cancer [91, 92], metastatic melanoma [93], prostate cancer [94, 95] and malignant glioma [96], demonstrated a good safety profile of the HSV1-TK/GCV suicide therapy, associated with moderate to encouraging efficacy.

Given the in chapter 1.2. described limitations of current therapy against glioma, the strategy of HSV1-TK/GCV suicide gene therapy is being under investigation as an alternative treatment of these neoplasms. Since the HSV1-TK/GCV system exerts its cytotoxic effect only in dividing cells, HSV1-TK and GCV are suitable for specific local targeting of the highly proliferating GBM cells [39]. Moreover, the immune privilege of the brain hampers the immune recognition of cellular cytotoxic processes and favours the transduction of the tumour with viral delivery vectors. Several encouraging phase I and II clinical trials towards malignant glioma, using retroviral [97, 98] and adenoviral [96, 99] delivery of HSV1-TK, pointed out the safety and feasibility of this suicide gene therapy. Rainov et al. reported minimal toxicity of adjuvant HSV1-TK gene therapy in GBM patients in a phase III clinical trial, but the limiting factor was the poor transduction efficiency of the retroviral delivery vector [100]. Though more encouraging than the trial of Rainov et al., the improvement of overall survival in a recent phase III GBM trial, using adenovirus-mediated gene therapy with HSV1-TK and GCV administration, was only minor [101]. In order to circumvent resistance of HSV1-TK-expressing cells to GCV, a combination of the HSV1-TK/GCV system with conventional chemo- and radiotherapy

became a necessary and successful treatment option, as it was shown in preclinical trials that HSV1-TK could sensitise glioma cells to radiation and cytostatic drugs like TMZ [102, 103].

1.3.5. Other suicide gene systems

It is of advantage to develop a broad range of suicide genes/prodrug combinations for cancer therapy, because not all cancers respond equally to the same prodrug and, in case of treatment failure with one suicide gene, it can be substituted by alternative suicide genes, against which there is no pre-existing immune response [56]. Over twenty suicide genes with different kinetic and cytotoxic properties are identified by now [57]. Besides HSV1-TK, other examples of widely used suicide gene systems include the enzymes cytosine deaminase (CD) and cytochrome P450. The CD enzyme, found in bacteria (bCD) and yeast (yCD), catalyses the conversion of the prodrug 5-fluorocytosine (5-FC) to the toxic metabolite 5-fluorouracil (5-FU) [104]. Cytochrome P450 enzymes are drug-metabolising enzymes of mammals, responsible for the conversion of the prodrugs ifosphamide (IFO) and cyclophosphamide (CPA) into their 4-hydroxy-forms, which induce cytotoxic effects [105]. Both CD/5-FU and cytochrome P450/IFO and CPA suicide gene systems have been investigated as approaches against cancer [106, 107].

1.4. Reporter genes for non-invasive imaging in cancer therapy

Non-invasive imaging with reporter genes in tumour therapy is applied for monitoring of delivery, distribution, expression and persistence of a therapeutic gene within a tumour, for visualising the therapeutic success as well as tumour regression or growth in living organisms. Non-invasive imaging can be performed e.g. by means of positron emission tomography (PET) with radionuclide probes. PET displays a higher sensitivity and spatial resolution than single photon emission computed tomography (SPECT). With its ability to detect about 10^{-10} M of a radiolabelled probe, PET allows the direct quantitation of tracer amounts of radiolabelled substrates within cells [108].

The most commonly applied reporter gene for non-invasive tumour imaging in experimental settings is *HSV1-TK*. The principle of non-invasive imaging with *HSV1-TK* as a reporter gene is based on the enzymatic conversion of various specific radiotracer substrates, such as the acycloguanosine derivative [^{18}F]-labelled 9-[4-fluoro-3-(hydroxymethyl)butyl]guanine (FHBG) or the uracil nucleoside derivative [^{124}I]- and [^{131}I]-labelled 2'-fluoro-2'-deoxy-5-iodo-1-β-D-arabinofuranosyl (FIAU) by the expressed HSV1-TK protein after gene transduction. The phosphorylated radiolabelled metabolites produced by this conversion are then trapped within the cell and can be visualised by PET ([^{18}F]-FHBG, [^{124}I]-FIAU) or SPECT ([^{131}I]-FIAU) imaging [109, 110] (figure 1.3). Crucial for the choice of the radiolabelled tracer FHBG and FIAU as reporter probes for HSV1-TK is that HSV1-TK and HSV1-sr39TK exhibit greater substrate specificity for these compounds than does mammalian TK [110].

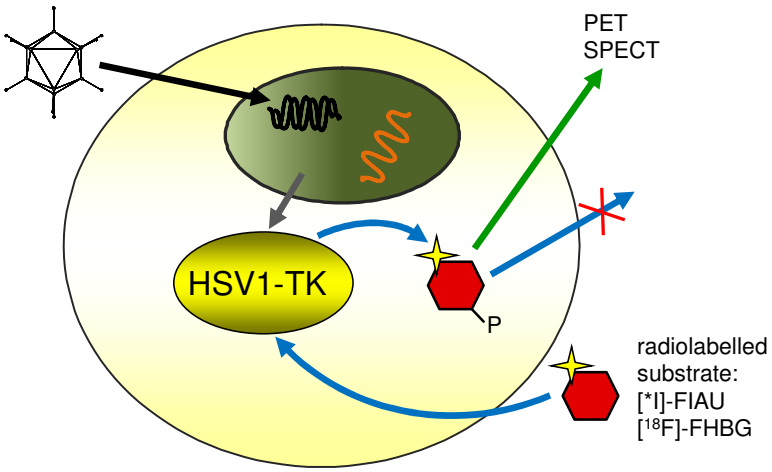

Figure 1.3: Principle of reporter gene imaging with HSV1-TK. The HSV1-TK enzyme, which is expressed after gene transduction of target cells, converts its specific radiolabelled substrates (e.g. [*I]-FIAU, [^{18}F]-FHBG) into phosphorylated metabolites. These cannot diffuse throughout the cell membrane and accumulate within the cell, enabling non-invasive imaging of HSV1-TK-transduced cells by means of PET and SPECT. *I: [^{124}I]- or [^{131}I]-FIAU.

Early investigations of hepatic reporter gene delivery have shown that adenoviral transfer of HSV1-TK or HSV1-sr39TK is promising for *in vivo* reporter gene PET imaging using radiolabelled acycloguanosines [111-113]. Some *in vitro* and *in vivo* studies of cardiovascular imaging [114-116] or tumour imaging [117-119] showed that HSV1-TK is more sensitive to [^{14}C]-FIAU and [^{124}I]-FIAU than to [^{18}F]-FHBG. In contrast, HSV1-sr39TK showed greater sensitivity to [^{18}F]-FHBG than to FIAU probes and the HSV1-sr39TK/[^{18}F]-FHBG combination yielded more radiotracer accumulation over time and higher imaging contrast for PET than the combination of HSV1-sr39TK and FIAU. Therefore, HSV1-sr39TK and [^{18}F]-FHBG have been used as an optimal combination of reporter gene and probe for non-invasive PET imaging. Non-invasive imaging with HSV1-sr39TK and [^{18}F]-FHBG in a dedicated small animal scanner with greater sensitivity than clinical PET scanners, termed microPET, was feasible for monitoring the HSV1-sr39TK/GCV-mediated effect in tumour xenografts [120-123]. The feasibility of FIAU-/FHBG-based HSV1-TK nuclear reporter gene imaging, its application for assessing the safety of transgene delivery vectors and for predicting the therapeutic response in cancer, was also demonstrated in several phase I and II clinical trials [124-127].

Another example of a widely used nuclear reporter gene is the human sodium-iodide symporter gene (*hNIS*). It mediates the uptake of radioisotopes suitable for imaging with scintigraphic techniques, such as ^{123}I, ^{131}I, and ^{99m}Tc-pertechnetate (^{99m}Tc), or with PET, as ^{124}I and ^{94m}Tc [128]. *hNIS* was applied for non-invasive imaging of the response of tumours to radioiodine therapy [129, 130]. Nuclear reporter genes can also code for extracellular receptors like human somatostatin receptor subtype 2 (*hSSTR2*) [131] or human dopamine 2 receptor (*hD2R*) [132].

1.5. Adenoviruses

1.5.1. Adenoviral structure

Human adenoviruses belong to the family of *Adenoviridae* and the genus of *Mastadenoviruses*. They were first isolated from human adenoids in 1953 by Rowe et al. [133]. Adenoviruses mainly cause infections of the respiratory tract that range from mild and self-limited to life threatening, associated with acute respiratory disease in immunocompromised patients [134-136]. Over 60 serotypes of human adenovirus, which are divided into seven species (A-H), have been identified so far [137].

Adenoviruses are non-enveloped viruses that have a capsid diameter of over 90 nm and a size of 150 MDa. Their genome consists of linear, double-stranded DNA of about 36 kb length [138, 139]. The mature adenovirus particle is composed of an outer capsid and an inner core that contains the viral DNA (figure 1.4). Recently, the visualisation of adenoviruses by X-ray crystallography [140] or cryoelectron microscopy [141] enabled the nearly atomic resolution of all structure components of the virion. The icosahedral virus capsid is composed of 240 pseudo-hexagonal homotrimers of hexon, the major capsid protein, on the faces and edges of the capsid and of a pentagon-shaped penton located on each of the 12 fivefold apices. Each penton consists of a covalent complex between the homopentameric penton base and a homotrimeric fiber protein [142-144]. Four minor capsid proteins (IIIa, VI, VIII and IX) are also involved in capsid assembly [141, 145]. The virus core contains six structural proteins, five of which are associated with the viral genome (V, VII, μ, IVa2 and the terminal protein). The sixth core protein, the 23K cysteine protease, plays a role in virion assembly [138, 144].

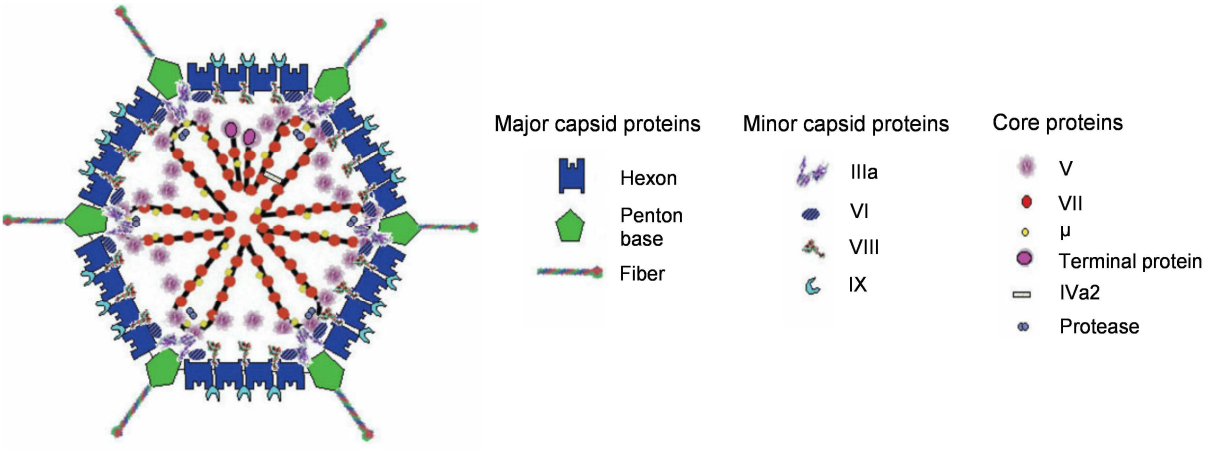

Figure 1.4: Adenovirus assembly. The adenovirus capsid is composed of the major capsid proteins hexon and penton (built up of penton base and fiber), and the minor capsid proteins IIIa, VI, VIII and IX. The core proteins V, VII, μ, the terminal protein and IVa2 stabilise the viral DNA. The viral protease plays a role in virion assembly (modified from [144]).

1.5.2. Adenoviral infection and life cycle

The initial contact between the adenovirus and the target cell is mediated by the interaction of the viral fiber protein with the coxsackie and adenovirus receptor (CAR), a cell membrane protein [146]. However, dependent on species, adenoviruses can also utilise alternative cell surface receptors for cell entry, e.g. CD46, CD80, CD86, sialic acid receptors or heparin sulphate glycosoaminoglycans [138, 144]. The virus-host interaction is further accomplished by the binding of an arginine-glycine-aspartic acid (RGD) peptide on the viral penton base to cellular $\alpha_v\beta_3/\alpha_v\beta_5$ integrins [147]. This binding triggers the internalisation of viral particles by clathrin-mediated endocytosis [148]. The delivery of the virus into an acidic endosome mediates the viral escape from the endosome and the transport of the virus towards the nucleus [149]. After docking to the nuclear pore complex, the viral particle disassembles and its DNA is imported into the nucleus, where the transcription of viral genes is initiated [150].

1.5.3. Adenoviral genome organisation

The linear DNA of the adenovirus is flanked by inverted terminal repeats (ITR) that contain the origins of DNA replication and, located close to the left ITR, the encapsidation signal [151, 152]. The viral genome is divided into transcription units defined as early and late according to the onset of their transcription [153] (figure 1.5). The early elements (*E1-4*) are the first to be transcribed shortly after infection and their gene products have regulatory functions. The *E1* region codes for the early region 1A (E1A) and early region 1B (E1B) proteins. E1A are the first proteins of the adenovirus that are expressed after infection. Crucial for mediating the regulatory functions of E1A are two transcripts of 12S and 13S mRNA, derived by alternative mRNA splicing, that encode proteins of 243 amino acid (aa) and 289 aa, respectively. *E1A* contains four conserved regions (CR1-4). The functional difference between the 289 aa and the 243 aa proteins arises from the lack of CR3 in the 243 aa protein. In the 289 aa protein, CR3 codes for a C4 zinc finger motif that acts as a transcriptional activator crucial for the transactivation of the delayed early *E2-4* genes and of some cellular genes [154-157]. A further function of the E1A proteins is the deregulation of the host cell cycle in order to facilitate adenoviral replication. Both splice variants of E1A bind to cellular retinoblastoma proteins (pRb) and inhibit their cell cycle suppressive activity by destroying pRb-E2F complexes. The released cellular transcription factor E2F mediates transition of the host cell cycle from G0/G1 into the S phase [156, 158]. Moreover, E1A proteins can directly target the cell division cycle 25 homolog a (cdc25a) phosphatase and thus force S phase entry [159].

The E1B protein family is subdivided into the proteins E1B55K and E1B19K. The E1B55K protein forms in cooperation with the *E4* encoded protein E4orf6 an ubiquitin-ligase complex that targets p53 and inhibits p53-mediated cell cycle arrest and apoptosis [160]. The E1B55K and E4orf6 complex is also responsible for the export of viral mRNA transcripts from the nucleus into the cytoplasm for the

biosynthesis of viral proteins. In addition, E1B55K and E4orf6 downregulate host protein synthesis [161]. The E1B19K protein is a homologue of the Bcl-2 protein and exerts anti-apoptotic effects in host cells [162].

The *E2* transcription unit, including the *E2A* and *E2B* genes, encode the viral DNA polymerase and other proteins that are directly involved in adenoviral DNA replication, DNA elongation, transcription control, mRNA stability, protection of viral DNA from degradation and prevention of DNA integration into the host genome [163, 164]. At the end of adenoviral replication, up to 10^6 new DNA molecules have been synthesised within 48 h after infection of human cells, which almost correlates with the cellular DNA content [152].

The gene products of the *E3* transcription unit are involved in mediation of lytic viral release from the infected cells and in adenovirus-mediated immune escape. The *E3* encoded adenovirus death protein (ADP, formerly E3 11.6K) facilitates host cell lysis and the release of newly synthesised viral particles at late stages of infection [165]. *E3* encoded proteins with immunomodulatory functions prevent detection of virus-infected cells by the host immune system by blocking MHC class I antigen presentation and inflammatory responses induced by cytokines [166].

The *E4* gene products are derived by alternative splicing of a primary mRNA transcript. Proteins expressed by the *E4* region exhibit diverse functions in viral DNA replication, RNA splicing, synthesis of late viral proteins, as well as in modulation of transcription, cell cycle, DNA repair and cell signalling [167].

Gene expression from the late regions *L1-5* is initiated about 8 h post infection. The late genes encode the viral structural proteins described in chapter 1.5.1. [168]. Besides its role in virion assembly [144], the *L3*-coded 23K proteinase cleaves the cellular cytokeratin network, thus rendering the host cell susceptible to lysis and release of newly synthesised viral particles [169]. An indication for cell lysis is the cytopathic effect (c.p.e.) that describes the typical swelling and rounding of adenovirus-infected cells, occurring one to two days after infection [170].

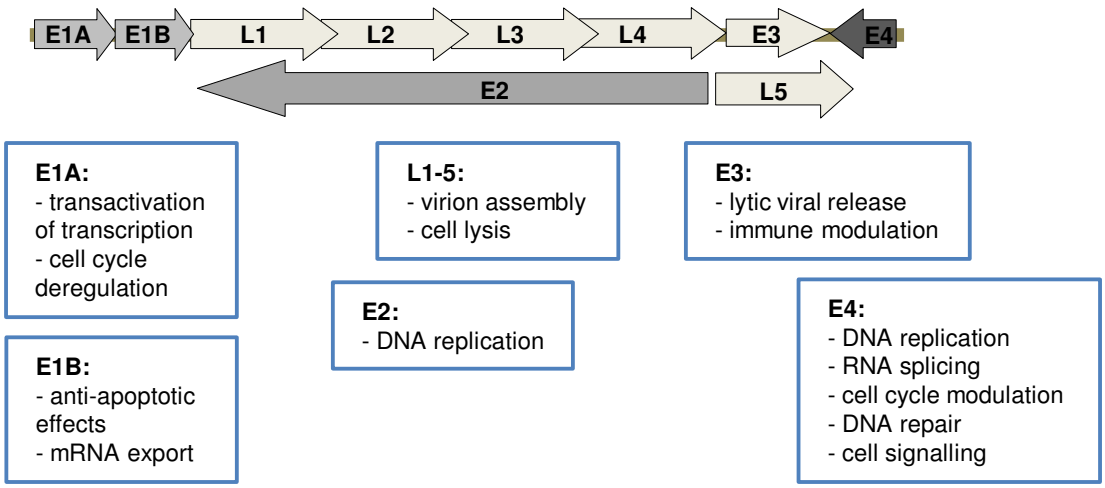

Figure 1.5: Organisation of the adenoviral genome. Location of the early (*E1-4*) and late (*L1-5*) gene regions in the adenoviral genome and their crucial gene functions.

1.6. Adenoviral vectors for gene therapy

Adenoviruses can be applied as vehicles for the delivery of therapeutic genes and adenovirus-based gene therapy is a promising alternative treatment for cancers that are refractory to conventional therapies. The advantages of adenoviral vectors in gene therapy are their broad host range and their ability to infect proliferating as well as quiescent cells, enabling efficient gene transfer. Moreover, they display low pathogenicity in humans and the non-integrative character of their genome allows for transient transgene expression and minimises the risk of mutagenesis. Finally, adenoviral vectors can be easily purified achieving high titres [168, 171]. The packaging capacity of adenoviral vectors for foreign DNA can be up to 105 % of the wild-type adenoviral genome size, which equals to an insert size of only about 2 kb, without impairing the genetic stability of the vectors [172]. In order to maximise the vector capacity for inserts, first generation vectors with deletions of the *E1* and/or *E3* regions that enable insertions of about 8 kb foreign DNA have been constructed, providing safe and efficient transgene delivery [153, 168, 173].

1.7. Oncolytic adenoviruses

1.7.1. Nature and modifications

Oncolytic viruses are biological therapeutic agents that are genetically modified to selectively kill tumour cells while sparing healthy tissue. The concept of cancer virotherapy is based on the ability of the viral agent to replicate in tumour cells and to spread its progeny throughout the tumour with the aim to eliminate the tumour burden completely [171, 174]. The strategy of oncolytic killing utilises the replicative and lytic life cycle of the viruses and its regulation by tumour-specific factors [174, 175]. According to the paradigm of virotherapy, viral oncolysis might also stimulate a systemic immune response against residual tumour cells [175]. There are some viruses with natural tropism for cancer cells, including reovirus [176], autonomous parvovirus [177], Newcastle disease virus [178, 179], mumps virus [180] and murine leukemia virus [181]. In contrast, viruses, such as adenovirus, measles virus, vesicular stomatitis virus, vaccinia virus and HSV need to be engineered to make them tumour specific [175].

Oncolytic adenoviruses are designed to overcome the limitations of replication-deficient vectors such as insufficient infectivity of solid tumours and impaired virus spread [171, 182]. Furthermore, all the benefits of attenuated adenoviral vectors, as listed in chapter 1.6., are applicable for oncolytic vectors [183]. Due to their ability to transduce also quiescent cells, oncolytic adenoviruses are suitable agents against cancer stem cell populations, which show a low proliferation rate [184-186].

In contrast to the non-selective replication of wild-type adenovirus, oncolytic adenoviruses are genetically modified to replicate exclusively in tumour cells. There are two major strategies to generate replicative adenoviral vectors with specific tumour tropism. The first strategy involves the introduction of loss-of-function mutations in adenoviral genes essential for viral replication in normal cells. These mutated viral genes are compensated by aberrant oncogenes, tumour suppressor genes or transcription factors in tumour cells, as p53, pRb or Y-box binding protein 1 (YB-1). The adenoviral replication is therefore restricted to tumour cells with dysfunctional gene expression [171, 174]. One of the most prominent examples for conditionally replicating adenoviruses with introduced mutations is ONYX-015 (formerly dl1520), which carries deletions of the *E1B55K* gene. It was originally proposed that this virus replicates selectively in tumour cells with a mutated p53 tumour suppressor gene and an aberrant p53-p14^{ARF} pathway, because the p53-binding protein E1B55K is not at disposal for inactivation of p53 and lack of p53 expression in tumours enables viral replication [187-189]. The p53-dependency of ONYX-015 is however rejected, as another study has stated that the replication of the virus does not depend on p53 or p14^{ARF} [190] and probably other mechanisms are involved. Another mutated conditionally replicating adenovirus is AdΔ24 that contains a 24 bp deletion of the CR2 of *E1A*, rendering the expressed protein unable to bind to pRb and to stimulate S phase entry. The virus can therefore replicate only in cancer cells with mutated pRb [191].

In the second strategy for generation of conditionally replicative adenoviral vectors, so called transcriptional targeting, viral promoters are replaced by cancer-specific promoters that restrict viral replication to tumour cells expressing specific transcription factors [171, 174, 183]. Several oncolytic adenoviruses that utilise transcriptional targeting have been designed using cancer-specific promoters of genes encoding for example prostate-specific antigen [192], α-fetoprotein [193] or human telomerase reverse transcriptase (hTERT) [194].

In order to augment the anti-tumour efficacy of conditionally replicating adenoviruses, several attempts to improve their cell targeting and delivery to the tumour, as well as their intratumoural spread, were performed. The rapid clearance of adenoviruses from blood by liver Kupffer cells [195] is a considerable obstacle especially for the targeting of disseminated cancers. Therefore, capsid modifications were performed in order to prevent the interaction of adenoviruses with hepatocytes and to increase adenovirus persistence in blood [174]. Although oncolytic adenoviruses are characterised by a high transduction efficiency *in vivo* [182], many tumours do not express CAR receptors sufficiently and adenoviral infection is therefore limited [196]. To enhance viral delivery and spread in CAR-deficient tumour cells significantly, an integrin-binding RGD motif [197] or a polylysine sequence [198] can be inserted into the adenoviral fiber knob gene. These fiber modifications increase both the CAR-independent tumour tropism and the oncolytic potential of the viruses [198-200]. A strategy to augment intratumoural spread of oncolytic adenoviruses by enhancing viral particle release is the deletion of the anti-apoptotic *E1B19K* gene [201] or the maintenance of the ADP protein [165]. Finally, the use of immune suppressive drugs can prevent recognition of oncolytic adenoviruses by the host adaptive immune response and can thus improve viral anti-tumour efficacy [175].

The potency of oncolytic adenoviruses can be further enhanced by arming them with suicide genes, as described in chapter 1.8., or transgenes that enhance intratumoural spread of the virus [202], modify the tumour microenvironment [203] and modulate immune responses in favour of tumour destruction [204].

1.7.2. In vitro 3D tumour models to explore oncolytic adenoviruses

Three-dimensional (3D) multicellular spheroids are convenient and feasible models for performing preliminary investigations of *in vivo* effects. A benefit of spheroids is that their complexity is intermediate between the conventional two-dimensional (2D) cell culture *in vitro* and tumours *in vivo*. The use of spheroids represents an approach to mimic micrometastases in order to study the biology of tumour microregions [205]. Because they resemble tumour tissue with regard to growth kinetics and metabolism [205], multicellular spheroids can be applied for the study of treatment efficacy and for drug screening in cancer therapy [206-209]. Spheroids are also a relevant and promising 3D model for exploring adenoviral replication, oncolysis, distribution and spread [210].

They were successfully applied in various preclinical analyses of conditionally replicating and tropism-modified oncolytic adenoviruses prior to *in vivo* application [211-213]. Moreover, spheroids derived from tumour cell lines were used as a convenient *in vitro* model to assess changes in cellular metabolism by means of imaging techniques after treatment with oncolytic adenoviruses [214].

1.7.3. Clinical application of oncolytic virotherapy

Modern oncolytic virotherapy undergoes a promising development towards clinical application, based on the recent success of some clinical trials. An adenoviral vector with similarity to ONYX-015, termed Oncorine (H101), was the first oncolytic adenovirus that was approved as a therapy of head and neck squamous cell carcinoma (HNSCC) in China in 2005 [215, 216]. A milestone in the development of oncolytic virotherapy was achieved with the first demonstration of significant anti-cancer efficacy by an attenuated oncolytic HSV-1, termed OncoVEX^{GM-CSF} (talimogene laherparepvec), encoding the immunostimulatory cytokine granulocyte macrophage colony-stimulating factor (GM-CSF) [217, 218]. Another notable clinical development of virotherapy was achieved by the study of JX-594, an oncolytic vaccinia virus armed with GM-CSF [219, 220]. Among oncolytic adenoviruses, some phase I and II clinical trials showed promising results by applying ONYX-015 with or without chemotherapy against various cancer types, including head and neck cancer [221, 222], ovarian cancer [223], solid tumours [224], pancreatic carcinoma [225], colorectal cancer [226, 227] and malignant glioma [228]. In addition, an oncolytic adenovirus under the control of the hTERT promoter and the RGD-modified version of AdΔ24 were tested in phase I trials against solid tumours [229] and ovarian cancer [199, 200], respectively.

HSV has been for a long time the vector of choice for oncolytic virotherapy against brain cancer [175, 230]. However, recombinant oncolytic HSV have shown only limited efficacy in clinical trials for malignant glioma probably due to deletions of crucial viral genes [231-233]. Oncolytic adenoviruses have emerged in the focus of malignant glioma therapy, as this tumour type provides favourable conditions for viral replication and spread. Malignant gliomas rarely metastasise and the viral load can be safely injected intratumourally. Moreover, the blood-brain barrier and the lack of tumour-specific antigen drainage to the cervical lymph nodes cause an immune privilege of the brain [234, 235]. ONYX-015 was tested as an adjuvant therapy in a phase I trial for recurrent malignant gliomas and demonstrated good viral tolerance and absence of severe anti-viral effects. This therapy was safe, but achieved no significant anti-tumour efficacy [228].

1.8. Arming oncolytic adenoviruses with suicide and reporter genes

Although clinical trials have demonstrated their good safety profile, oncolytic adenoviruses are not able to improve the outcome of the disease significantly, as described above. Due to the heterogeneous expression of cell surface receptors [236] and tumour-specific promoters from one tumour type to the other, a treatment with a single oncolytic adenovirus has often not the desired efficacy. Oncolytic adenoviruses can be therefore combined with suicide and reporter genes in order to improve cell killing and to directly monitor the viral distribution, spread and therapeutic efficacy in living systems.

The HSV1-TK/GCV suicide system was shown to enhance the oncolytic activity of HSV1-TK-armed conditionally replicating [237-239] and non-conditionally replicating [240] adenoviruses and thus to improve the treatment efficacy in different preclinical tumour models compared to virus treatment only. Other studies demonstrated a potent anti-tumour synergistic effect of HSV1-TK-expressing conditionally replicating adenoviruses driven by the hTERT promoter and the HSV1-TK/GCV suicide system [241, 242].

Further improvement of armed virotherapy includes the development of oncolytic adenoviruses containing *bCD/HSV1-TK* or *yCD/HSV1-sr39TK* fusion genes, which allow the concomitant delivery of both suicide gene types to tumours [243, 244]. Encouraging results from phase I clinical trials demonstrated the potential therapeutic benefit and safety of the combined approach using viral oncolysis, activity of both CD/5-FC and HSV1-TK/GCV suicide systems and radiation therapy for prostate cancer [245-247]. Oncolytic adenoviruses expressing HSV1-sr39TK [244] or a mutant of HSV1-TK that incorporates an 8 aa-domain derived from the Tat protein of the human immunodeficiency virus (Tat8TK) [248] can facilitate *in vivo* PET imaging of viral distribution, transgene activity and of the progress of combined anti-tumour oncolytic- and suicide gene therapy. Furthermore, the delivery of the *hNIS* reporter gene to conditionally replicating adenoviruses [249, 250] or to tropism-modified replication-selective adenoviruses [251-253] was proven to be effective for non-invasive imaging of the combined potential of oncolytic virotherapy and hNIS-mediated radioiodine treatment against cancer.

Besides *HSV1-TK/HSV1-sr39TK* and *CD*, there are further suicide genes delivered by replication-competent adenoviruses that were shown to enhance the oncolytic potential of their delivery vectors in cancer. One example thereof is the suicide gene *FCU1*, encoding a bifunctional chimeric protein that combines the enzymatic properties of yCD and uracil phosphoribosyl transferase (FUR1 or UPRT) and catalyses the conversion of 5-FC [254]. Another example is the novel suicide gene deoxyribonucleoside kinase of *Drosophila melanogaster* (*Dm-dNK*), which sensitises mammalian cells to the prodrugs (E)-5-(2-bromovinyl)-20-deoxyuridine (BVDU) and 2',2'-difluoro-deoxycytidine (dFdC) [255].

1.9. YB-1 dependent oncolytic adenoviruses

1.9.1. The multifunctional protein YB-1

The Y-box binding protein 1 (YB-1) is a protein with multiple functions, concerning the regulation of various biological processes. It belongs to the superfamily of the cold-shock proteins and contains a highly conserved nucleic-acid-binding motif [256]. Whereas YB-1 is barely present in healthy cells, except in certain embryonic tissues [257], it is overexpressed in various cancer types and is located mostly in the nucleus of tumour cells [258, 259]. The pleiotropic functions of YB-1 arise from the localisation of the protein either in the nucleus or in the cytoplasm of cells. In the cytoplasm, YB-1 is involved in regulation of mRNA translation and transport of mRNA to polysomes [260, 261]. Translocation of YB-1 into the nucleus of highly proliferating or tumour cells results from environmental stressors like chemotherapy [258], UV irradiation [262], hyperthermia [263] or takes place at the G1/S phase transition of the cell cycle [264]. YB-1 also accumulates in the nucleus of adenovirus-infected cells [259, 265]. Following accumulation in the nucleus, YB-1 binds with its cold-shock domain to an inverted CCAAT element within a gene promoter region, termed Y-box [264, 266], and functions as a transcription factor that regulates a variety of genes, associated with cancer malignancy [264, 267-272]. YB-1 also promotes an epithelial-mesenchymal transition that contributes to the metastatic potential of tumours [273]. It has also been shown that YB-1 is associated with the transactivation of genes responsible for tumour proliferation and relapse [274, 275]. YB-1 directly interacts with p53 or represses the transcription of *p53*, thus reducing its pro-apoptotic activity [276, 277]. Evidence exist that many tumours exhibit multidrug-resistant phenotype as a result of the transactivation of *MDR1* and multidrug resistance-related protein (*MRP1*) gene expression by nuclear accumulated YB-1 [258, 263, 266, 278]. Due to its multiple functions in tumourigenesis, nuclear localisation of YB-1 is a prognostic factor for poor clinical outcome of many malignancies, including amongst others pediatric GBM [279], breast cancer [280], ovarian cancer [281], non-small cell lung cancer [282], HNSCC [283]. Furthermore, high levels of YB-1 mRNA are observed in GBM [284]. The pleotropic functions of YB-1 as a regulator of genes and signalling pathways responsible for development of cancer and malignant phenotype turn this protein into an oncogenic factor and an excellent therapeutic target against cancer [285].

1.9.2. Regulation of adenoviral replication by YB-1 and YB-1 dependent virotherapy

The adenoviral DNA replication depends on viral replication factors encoded by the adenoviral *E2* region, as described in chapter 1.5.3. The expression of the *E2* genes is controlled by the E2-early and E2-late promoters [286]. The interaction of the CR1 and CR2 of E1A with pRb releases the host cell factor E2F from the pRb-E2F complex, leading amongst others to activation of the E2-early promoter by E2F [156, 287]. In contrast, the activity of the E2-late promoter does not depend on E1A or E2F

and is required for the accomplishment of adenoviral replication [265]. It was demonstrated that YB-1 is translocated to the nucleus of adenovirus-infected cells by the adenoviral proteins E1B55K and E4orf6. Following nuclear accumulation, YB-1 binds to the proximal Y-boxes of the adenoviral E2-late promoter and activates the *E2* gene transcription [259, 265]. As mentioned in chapter 1.5.3., *E1B55K* and *E4orf6* are expressed after transactivation by the CR3-containing E1A 289 aa protein (E1A 13S mRNA) [156]. Interestingly, after infection of tumour cells with adenoviruses that do not produce the E1A 289 aa protein as a result of deletion in the CR3 transactivation domain, YB-1 can relocate into the nucleus independently of E1A, E1B55K and E4orf6 and can activate the E2-late promoter, leading to adenoviral replication [259, 288] (figure 1.6). Therefore, this YB-1-based strategy can be applied for the development of conditionally replicating E1A-mutated adenoviruses that replicate in the presence of YB-1, which is already accumulated in the nucleus of tumour cells due to overexpression [284] or environmental stress [258, 262, 263]. In this context, YB-1 dependent adenoviruses showed efficient E1A-independent replication and oncolytic potential in multidrug-resistant cancer cells with nuclear localisation of YB-1 [288], as YB-1 induces *MDR1* gene expression [258].

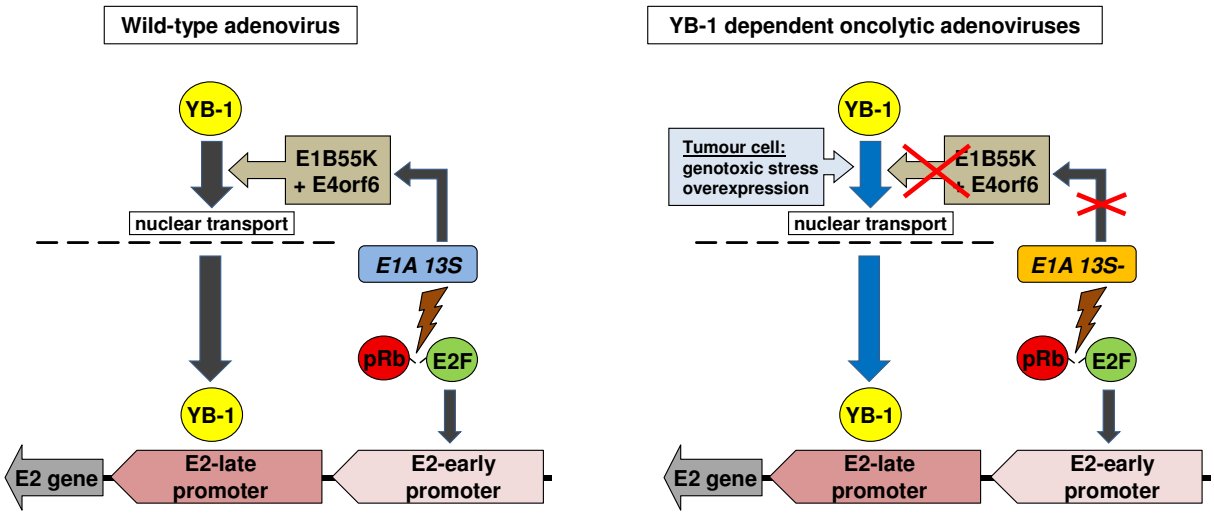

Figure 1.6: Concept of YB-1 dependent oncolytic adenoviruses. The DNA replication of adenoviruses is activated by adenoviral E1A proteins, which disrupt the pRb-E2F complex and enable binding of E2F to the E2-early promoter. However, the E2-late promoter plays the main role in the activation of *E2* gene transcription. The E1A 289 aa protein, encoded by the E1A 13S mRNA transcript of wild-type adenoviruses (left), transactivate the expression of E1B55K and E4orf6. YB-1 is translocated by E1B55K and E4orf6 to the cell nucleus and activates the E2-late promoter. In adenoviruses that do not produce E1A 13S mRNA (right), gene transactivation is dysfunctional and E1B55K and E4orf6 are consequently not at disposal for nuclear transport of YB-1. The replication of these adenoviruses is YB-1 dependent, because the E2-late promoter is activated only in tumour cells with already nuclear accumulated YB-1. The transport of YB-1 to the nucleus of these tumour cells is induced by stress responses or overexpression of YB-1 (modified from [265]).

Several studies demonstrated the relation between chemotherapeutic stress, nuclear localisation of YB-1 and adenoviral replication. Among them, a study showed that YB-1 dependent oncolytic adenoviruses cause oncolysis and downregulation of *MDR1* and *MRP1* gene expression, leading to resensitization of multidrug-resistant tumour cells to chemotherapy [265]. It was also demonstrated that genotoxic stress induced by chemotherapy or radiation enhances the nuclear accumulation of YB-1 and augments the replication and oncolytic potential of YB-1 dependent adenoviruses [289-292].

A novel oncolytic adenovirus that is based on the concept of YB-1 dependent virotherapy is the vector Ad-delo3-RGD [291]. The structure of this adenovirus is partly based on the genome of the adenoviral vector dl520 and accordingly, Ad-delo3-RGD contains a deletion of 11 bp in CR3 of *E1A* [293]. Because of this deletion, the adenovirus does not express the 289 aa E1A protein containing the transactivation domain encoded by CR3. The *E1A* deletion renders the virus conditionally replicating in the presence of YB-1 [291]. Ad-delo3-RGD also carries a deletion in the *E1B19K* gene, resulting in improved viral spread [201]. A deletion of most of the *E3* region enables transgene insertion for future applications. Finally, the viral fiber was modified with a RGD motif in order to improve infectivity [197]. Ad-delo3-RGD was shown to replicate YB-1 dependently and to exert selective oncolytic killing of tumour cells *in vitro* and *in vivo* in xenograft models of pancreatic cancer and malignant glioma [291, 292]. The oncolytic activity of the virus against pancreatic cancer cells was augmented after combination of oncolytic virotherapy with paclitaxel treatment [291]. In malignant glioma cells, treatment with TMZ enhanced nuclear accumulation of YB-1, which resulted in significant increase in viral replication and in potentiation of the viral anti-tumour effect [292]. Encouraging therapeutic efficacy has been obtained recently by the combination of Ad-delo3-RGD and TMZ in brain cancer stem cells, suggesting that YB-1 based virotherapy could be promising against this subset of cells [294].

1.10. Aims of the thesis

Standard and alternative molecular therapies for GBM and malignant glioma are currently facing limited success. Promising strategies to address existing limitations of anti-GBM and anti-cancer therapy in general represent suicide gene therapy and oncolytic virotherapy. Oncolytic adenoviruses modified to replicate selectively in tumour cells that express the oncogenic factor YB-1 have already demonstrated anti-tumour efficacy *in vitro* and *in vivo*, also in combination with chemotherapy.

Based on the finding that YB-1 is overexpressed in GBM, it is of special interest to develop a novel targeted approach against GBM, combining YB-1 dependent virotherapy with a HSV1-sr39TK/GCV-mediated suicide and reporter gene strategy, and TMZ therapy. The aim of this work is first to characterise an *E1*-mutated YB-1 dependent oncolytic adenovirus armed with the suicide and reporter gene *HSV1-sr39TK* with respect to viral replication, release and dissemination, as well as induction of oncolytic effect and transgene expression in GBM cells *in vitro*. Furthermore, the combined oncolytic effect and HSV1-sr39TK/GCV-mediated cytotoxicity of the vector is to be analysed, regarding the timing of GCV addition and induction of bystander killing effect. Considering that YB-1 is accumulated within the cell nucleus upon chemotherapy-induced stress, a further goal of this work is to evaluate the influence of TMZ on adenoviral replication and oncolytic effect in GBM cells. In addition, the potential synergy between TMZ, viral oncolysis and HSV1-sr39TK/GCV-mediated cytotoxicity is to be analysed. The application of HSV1-sr39TK in the context of viral oncolysis for non-invasive nuclear PET imaging is also to be examined *in vitro*. The oncolytic, cytotoxicity-mediating and imaging properties of the armed vector are to be compared to other YB-1 dependent oncolytic adenoviruses and a HSV1-sr39TK-expressing replication-deficient adenoviral vector, as well as to be analysed in an *in vitro* 3D multicellular spheroid model. The data obtained in this thesis are fundamental for future preclinical investigations *in vivo*.

2. MATERIALS

2.1. Laboratory equipment

Table 2.1: Laboratory equipment

Laboratory equipment	Manufacturer
Analytical balances: PCE-LSM 2000 Research RC210P	 PCE GmbH, Meschede, Germany Sartorius AG, Göttingen, Germany
Centrifuges: Biofuge fresco EBA 12 R Megafuge 2.0 R Ultracentrifuge Optima™ LE-80K	 Heraeus Instruments, Hanau, Germany Hettich GmbH & Co.KG, Tuttlingen,Germany Heraeus Instruments, Hanau, Germany Beckman Coulter GmbH, Krefeld, Germany
CO_2 incubator HERAcell 150i	Thermo Scientific Inc., Rockford, IL, USA
Concentrator 5301	Eppendorf AG, Hamburg, Germany
Cross-linker UV Stratalinker 2400	Stratagene, La Jolla, CA, USA
Cryostat microtome HM 560	Microm GmbH, Walldorf, Germany
Electrophoresis power supply PowerPac 300	Bio-Rad, Munich, Germany
Gamma-counter Wallac 1480-011	PerkinElmer LAS GmbH, Rodgau, Germany
Gel electrophoresis units: Mini horizontal submarine unit HE33 Sub-Cell GT system	 Amersham Biosciences, Buckinghamshire, UK Bio-Rad, Munich, Germany
Hybridisation oven Personal Hyb	Stratagene, La Jolla, CA, USA
INVEON PET/CT System	Siemens Healthcare, Erlangen, Germany
Microscopes: Axiovert 25 and 135 with AxioCam MRc Eclipse TE2000-S	 Carl Zeiss GmbH, Jena, Germany Nikon Instruments, Melville, NY, USA
Microtiter shaker MTS 2/4	IKA Werke GmbH, Staufen, Germany
Minishaker MS2	IKA Werke GmbH, Staufen, Germany
Multilabel counter Wallac Victor^2 1420	PerkinElmer LAS GmbH, Rodgau, Germany
Neubauer cell counting chamber	Brand GmbH, Wertheim, Germany
Pipettes (10/20/200/1000 µl)	Eppendorf AG, Hamburg, Germany
Pipette controller Accu-jet®	Brand GmbH, Wertheim, Germany
Real-time PCR Sequence Detection System ABI 7900HT	Applied Biosystems®, Life Technologies GmbH, Darmstadt, Germany
SDS-PAGE unit Mini-PROTEAN 3 Cell	Bio-Rad, Munich, Germany
Spectrophotometer DU 640	Beckman Coulter GmbH, Krefeld, Germany
Sterile bench Hera Safe HS 12	Heraeus Instruments, Hanau, Germany
Thermal cyclers for PCR: Mastercycler® PTC-100™	 Eppendorf AG, Hamburg, Germany MJ Research Inc., Watertown, MA, USA
Thermomixer comfort	Eppendorf AG, Hamburg, Germany
UV gel documentation system	LTF Labortechnik GmbH, Wasserburg, Germany
UV transilluminator	Biotec-Fischer GmbH, Reiskirchen, Germany
Water bath	Memmert GmbH, Schwabach, Germany
Western blot: Image Station 440CF	Kodak Digital Science, Rochester, NY, USA
Western blot: Transphor Electrophoresis unit	Hoefer Inc., San Francisco, CA, USA

2.2. Consumables

Table 2.2: Consumables

Consumable	Manufacturer
Cell culture dishes (6, 10 and 15 cm)	TPP AG, Trasadingen, Switzerland
Cell culture test plates (6-, 24-, 96-well)	TPP AG, Trasadingen, Switzerland
Cell lifter	Corning Inc., Corning, NY, USA
Centrifuge tubes, conical (15 and 50 ml)	TPP AG, Trasadingen, Switzerland
Cover slips (24 x 50 mm)	G. Menzel GmbH, Braunschweig, Germany
Cryomold Intermediate (15 x 15 x 5 mm)	Sakura Finetek, Torrance, CA, USA
Cryopreservation tubes CryoPure (1.6 ml)	Sarstedt AG & Co., Nümbrecht, Germany
Dialysis Cassette Slide-A-Lyzer®, 10K Molecular Weight Cut-Off (MWCO)	Pierce Biotechnology Inc., Rockford, IL, USA
Disposable scalpel	Feather Co., Osaka, Japan
GeneScreen Hybridisation Transfer Membrane	PerkinElmer LAS GmbH, Rodgau, Germany
Micro Amp® Optical 96-well real-time PCR Reaction Plate with Optical Adhesive Film	Applied Biosystems®, Life Technologies GmbH, Darmstadt, Germany
Microscope slides Superfrost Plus	G. Menzel GmbH, Braunschweig, Germany
Needles, sterile (18G x 1½") Microlance™ 3	BD Biosciences, Heidelberg, Germany
Pipette tips Axygen®	Corning Inc., Corning, NY, USA
Polystyrene Reagent Reservoir (50 ml)	Corning Inc., Corning, NY, USA
Precise Protein Gels (10 %)	Thermo Scientific Inc., Rockford, IL, USA
Polyvinylidene fluoride (PVDF) membrane	Millipore, Merck KGaA, Darmstadt, Germany
Reaction tubes (0.5, 1.5 and 2 ml)	Josef Peske GmbH, Aindling, Germany
Serological pipettes (1, 2, 5, 10, 25, 50 ml)	Greiner Bio-One GmbH, Solingen, Germany
Syringe filter, sterile (0.22 µm)	TPP AG, Trasadingen, Switzerland
Syringes, sterile	B. Braun Medical Inc., Melsungen, Germany
Ultra-clear centrifuge tubes (16 x 102 mm)	Beckman Coulter GmbH, Krefeld, Germany
UV-Cuvette micro with caps	Brand GmbH, Wertheim, Germany
Whatman paper	Schleicher & Schuell Bioscience GmbH, Dassel, Germany

2.3. Chemicals

Table 2.3: Chemicals

Chemical	Manufacturer
Acetic acid	Merck KGaA, Darmstadt, Germany
Acetone	Pharmacy of Klinikum rechts der Isar, Munich, Germany
Ammonium acetate ($NH_4C_2H_3O_2$)	Merck KGaA, Darmstadt, Germany
Bromophenol blue	Sigma-Aldrich GmbH, Steinheim, Germany
Calcium chloride ($CaCl_2$)	Fluka GmbH, Neu-Ulm, Germany
Cesium chloride (CsCl)	Serva, Heidelberg, Germany
Chloroform	Merck KGaA, Darmstadt, Germany
Dimethyl sulfoxide (DMSO)	Sigma-Aldrich GmbH, Steinheim, Germany
Ethanol	Merck KGaA, Darmstadt, Germany
Ethylenediamine-tetraacetic acid (EDTA)	Merck KGaA, Darmstadt, Germany
Glycerol	Merck KGaA, Darmstadt, Germany
Glycine	Sigma-Aldrich GmbH, Steinheim, Germany

Hydrochloric acid (HCl) 37 %	Merck KGaA, Darmstadt, Germany
Isopropyl alcohol	Pharmacy of Klinikum rechts der Isar, Munich, Germany
Magnesium chloride ($MgCl_2$)	Merck KGaA, Darmstadt, Germany
Maleic acid	Sigma-Aldrich GmbH, Steinheim, Germany
β-Mercaptoethanol	Sigma-Aldrich GmbH, Steinheim, Germany
Methanol	Merck KGaA, Darmstadt, Germany
Phenol:Chloroform:Isoamyl Alcohol 25:24:1	Sigma-Aldrich GmbH, Steinheim, Germany
Potassium chloride (KCl)	Sigma-Aldrich GmbH, Steinheim, Germany
Potassium dihydrogen phosphate (KH_2PO_4)	Merck KGaA, Darmstadt, Germany
Sodium acetate ($C_2H_3NaO_2$)	Sigma-Aldrich GmbH, Steinheim, Germany
Sodium chloride (NaCl)	Sigma-Aldrich GmbH, Steinheim, Germany
Sodium citrate dihydrate	Merck KGaA, Darmstadt, Germany
Sodium deoxycholate	Sigma-Aldrich GmbH, Steinheim, Germany
Sodium dodecyl sulfate (SDS)	SERVA Electrophoresis GmbH, Heidelberg, Germany
Sodium hydrogen carbonate ($NaHCO_3$)	Fluka GmbH, Neu-Ulm, Germany
Sodium hydroxide (NaOH)	Merck KGaA, Darmstadt, Germany
Sodium phosphate (Na_2HPO_4)	Sigma-Aldrich GmbH, Steinheim, Germany
Sulforhodamine B (SRB), sodium salt	Sigma-Aldrich GmbH, Steinheim, Germany
Trichloroacetic acid (TCA)	Sigma-Aldrich GmbH, Steinheim, Germany
Tris base	Carl Roth GmbH, Karlsruhe, Germany
Triton-X 100	Sigma-Aldrich GmbH, Steinheim, Germany
Trizol Reagent	Invitrogen GmbH, Karlsruhe, Germany
Tween 20	Sigma-Aldrich GmbH, Steinheim, Germany

2.4. Biochemical reagents and commercial available substances

Table 2.4: Biochemical reagents and commercial available substances

Substance	Manufacturer
Agar noble, ultrapure	Affymetrix, Cleveland, USA
Agarose	Peqlab Biotechnologie GmbH, Erlangen, Germany
Bovine Serum Albumin Fraction V (BSA), pH 5.2	Carl Roth GmbH, Karlsruhe, Germany
Cresol red	Sigma-Aldrich GmbH, Steinheim, Germany
Distilled water (DNase/RNase free)	Gibco®, Life Technologies GmbH, Darmstadt, Germany
DNA ladder (1 kb)	Invitrogen™, Life Technologies GmbH, Darmstadt, Germany
DNA loading dye (6x)	Sigma-Aldrich GmbH, Steinheim, Germany
ECL™ Western Blotting Detection Reagent	GE Healthcare GmbH, Munich, Germany
Embedding compound Tissue-Tek® O.C.T.™	Sakura Finetek, Torrance, CA, USA
Ethidium bromide (10 mg/ml)	Sigma-Aldrich GmbH, Steinheim, Germany
Glycogen	Sigma-Aldrich GmbH, Steinheim, Germany
High-Range Rainbow Molecular Weight Marker for SDS-PAGE	GE Healthcare GmbH, Munich, Germany
$MgCl_2$ for PCR	Fermentas GmbH, St. Leon-Rot, Germany
Milk powder	AppliChem GmbH, Darmstadt, Germany
PCR dNTP mix (10 mM each)	Roche Diagnostics, Mannheim, Germany

PreDeveloped TaqMan Assay Reagent Human 18S rRNA	Applied Biosystems®, Life Technologies GmbH, Darmstadt, Germany
Protease inhibitor cocktail tablets	Roche Diagnostics, Mannheim, Germany
Protein Assay (Dye reagent)	Bio-Rad, Munich, Germany
qPCR Master Mix Plus	Eurogentec s.a., Seraing, Belgium
qPCR Master Mix Plus for SYBR® Assay I	Eurogentec s.a., Seraing, Belgium
Recombinant green fluorescent protein (rGFP)	MP Biomedicals, Heidelberg, Germany
Taq buffer with $(NH_4)_2SO_4$	Fermentas GmbH, St. Leon-Rot, Germany
Trypan blue (0.4 %)	Sigma-Aldrich GmbH, Steinheim, Germany
Vectashield mounting medium containing 4´,6´-diamidino-2-phenylindole (DAPI)	Vector Laboratories, Burlingame, CA, USA
Western blot: BupH™ Tris-HEPES-SDS Running Buffer	Thermo Scientific Inc., Rockford, IL, USA

2.5. Prepared buffers and solutions

Table 2.5: Prepared buffers and solutions

Buffer or solution	Composition
CsCl, ρ 1.25 g/cm^3	33.75 g CsCl in 100 ml 10 mM Tris, pH 8.0
CsCl, ρ 1.35 g/cm^3	47.57 g CsCl in 100 ml 10 mM Tris, pH 8.0
Digestion buffer for DNA isolation	100 mM NaCl, 25m M EDTA (pH 8.0), 10 mM Tris (pH 8.0), 0.5 % SDS
GCV	50 mg/ml stock, dissolved in dH_2O
Lysis buffer	250 mM Tris (pH 8.0), 0.1 % Triton X-100
Radio-Immunoprecipitation Assay (RIPA) buffer	50 mM Tris (pH 7.2), 150 mM NaCl, 0.1 % SDS, 0.5 % Na-deoxycholate, 1 % Triton X-100, 1x Protease inhibitor cocktail
TMZ	100 mM stock, dissolved in DMSO
Tris (1 M)	121.1 g Tris base dissolved in 1l dH_2O, pH adjusted with 37 % HCl
PCR master mix	1 x Taq buffer, 1.5 mM $MgCl_2$, 0.4 mM dNTPs, 5 U Taq polymerase
Phosphate Buffered Saline (PBS), 20x	200 mM Na_2HPO_4, 2.8 M NaCl, 36 mM KH_2PO_4, 54 mM KCl (pH 7.4)
PBS^{2+}	1 x PBS, 0.68 mM $CaCl_2$, 0.49 mM $MgCl_2$
PBS/Tween	1 x PBS, 0.05 % Tween 20
Precipitation buffer for DNA isolation I	94 % ethanol, 588 mM $NH_4C_2H_3O_2$
Precipitation buffer for DNA isolation II	97 % ethanol, 300 mM $C_2H_3NaO_2$
SDS-Pronase buffer for DNA isolation	10 mM Tris (pH 7.5), 10 mM EDTA (pH 8.0), 0.5 % SDS, 0.5 mg/ml Pronase
Sodium chloride-sodium citrate buffer (SSC), 20x	3 M NaCl, 0.3 M sodium citrate
SRB staining solution	0.5 % (w/v) SRB in 1 % acetic acid
Tris-acetate-EDTA (TAE) buffer	40 mM Tris (pH 8.0), 1 mM EDTA (pH 8.0), 0.1% acetic acid
Western blot: blocking buffer	5 % (w/v) milk powder, 50 mM Tris (pH 7.5), 150 mM NaCl
Western blot: blotting buffer (10x)	250 mM Tris base, 1.92 M Glycin, 1 % SDS, 20 % Methanol
Western blot: Laemmli buffer (5x)	300 mM Tris (pH 6.8), 1.5 g SDS, 50 % Glycerol, 12.5 %

	β-Mercaptoethanol, 100 mg Bromophenol blue
Immunofluorescence: blocking buffer	1 % BSA (w/v) in 1 x PBS, 0.05 % Tween 20
Southern blot: denaturation solution	0.5 M NaOH, 1.5 M NaCl
Southern blot: neutralisation solution	0.5 M Tris (pH 7.5), 1.5 M NaCl
Southern blot (detection): maleic acid buffer	0.1 M maleic acid, 150 mM NaCl, adjust to pH 7.5 with solid NaOH
Southern blot (detection): detection buffer	0.1 M Tris, 0.1 M NaCl, adjust to pH 9.5 with solid NaOH, 0.3 % Tween 20
Southern blot (detection): washing buffer	0.1 M maleic acid, 150 mM NaCl, adjust to pH 7.5 with solid NaOH
Southern blot: stripping buffer	0.2 M NaOH, 0.1 % SDS

2.6. Kits

Table 2.6: Kits

Kit	Manufacturer
Adeno-X™ Rapid Titer Kit	Clontech Laboratories, Mountain View, CA, USA
DNA Blood and Tissue Kit	Qiagen GmbH, Hilden, Germany
DIG High Prime DNA Labelling and Detection Starter Kit II	Roche Diagnostics, Mannheim, Germany
High Capacity cDNA Reverse Transcription Kit	Applied Biosystems®, Life Technologies GmbH, Darmstadt, Germany
QIAquick Gel Extraction Kit	Qiagen GmbH, Hilden, Germany
Quant-iT™ PicoGreen® dsDNA Assay Kit	Invitrogen™, Life Technologies GmbH, Darmstadt, Germany
XTT Cell Proliferation Kit II	Roche Diagnostics, Mannheim, Germany

2.7. Enzymes

Table 2.7: Enzymes

Enzyme	Manufacturer
Benzonase Nuclease (25 U/µl)	Novagen, San Diego, USA
Pronase	Boehringer, Mannheim, Germany
Proteinase K	Qiagen GmbH, Hilden, Germany
Restriction enzymes	New England Biolabs GmbH, Frankfurt am Main, Germany (*Pvu*I with buffer R^+: Fermentas GmbH, St. Leon-Rot, Germany)
RNase A	Roche Diagnostics, Mannheim, Germany
Taq DNA polymerase	Fermentas GmbH, St. Leon-Rot, Germany

2.8. Antibodies

Table 2.8: Antibodies

Target	Isotype, host	Conjugate	Manufacturer	Application
anti-goat	IgG, donkey	HRP	Santa Cruz Biotechnology, Inc., Heidelberg, Germany	WB
anti-mouse	IgG, goat polyclonal	FITC	Serotec, Oxford, UK	IF
anti-rabbit	IgG-H&L, goat polyclonal	Texas Red	Abcam, Cambridge, UK	IF
Hexon	IgG, mouse		Clontech Laboratories, Mountain View, CA, USA	IF
HSV1-TK	IgG, rabbit polyclonal		Prof. William Summers, Yale University, USA	IF
HSV1-TK (N-terminus) *	IgG, goat polyclonal		Santa Cruz Biotechnology, Inc., Heidelberg, Germany	WB

Abbreviations: Fluorescein isothiocyanate (FITC), Horseradish peroxidase (HRP), Immunofluorescence (IF), Western blot (WB).
* Supplied together with a blocking peptide (0.2 µg/µl; Santa Cruz Biotechnology, Inc., Heidelberg, Germany) for competition studies.

2.9. Primers and oligonucleotide probes

Table 2.9: Primer and probe sequences

Target gene	Sequence	T_m	Application
Adenoviral E1A	fw: 5'-ATG GCC GCC AGT CTT TTG-3' rev: 5'-GCC ATG CAA GTT AAA CAT TAT C-3'	56°C 60°C	PCR
Adenoviral E2	fw: 5'-GGC TGC TCT GCT CGG AAG AC-3' rev: 5'-GTA ATT AAC AAC CGT TCC GAG G-3'	65°C 60°C	PCR
Adenoviral E1A-pIX	fw: 5'-GGG AAA ACT GAA TAA GAG G-3' rev: 5'-AAC GAG TTG GTG CTC ATG G-3'	52.4°C 56.7°C	PCR
Adenoviral E3	fw: 5'-CGA GCT CAG CTA CTC CAT C-3' rev: 5'-GTA ATT AGC ATA GCA GTG CAG C-3'	60°C 64°C	PCR
HSV1-sr39TK	fw: 5'-ATC AAC ACG CGT CTG CGT TCG-3' rev: 5'-TCA GTT AGC CTC CCC CAT CTC-3'	61.8°C 61.8°C	PCR
Adenoviral Fiber 5	fw: 5'-AAG CTA GCC CTG CAA ACA TCA-3' rev: 5'- CCC AAG CTA CCA GTG GCA GTA-3'	59°C 63°C	real-time PCR
HSV1-sr39TK	fw: 5'-GTA CCC GAG CCG ATG ACT TAC T-3' rev: 5'-CCC GGC CGA TAT CTC A-3'	61°C 58°C	real-time PCR
	Probe: 6-FAM – 5'-CTT CCG AGA CAA TCG CGA ACA TCT ACA CC-3' – TAMRA		

All primers applied for Polymerase chain reaction (PCR) analysis and the adenoviral Fiber 5 primers used in real-time PCR analysis were purchased from Metabion International AG, Martinsried, Germany. They were dissolved in dH_2O to obtain a stock concentration of 100 µM. The adenoviral E1A-pIX primers amplify a sequence located between *E1A* and the gene coding for minor capsid protein IX (pIX). The HSV1-TK primers and probe applied for real-time PCR analysis were designed

according to Ebeling et al. [295] and were obtained from Applied Biosystems®, Life Technologies GmbH, Darmstadt, Germany. The primers were diluted in 1 mM Tris-HCl, pH 8.0/0.01 mM EDTA to a stock concentration of 10 µM. The specific HSV1-TK probe, coupled to the 5' reporter dye 6-carboxyfluorescein (FAM) and the 3' quencher dye 6-carboxytertramethylrhodamine (TAMRA), was supplied at a concentration of 100 µM.

2.10. Plasmids

pXC1

pXC1 is a cloning vector that contains the left terminal 16 % of human adenovirus 5 (Ad5) DNA [296]. It was used within this thesis as a positive reference for detection of adenoviral *E1A* in the test of adenovirus preparations for contamination with wild-type adenovirus.

pBHGloxΔE1,3 Cre

The plasmid pBHGloxΔE1,3 Cre is an *E1*- and *E3*-deleted Ad5 backbone vector for adenovirus construction and transgene expression. It contains a *loxP*-site (locus of X-over of P1) and a coding sequence for Cre recombinase (cyclization recombinase), enabling vector construction by means of the Cre-loxP recombination system [297]. pBHGloxΔE1,3 Cre was used within this thesis as a positive reference for detection of adenoviral *E2* region in the test of adenovirus preparations for contamination with wild-type adenovirus.

pBHG10

The *E1*- and *E3*-deleted Ad5 backbone plasmid pBHG10 is used for adenovirus construction by means of homologue recombination [173]. The vector was used within this thesis for the derivation of template-specific DNA hybridisation probe for detection of adenoviral *E2* region.

pDC316sr39TK

The plasmid pDC316sr39TK is a transfer vector used for adenovirus construction containing the transgene *HSV1-sr39TK*. The vector was used within this thesis for the generation of a template-specific DNA hybridisation probe for detection of *HSV1-sr39TK*.

The plasmids pXC1, pBHGloxΔE1,3 Cre and pBHG10 were obtained from Microbix Biosystems, Toronto, Canada. The plasmid pDC316sr39TK was constructed in the laboratory of Dr. Martina Anton, Klinikum rechts der Isar, Munich, Germany.

2.11. Prodrugs, cytostatic drugs and radiolabelled compounds

GCV

GCV (Cymeven®) is a prodrug that is converted by HSV1-TK into the toxic metabolite GCV-triphosphate, which induces cytotoxicity through inhibition of DNA synthesis [61, 62, 64]. GCV was purchased from Hoffmann-La Roche, Grenzach-Wyhlen, Germany and a stock solution was prepared as described in table 2.5.

Daunorubicin

The cytostatic drug daunorubicin (daunoblastin) is a member of the group of anthracyclines. As a DNA intercalator, it inhibits DNA and RNA synthesis [298]. The drug was used within this thesis as a substrate for P-gp in order to maintain the multidrug-resistant phenotype of the cell line EPP85-181RDB. Daunorubicin was purchased from Sigma-Aldrich GmbH, Steinheim, Germany.

TMZ

The cytostatic drug TMZ is a DNA alkylating agent, which exerts its cytostatic effect through formation of a reactive methyldiazonium cation and DNA methylation of guanine at the O^6 position [13, 14]. TMZ was purchased from Sigma-Aldrich GmbH, Steinheim, Germany and a stock solution was prepared as described in table 2.5.

[^{18}F]-FHBG

[^{18}F]-FHBG is a radiolabelled GCV analogue, converted by HSV1-TK into an insoluble metabolite that is trapped within the cell and can be detected by a gamma-counter or a PET system [109]. The radiotracer was synthesised at the Department of Nuclear Medicine, Klinikum rechts der Isar, Munich, Germany [114, 299], yielding [^{18}F]-FHBG at an average specific activity of 33.4 GBq/µmol.

2.12. Cell culture media and supplements

Table 2.10: Cell culture media and supplements

Cell culture medium or supplement	Manufacturer
Eagle's Minimum Essential Medium (MEM) with Earle's salts and 2 mM L-glutamine	Gibco®, Life Technologies GmbH, Darmstadt, Germany
Dulbecco's Modified Eagle's Medium (DMEM)	Biochrom AG, Berlin, Germany
D-glucose	Merck KGaA, Darmstadt, Germany
Fetal bovine serum (FBS)	PAN-Biotech GmbH, Aidenbach, Germany
Fetuin	Sigma-Aldrich GmbH, Steinheim, Germany
Fungizone® Antimycotic	Gibco®, Life Technologies GmbH, Darmstadt, Germany
Horse serum (HS)	Gibco®, Life Technologies GmbH, Darmstadt, Germany
L-alanyl-L-glutamine	Biochrom AG, Berlin, Germany

Leibovitz's L-15 medium	BioWhittaker™, Lonza GmbH, Cologne, Germany
MEM-vitamins, 100x	Biochrom AG, Berlin, Germany
$NaHCO_3$, pH 7.5	Fluka GmbH, Neu-Ulm, Germany
Non-essential amino acids (NEAA)	Gibco®, Life Technologies GmbH, Darmstadt, Germany
Transferrin	Sigma-Aldrich GmbH, Steinheim, Germany
Trasylol	Pharmacy of Klinikum rechts der Isar, Munich, Germany
Trypsin/EDTA (0.25 %/0.02 %)	Biochrom AG, Berlin, Germany
Opti-MEM® I + GlutaMAX™ I	Gibco®, Life Technologies GmbH, Darmstadt, Germany
PBS-Dulbecco, 1x	Biochrom AG, Berlin, Germany
Penicillin/Streptomycin (PS), 100x	Biochrom AG, Berlin, Germany

DMEM was supplemented with 10 % FBS and 2 mM L-glutamine. The culture medium of adenovirus-infected HEK293 cells consisted of DMEM supplemented with 5 % HS and 2 mM L-glutamine. Eagle's MEM with Earle's salts and 2 mM L-glutamine was supplemented with 10 % FBS and 1 % NEAA. U87-MG spheroid growth medium consisted of Eagle's MEM with Earle's salts and 2 mM L-glutamine supplemented with 10 % FBS, 1 % NEAA, 1 % PS, 1 % $NaHCO_3$ (0.22 µm filtered) and 0.25 µg/ml Fungizone®. The L-15 medium was replenished with 10 % FBS, 1 mM L-glutamine, 1 g/l glucose (0.22 µm filtered), 1,1 g/l $NaHCO_3$ (0.22 µm filtered), MEM-vitamins (1x), 6.25 mg/l fetuin, 2.5 mg/l transferrin and 20,000 kIU (Kallikrein Inhibitor Units)/l Trasylol.

2.13. Cell lines

HEK293

The human embryonic kidney (HEK) cell line 293 (Microbix Biosystems, Toronto, Canada) is used for the production and titration of adenoviruses. The HEK293 cells are stably transformed with 4.5 kb of the left end of the Ad5 genome, enabling a transcomplementation of the *E1* region and rendering the cell line permissive for Ad5 infection [300]. In this thesis, all adenoviruses were produced within this cell line. HEK293 cells were maintained in DMEM with supplements.

U87-MG

U87-MG (wt-p53) is a human, epithelial glioblastoma-astrocytoma (grade IV) cell line, derived from malignant glioma of a Caucasian 44-year-old woman and first characterised by J. Ponten [301]. U87-MG (HTB-14) were purchased from American Type Culture Collection (ATCC), Rockville, MD, USA and cultured in Eagle's MEM with Earle's salts and 2 mM L-glutamine with supplements. The cell line is characterised by a high expression level and partial nuclear localisation of YB-1 [290].

EPP85-181RDB

The human pancreatic carcinoma cell line EPP85-181RDB (RDB: resistant to daunoblastin) is characterised by a multidrug-resistant phenotype and was derived as a subclone from the parental, drug-sensitive cell line EPP85-181, established by Hermann Lage [51]. The cell line EPP85-181RDB was kindly provided by PD Dr. Per Sonne Holm, Klinikum rechts der Isar, Munich, Germany and cultured in L-15 medium with supplements. Its classical multidrug-resistant phenotype, conferred by overexpression of MDR1/P-gp, was maintained by addition of 2.5 µg/ml daunorubicin to the culture medium every two weeks [51]. Nuclear distribution of YB-1 had been already verified [288].

2.14. Adenoviruses

Ad-delo3-RGD

The structure of the oncolytic adenovirus Ad-delo3-RGD (chapter 1.9.2.) is partially based on the genome of the Ad5-derived dl520 [293]. In this context, dl520 DNA from *Ssp*BI (Ad5 wild-type position nt193) to *Mun*I (Ad5 wild-type nt3925) was subcloned into the shuttle plasmid of the AdEasy system (Qbiogene). This fragment carries an 11 bp deletion in the CR3 region of the *E1A* gene, resulting in lack of expression of the transactivating 289 aa protein by the *E1A13S* splice variant. Ad-delo3-RGD contains also a partial deletion of *E1B19K* due to restriction with *Eco*NI (Ad5 wild-type position nt1715) and *Bst*EII (Ad5 wild-type position nt1916), which abrogates E1B19K expression. The open reading frame of *E1B55K* has not been affected. The vector carries also a deletion of the *E3* region. Ad-delo3-RGD as well as the following oncolytic vectors were derived by homologous recombination with a RGD-modified [197] AdEasy backbone [291]. All oncolytic vectors were constructed and kindly provided by PD Dr. Per S. Holm and Klaus Mantwill, Klinikum rechts der Isar, Munich, Germany (figure 2.1).

Ad-delo-sr39TK-RGD

The Ad5-based, oncolytic adenovirus Ad-delo-sr39TK-RGD (Ad-delo2-sr39TK-RGD) contains the same deletions of *E1A13S* and *E1B19K* as Ad-delo3-RGD. However, the *ADP* gene was retained and the transgene *HSV1*-sr39TK, controlled by a human cytomegalovirus (CMV) promoter and a simian virus 40-polyadenylation (SV40-poly(A)) recognition sequence, was inserted into the otherwise deleted *E3* region of the RGD-modified backbone of Ad-delo-sr39TK-RGD (figure 2.1).

Ad-delo-shMGMT-RGD

Ad-delo-shMGMT-RGD is an Ad5-based oncolytic vector containing the same deletion of *E1A13S* as Ad-delo3-RGD and Ad-delo-sr39TK-RGD, but without ablation of the *E1B19K* gene. The partially deleted *E3* region expresses a short hairpin RNA (shRNA) insert, which is processed into a small

interfering RNA (siRNA) sequence against the cellular *MGMT* gene, and contains also the *ADP* gene and the RGD motif (figure 2.1).

Ad-sr39TK

Ad-sr39TK is a replication-deficient, *E1*- and *E3*-deleted adenovirus. The vector was derived by homologous recombination of a transfer vector, containing the human CMV promoter-controlled transgene *HSV1-sr39TK* together with a SV40-poly(A) recognition sequence, with an adenoviral packaging plasmid [113]. The transgene was thereby inserted into the deleted *E1* region of the packaging plasmid. Ad-sr39TK was kindly provided by Prof. Dr. Sanjiv S. Gambhir, University of California School of Medicine, Los Angeles, CA, USA (figure 2.1).

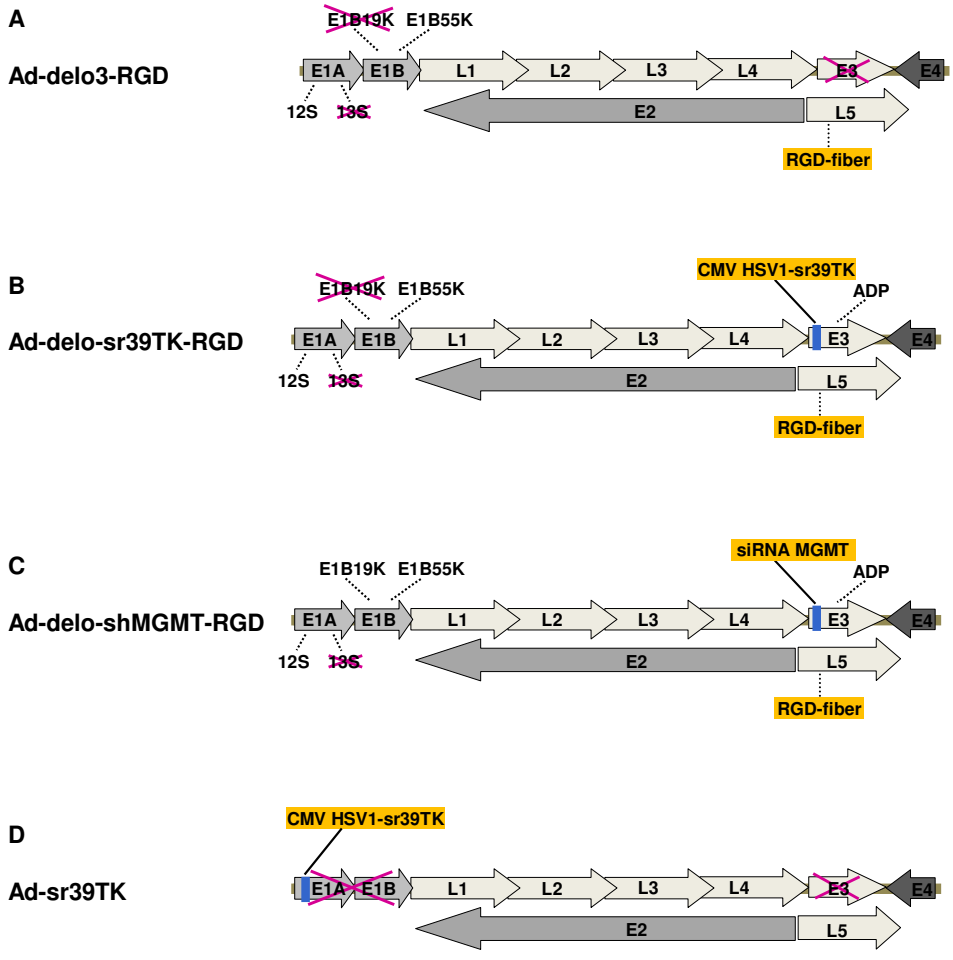

Figure 2.1: Structure of YB-1 dependent oncolytic adenoviruses and of HSV1-sr39TK-armed replication-deficient adenovirus. Mutations of the oncolytic vectors Ad-delo3-RGD (A), Ad-delo-sr39TK-RGD (B) and Ad-delo-shMGMT-RGD (C), as well as of the replication-deficient vector Ad-sr39TK (D) are described in detail in chapter 2.14. Blue bars indicate insertions.

Ad5-wt

Ad5-wt (wild-type) denotes the wild-type adenovirus of serotype 5. Ad5-wt DNA was applied as a reference for the verification of the genetic structure of the oncolytic adenoviruses and was kindly provided by Klaus Mantwill, Klinikum rechts der Isar, Munich, Germany.

Ad-mCMVeGFP

The replication-deficient, *E1*- and *E3*-deleted adenovirus contains the murine CMV (mCMV) promoter-controlled transgene enhanced green fluorescent protein (*eGFP*) inserted into the deleted *E3* region. Ad-mCMVeGFP was produced by Cre-loxP recombination of a transgene-containing transfer vector with the adenoviral packaging vector pBHGlox. The virus was applied as an indicator of adenoviral infectivity of U87-MG-derived spheroids. The vector was constructed in the laboratory of Dr. Martina Anton, Klinikum rechts der Isar, Munich, Germany.

2.15. Software and databases

Table 2.11: Software and databases

Software or database	Application	Company or URL
EndNote	citation management	Thomson Reuters, New York City, NY, USA
GraphPad Prism	data analysis, statistics	GraphPad Software, San Diego, CA, USA
Image J	image processing	National Institutes of Health, Bethesda, MD, USA
INVEON Acquisition and Research Workplace	PET data analysis	Siemens Healthcare, Erlangen, Germany
Microsoft Office	word processing, data analysis	Microsoft GmbH, Unterschleißheim, Germany
National Center for Biotechnology Information (NCBI)	literature, gene and protein database	http://www.ncbi.nlm.nih.gov
SDS2.2	real-time PCR analysis	Life Technologies GmbH, Darmstadt, Germany
Universal Protein Resource Knowledgebase (UniProtKB)	protein database	http://www.uniprot.org
VectorNTI	gene sequence analysis	Life Technologies GmbH, Darmstadt, Germany

3. METHODS

3.1. Cell culture

3.1.1. 2D monolayer cell culture

All cell lines were cultured in appropriate culture medium at 37°C in a humidified atmosphere containing 5 % CO_2. The cells were passaged, when reaching 70-80 % confluence, by detaching the cell monolayer with Trypsin and resuspending it in fresh culture medium. When used for experiments, the number of living cells for plating was determined by a Neubauer cell counting chamber and the total number of living cells was calculated according to following equation: average number of cells per one large square x 10^4 x dilution factor = cell number per ml. To exclude dead cells from counting, the cell suspension was stained in a 1:1 ratio with Trypan blue. The anionic diazo dye of Trypan blue passes through the leaky membranes of non-living cells and is microscopically visible after accumulation within the cell lumen. Dead cells can thus be excluded from counting.

For freezing, cells were detached as described above, centrifuged at 1200 rpm for 3 min at room temperature (RT) and resuspended in 90 % FBS and 10 % DMSO per 1-2 x 10^6 cells. The cell suspension was immediately frozen in an isopropyl alcohol containing freezing container at -80°C and was transferred to the vapour phase of liquid nitrogen for long-term storage after 24 h. Cryo-conserved cells were thawed in a 37°C water bath and immediately transferred into fresh culture medium. When the cells had attached to the culture dish, the medium was changed to remove traces of DMSO and the cells were cultured as described above.

3.1.2. 3D spheroid cell culture

Spheroids of U87-MG cells were cultured at 37°C in a humidified atmosphere containing 5 % CO_2 and were established as described by Leske et al. [302]. Accordingly, 4000 cells per well were dissociated and seeded into wells of a 96-well plate coated with 60 µl of 1 % noble agar dissolved in PBS, using the appropriate culture medium. Spheroids formed within 24 h and were allowed to grow for three days, before performing experiments. For long-term cultivation of spheroids, culture medium was changed three times a week. Spheroid diameter was measured with an inverted microscope and their volumes were calculated using the equation $V = \frac{4}{3}\pi r^3$. The migration of cells from spheroids, formed as described above and attached to an uncoated well of a 24-well plate, was microscopically monitored 24 h to 7 days after attachment. Migration distance was measured using transmitted light microscopy.

3.2. Adenovirus amplification and purification

All infections of HEK293 cells with adenoviruses during the adenoviral amplification process were performed as described in chapter 3.4. When first signs of c.p.e. of the assembled adenoviruses occurred, cell supernatants containing released viral particles were collected and several small-scale viral amplification steps were performed. During all expansion steps, adenoviruses were released from the producer cells by three freezing and thawing steps of the virus-containing supernatant or cell suspension. After an expansion step in 8 x 15 cm culture dishes of HEK293 cells, the scraped cells were harvested about 48 h post infection by centrifugation at 2700 rpm and RT for 20 min and the pellet was resuspended in 6-10 ml PBS^{2+} (table 2.5). The viral titre was determined by End-point dilution assay as described in chapter 3.3.2. This suspension, so called “crude stock”, was applied for large-scale adenovirus expansion. For expansion to a large format prior to adenovirus purification, 20-30 x 15 cm culture dishes of HEK293 cells were infected with the “crude stock” at a multiplicity of infection (MOI) of 10 (pfu/cell, see chapter 3.3.2). When c.p.e. was almost complete, usually after about 48 h, the cells were harvested by centrifugation at 2700 rpm and RT for 20 min and the pellet was resuspended in 10-15 ml of 0.1 M Tris, pH 8.0. To separate the viral particles from the cell debris, the suspension was centrifuged for 10 min at 2000 rpm and RT and once again in an ultracentrifuge for 15 min at 8000 rpm and RT. The supernatant was incubated with 200 units of Benzonase Nuclease for 45 min, in order to degrade remaining cellular nucleic acids. The adenoviruses were then purified by two subsequent CsCl step-gradient centrifugations at 30,000 rpm and 10 °C. The first gradient consisted of CsCl (ρ 1.35 g/cm^3), overlaid with CsCl (ρ 1.25 g/cm^3). The viral suspension was applied on top of the gradient and centrifuged for 3 h. The viral band from the first step-gradient was then added to a second gradient, consisting of CsCl with a density of 1.35 g/cm^3 and centrifuged for 16-24 h. Afterwards, the virus was pooled from the ultracentrifuge tube with a syringe and a needle, and purified by three consecutive dialysis steps against PBS in a Slide-A-Lyzer® dialysis cassette. The purified virus was stored in PBS^{2+} supplemented with 10 % glycerol at -80 °C.

3.3. Determination of viral titre

3.3.1. Infectious units

The number of infectious units (ifu) per ml of adenoviral preparations was determined in HEK293 cells by Adeno-X^{TM} Rapid Titer Kit according to manufacturer's instructions.

3.3.2. Plaque forming units

Adenoviral particles cause c.p.e. in infected cells, which results in detachment of the adherent cell layer and formation of clear spots, so called "plaques". The number of viral plaque forming units (pfu) per ml was determined by End-point dilution assay, according to Clontech's titration protocol based on the Spearman-Karber method (Clontech Laboratories, USA). To perform the titration, HEK293 cells were seeded into a 96-well plate and infected with serial dilutions of the virus solution, either in form of CsCl-purified stocks, "crude stocks" or supernatants of infected U87-MG cells or spheroids containing released viral particles. The infected HEK293 cells were incubated in a humidified atmosphere for 10 days at 37°C. The fraction of c.p.e.-positive wells for each of the serial dilutions was determined and viral titre (pfu/ml) was calculated according to the following formula:

Titre (pfu/ml) = $10^{(x + 0.8)}$

x = the sum of the fractions of c.p.e.-positive wells

3.3.3. Viral particle number and aggregate formation

The amount of viral particles (VP) was determined by optical densitometry. The virus stock was diluted 1:20 in a 0.1 % SDS solution in order to inactivate the functional virus and the optical density (OD) in nm was measured by a spectrometer. The amount of VP/ml was calculated according to OD_{260} x 1.1 x 10^{12} VP/ml [303]. An OD_{260}/OD_{280} ratio about 1.4 indicated optimal purity.

To test adenoviruses for aggregation, viral solutions were diluted 1:50 in CsCl (ρ 1.35 g/cm^3) prior to desalting in a dialysis cassette and OD_{260}, OD_{320} and OD_{340} were determined. Ratios of OD_{320}/OD_{260} and OD_{340}/OD_{260} below 0.26 ensured that the viral stock was not aggregated.

According to the above described measurements, the adenoviral stocks applied in this thesis had an optimal purity and were not aggregated.

3.4. Adenovirus infections

The total MOI for all infections, referred to as either ifu or pfu, was derived by multiplication of the required MOI (ifu/cell or pfu/cell) with the cell number to be infected.

3.4.1. 2D cell culture

Infections of HEK293 cells were performed by diluting the virus at the required MOI (pfu/cell) in PBS^{2+} and applying the viral solution onto the cell monolayer. After incubation in a humidified atmosphere at 37°C for 30 min, HEK293 culture medium for infections was added to the cells. U87-MG and EPP85-181RDB cells were infected with viruses at the required MOI (ifu/ml) in Opti-MEM® I + GlutaMAX™ I. U87-MG and EPP85-181RDB cells were incubated for 30 min and 1 h at 37°C, respectively, and cultured subsequently in growth medium for a period of time dependent on experiment. Morphological changes of the cells and the occurrence of c.p.e. was monitored by transmitted-light microscopy.

3.4.2. 3D spheroid culture

3.4.2.1. Infection

U87-MG-derived spheroids with a volume of 0.1-0.18 mm^3 were infected three days after formation in 50 µl Opti-MEM® I + GlutaMAX™ I for 30 min in a humidified atmosphere at 37°C without removing the spheroids from the coated wells and cultured in growth medium for a period of time, dependent on experiment. The cell number per spheroid was extrapolated from a spheroid growth curve with known initial number of cells and the MOI (ifu/cell) per spheroid was calculated accordingly. Spheroid growth was monitored at different time points and their volume was calculated as described in chapter 3.1.2.

3.4.2.2. Determination of infectivity

The infectivity of spheroids was explored by infections with Ad-mCMVeGFP at different MOIs (pfu/cell) as described above. The fluorescent signal intensity of eGFP was detected microscopically. In addition, spheroids were digested with 10 µl lysis buffer (table 2.5) for 15 min at RT. The lysates were used to quantify the fluorescent signal according to a standard consisting of serial dilutions with known concentrations of rGFP. The protein amount in the spheroid samples was determined by Bio-Rad Protein Assay as described in chapter 3.12.2. The fluorescent signal intensity of eGFP was measured in a black 96-well plate using a multilabel counter with excitation at 485 nm and emission at 535 nm wavelength. The amount of eGFP in the samples was calculated by extrapolation from the standard curve and normalised to the protein amount.

3.5. DNA isolation

3.5.1. Viral DNA isolation

DNA from purified virus stocks was isolated by phenol-chloroform extraction. 200 µl digestion buffer (table 2.5) was added to 10 µl of the virus together with 0.6 mAU (milli-arbitrary unit) proteinase K to degrade the viral capsid. After incubation for 1 h at 50°C, equal volume of phenol-chloroform-isoamyl alcohol was added to the suspension and centrifuged for 15 min at 14,000 rpm and 4°C. An equal volume of chloroform was added together with cresol red to the upper, aqueous phase containing the DNA for removal of phenol residuals and centrifuged again. The DNA from the aqueous phase was precipitated by addition of the 4.25-fold volume of precipitation buffer I (table 2.5) with 35 µg/ml of glycogen as a DNA carrier and collected by centrifugation for 30 min at 14,000 rpm and 4°C. The DNA pellet was washed from remaining salts with 70 % ethanol, air dried and resuspended in dH_2O. DNA concentration was determined by Quant-iT™ PicoGreen® dsDNA Assay Kit as described in chapter 3.7.2.

3.5.2. Extraction of cellular DNA

In order to perform adenoviral replication analysis by Southern blot or by real-time quantitative PCR, infected U87-MG or EPP85-181RDB cells were lysed over night at 37°C by 500 µl SDS-Pronase buffer (table 2.5) for DNA extraction. The cell lysates were then mixed with an equal volume of phenol-chloroform-isoamyl alcohol and centrifuged for 15 min at 15°C and 14,000 rpm. The DNA from the aqueous phase was precipitated by addition of precipitation buffer II (table 2.5) and mixing by inversion until a visible DNA filament was formed. After three washing steps with 70 % ethanol, the DNA was air dried and resuspended in dH_2O. The DNA concentration was determined by optical densitometry as described in chapter 3.7.1.

3.6. RNA isolation and reverse transcription

3.6.1. Isolation of cellular RNA

For RNA isolation infected U87-MG or EPP85-181RDB cells were lysed by incubation for 5 min with 1 ml Trizol reagent/1 x 10^6 cells. 200 µl chloroform per ml Trizol was then applied to the cell lysates, mixed well and centrifuged for 15 min at 13,000 rpm and 4°C. The RNA from the upper aqueous phase was precipitated by addition of one volume of isopropyl alcohol and, after an incubation step, centrifugation for 10 min at 13,000 rpm and 4°C. The RNA pellet was washed out from residual salts with 80 % ethanol, centrifuged for 5 min at 7600 rpm and 4°C and air dried. The pellet was finally resuspended in nuclease-free water, followed by denaturation of the RNA at 65°C for 10 min. The RNA concentration was determined by optical densitometry. The integrity of RNA was verified by

electrophoretic separation in a 1 % agarose gel as described in chapter 3.8. Extracted RNA was stored at -80°C.

3.6.2. Reverse transcription from RNA into cDNA

The reverse transcription of RNA into complementary DNA (cDNA) was performed using the High capacity cDNA reverse transcription kit according to manufacturer's instructions. 1 µg RNA per reaction was reverse transcribed in a thermal cycler (PTC-100™). The cDNA was stored at -20°C.

3.7. Determination of DNA and RNA concentration

3.7.1. Measurement of optical density

DNA and RNA concentration was determined by optical densitometry of OD_{260}/OD_{280} in a spectrophotometer. Provided that the path length of light, passing through a sample, is 1 cm, an OD_{260} of 1.0 corresponds to a concentration of 50 µg/ml for double-stranded (ds)DNA or 40 µg/ml for single-stranded (ss)RNA according to the Beer-Lambert law. Thus, the concentration was calculated as follows:

dsDNA (µg/ml): 50 µg/ml × OD_{260} × dilution factor

ssRNA (µg/ml): 40 µg/ml × OD_{260} × dilution factor

An OD_{260}/OD_{280} ratio of about 1.8 for DNA and of 1.8-2 for RNA is indicative for maximal purity.

3.7.2. PicoGreen assay for DNA quantification

In case of low DNA yield the concentration of DNA was determined using Quant-iT™ PicoGreen® dsDNA Assay Kit. The DNA was labelled by the fluorescent nucleic acid stain PicoGreen and fluorescence was measured at 538 nm after excitation at 485 nm in a multilabel counter. The DNA amount was quantified by means of a standard curve with bacteriophage λ-DNA (provided by the kit), treated as the unknown samples.

3.8. Agarose gel electrophoresis

DNA and RNA fragments were subjected to electrophoretic gel separation in order to determine the length of DNA fragments, to isolate DNA fragments of interest or to analyse the integrity of RNA. The agarose gels were prepared by melting of 1 % or, when large fragments were analysed, 0.8 % agarose in 1 x TAE. Prior to polymerisation, 0.5 µg/ml of ethidium bromide was added to the gel. DNA or RNA reactions were mixed in a ratio of 1:6 with 6 x DNA loading dye and loaded next to a DNA ladder on the gel. Electrophoresis was run in gel units with power supply at 90 V or at 20-30 V depending on experiment. Because of the intercalation with ethidium bromide, the DNA emits visible light after

excitation with UV light at 366 nm and the DNA fragments can be visualised in an UV gel documentation system or transilluminator.

3.9. Southern blot

Southern blot is a method for transferring electrophoretic separated DNA fragments from a gel to a solid support in order to detect a gene or DNA region of interest with a specific fluorescent or radiolabelled DNA probe. The probe hybridises to the complementary DNA fragments and can be visualised in a chemiluminescent or autoradiographic reaction [304].

In order to perform adenoviral replication analysis by Southern blot, DNA from infected and/or GCV-treated U87-MG cells was extracted as described in chapter 3.5.2. 1 µg DNA was digested with 10 U *Pvu*I in a 20 µl reaction mix of 1 x buffer R^+ and 10 µg RNase A for 90 min at 37°C. The restriction was terminated by incubation of the reaction for 5 min at RT with 5 µg pronase. DNA fragments, which were in a range from 1.67 to 13.81 kb depending on virus, were obtained by electrophoretic separation on a 0.8 % agarose gel over night at 20-30 V. The separated DNA fragments on the gel were then exposed to 250 mM HCl for 10-20 min, followed by incubation in denaturation solution and subsequently in neutralisation solution (table 2.5) for 2 x 15 min, each. The exposal to weak acid results in partial depurination of the DNA and the strong base in the denaturation solution hydrolyses the phosphodiester backbone at the sites of depurination. The resulting about 1 kb fragments can then be transferred from the gel with high efficiency [305]. The DNA fragments were blotted onto a GeneScreen Hybridisation Transfer Membrane by capillary transfer overnight at RT. 20 x SSC was used to elute the DNA from the gel and a weight on top of the transfer system was applied to ensure tight connection between the layers of material used within it. The DNA was immobilised on the membrane by UV irradiation at 120 mJ in a Cross-linker.

Probe generation, hybridisation of template DNA with specific DNA probes and signal detection were performed according to DIG High Prime DNA Labelling and Detection Starter Kit II. To generate a complementary DNA probe for the detection of a template in the *E2* region, a 1669 bp fragment was obtained by *Pvu*I-restriction (nt6149/nt7818) of the adenoviral backbone plasmid pBHG10. A specific 1146 bp probe for detection of the *HSV1-sr39TK* gene was derived by restriction of the shuttle plasmid pDC316sr39TK with *Eco*RI (nt993) and *Hind*III (nt2139). Both probes were purified using QIAquick Gel Extraction Kit and their concentration was determined by Quant-iT™ PicoGreen® dsDNA Assay Kit (chapter 3.7.2). The probes were labelled with the steroid hapten digoxigenin (DIG) coupled to 2´-deoxyuridine 5´-triphosphate (dUTP). The optimal hybridisation temperature of the probes was based on their melting temperature (T_m) and was calculated following the

manufacturer's instructions. The labelling efficiency of the probes was determined in a preliminary experiment to be sufficient to label 1-3 pg/µl of template DNA.

After hybridisation of the template DNA with its complementary DNA probes, signals were detected in a chemiluminescent reaction at 477 nm by a Kodak image station. All buffers used within the kit for immunological detection are listed in table 2.5. If it was necessary for the DNA blot to be re-probed, the first DNA probe was removed by washing the transfer membrane in Stripping buffer (table 2.5), following the manufacturer's instructions of the DIG High Prime kit. The template DNA was hybridised with a second DIG-labelled DNA probe and detected as described above.

3.10. Polymerase chain reaction

PCR analysis of adenoviral DNA as a control to exclude an unintentional contamination with wild-type adenovirus was performed using PCR master mix (table 2.5), 0.2 µM of each forward and reverse *E1A*- and *E2*-specific primers (table 2.9) and 50 ng adenoviral template DNA, isolated as described in chapter 3.5.1, in a total reaction volume of 50 µl. The plasmids pXC1 and pBHGlox were used as positive amplification controls for *E1A* and *E2*, respectively. DNA was amplified on a thermal cycler according to table 3.1. PCR analysis for verification of the genetic modifications of the adenoviral vectors was performed as described above with 0.2 µM of each forward and reverse *E1A-pIX*-, *E3*- and *HSV1-sr39TK*-specific primers (table 2.9). Amplifications were carried out on a thermal cycler as described in table 3.1.

Table 3.1: PCR cycling conditions

Target / PCR step	Adenoviral E1A/E2	Adenoviral E1A-pIX/E3	HSV1-sr39TK
Initial denaturation	94 °C 2 min 1x	94 °C 2 min 1x	94 °C 2 min 1x
Denaturation	94 °C 45 sec 35x	94 °C 45 sec 30x	94 °C 45 sec 35x
Annealing	57 °C 45 sec 35x	50 °C 45 sec 30x	57 °C 45 sec 35x
Extension	72 °C 1 min 35x	72 °C 5 min 30x	72 °C 1 min 35x
Final extension	72 °C 10 min 1x	72 °C 10 min 1x	72 °C 10 min 1x

The length of the PCR products was determined by electrophoretic separation on a 1 % agarose gel at 90 V as described in chapter 3.8.

3.11. Real-time quantitative PCR analysis

Real-time quantitative PCR (qPCR) is a method for monitoring the amplification throughout the PCR process in real time and provides a powerful tool to quantify gene replication or expression. The quantity of PCR products correlates with the time point when the target amplification is first detected. This value is defined as cycle threshold (C_t), the cycle in which the fluorescence intensity of the target is greater than background fluorescence. The greater the quantity of initial target DNA, the faster a fluorescent signal exceeds the background level, resulting in a lower C_t [306].

Two real-time qPCR data analysis types can be discriminated: absolute and relative quantification. Absolute quantification is used to determine the input copy number of a sample, interpolating it from a standard curve. The standard curve enables a linear correlation between C_t and initial amount of nucleic acids, allowing quantification of unknown samples based on their C_t values [306]. Relative quantification is applied to determine changes in gene expression of a target sample in relation to a reference (calibrator). Target gene expression is normalised to an endogenous control, usually a housekeeping gene or ribosomal RNA (rRNA). In this thesis, relative gene expression was calculated by the comparative C_t ($2^{-\Delta\Delta Ct}$) method, which determines changes in gene expression as a relative fold difference between a target and reference sample [307].

Real-time qPCR can be performed with different detection chemistries, as SYBR green dye or TaqMan® hydrolysis probes. The fluorescent cyanine dye SYBR green binds to the minor groove of dsDNA and emits fluorescence at 524 nm [308]. Thus, increase of fluorescence intensity correlates directly with dsDNA accumulation. The group of TaqMan® probes comprises sequence-specific oligonucleotides containing a fluorescent reporter dye on the 5´ end and a quencher dye on the 3´ end [306]. The quencher dye reduces the fluorescence emitted by the reporter dye by fluorescence resonance energy transfer [309], when the probe is intact. When annealed to the target sequence, the probe is cleaved by the 5´ exonuclease activity of *Thermus aquaticus* (Taq) DNA polymerase during the extension step of the PCR, the quencher is separated from the reporter and fluorescence emission increases [306, 310].

3.11.1. Absolute DNA quantification

In order to perform absolute quantification of *Fiber 5* and *HSV1-sr39TK* genes, a standard of known copy number was generated by extraction of DNA from a highly concentrated purified Ad-delo-sr39TK-RGD-stock using DNeasy Blood and Tissue Kit according to manufacturer's instruction. The copy number of the DNA per µl was calculated by means of its concentration and molecular weight and serial dilutions were prepared in order to derive a standard curve. Each standard dilution was mixed with 5 ng of genomic (U87-MG) DNA to mimic an "in vivo" adenoviral infection. DNA from infected cells was isolated (chapter 3.5.2) and DNA concentration was determined as described in

chapter 3.7.1. DNA from 100 µl of virus-containing cellular supernatants was extracted according to DNeasy Blood and Tissue Kit and the DNA concentration was determined by Quant-iT™ PicoGreen® dsDNA Assay Kit (chapter 3.7.2). The absolute qPCR of *Fiber 5* was performed using 12.5 µl of the qPCR Master Mix Plus for SYBR® Assay per reaction, 0.4 µM of each specific forward and reverse primers (table 2.9) and 2-2.5 ng of template DNA in a total reaction volume of 25 µl. The absolute qPCR of *HSV1-sr39TK* was performed with 12.5 µl of qPCR Master Mix Plus, 300 nM of each primer, 200 nM of the probe (table 2.9) and 5 ng of template DNA in a total reaction volume of 25 µl. The template DNA was amplified in a real-time PCR sequence detection system according to the cycling conditions listed in table 3.2 and table 3.3. The amount of gene copies was calculated by means of the standard curve using SDS 2.2 software.

Table 3.2: Real-time qPCR cycling conditions for SYBR® Green assay

	Stage	Temperature (°C)	Time	Cycles
1.	Initial denaturation	95	15 min	1
2.	Denaturation	95	15 sec	40
	Annealing	58	15 sec	40
	Extension	72	15 sec	40
3.	Dissociation (melting curve analysis)	95	15 sec	1
		60	15 sec	1
		95	15 sec	1

Table 3.3: Real-time qPCR cycling conditions for TaqMan® assay

	Stage	Temperature (°C)	Time	Cycles
1.	Initial denaturation	50	2 min	1
2.	Denaturation	95	10 min	1
3.	Annealing	95	15 sec	40
	Extension	60	1 min	40

3.11.2. Relative mRNA quantification

For the relative quantification of HSV1-sr39TK mRNA expression, total RNA was isolated from infected U87-MG or EPP85-181RDB cells (chapter 3.6.1) and reverse transcribed into cDNA (chapter 3.6.2). The qPCR was performed with master mix, primers and probe as described in chapter 3.11.1, using 5 ng of cDNA per reaction. cDNA from uninfected cells served as a reference. The transgene expression was normalised to the expression of the endogenous control 18S rRNA, which was detected in parallel using PreDeveloped TaqMan Assay Reagent Human 18S rRNA in 1 ng cDNA per reaction. The amplification was performed according to table 3.3.

3.12. Protein analysis

3.12.1. Extraction of cellular proteins

For analysis of HSV1-sr39TK protein expression, infected and/or GCV-treated U87-MG or EPP85-181RDB cells were harvested by centrifugation at 2700 rpm for 10 min, when cells infected with oncolytic adenoviruses showed indication of c.p.e. After two washing steps with 1 x PBS, cells were lysed in 500 µl/1 x 10^6 cells ice-cold RIPA buffer (table 2.5) for 30 min on ice. DNA was removed from the lysates by centrifugation for 30 min at 10,000 rpm and 4°C. Supernatants containing the extracted cellular and viral proteins were stored at -80°C.

3.12.2. Protein quantification

Protein concentration was quantified by the Bio-Rad Protein Assay, which is based on the method of Bradford [311]. Accordingly, the absorbance maximum for an acidic solution of Coomassie® Brilliant Blue G-250 dye, included in the dye reagent, shifts from 465 nm to 595 nm when forming complexes with proteins. For quantification, protein standard consisting of BSA (stock solution 1.45 mg/ml in 20 % RIPA buffer) was prepared by serial dilutions. The protein sample and the standard dilutions were mixed 1:4 with dye reagent and incubated for 20 min. The absorbance at 590 nm was measured in a multilabel counter and protein concentration was calculated according to the standard curve.

3.12.3. TCA precipitation

Samples containing a low protein amount, mostly because of c.p.e., were concentrated by TCA precipitation. For this purpose, protein extracts were treated with ¼-fold volume of 50 % ice-cold TCA and incubated for 15 min on ice. After centrifugation for 15 min at 14,000 rpm and 2°C, the pellets were resuspended in 500 µl ice-cold acetone to remove residual TCA and centrifuged again for 15 min at 2°C and 14,000 rpm. Pellets were vacuum-dried in a concentrator and resuspended in 5 x Laemmli buffer (table 2.5).

3.12.4. SDS-polyacrylamide gel electrophoresis and Western blot

SDS-polyacrylamide gel electrophoresis (SDS-PAGE) is applied in order to separate proteins according to their size, using SDS as a detergent [312]. SDS acts as an anionic, denaturing detergent that binds to proteins directly proportional to their molecular weight and enables their motility in an electric field through its negative charge.

Prior to subjecting proteins to SDS-PAGE, precipitated and in Laemmli buffer diluted samples were boiled at 95°C for 5 min to further denature the proteins by breaking up secondary and tertiary structures. 150 µg of the protein samples were loaded together with a molecular weight marker on 10 % polyacryamid gels and separated according to their size by electrophoresis at 25 mA per gel, using BupH™ Tris-HEPES-SDS Running Buffer (table 2.4).

Proteins were then blotted onto a PVDF membrane by electrophoretic transfer in a transfer unit filled with blotting buffer (table 2.5) for 1 h at 400 mA. The membrane was blocked to avoid unspecific antibody binding by incubation in blocking buffer (table 2.5) for 30 min at RT. The primary antibody against HSV1-TK (table 2.8) was diluted 1:1000 in blocking buffer and incubated for overnight at 4°C onto the membrane. In a parallel reaction, the primary antibody (1:1000) was incubated with 1 µg/ml of a blocking peptide (table 2.8) against the HSV1-TK-specific antibody for 30 min at RT to test the specificity of the antibody. The antibody-blocking peptide complex was then applied to a protein sample on the membrane and incubated overnight at 4°C. The antibody that is neutralised by the blocking peptide is no longer able to bind to the epitope of its target protein and thus no signal is detected. After three washing steps with PBS/Tween (table 2.5) for 10 min, a 1:3000 dilution of the secondary antibody (table 2.8) in blocking buffer was applied for 1 h at RT. Following four washing steps of 15 min with PBS/Tween and one with PBS, protein detection was performed using the ECL™ ("Enhanced Chemiluminescence") detection reagent. The enzyme HRP coupled to the secondary antibody catalyses the oxidation of luminol and generates chemiluminescence at 425 nm wavelength. Signals were detected by an image station. Mean intensity was quantified using Image J software.

3.13. Cytotoxicity assays

3.13.1. SRB staining

In order to quantify c.p.e., HSV1-sr39TK/GCV-mediated cytotoxicity or the combined cell killing effect of adenoviral infection, TMZ and the HSV1-sr39TK/GCV-system, cell staining with SRB was performed [313]. SRB is a fluorescent aminoxanthene dye that binds to basic amino acid residues of cellular proteins under mild acetic conditions. Hence, SRB staining enables quantification of cell survival after treatment. The remaining adherent cells were first fixed in 10 % cold TCA solution (50 µl/well, 96-well plate) overnight at 4°C. After rinsing of TCA by five washing steps with distilled water, cells were stained by SRB staining solution (table 2.5; 50 µl/well, 96-well plate) for 10 min at RT. Subsequently, the dye was removed by five times washing with 1 % acetic acid and the stained cells were air dried. In addition, images of SRB-stained cells were taken. To quantify cell survival, dried SRB dye was dissolved in 10 mM non-buffered Tris (100 µl/well, 96-well plate) for 1 h and the OD at 590 nm was measured in a multilabel counter.

3.13.2. XTT assay

Metabolic activity of cells or U87-MG-derived spheroids, subjected to viral infections or GCV and TMZ treatment, was verified using the XTT Cell Proliferation Kit II according to the manufacturer's instructions. Briefly, cells or spheroids were incubated in growth medium with XTT solution for 4-24

h. The solution contains the yellow tetrazolium salt XTT that is cleaved by metabolically active cells to form an orange formazan dye [314, 315]. As this conversion occurs only in viable cells, the amount of orange formazan formed correlates with the increase in viability and can be quantified spectrometrically in a multilabel counter at absorbance of 490 nm with background correction at 630 nm. The number of viable cells in 2D monolayer culture was determined by means of an equally treated standard curve, consisting of serial dilutions with known cell number.

In contrary to SRB staining, the XTT assay enables the quantification of metabolically active cells, whereas SRB detects intact cells, regardless of functional metabolism.

3.14. Preparation of cryosections and immunofluorescence staining

For immunofluorescence analysis of adenoviral distribution, infected and drug-treated U87-MG-derived spheroids were fixed 48 h post infection in acetone/methanol (1:1) for 20 min at -20°C and embedded in Cryo Tissue Tek medium for cryosectioning. Cryosections of 14 µm thickness were generated using a cryostat microtome and mounted onto microscope slides. Prior to immunostaining, frozen sections at -20°C were warmed to RT and fixed for permeabilisation of cells in acetone/methanol (1:1) for 10 min at RT. After washing with 1 x cold PBS, unspecific antibody binding was avoided by incubation of the sections in blocking buffer (table 2.5) for 30 min RT. The slides were washed once with PBS/Tween (table 2.5) and incubated simultaneously with 1:1000 dilutions of the primary anti-Hexon or anti-HSV1-TK antibodies (table 2.8) overnight at 4°C. After three times rinsing with 1 x PBS, the sections were treated with 1:50 dilutions of the corresponding FITC- and Texas Red-coupled secondary antibodies (table 2.8) for 1 h at RT. After three times rinsing with 1 x PBS, the sections were air dried and mounted in Vectashield mounting medium containing DAPI. Fluorescent signals were analysed on a Nikon Eclipse fluorescence microscope.

3.15. [^{18}F]-FHBG radiotracer uptake

The radiotracer uptake activity of HSV1-sr39TK as an indicator of the enzymatic function of HSV1-sr39TK was analysed by *in vitro* uptake of [^{18}F]-FHBG in infected and/or treated U87-MG cells or spheroids. For uptake analysis, 1 x 10^5 cells and spheroids containing approximately 1 x 10^5 cells were washed once with 1 x PBS and labelled with 0.1 MBq [^{18}F]-FHBG. All probes were incubated for a minimum of 1 h at 37°C and washed twice with ice-cold PBS, before the accumulated radiotracer was released from the cells by addition of 1 ml 1 M NaOH. A standard curve, containing serial dilutions of the [^{18}F]-FHBG solution, was prepared in order to determine the uptake dose of the samples. The

radiotracer activity per 1 x 10^5 cells was measured as counts per minute (cpm) using a gamma-counter and decay-corrected.

To measure the spatial accumulation of radiotracer without disrupting the spheroid morphology, infected and/or treated spheroids consisting of 4 x 10^5 cells were labelled with [^{18}F]-FHBG as described above. After labelling, spheroids were transferred to a 24-well plate, containing one spheroid per well, and radioactivity was detected on a combined small-animal positron emission tomography (PET)/computed tomography (CT) system. The analysis of the regions of interest (ROI) was performed with INVEON Research Workplace software using the statistical iterative reconstruction algorithm of ordered subset expectation maximisation (OSEM 3D) with attenuation correction/scatter correction (ACSC). Decay correction was performed and the measured activity was validated by means of a standard curve with serial radiotracer dilutions.

3.16. Statistical analysis

Statistical analysis of TMZ-enhanced adenoviral replication was performed by using Student's t-test (paired, two-sided). The criterion for statistical significance was taken as $p < 0.05$. To analyse spheroid growth after subjection to viral infections and TMZ or GCV treatment in a time-course, two-way ANOVA at 5 % level of significance (alpha value of 0.05) was performed. Correction of alpha error level was subsequently conducted by Tukey's multiple comparison test (95 % confidence interval) for the significance of multiple independent groups. Metabolic activity of spheroids after treatment was analysed by Student's t-test (paired, two-sided, $p < 0.05$). The radiotracer uptake studies were evaluated by one-way ANOVA at a 5 % level of significance (alpha value of 0.05) with Tukey's multiple comparison test (95 % confidence interval) as described above.

4. RESULTS

4.1. Characterisation of adenoviral vectors

The adenoviral vectors (figure 2.1) applied in this work were characterised in order to verify their correct genetic structure prior to the beginning of all experiments. Additionally, the adenoviral preparations were examined for potential contamination with wild-type adenovirus.

4.1.1. Verification of crucial genetic modifications

The integrity of essential mutated adenoviral regions and the maintenance of the transgene *HSV1-sr39TK* in Ad-delo-sr39TK-RGD were verified after virus production and compared to respective gene regions of a *HSV1-sr39TK*-armed and non-armed adenovirus. The verification was performed by means of PCR analysis of DNA extracted from CsCl-purified adenovirus preparations. The expected PCR products are summarised in table 4.1 and the derived PCR signals are depicted in figure 4.1.

The *E1* region-specific primers amplify a DNA fragment, which comprises the *E1A, E1B19K and E1B55K* genes. This fragment was detected in its full length in Ad5-wt DNA. The vectors Ad-delo-sr39TK-RGD and Ad-delo3-RGD contain an 11 bp deletion in the CR3 region of the *E1A* gene and a 201 bp deletion in the *E1B19K* gene (chapter 2.14.). Because of these two manipulations, a shorter PCR product than the one in Ad5-wt was derived from Ad-delo-sr39TK-RGD and Ad-delo3-RGD, as expected. In the replication-deficient adenovirus Ad-sr39TK, the detected fragment in the *E1* region is for the most part deleted and replaced by the transgene *HSV1-sr39TK* (chapter 2.14.). The specific amplification resulted therefore in a PCR product shorter than that of Ad5-wt and the oncolytic adenoviruses.

The *E3* region-specific primers amplified a sequence located in the *E3* region of Ad5-wt. In Ad-delo-sr39TK-RGD, this part of the *E3* region is replaced by the 1131 bp insertion of the *HSV1-sr39TK* gene. This insertion resulted in a larger PCR product, compared to Ad5-wt, when detected with *E3*-specific primers. No respective PCR signal was obtained in the *E3*-deleted Ad-delo3-RGD vector. A fragment, localised outside of the deletion in the *E3* region and corresponding to the respective PCR sequence derived from Ad5-wt, was detected in Ad-sr39TK DNA.

Both Ad-delo-sr39TK-RGD and Ad-sr39TK yielded a positive amplification signal for the transgene *HSV1-sr39TK*. The vectors armed with the transgene *HSV1-sr39TK* were also verified by sequencing (data not shown). The oncolytic vector Ad-delo-shMGMT-RGD had already been verified previously.

Table 4.1: Expected PCR products after specific detection of adenoviral *E1*/*E3* region and *HSV1-sr39TK*.

Virus	PCR product (size in bp)		
	E1	*E3*	*HSV1-sr39TK*
Ad5-wt	3345	796	n.a.
Ad-delo-sr39TK-RGD	3163	2147	1070
Ad-delo3-RGD	3163	-	n.a.
Ad-sr39TK	2935	796	1112

Ad5-wt: wild-type adenovirus 5; n.a.: not analysed

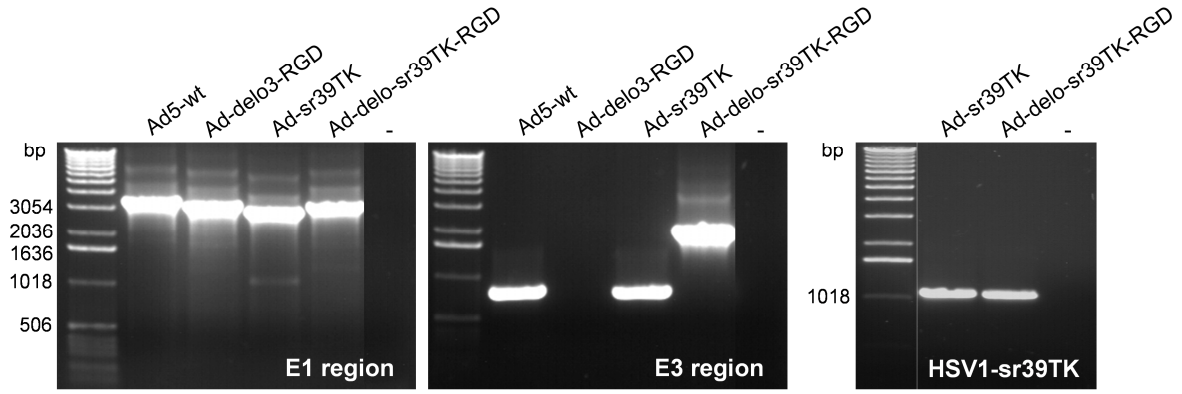

Figure 4.1: Verification of key adenoviral modifications. DNA was isolated by phenol-chloroform extraction from CsCl-purifications of the indicated adenoviruses and subjected to PCR analysis with specific primers for the amplification of adenoviral *E1A-pIX* region (left), *E3* region (middle) and *HSV1-sr39TK* gene (right). Lane 1: 1 kb DNA ladder with DNA bands of indicated length. - : negative control.

4.1.2. Control for contamination with wild-type Ad5 recombinants

Recombinant replication-competent adenoviruses (RCA) arise from the recovery of *E1* sequences during accidental homologous recombination between *E1*-deleted or *E1*-mutated adenoviruses and the wild-type *E1* sequence provided by the producer cell line HEK293 [316]. In order to exclude possible contamination of the adenoviruses with wild-type Ad5 RCA, the adenoviral vectors were examined by specific PCR amplification of DNA extracted from CsCl-purified adenovirus preparations. If the PCR analysis with specific primers for *E1A* is positive in replication-deficient, *E1A*-deleted adenoviruses, the virus of interest is contaminated with RCA. However, oncolytic adenoviruses like Ad-delo-sr39TK-RGD, Ad-delo3-RGD and Ad-delo-shMGMT-RGD, which contain an 11 bp deletion in the CR3 region of the *E1A* gene, yield a positive amplification signal despite being devoid of contamination with wild-type recombinants. The results of the PCR analysis for wild-type RCA contamination are summarised in table 4.2 and the signals derived by the PCR are depicted in figure 4.2. Amplification of all oncolytic vectors with *E1A*-specific primers resulted in the expected PCR products, which are 11 bp shorter than the respective product of the Ad5-derived vector pXC1. However, due to the similar length of the PCR products derived from the oncolytic vectors and of those derived from the Ad5-vector pXC1, a potential wild-type RCA contamination of the oncolytic

vectors could not be definitely excluded. Absence of RCA contamination was therefore verified by the distinctive PCR signals of the oncolytic vectors in figure 4.1. No PCR signal was derived by *E1A*-specific amplification of Ad-sr39TK. The sensitivity of the amplification was high, given that the detection limit of the *E1A*-specific PCR had been proved to be 10 fg of pXC1 DNA that corresponds to 912 DNA copies (Dr. Martina Anton, personal communication). The presence of adenoviral DNA was verified by successful *E2*-specific PCR amplification, using the vector pBHGlox as a positive reference.

Table 4.2: Expected PCR products after specific detection of fragments in adenoviral *E1A* and *E2* regions for proof of contamination with wild-type RCA.

Virus	PCR product (size in bp)	
	E1A	*E2*
pXC1	1042	n.a.
pBHGlox	n.a.	631
Ad-sr39TK	-	631
Ad-delo-sr39TK-RGD	1031	631
Ad-delo-shMGMT-RGD	1031	631
Ad-delo3-RGD	1031	631

n.a.: not analysed

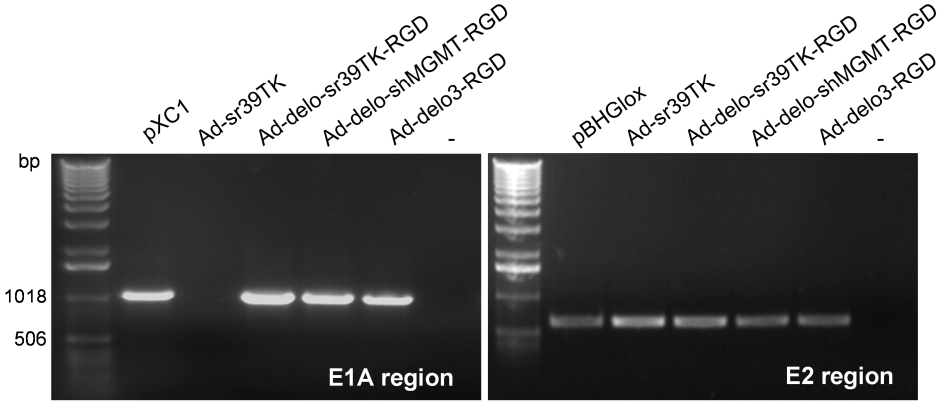

Figure 4.2: Control of contamination with wild-type RCA. DNA was isolated by phenol-chloroform extraction from CsCl-purifications of the indicated adenoviruses and subjected to PCR analysis with specific primers for the amplification of adenoviral *E1A* (left) and *E2* region (right). Plasmid DNA of pXC1 and pBHGlox was used as a positive control for *E1A* and *E2* amplification, respectively. Lane 1: 1 kb DNA ladder showing relevant DNA bands. - : negative control.

The results described in 4.1.1. and 4.2.1. demonstrate that Ad-delo-sr39TK-RGD contains the correct modifications of its genome and that the replication-deficient adenovirus Ad-sr39TK was devoid of any detectable wild-type RCA contamination. Due to the presence of the *E1A* region, the lack of RCA contamination in the oncolytic adenovirus preparations was only partially confirmed. The adenoviruses could be applied in the subsequent experiments.

4.2. Induction of cytopathic effect by YB-1 dependent oncolytic adenoviruses in tumour cell lines

Cytopathic effect (c.p.e.) is a characteristic of infection with replicating adenoviruses and a prerequisite for lysis of infected cells. The ability of oncolytic adenoviruses to induce c.p.e. is therefore a crucial step for efficient tumour cell eradication. The vectors Ad-delo-sr39TK-RGD, Ad-delo3-RGD and Ad-delo-shMGMT-RGD were rendered YB-1 dependent by deleting the CR3 domain of *E1A* (figure 2.1). Thus, it was of interest to examine the potential of YB-1 dependent oncolytic adenoviruses in mediating c.p.e in the glioma cell line U87-MG and in the multidrug-resistant pancreatic cell line EPP85-181RDB as a reference. The replication of YB-1 dependent oncolytic adenoviruses is stimulated by nuclear accumulated YB-1 [259, 265]. In this context, the U87-MG cell line had been characterised by a high expression level and partial nuclear localisation of YB-1 [290]. Nuclear distribution of YB-1 in EPP85-181RDB cells had also been verified [288].

As shown in figure 4.3, c.p.e. was microscopically visible as colonies of rounded cells detached from the cell monolayer. Ad-delo-sr39TK-RGD was able to induce complete c.p.e. in U87-MG cells at MOI of 100 ifu/cell already 48 h after infection. At MOI of 10 ifu/cell, Ad-delo-sr39TK-RGD could induce c.p.e. in only about 50-70 % of the cell population 72 h after infection (data not shown). The c.p.e. elicited by Ad-delo3-RGD 48 h after infection was as strong as that of the armed virus, but started with a delay of one day compared to Ad-delo-sr39TK-RGD, when a MOI of 10 ifu/cell was applied (data not shown). Ad-delo-shMGMT-RGD induced a similar c.p.e. as Ad-delo-sr39TK-RGD and Ad-delo3-RGD, regarding its strength and onset time-point. C.p.e. was absent after infection of the tumour cells lines with Ad-sr39TK. In EPP85-181RDB, all oncolytic adenoviruses were able to mediate c.p.e. successfully and at the same level as in U87-MG cells, but 72 h after infection.

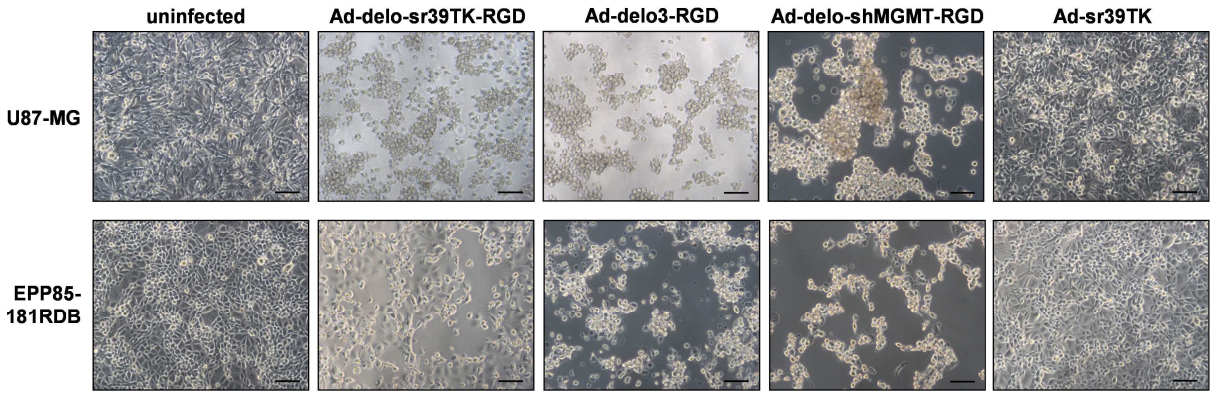

Figure 4.3: Induction of c.p.e. by YB-1 dependent oncolytic adenoviruses in tumour cell lines. U87-MG and EPP85-181RDB cells (5 x 10^5) were infected with the indicated adenoviruses at MOI of 100 ifu/cell and analysed in an inverted microscope for occurrence of c.p.e. 48 h (U87-MG) or 72 h (EPP85-181RDB) after infection. Scale bar: 100 µm.

Taking the above described results into account, all YB-1 dependent adenoviruses successfully induced c.p.e. and thus oncolytic effect in tumour cells. As a next step, the contribution of viral replication to c.p.e. was explored.

4.3. Replication competence of YB-1 dependent oncolytic adenoviruses

4.3.1. Replication of oncolytic adenoviruses in tumour cells

Given that adenoviral replication is a prerequisite for successful induction of c.p.e. and oncolytic effect in target cells, it was of interest to examine the replication capacity of oncolytic adenoviruses. Moreover, it was analysed whether the replication kinetics of the transgene *HSV1-sr39TK* in Ad-delo-sr39TK-RGD correlated with the replication potential of the virus. These examinations were performed by Southern blot and real-time qPCR analyses.

In accordance with their strong induction of c.p.e., the oncolytic adenoviruses replicated efficiently in U87-MG cells, as shown by Southern blot detection of viral DNA (figure 4.4 A). A time-dependent and cumulative increase of the DNA amount of all oncolytic viruses was observed from 24 h up to 96 h after infection. *HSV1-sr39TK* gene replication also increased slightly from 24 h to 96 h after infection with Ad-delo-sr39TK-RGD. The transgene was not detected in the DNA of Ad-delo3-RGD and Ad-delo-shMGMT-RGD. No DNA replication was observed after infection with Ad-sr39TK. Addition of GCV to infected U87-MG cells immediately after infection resulted in absence of Ad-delo-sr39TK-RGD DNA replication, even when high viral doses (MOI of 100 ifu/cell) were applied, as shown by the specific detection of *HSV1-sr39TK* (figure 4.4 B).

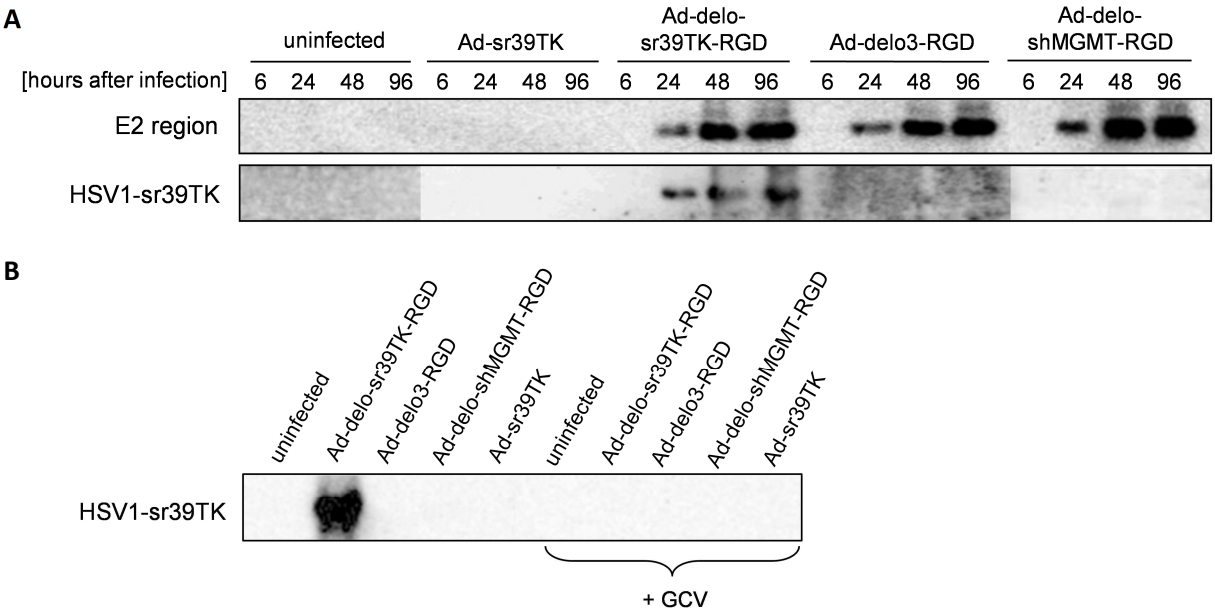

Figure 4.4: Analysis of adenoviral replication in glioma cells. U87-MG cells (5 x 10^5) were infected with the indicated adenoviruses at MOI of 100 ifu/cell. **A:** DNA was isolated from cells 6 h, 24 h, 48 h and 96 h after

infection using phenol-chloroform extraction. Southern blot analysis was performed with 1 µg DNA, digested with *PvuI*. A 1669 bp fragment of the adenoviral *E2* region and, after stripping and re-probing, a 1146 bp fragment of *HSV1-sr39TK* were detected by hybridisation with complementary DIG-dUTP-labelled DNA probes. **B:** GCV [50 µg/ml] was added to U87-MG cells immediately after infection. DNA was isolated 72 h after infection and subjected to Southern blot analysis and specific detection of *HSV1-sr39TK* as described in A.

Consistent with the detection of viral DNA by Southern blot analysis, but more accurately, the replication of the oncolytic adenoviruses was demonstrated by real-time qPCR analysis of adenoviral *Fiber 5* gene copy number in U87-MG glioma cells and in the multidrug-resistant cell line EPP85-181RDB (figure 4.5). A significant replication burst of Ad-delo-sr39TK-RGD was observed in U87-MG cells from 24 h to 48 h (150-fold) and in EPP85-181RDB cells from 12 h to 24 h (260-fold) after infection. The overall DNA accumulation from 6 h to 72 h post infection was about 180,000-fold in U87-MG cells and only about 1700-fold in EPP85-181RDB cells. In contrast, the DNA copy number of Ad-sr39TK remained constant over time in both cell lines, which confirmed the replication-deficient character of the virus. In comparison to Ad-delo-sr39TK-RGD, the replication of Ad-delo3-RGD increased only 8300-fold from 6 h to 72 h in U87-MG cells, despite identical *E1A* genetic backbone. The lower replication level obtained by Ad-delo3-RGD reflected the 24 h-delayed induction of c.p.e. by Ad-delo3-RGD compared to Ad-delo-sr39TK-RGD, as described in chapter 4.2. In EPP85-181RDB cells, the DNA accumulation of Ad-delo3-RGD reached a similar level as Ad-delo-sr39TK-RGD replication 48 h and 72 h post infection. Hence, Ad-delo-sr39TK-RGD not only replicates effectively, but has an improved replication competence over Ad-delo3-RGD in glioma cells.

The gene copy number of *HSV1-sr39TK* paralleled the increase in Ad-delo-sr39TK-RGD replication and accumulated about 5000-fold in U87-MG cells and only about 500-fold in EPP85-181RDB cells from 6 h to 72 h post infection. The transgene copy number remained constant in Ad-sr39TK and was not detectable in Ad-delo3-RGD. The difference between the accumulated DNA copy number of *Fiber 5* and that of *HSV1-sr39TK* resulted most probably from the different efficiency of the detection chemistries (SYBR green dye for *Fiber 5* and TaqMan® probe for *HSV1-sr39TK*) used for quantification of the genes.

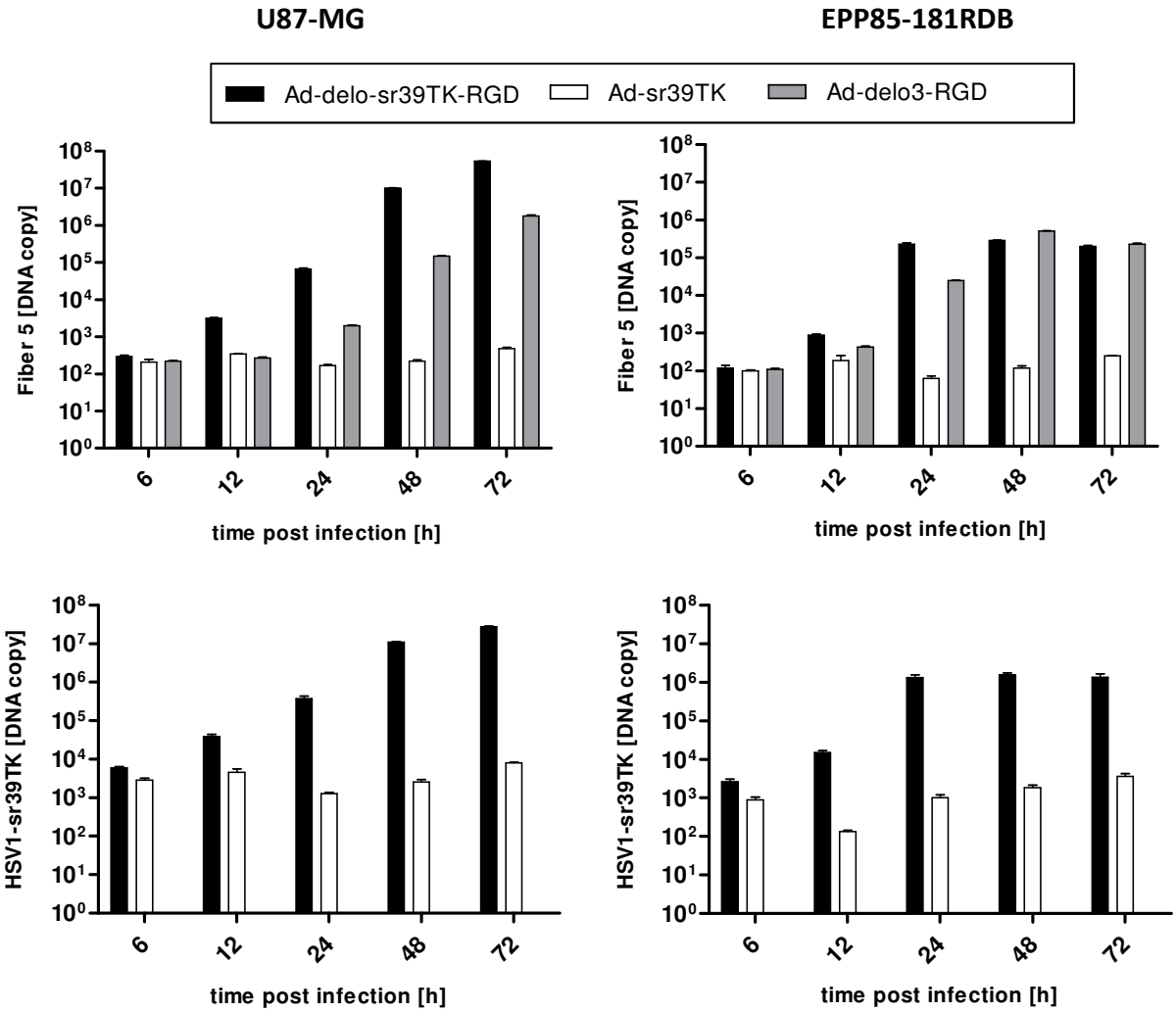

Figure 4.5: Accumulation of adenoviral DNA in glioma and pancreatic carcinoma cells. U87-MG and EPP85-181RDB cells (1 x 10^6) were infected with the indicated adenoviruses at MOI of 10 ifu/cell. DNA was isolated from infected cells 6-72 h after infection by phenol-chloroform extraction. The copy number of adenoviral *Fiber 5* gene and *HSV1-sr39TK* transgene was quantified by means of absolute real-time qPCR of 2.5 ng (*Fiber 5*) and 5 ng (*HSV1-sr39TK*) DNA per reaction (mean±SD); n=3.

4.3.2. Release of newly synthesised adenoviral particles

In order to spread to, infect and lyse neighbouring cells, an oncolytic adenovirus should be able to produce functional viral progeny. Therefore, the release of newly synthesised viral particles by U87-MG and EPP85-181RDB cells infected with oncolytic adenoviruses was analysed by absolute real-time qPCR of *Fiber 5* DNA copy number. Release of newly synthesised Ad-delo-sr39TK-RGD oncolytic adenoviral particles from both tumour cell lines was first detected 48 h after infection (figure 4.6). The values measured 6 h, 12 h and 24 h after infection indicate most probably not internalised adenoviruses, as viral release usually starts about 48 h to 72 h post infection [165]. After 96 h, viral release from U87-MG and EPP85-181RDB cells reached a 9020-fold and an about 25-fold higher level than the initial value, respectively. This finding correlated with the enhanced intracellular replication of viral DNA up to 72 h after infection (figure 4.5). In comparison, the cumulative release of Ad-delo3-

RGD and Ad-delo-shMGMT-RGD particles from U87-MG and EPP85-181RDB cells started 72 h or 96 h post infection (figure 4.6).

In addition to its delayed release, Ad-delo3-RGD yielded 16,000-times and 70-times less viral particles than Ad-delo-sr39TK-RGD from U87-MG and EPP85-181RDB cells, respectively, 96 h post infection. This finding was in accordance with the attenuated intracellular DNA replication efficacy of Ad-delo3-RGD compared to the armed oncolytic adenovirus. Ad-delo-shMGMT-RGD was characterised by a 400-fold and 6-fold lower particle release than Ad-delo-sr39TK-RGD from U87-MG and EPP85-181RDB cells, respectively, 96 h post infection.

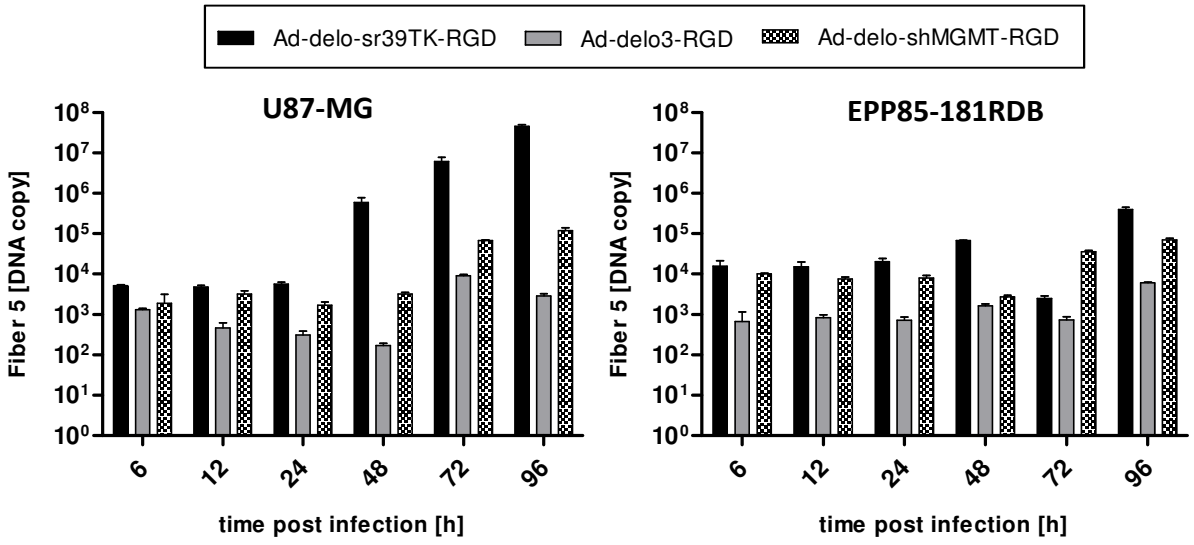

Figure 4.6: Release of newly synthesised adenoviral particles from glioma and pancreatic carcinoma cells. U87-MG and EPP85-181RDB cells (2 x 10^5) were infected with the indicated oncolytic adenoviruses at MOI of 10 ifu/cell. DNA was isolated from supernatants of infected cells 6-96 h after infection using DNeasy Blood and Tissue Kit (Qiagen). Cumulative release of newly synthesised adenoviral particles was analysed by detection of *Fiber 5* gene copy number by absolute real-time qPCR of 2.5 ng DNA per reaction (mean±SD); n=3.

4.3.3. Oncolytic adenoviruses produce infectious progeny

The infectivity of released oncolytic viral progeny from U87-MG glioma cells was examined by End-point dilution assay on HEK293 cells and the infectious titre was determined accordingly (figure 4.7). The infectious titre of released Ad-delo-sr39TK-RGD particles was 7.94 x 10^6 pfu/ml 5 days after infection of U87-MG cells. Ad-delo3-RGD and Ad-delo-shMGMT-RGD particles yielded 25-fold and 3-fold lower titres than Ad-delo-sr39TK-RGD, respectively. The low amount of infectious particles of Ad-delo3-RGD was associated with the attenuated replication efficiency and progeny release of the virus, as shown in figures 4.5 and 4.6. No infectious particles were produced by Ad-sr39TK-infected glioma cells.

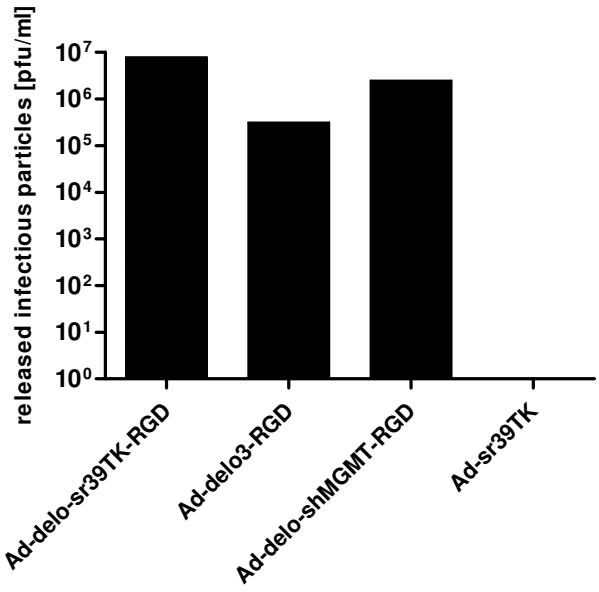

Figure 4.7: Infectivity of newly synthesised adenoviral particles. U87-MG cells (2 x 10^5) were infected with the indicated adenoviruses at MOI of 10 ifu/cell and supernatants containing released viral particles were collected 5 days post infection. The titres of released viral particles, defined as plaque forming units per ml (pfu/ml), were determined by End-point dilution assay in HEK293 cells.

The results described in chapter 4.3. demonstrate the strong replication competence of Ad-delo-sr39TK-RGD, as well as the efficient production and release of viral progeny, which was in accordance with the successful induction of c.p.e in infected tumour cells and proved the oncolytic potential of the virus. Moreover, Ad-delo-sr39TK-RGD displayed improved replication capacity and viral release as compared to the *E3*-deleted vector Ad-delo3-RGD. The accumulation of *HSV1-sr39TK* copy number over time correlated with adenoviral replication. The replication competence of Ad-delo-sr39TK-RGD in glioma cells was 100-times higher than in multidrug-resistant pancreatic carcinoma cells at late time points of viral infection. In addition, Ad-delo-sr39TK-RGD was able to produce high amount of viral progeny to re-infect tumour cells.

4.4. Expression of adenovirus-delivered HSV1-sr39TK in tumour cells

In order to investigate the expression kinetics of the transgene *HSV1-sr39TK*, U87-MG and EPP85-181RDB cells infected with armed oncolytic and replication-deficient vectors were subjected to specific mRNA real-time quantification and immunodetection of the protein by SDS-PAGE and Western blot.

The relative mRNA levels of HSV1-sr39TK synthesised by Ad-delo-sr39TK-RGD-infected U87-MG and EPP85-181RDB cells increased 52-fold and 87-fold, respectively, from 6 h to 72 h post infection, whereas mRNA delivered by Ad-sr39TK did not accumulate over time in both cell lines (figure 4.8). The highest HSV1-sr39TK mRNA level in Ad-delo-sr39TK-RGD-infected EPP85-181RDB cells was detected 48 h post infection. However, the mRNA levels in infected U87-MG cells were about 10-times higher than the mRNA levels derived from infected EPP85-181RDB cells at each time point analysed.

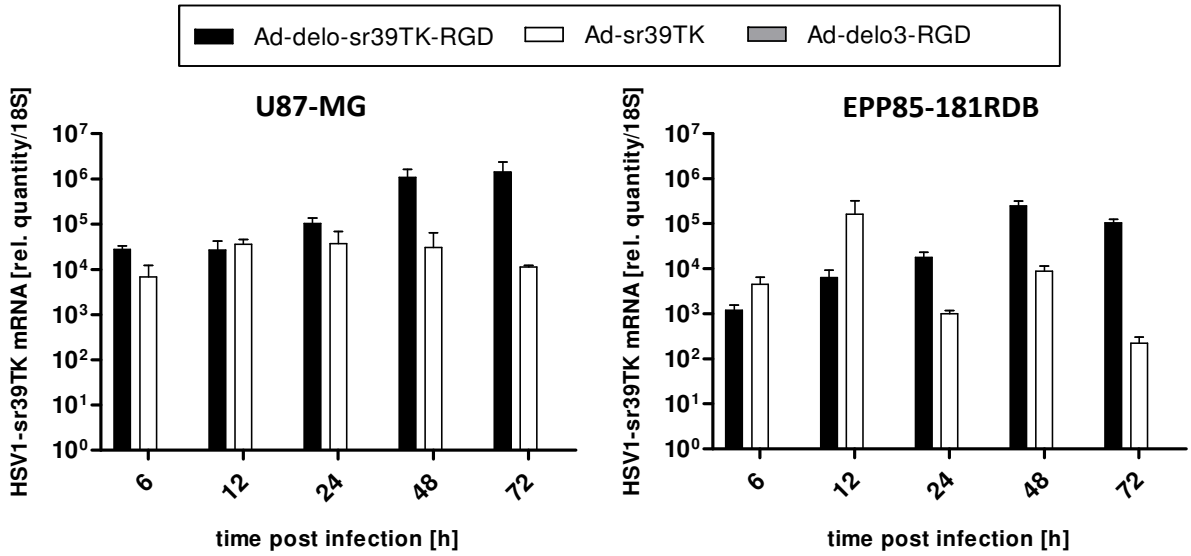

Figure 4.8: Relative quantification of adenovirus-delivered HSV1-sr39TK mRNA transcripts. U87-MG and EPP85-181RDB cells (1 x 10^6) were infected with the indicated adenoviruses at MOI of 10 ifu/cell. Total RNA was isolated 6-72 h post infection using Trizol reagent (Invitrogen) and reverse transcription into cDNA was performed. HSV1-sr39TK mRNA transcripts were deduced from cDNA amount (5 ng per reaction) in a relative real-time qPCR and normalised to 18S rRNA endogenous control (mean±SD); n=3.

The results of the mRNA quantification were supported by analysis of protein expression (figure 4.9). The HSV1-sr39TK protein of 40.97 kDa (UniProtKB) delivered by Ad-delo-sr39TK-RGD and Ad-sr39TK was successfully detected 48 h after infection of U87-MG cells and 72 h after infection of EPP85-181RDB cells (figure 4.9 A left), when first signs of c.p.e. were visible (figure 4.3). As shown by the analysis of signal intensity (figure 4.9 A right), the protein expression level of the transgene in Ad-delo-sr39TK-RGD (second lane) was comparable to that of the transgene in Ad-sr39TK (third lane) in both cell lines. The expression levels of the HSV1-sr39TK protein in the EPP85-181RDB cell line were lower than those in U87-MG cells, regardless of delivery vector.

It was further investigated if GCV had an impact on HSV1-sr39TK expression in infected U87-MG cells (figure 4.9 B). Ad-delo-sr39TK-RGD- as well as Ad-sr39TK-delivered HSV1-sr39TK was weakly expressed when GCV was applied 24 h or 48 h after infection. After GCV addition 72 h post infection, a significant level of HSV1-sr39TK expressed by Ad-sr39TK (lane 6) was detected, compared to a lower expression by Ad-delo-sr39TK-RGD (lane 5). This finding could result from an enhanced cell killing by Ad-delo-sr39TK-RGD 72 h after infection. The lack of a HSV1-sr39TK protein signal, when the primary antibody was neutralised by a blocking peptide against HSV1-TK and applied to lysates of Ad-delo-sr39TK-RGD-infected cells, proved the specificity of the anti-HSV1-TK antibody (figure 4.9 C).

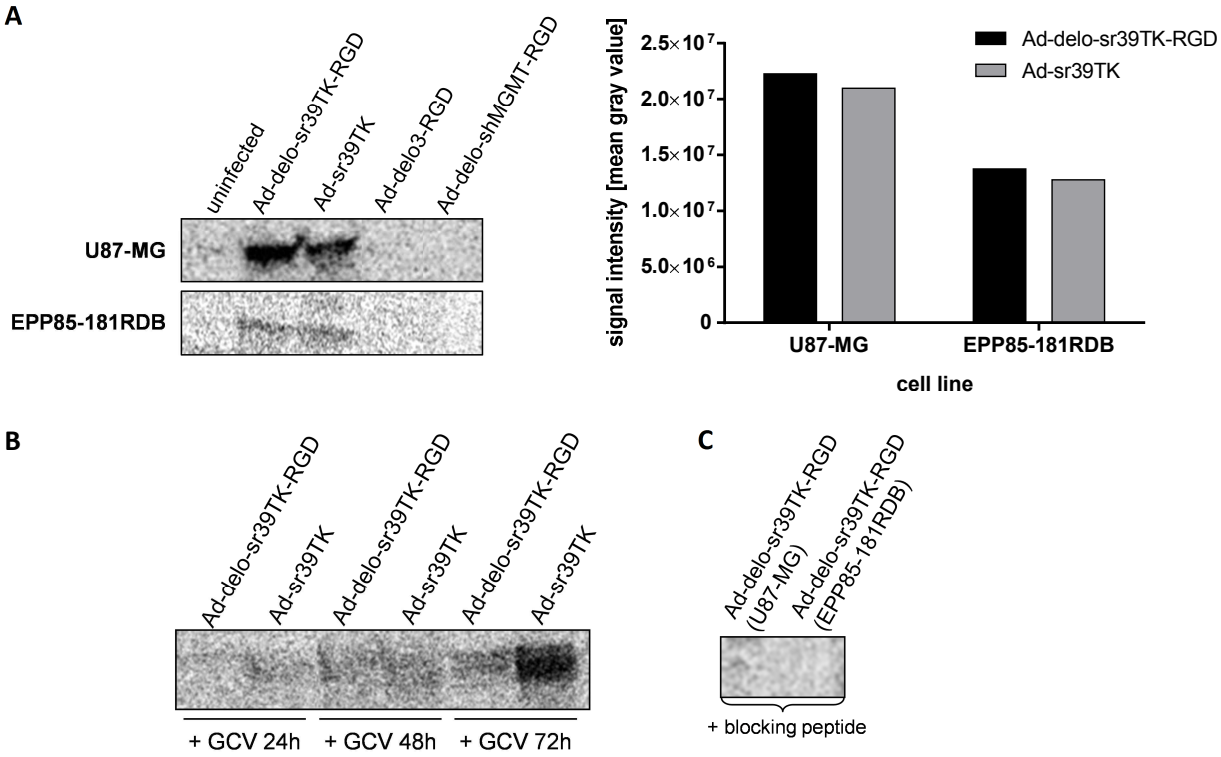

Figure 4.9: Expression of adenovirus-delivered HSV1-sr39TK in tumour cells. U87-MG and EPP85-181RDB cells (1 x 10^6) were infected with the indicated adenoviruses at MOI of 100 ifu/cell. Protein extractions were derived at indicated time points using RIPA buffer, concentrated by TCA precipitation and subjected to Western blot analysis. HSV1-sr39TK protein expression was analysed in 150 µg protein lysates by immunodetection. **A:** HSV1-sr39TK protein was detected 48 h (U87-MG) and 72 h (EPP85-181RDB) after infection (left) and the protein signal intensity was determined by densitometry (right). **B:** U87-MG cells were treated with GCV [50 µg/ml] 24 h, 48 h and 72 h after infection. Protein expression was analysed 48 h after GCV addition. **C:** The specificity of the primary antibody against HSV1-sr39TK was verified in protein extractions of Ad-delo-sr39TK-RGD-infected cells by the incubation of the antibody with a blocking peptide [1 µg/ml].

To sum up, the increasing HSV1-sr39TK expression from Ad-delo-sr39TK-RGD 6 h to 72 h after infection was due to the replication competence of the oncolytic virus and thus due to accumulation of transgene DNA copies, as shown by the replication analysis. Moreover, it could be shown that GCV had a negative impact on protein expression at early time points of infection, probably due to HSV1-sr39TK/GCV-mediated cytotoxicity.

4.5. Analysis of growth, cellular migration and infectivity of glioma spheroids

Spheroids are convenient models to mimic tumour behaviour *in vitro* and to study anti-tumour treatment effects. Therefore, spheroids were first analysed in respect of various parameters concerning their growth, migration ability of cells out of the spheroidal structure and infectivity with adenoviruses.

4.5.1. Spheroids exhibit tumour-like growth pattern

In order to examine U87-MG spheroid growth, spheroids were cultivated for 28 days after formation. During that time-course the surface areas and the volumes of the spheroids were calculated, as depicted in figure 4.10. The increase of the spheroid surface areas corresponded to the increase of their volumes. All of the 12 spheroids analysed displayed similar growth pattern with some fluctuations of their volumes from day 17 to day 28 of monitoring, characteristic of tumour-like growth. The spheroids grew exponentially until reaching a plateau phase of growth after 14 days. At day 14 they had increased up to 6-fold of their initial volumes. After 28 days the spheroids reached mean volumes of 0.4 ± 0.11 mm³ that corresponded to an 8-fold increase relative to the initial values. All spheroids had mostly uniform morphology at each time point analysed, as depicted in figure 4.10, below.

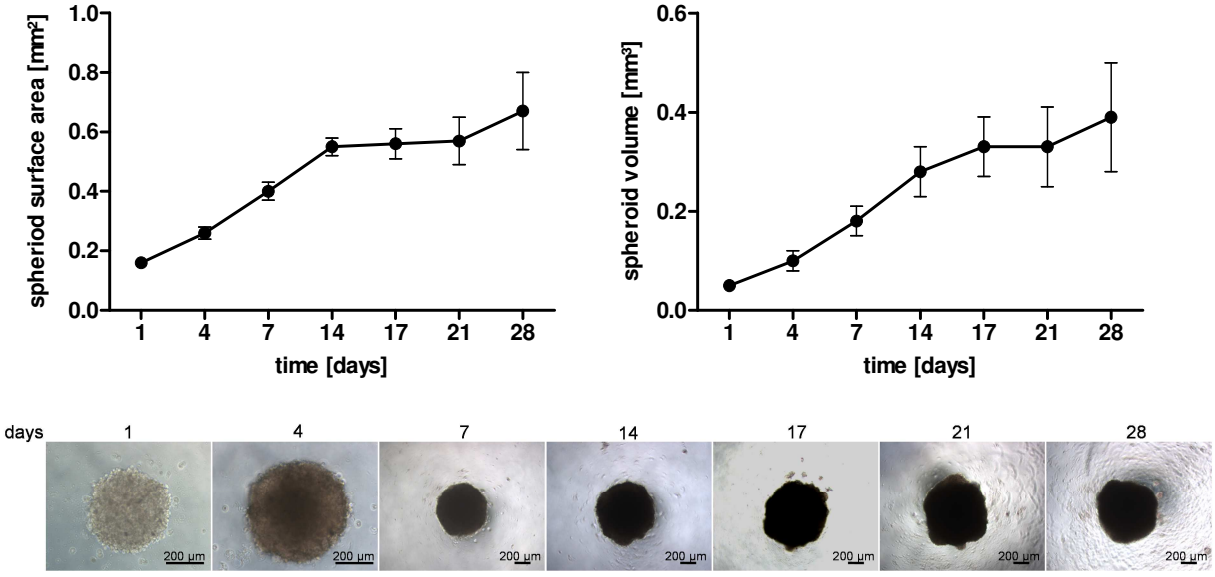

Figure 4.10: Growth analysis of U87-MG-derived multicellular spheroids. The growth of glioma spheroids, consisting of an initial number of about 1 x 10^5 cells, was monitored in a time-course of 28 days after formation. Spheroid diameter was measured in an inverted microscope. The surface areas and volumes were calculated accordingly at the indicated time points (mean±SD); n=12. Representative spheroids are shown below (magnification: days 1-4: x 100, days 7-28: x 40).

4.5.2. Migration potential of cells from spheroids

The migration behaviour of U87-MG cells, detached from spheroids, was explored in the following one to seven days after adherence of spheroids to solid substrate. Representative images of migrating glioma cells from attached spheroids are displayed in figure 4.11. It could be shown that only one day after adherence cells started to migrate from the spheroids and reached migration distances in a range of 175-300 µm. Migration continued after two and three days with increasing migration behaviour of the cells, spreading at distances of up to 700 µm. Cell filaments outgrowing from the spheroids were formed during the migration process. After seven days a significant number of cells had detached from the spheroids and migrated at distances of up to 1000 µm, forming specific clusters and cell networks.

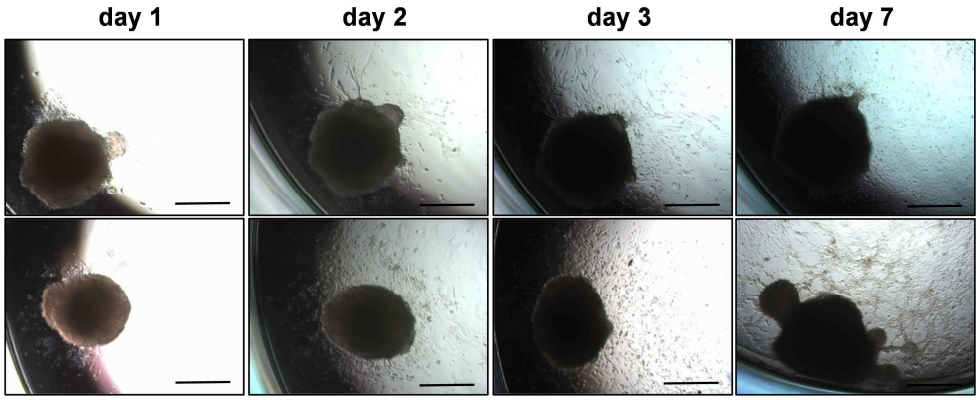

Figure 4.11: Cellular migration from U87-MG-derived spheroids. Glioma spheroids consisting of about 1 x 10^5 cells were attached after formation to uncoated wells of a 24-well plate. The migration behaviour of cells from spheroids (n=2) was monitored 1-7 days after spheroid attachment to the surface. Scale bar: 500 µm.

4.5.3. Spheroids allow for adenoviral infections

Prior to infection with oncolytic and armed replication-deficient adenoviruses, the infectivity of spheroid culture was investigated by infection of spheroids with the eGFP-expressing adenovirus Ad-mCMVeGFP (chapter 2.14). Fluorescent microscopic analysis of infected spheroids revealed that eGFP expression was visible already one to two days post infection, especially at MOI of 20, 50 and 100 pfu/cell, and was stable up to seven days (figure 4.12 A). However, as Ad-mCMVeGFP is a replication-deficient adenovirus, the infection takes place in the outer spheroid layers, giving no information about the infectivity of the inner layers. The microscopic observations were confirmed by fluorimetric quantification of eGFP expression in spheroid lysates (figure 4.12 B). Both microscopic and fluorimetric evaluation methods revealed that the signal intensity of eGFP was directly proportional to the viral MOI applied. According to these results and considering that replication-competent adenoviruses yield better infectivity than replication-deficient viruses, MOI of 50 was chosen for further infections.

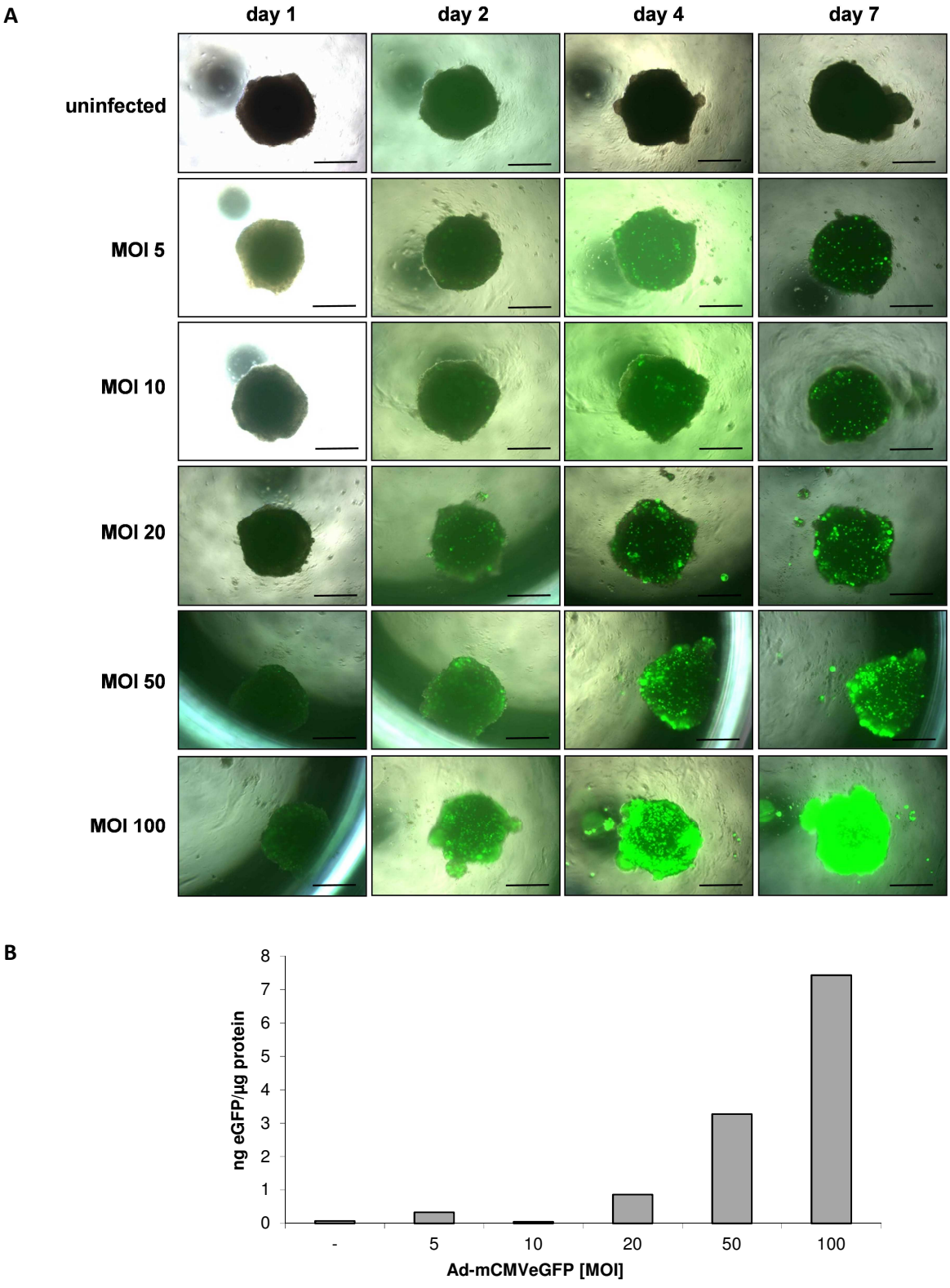

Figure 4.12: Infectivity of U87-MG-derived spheroids. Glioma spheroids with volumes of 0.1-0.18 mm³, consisting of an initial number of about 1 x 10^5 cells, were infected with MOI of 5 to 100 pfu/cell of the replication-deficient adenovirus Ad-mCMVeGFP. **A:** Merged transmitted light and fluorescent images demonstrate expression of the reporter gene *eGFP* as an indicator of spheroid infectivity at indicated time points post infection. Scale bar: 500 µm. **B:** The expression of eGFP at each MOI was quantified at 485/535 nm wavelength in lysates of spheroids 7 days after infection according to a standard curve. Quantity of eGFP [ng] was normalised to total protein amount [µg]; n=1.

Regarding the characterisation of glioma spheroids with respect to their growth, cellular migration and infectivity, the spheroids displayed tumour-like growth pattern and characteristics, and were susceptible to adenoviral infections. These properties classified them as a suitable *in vitro* model to explore the effects of viral oncolysis and of the HSV1-sr39TK/GCV system against tumours.

4.6. Overlapping time- and dose-dependent HSV1-sr39TK/GCV-mediated cytotoxicity and oncolytic effect

Initially, the influence of overlapping oncolytic potential and HSV1-sr39TK/GCV-mediated cytotoxicity on tumour cells was investigated. Bearing in mind that both effects are exerted by Ad-delo-sr39TK-RGD, it was expected that they should mutually potentiate their action. In this context, it was analysed whether the time point of GCV addition and the prodrug dose were crucial for the strength of the HSV1-sr39TK/GCV-mediated cytotoxicity and/or oncolytic effect. The highest concentration of GCV corresponded to therapeutically relevant GCV concentrations used in preclinical and clinical studies [96, 98, 101, 317]. The experiment was performed by means of SRB quantification of cell survival and XTT assay for analysis of metabolic activity, using the drug-sensitive cell line U87-MG and the multidrug-resistant cell line EPP85-181RDB as a reference.

As shown in figure 4.13 A, when GCV was added to glioma cells immediately after infection (0 h), the GCV dose mediating the strongest cytotoxicity was 100 µg/ml, leading to cell survival of 16.1 ± 5 % with Ad-delo-sr39TK-RGD, compared to 7.1 ± 0.11 % cell survival with Ad-sr39TK (figure 4.13 A). The XTT cytotoxicity assay displayed the percentage of metabolically active cells. After GCV addition directly post infection, the metabolic activity of Ad-delo-sr39TK-RGD-infected cells decreased in a dose-dependent way, paralleling SRB quantification (figure 4.13 B). The amount of metabolically active cells was 44 ± 8.55 % at 1 µg/ml GCV and only 9 ± 3.19 % at 10 µg/ml GCV. Addition of GCV 24 h, 48 h or 72 h post infection revealed effective cell killing at the lowest GCV dose of 0.001 µg/ml for the oncolytic adenovirus. Glioma cell survival with Ad-delo-sr39TK-RGD and 0.001 µg/ml GCV was 5.6 ± 0.18 %, compared to 106.5 ± 4.6 % survival with Ad-sr39TK, when GCV was added 24 h post infection. Cell killing activity was most effective by applying GCV 48 h or 72 h after infection, when the least survival of Ad-delo-sr39TK-RGD-infected cells was 4.1 ± 0.02 % (48 h) and 4.1 ± 0.16 % (72 h) at 0.001 µg/ml GCV (figure 4.13 A). In contrast, the survival of Ad-sr39TK-infected cells at 0.001 µg/ml GCV was 99.4 ± 4.98 % (48 h) and 87.6 ± 4.05 % (72 h). These results indicate that addition of GCV 48 h or 72 h post infection leads to a significant overlap of viral oncolysis and HSV1-sr39TK/GCV-mediated cytotoxicity in U87-MG cells regardless of GCV dose, compared to the exclusively prodrug dose-dependent cytotoxicity of the replication-deficient Ad-sr39TK at each time point analysed.

Supporting the results of the SRB quantification, when GCV was applied 48 h post infection with Ad-delo-sr39TK-RGD, no metabolically active cells remained, unlike infection with Ad-delo3-RGD plus GCV application (figure 4.13 B). Although cell killing was enhanced by rising GCV doses (figure 4.13 A), Ad-sr39TK-infected cells remained metabolically active (figure 4.13 B). The IC_{50} values of the Ad-sr39TK/GCV-mediated cytotoxicity varied from 9.8 µg/ml (72 h) to 0.35 µg/ml (24 h) (figure 4.13 A).

Although the contribution of suicide system and oncolysis to cell killing could not be clearly dissected, the HSV1-sr39TK/GCV-mediated cytotoxicity of Ad-delo-sr39TK-RGD predominated its oncolytic activity from GCV concentrations of 1 to 100 µg/ml when applied 0 h and 24 h post infection (figure 4.13 A). This finding was confirmed by the strong cytotoxic effects of Ad-sr39TK at 1 to 100 µg/ml GCV, but less cytotoxicity at lower doses. A peak value of cell survival was observed at 0.1 µg/ml GCV after infection with Ad-delo-sr39TK-RGD and GCV addition 0 h or 24 h post infection. This gave rise to the assumption that viral replication was prevented by the cytotoxicity of the HSV1-sr39TK/GCV system, acting on the initial number of infected cells. The inhibition of oncolysis was overcome when GCV was added 48 h or 72 h post infection, because the oncolytic effect of the virus had already been initiated before GCV addition and thus predominated over the HSV1-sr39TK/GCV-mediated cytotoxicity.

The oncolytic activity of Ad-delo-sr39TK-RGD (0 µg/ml GCV) promoted strong cell killing. The cell survival after oncolysis by Ad-delo-sr39TK-RGD was between 33 ± 2.98 % to 4.2 ± 0.18 % 10 days after infection and the cell killing was accordingly 67-96 % (not shown in figure 4.13 A). However, without addition of GCV most of the Ad-delo-sr39TK-RGD-infected cells (89 ± 11.7 %) remained metabolically active 10 days after infection, despite oncolytic effect (not shown in figure 4.13 B). In contrast, progressive cell death mediated by Ad-delo-sr39TK-RGD and GCV could be observed microscopically already 3-4 days after infection (data not shown).

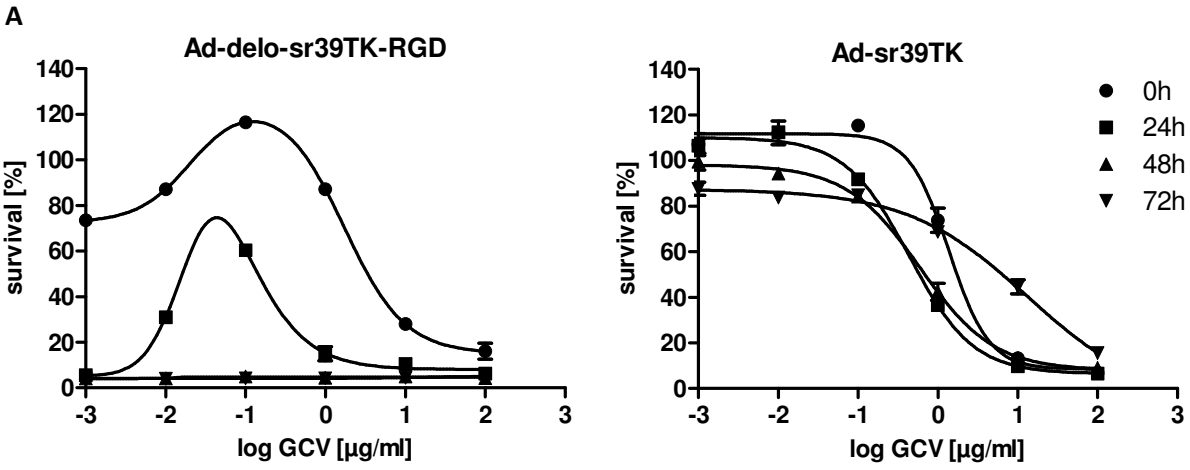

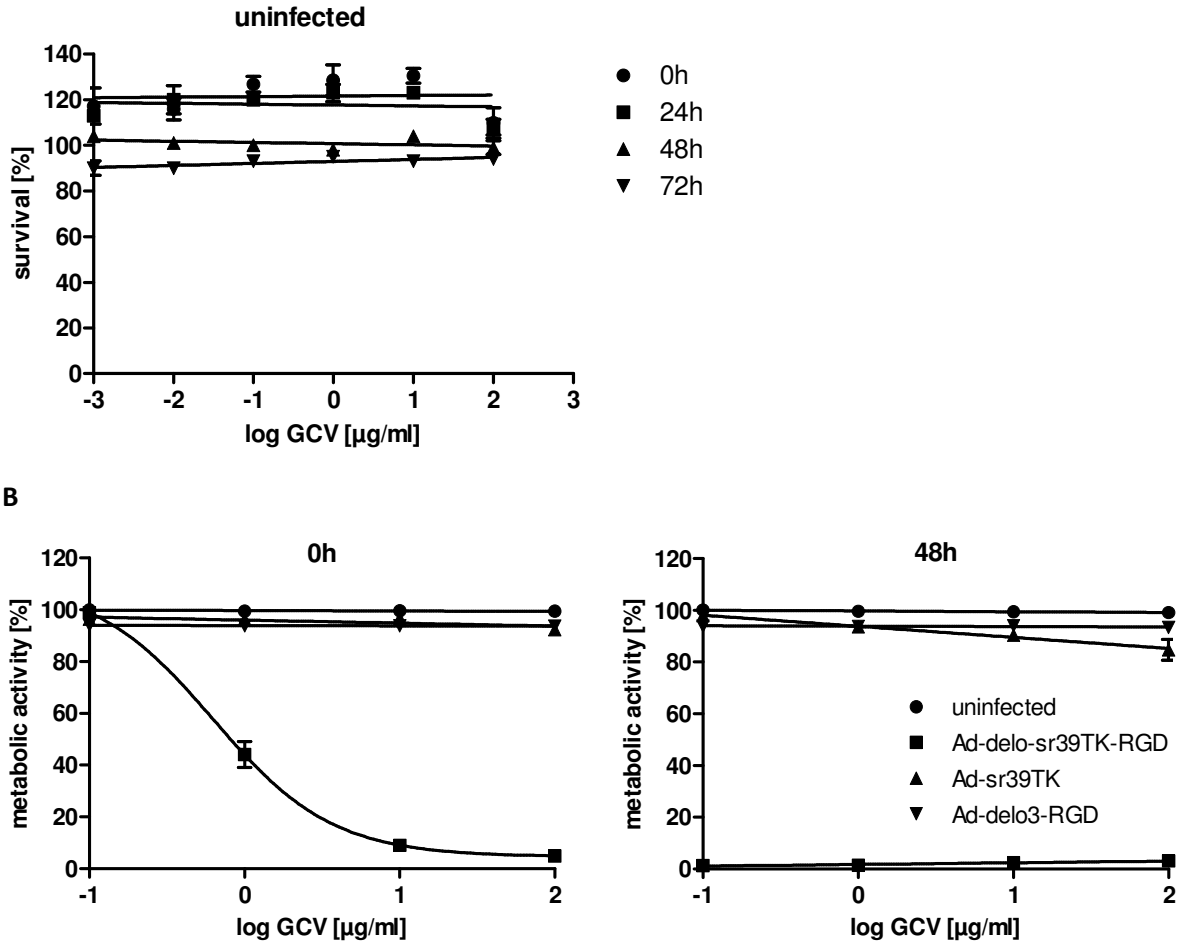

Figure 4.13: Overlapping time- and dose-dependent HSV1-sr39TK/GCV-mediated cytotoxicity and oncolytic effect in glioma cells. U87-MG cells (2 x 10^3) were infected at MOI of 100 ifu/cell with the indicated adenoviruses. GCV was added at increasing concentrations starting 0 h, 24 h, 48 h and 72 h after infection and applied again after 72 h. **A:** Cell killing was detected 10 days after infection using SRB staining and quantification of cell survival by measurement of the absorbance at 590 nm. Cell survival was quantified in percentage (mean±SD), referring to the survival of uninfected cells (100 %); n=3. **B:** After GCV addition directly (0 h) or 48 h post infection with the indicated adenoviruses, the metabolic activity was quantified by XTT assay 10 days after infection. The number of metabolically active cells was calculated using a standard curve and quantified in percentage (mean±SD) referring to the metabolic activity of uninfected cells (100 %); n=3.

Ad-delo-sr39TK-RGD and its HSV1-sr39TK/GCV-mediated cytotoxicity induced an overall weaker cell killing in EPP85-181RDB cells compared to U87-MG cells at equal viral MOI and when GCV was applied 24 h post infection (figure 4.14). The lowest cell survival amounted to 51 ± 6.31 % at a GCV concentration of 10 µg/ml. The IC_{50} value for the Ad-sr39TK/GCV-mediated cytotoxicity was about 5-times higher than that for Ad-delo-sr39TK-RGD/GCV. In addition, the IC_{50} for the Ad-sr39TK/GCV-mediated cytotoxicity in EPP85-181RDB cells was about 140-times higher than that in U87-MG cells (figure 4.13 A) at the same time point of GCV application. In comparison, the oncolytic effect of Ad-delo-sr39TK-RGD alone led to a cell survival of 61 ± 7.74 % (not shown in figure 4.14). As in Ad-delo-sr39TK-RGD-infected U87-MG cells, the replication and oncolytic potential of Ad-delo-sr39TK-RGD in

EPP85-181RDB cells was inhibited by GCV at a concentration of 0.01 µg/ml. Ad-sr39TK was not successful in inducing HSV1-sr39TK/GCV-mediated cytotoxicity, as cell survival was not below 79 ± 2.34 % at 10 µg/ml GCV. In this context, the HSV1-sr39TK/GCV-mediated effect might be attenuated through hampering the activity of GCV by the multidrug-resistant phenotype of the pancreatic carcinoma cells.

Ad-delo3-RGD and Ad-delo-shMGMT-RGD were limited in their oncolytic potential. EPP85-181RDB cells infected with Ad-delo3-RGD and Ad-delo-shMGMT-RGD displayed an average cell survival of 90 % and 50 %, respectively, independent of GCV dose. The application of GCV immediately after infection with oncolytic and replication-deficient adenoviruses or two to three days after infection did not potentiate the killing of EPP85-181RDB cells (data not shown). A GCV concentration of 100 µg/ml exerted unspecific toxicity.

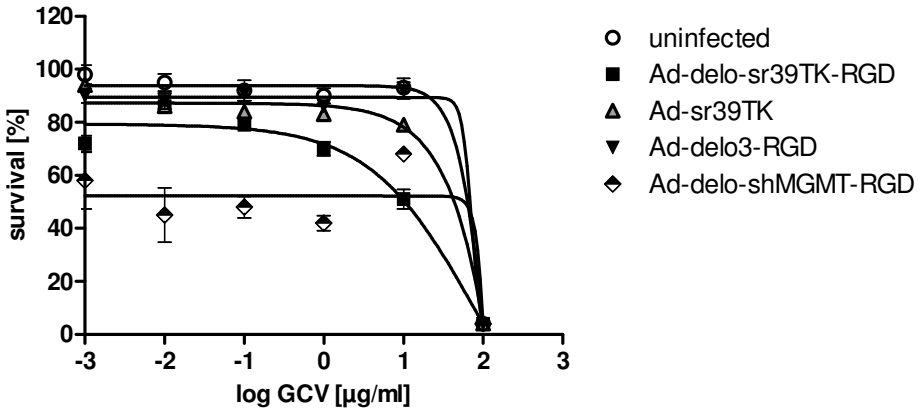

Figure 4.14: Overlapping dose-dependent HSV1sr39TK/GCV-mediated cytotoxicity and oncolytic effect in multidrug-resistant pancreatic carcinoma cells. EPP85-181RDB cells (2 x 10^3) were infected at MOI of 100 ifu/cell with indicated adenoviruses. GCV was added at increasing concentrations 24 h after infection and again after 72 h. Cell killing was detected 10 days after infection using SRB staining and quantification of cell survival by measurement of the absorbance at 590 nm. Cell survival was quantified in percentage (mean±SD), referring to the survival of uninfected cells (100 %); n=3.

These results show that the oncolytic effect of Ad-delo-sr39TK-RGD in glioma cells was enhanced by the HSV1-sr39TK/GCV-mediated cytotoxicity in a prodrug dose-dependent way, although virus-mediated cell killing was inhibited at critical GCV concentrations applied immediately after infection, even at a high viral dose. However, by applying GCV at later time points following infection, the combined action of oncolytic effect and the suicide system induced an equally strong cell killing, so that the oncolytic effect of the virus could not be further augmented. Due to their multidrug-resistant phenotype, over 50 % of the EPP85-181RDB cells survived the combined treatment with Ad-delo-sr39TK-RGD and the HSV1-sr39TK/GCV suicide system.

4.7. Bystander effect of viral oncolysis and HSV1-sr39TK/GCV-mediated cytotoxicity

The aim of the following experiment was to prove if the bystander effect, described for the HSV1-TK/GCV system [55], can be translated into glioma cells infected with oncolytic HSV1-sr39TK-armed adenoviruses. The potential of bystander cell killing in glioma cells was compared to the respective effect in multidrug-resistant pancreatic carcinoma cells. The major challenge was to distinguish between HSV1-sr39TK/GCV-mediated bystander effect and bystander effect by viral replication. A GCV concentration of 10 µg/ml was chosen for the analysis of bystander effect in order to circumvent inhibition of oncolytic cell killing by GCV at lower doses (figure 4.13, Ad-delo-sr39TK-RGD). To ensure that the oncolytic effect did not dominate the HSV1-sr39TK/GCV-mediated cytotoxicity (figure 4.13, Ad-delo-sr39TK-RGD), the prodrug was applied shortly after infection to co-cultured infected and uninfected cells. Cell survival was analysed by SRB staining and subsequent quantification.

As shown in figure 4.15, it was demonstrated that the survival of U87-MG glioma cells, treated with GCV, decreased exponentially with increasing ratio of Ad-sr39TK-infected to uninfected cells. Cell survival was 18 ± 0.01 % even if only 17 % of the whole cell population was infected with Ad-sr39TK, compared to the same approach without addition of GCV. This data indicates the action of an Ad-sr39TK-induced, HSV1-sr39TK/GCV-mediated bystander effect. No bystander effect was observed without GCV addition. Ad-delo-sr39TK-RGD also induced a bystander effect after addition of GCV, indicated by an inversely proportional decrease in cell survival with increasing ratio of infected to uninfected cells. When only 17 % of the cell population were infected, the cell survival was 45.9 ± 9.7 %. The larger amount of eradicated cells compared to the fraction of virus-infected cells indicated a bystander effect of the HSV1-sr39TK/GCV system. Ad-delo-sr39TK-RGD and Ad-sr39TK induced a similar bystander effect with GCV. The oncolytic activity of Ad-delo-sr39TK-RGD, shown in the setting without GCV, was directly proportional to the fraction of infected cells. The bystander effect, induced by GCV, led to enhanced cell killing compared to the oncolytic effect alone.

In EPP85-181RDB cells, there was a decrease of survival mediated by the HSV1-sr39TK/GCV-effect to 61 ± 0.04 %, when 50 % of the cell population were infected with Ad-sr39TK (figure 4.15). Survival reached 34 ± 0.002 % when 100 % of the cells were infected with Ad-sr39TK and subjected to GCV. As expected, there was no influence of Ad-sr39TK-infected cells without GCV on cell survival. In Ad-delo-sr39TK-RGD-infected cells with GCV, survival decreased with increasing ratio of infected to uninfected cells. Survival reached 65 ± 0.02 % even with 50 % infected cells. As observed with Ad-sr39TK and GCV, the fraction of infected cells corresponded to the fraction of dead cells (cell survival), indicating no additional bystander killing. Moreover, the oncolytic effect of Ad-delo-sr39TK-RGD alone resulted in stronger cell killing of the multidrug-resistant cell line than the combination of

virus and HSV1-sr39TK/GCV-mediated cytotoxicity, as only 30 % infected cells led to survival of 8 ± 0.001 %. A GCV concentration of 50 µg/ml was needed for Ad-delo-sr39TK-RGD- and Ad-sr39TK-infected EPP85-181RDB cells in order to cause a bystander cell killing with GCV similar to that in U87-MG cells (data not shown).

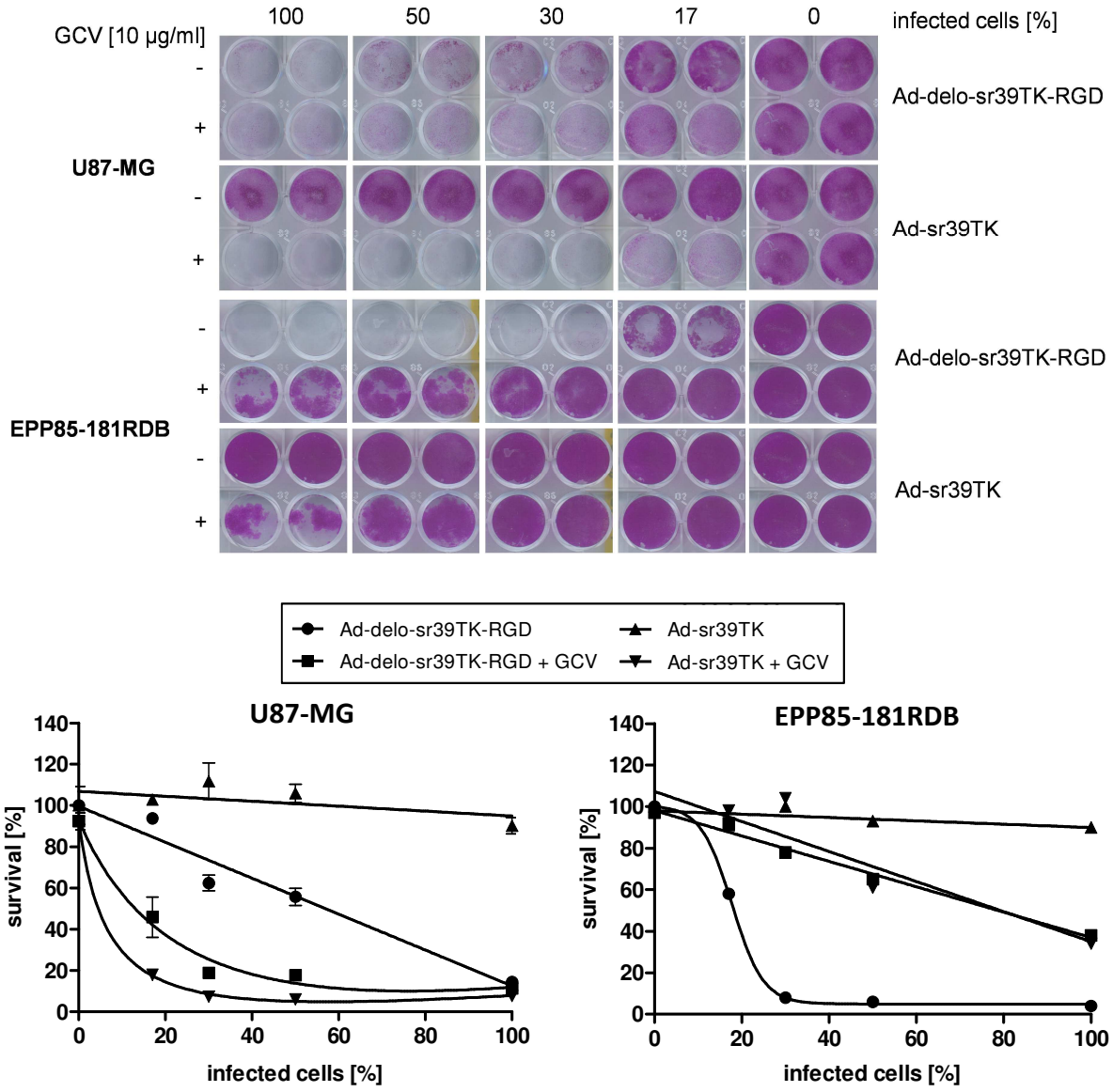

Figure 4.15: Bystander effect of oncolysis and HSV1-sr39TK/GCV-mediated cytotoxicity. U87-MG and EPP85-181RDB cells were infected with Ad-delo-sr39TK-RGD and Ad-sr39TK at MOI of 10 ifu/cell. Infected and uninfected cells were co-cultured at ratios 1:0 (100 % infected cells) to 1:5 (17 % infected cells) in a total population of 5 x 10^4 cells. GCV [10 µg/ml] was added 3 h after co-culturing and re-added 72 h after the first treatment. The potential bystander effect conducted by the adenoviruses in combination with GCV was evaluated by SRB-staining (above) and photometric quantification (below) 10 days after co-culture. Cell survival was quantified in percentage (mean±SD), referring to the survival of uninfected cells (100 %); n=2.

These results show that Ad-delo-sr39TK-RGD in cooperation with the HSV1-sr39TK/GCV-system exerted a strong bystander effect, which induced efficient cytotoxicity even in glioma cell populations

with a low fraction of infected cells. In multidrug-resistant pancreatic carcinoma cells, however, no significant enhancement of cell killing by a bystander effect with GCV was observed, as the fraction of infected cells corresponded to the amount of eradicated cells. This finding indicates a low susceptibility of the multidrug-resistant cells to GCV. Taking the results described in chapters 4.6. and 4.7. into account, EPP85-181RDB cells were not as successfully eradicated through the HSV1-sr39TK/GCV-mediated cytotoxicity as U87-MG cells and were not further investigated in this context.

4.8. Enhancement of the oncolytic potential of YB-1 dependent adenoviruses by TMZ

It is known that cytostatic drugs are able to enhance the translocation of YB-1 to the nucleus of tumour cells. Enhanced nuclear YB-1 accumulation results in augmented replication of YB-1 dependent oncolytic adenoviruses that consequently leads to an enhanced oncolytic effect [291, 292]. In order to prove whether treatment with TMZ leads to potentiated oncolytic effect of the adenoviruses in tumour cells, different experimental approaches were investigated by varying TMZ and viral doses. TMZ concentrations, similar to those used in clinical trials for the study of TMZ pharmacokinetics in human plasma [318, 319], were used in this experiment. Cell survival after treatment was analysed by SRB staining and quantification. The IC_{50} value of TMZ was higher than 500 µM in uninfected U87-MG and EPP85-181RDB cells. It was expected that a combined treatment of TMZ and oncolytic adenoviruses should decrease cell survival substantially.

Ad-delo-sr39TK-RGD led to cell eradication even at a MOI of 5 with rising TMZ concentrations (figure 4.16). MOI of 5 and 25 µM TMZ led to 49 ± 19.39 % survival of glioma cells. 25 µM TMZ was needed to decrease the survival to 10 ± 2.66 % at MOI of 10, and at MOI of 20 and 10 µM TMZ it was reduced to 12 ± 2.55 %. A potent oncolytic effect was observed at MOI of 50 and 100 regardless of TMZ concentration, resulting in reduction of survival to 6 %.

Ad-delo3-RGD did not result in enhanced oncolytic cell killing in combination with TMZ pre-treatment at the same level as Ad-delo-sr39TK-RGD at MOI of 5, 10 and 20 (figure 4.16). The cell survival at MOI of 5 and 10 with 250 µM TMZ was 61 ± 3.57 % and 55 ± 0.88 %, respectively. MOI of 20 of Ad-delo-3-RGD caused a more prominent decrease in cell survival than MOI of 5 and 10. At MOI of 20 and 50 µM TMZ, the fraction of surviving cells was 33 ± 4.75 %. A significant cell killing potential, similar to that of Ad-delo-sr39TK-RGD, was observed at MOI of 50 and 100, regardless of TMZ dose.

Ad-delo-shMGMT-RGD carries a shRNA sequence for silencing the expression of the cellular *MGMT* gene (figure 2.1). Silenced MGMT is no longer able to remove the cytotoxic adducts caused by TMZ and consequently the lack of MGMT-mediated repair mechanism leads to improved outcome of TMZ therapy [320]. Ad-delo-shMGMT-RGD is therefore expected to enhance tumour cell killing on the one

hand through TMZ-mediated and YB-1 dependent replication and on the other hand, by stimulation of the cytotoxic activity of TMZ. As shown in figure 4.16, Ad-delo-shMGMT-RGD displayed an MOI- and TMZ dose-dependent oncolytic potential, similar to that of Ad-delo-sr39TK-RGD. The cell survival at MOI of 5 and 50 µM TMZ was 46 ± 4.4 %. MOI of 10 and 50 µM TMZ resulted in 19 ± 11.9 % survival. At MOI of 20, 2.5 µM TMZ was necessary to reduce the cell survival to 19 ± 13.6 %. Similar to Ad-delo-sr39TK-RGD and Ad-delo3-RGD, MOI of 50 and 100 of Ad-delo-shMGMT-RGD caused almost complete eradication of glioma cells, regardless of TMZ dose.

Infection with Ad-sr39TK did not cause oncolytic activity in TMZ pre-treated cells (figure 4.16). The decrease of cell survival after infection with Ad-sr39TK was rather due to non-virally induced cytotoxicity by rising TMZ doses, as also observed in uninfected cells.

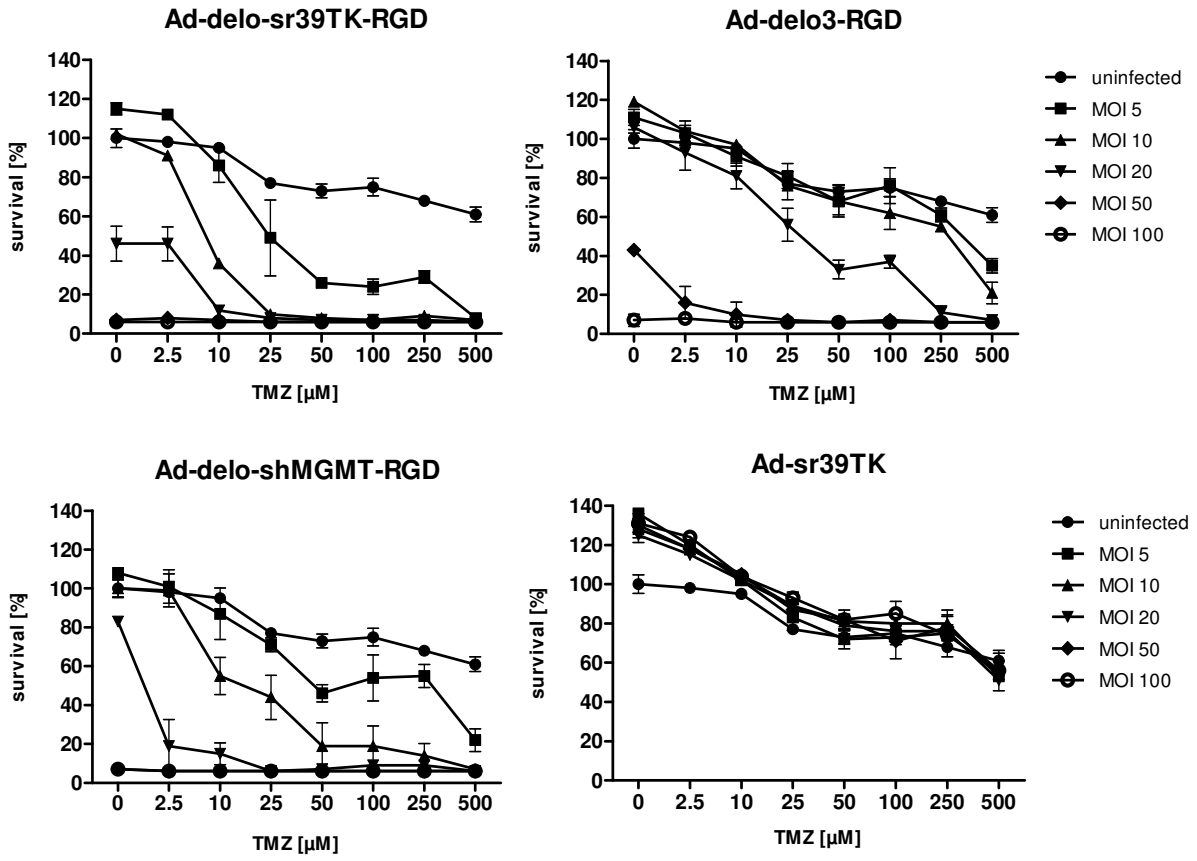

Figure 4.16: Enhancement of oncolytic effect by TMZ in glioma cells. U87-MG cells (2 x 10^3) were pre-treated for 24 h with varying doses of TMZ and infected at MOI of 5-100 ifu/cell with the indicated adenoviruses. Cell survival was determined 7 days post infection by photometric quantification of SRB-staining and displayed in percentage (mean±SD), referring to the survival of uninfected and untreated cells (100 %); n=3.

In EPP85-181RDB cells, TMZ post-treatment (figure 4.17) was more efficient for potentiation of oncolysis than TMZ pre-treatment (data not shown). 250 µM TMZ was necessary to be applied after infection with Ad-delo-sr39TK-RGD at a MOI of 100 to reduce the percentage of living cells to 35 ±

0.09 %, whereas 500 µM TMZ and MOI of 100 resulted in a decrease to only 4 ± 0.01 % survival (figure 4.17). Ad-delo3-RGD and Ad-delo-shMGMT-RGD mediated significant oncolysis and decrease in survival to 44 ± 0.05 % and 17 ± 0.1 %, respectively, with 500 µM TMZ. Ad-sr39TK-infected and uninfected cells were not affected by TMZ, except at a cytotoxic dose of 500 µM. Considering the low efficiency of TMZ-enhanced oncolysis in EPP85-181RDB cells, the cell line was not taken into account for further analyses.

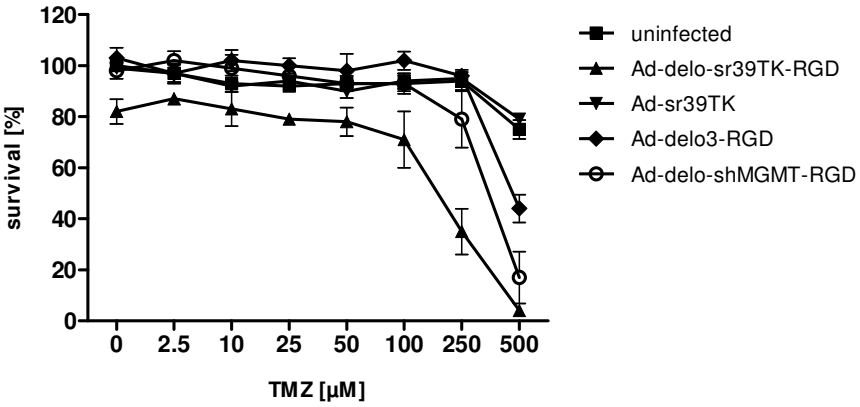

Figure 4.17: Enhancement of oncolytic effect by TMZ in multidrug resistant pancreatic carcinoma cells. EPP85-181RDB cells (2 x 10^3) were infected at MOI of 100 ifu/cell with the indicated adenoviruses and treated with varying doses of TMZ after infection. Cell survival after treatment was determined 7 days post infection by photometric quantification of SRB-staining. Cell survival is displayed in percentage (mean±SD), referring to the survival of uninfected and untreated cells (100 %); n=3.

The above described results show efficient TMZ-mediated augmentation of the oncolytic activity of YB-1 dependent adenoviruses in glioma cells. The oncolytic activity correlated with viral MOI and cytostatic drug dose, and was potentiated by TMZ even at low virus and TMZ doses. The oncolytic potential of Ad-delo-sr39TK-RGD was similar to that of Ad-delo-shMGMT-RGD, which has a dual function of mediating YB-1 dependent oncolysis and potentiation of TMZ cytotoxicity by silencing of *MGMT*. The enhancement of the oncolytic effect by TMZ in the multidrug-resistant EPP85-181RDB cell line was successful only after infection of cells at a high viral MOI and treatment with high TMZ doses post infection.

4.9. Improved cell killing by the combination of oncolytic potential, TMZ and HSV1-sr39TK/GCV-mediated cytotoxicity

4.9.1. Combined cell killing in 2D glioma culture

It was further analysed if TMZ and GCV enhance the killing of infected glioma cells through the combined activity of TMZ-mediated potentiation of oncolysis and HSV1-sr39TK/GCV-mediated cytotoxicity. Cell survival after virus infection and treatment with TMZ, GCV or TMZ plus GCV was analysed by SRB staining and quantification. In addition, the metabolic activity was investigated by XTT assay. As described in chapter 3.13.2, the XTT assay quantifies living and metabolically active cells, whereas SRB staining detects detached but intact cells, regardless of their viability and functional metabolism. A low concentration of GCV [0.5 µg/ml] and variable concentrations of TMZ, as well as a viral dose of 10 ifu/cell were chosen in order to be able to detect subtle effects.

In 2D glioma culture, GCV addition to Ad-delo-sr39TK-RGD-infected TMZ-untreated cells resulted in cell survival of 24 ± 10.66 % (cell killing of 80 %), compared to survival of 36 ± 13.41 % (cell killing of 60 %, not shown) after infection with Ad-delo-sr39TK-RGD and without treatment (figure 4.18 A). TMZ pre-treatment of Ad-delo-sr39TK-RGD-infected cells in combination with GCV led to a potentiated GCV-enhanced cytotoxic effect, even with only 2.5 µM TMZ (survival 13 ± 0.58 %). This effect caused a 2.7-fold reduction in survival compared to infected and untreated cells. Therefore, 2.5 µM TMZ in combination with 0.5 µg/ml GCV was sufficient to induce an oncolytic effect, which was able to eradicate about 90 % of the cell population. In addition, the reduction of cell survival by Ad-delo-sr39TK-RGD in combination with TMZ and GCV was stronger than TMZ-enhanced oncolysis elicited by Ad-delo3-RGD and Ad-delo-shMGMT-RGD at all TMZ concentrations analysed. The combination of TMZ pre-treatment and GCV reduced the cell survival of uninfected and Ad-sr39TK-infected glioma cells, probably due to toxicity of TMZ.

The results of the survival analysis by SRB quantification were confirmed by measurement of the metabolic activity of infected and treated cells. As shown in figure 4.18 B, the amount of metabolically active Ad-delo-sr39TK-RGD-infected cells was decreased from about 50 % to < 30 % when treated with TMZ plus GCV and correlated with cell survival, as demonstrated by SRB quantification. The reduction of the metabolic activity of Ad-delo3-RGD- and Ad-delo-shMGMT-RGD-infected cells upon combined treatment paralleled cell survival, as shown in figure 4.18 A. However, the oncolytic effect of Ad-delo-shMGMT-RGD (0 µM TMZ) resulted in a lower amount of living cells than detected by the analysis of cell survival in figure 4.18 A. Despite of the toxicity exerted by TMZ and GCV upon uninfected and Ad-sr39TK-infected cells (figure 4.18 A), over 60 % of these cells remained metabolically active after double treatment.

As demonstrated by some representative images of cell survival (figure 4.18 C), GCV addition to TMZ-pre-treated and Ad-delo-sr39TK-RGD-infected cells altered the morphology and induced lysis of the affected cells. While untreated oncolytic adenovirus-infected cells, or either TMZ- or GCV-treated Ad-delo-sr39TK-RGD-infected cells showed only signs of c.p.e. and appeared rounded, but without disrupted membranes (no necrosis), simultaneous TMZ and GCV treatment of cells infected with Ad-delo-sr39TK-RGD resulted in massive cell death (arrows). Cell death was also observed when TMZ concentrations lower than 10 µM were applied (data not shown). Cells, subjected to the combined effect of oncolysis, HSV1-sr39TK/GCV-mediated cytotoxicity and TMZ treatment, showed indications of a mixed type of cell death. On the one hand, some cells probably displayed apoptotic characteristics, indicated by formation and lysis of apoptotic bodies. On the other hand, few cells had a necrotic appearance, indicated by swelling and an enlarged nucleus. In contrast, Ad-delo3-RGD- and Ad-delo-shMGMT-RGD-infected cells displayed c.p.e. that was potentiated by TMZ, but not further enhanced by GCV. Thus, the mode of cell death, induced by HSV1-sr39TK/GCV, contributed to the combined TMZ-mediated- and oncolytic effect of the virus and was responsible for the low metabolic activity of Ad-delo-sr39TK-RGD-infected cells, as shown in figure 4.18 B. No major alteration in cellular morphology was observed in uninfected cells and cells infected with Ad-sr39TK and treated with TMZ and GCV, their number was however slightly reduced upon treatment.

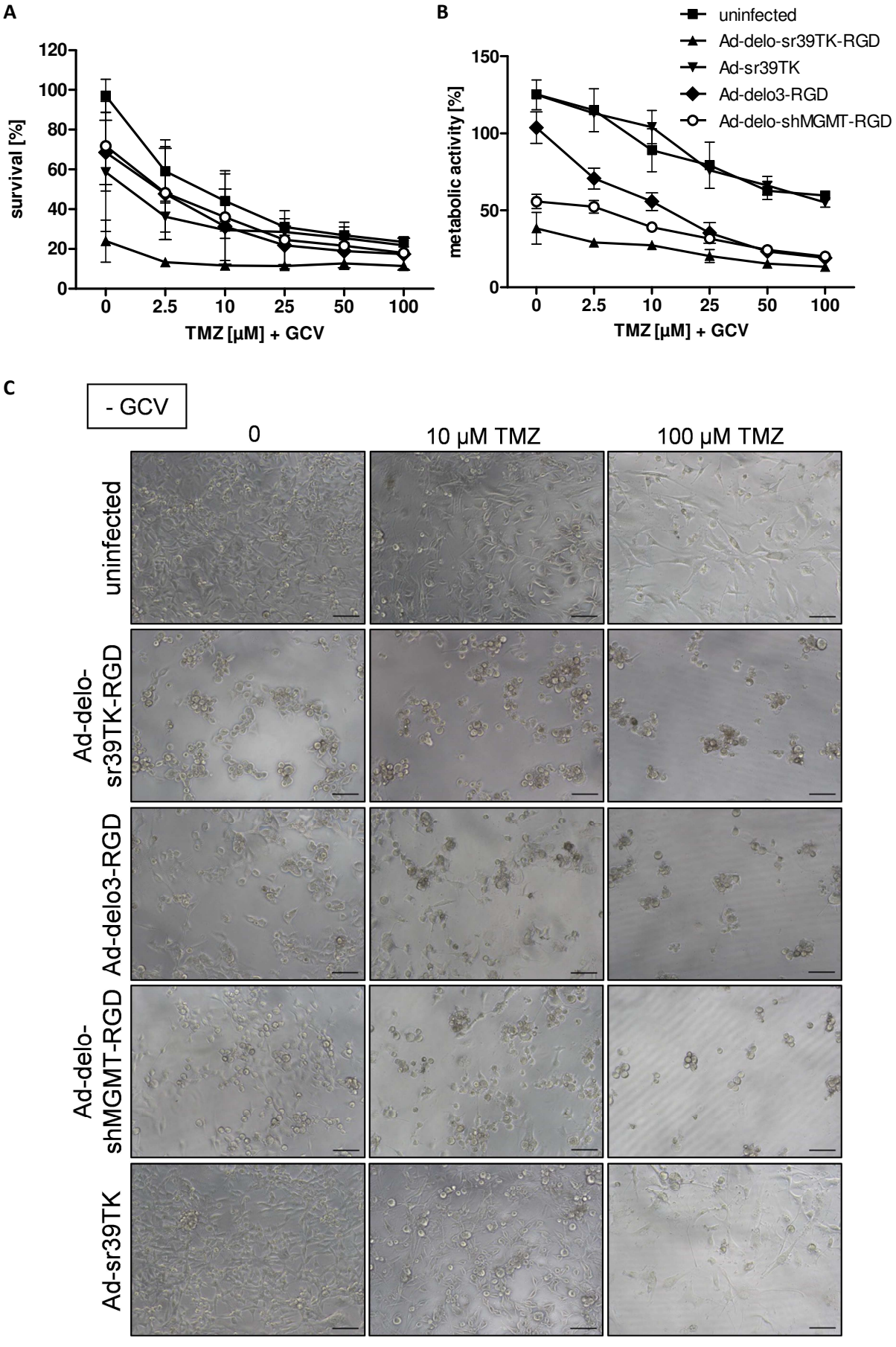
A
survival [%]
120
100
80
60
40
20
0
0
2.5
10
25
50
100
TMZ [µM] + GCV
B
metabolic activity [%]
150
100
50
0
uninfected
Ad-delo-sr39TK-RGD
Ad-sr39TK
Ad-delo3-RGD
Ad-delo-shMGMT-RGD
TMZ [µM] + GCV
C
- GCV
0
10 µM TMZ
100 µM TMZ
uninfected
Ad-delo-sr39TK-RGD
Ad-delo3-RGD
Ad-delo-shMGMT-RGD
Ad-sr39TK

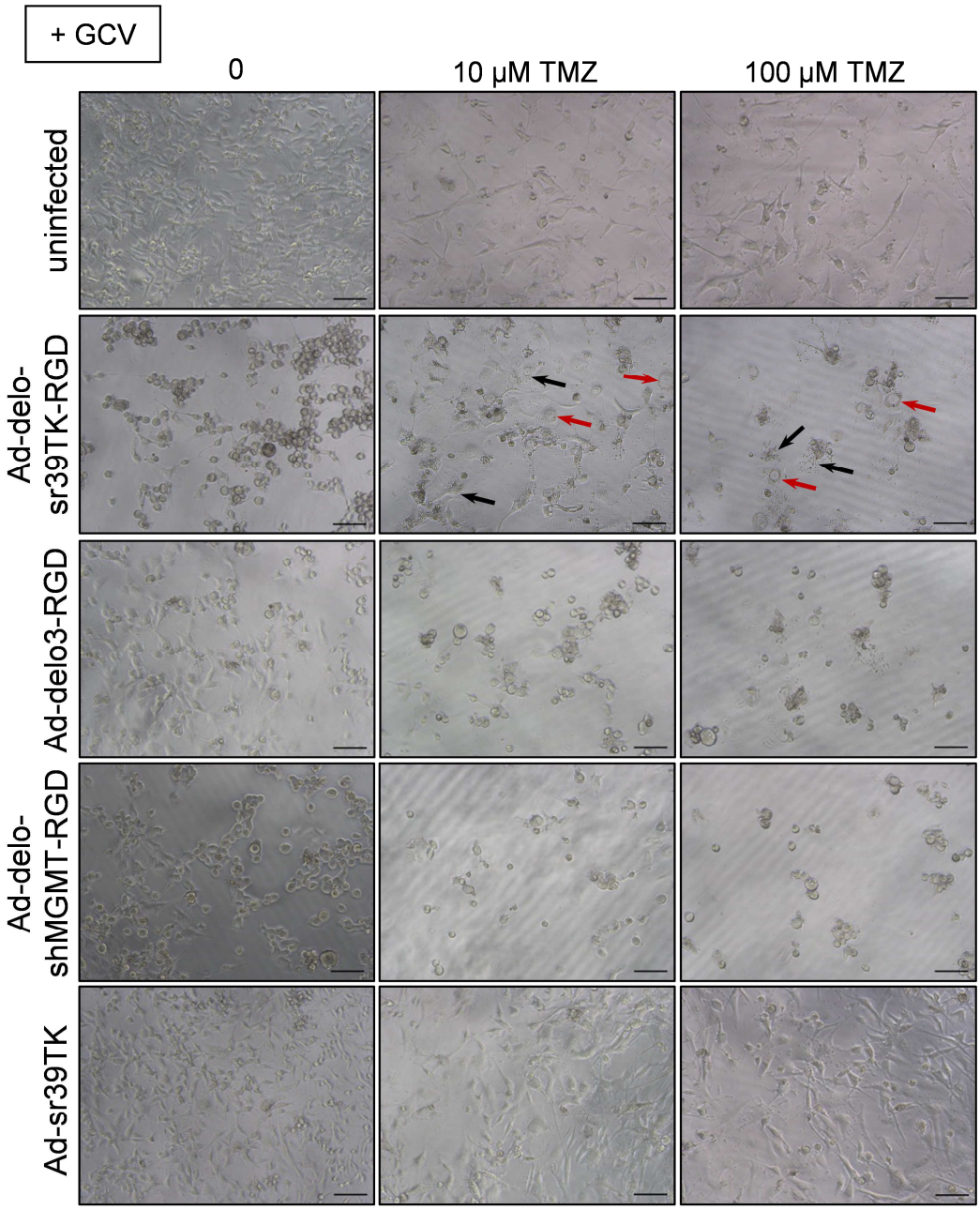

Figure 4.18: Improved cell killing by the combination of oncolytic effect, TMZ and HSV1-sr39TK/GCV-mediated cytotoxicity in glioma cells. U87-MG cells (2 x 10^3) were pre-treated for 24 h with varying doses of TMZ and infected at MOI of 10 ifu/cell with the indicated adenoviruses. GCV [0.5 µg/ml] was applied 24 h post infection. Cell survival after combined treatment was assessed 5 days post infection by photometric quantification of SRB-staining **(A)** and metabolic activity was analysed by XTT assay **(B)**. Cell survival or metabolic activity are displayed in percentage (mean±SD), referring to the survival or metabolic activity of uninfected and untreated cells (100 %); n=3. **C:** Representative images of U87-MG cells pre-treated with 0, 10 and 100 µM TMZ and infected as described above with or without GCV addition were taken in an inverted microscope 5 days post infection. Arrows indicate morphologic changes due to apoptotic (black) or necrosis-like (red) cell death. Scale bar: 100 µm.

4.9.2. Combined cell killing in 3D glioma spheroids

It was further investigated whether the HSV1-sr39TK/GCV-mediated cytotoxicity and TMZ-enhanced oncolysis can be translated from U87-MG monolayer culture into 3D spheroids of glioma cells. To increase the accessibility of cells in the inner spheroid layers and because of low cell killing at MOI of 10 ifu/cell (data not shown), spheroids were transduced with MOI of 50 ifu/cell. Moreover, 100 µM TMZ was applied in order to increase penetration of the drug into the 3D cell structure. The effect of viral oncolysis and single or combined TMZ and GCV treatment on spheroids was assessed by monitoring the spheroid growth and metabolic activity.

As indicated in figure 4.19 A, a combined application of TMZ [100 µM] and GCV [0.5 µg/ml] induced the strongest decrease of spheroid volume in Ad-delo-sr39TK-RGD-infected spheroids and resulted in growth retardation from day 4 till day 10 after infection, when spheroids were markedly reduced to their initial volume of 0.06 ± 0.003 mm^3. The combination between TMZ and GCV seemed to have a more pronounced effect than TMZ and GCV treatment alone. The volume of TMZ-treated or untreated Ad-delo-sr39TK-RGD-infected spheroids started to reduce 7 days post infection. At that time point the combined treatment was 3-times more effective than Ad-delo-sr39TK-RGD alone and 2-times more effective than Ad-delo-sr39TK-RGD in combination with TMZ. Ad-delo3-RGD- and Ad-delo-shMGMT-RGD-infected spheroids also displayed stronger growth retardation from day 2 to 4 due to the TMZ treatment, compared to virus alone. Their growth was not further affected by GCV. The oncolytic effect of Ad-delo-shMGMT-RGD alone was able to reduce spheroid growth 10 days after infection, whereas the oncolytic effect of Ad-delo3-RGD only prevented further spheroid growth 7 to 10 days post infection. However, TMZ elicited cellular toxicity also without oncolytic virus activity, as shown in untreated and in Ad-sr39TK-infected spheroids. Compared to Ad-delo-sr39TK-RGD, Ad-sr39TK did not induce a pronounced reduction in spheroid volume in combination with simultaneous TMZ and GCV treatment.

According to the results observed in Ad-delo-sr39TK-RGD-infected spheroids (figure 4.19 B), TMZ and GCV treatment alone as well as combined TMZ plus GCV treatment resulted in significant reduction of the cellular metabolic activity to 14 ± 0.4 %, 19 ± 1 % and 16 ± 1 %, respectively, compared to 26 ± 3 % metabolic activity of infected and untreated spheroids. TMZ induced a 2- to 4-fold reduction in the metabolic activity of Ad-delo3-RGD- and Ad-delo-shMGMT-RGD-infected spheroids, in relation to virus infection alone and virus with GCV treatment. In comparison, TMZ attenuated the metabolic activity of uninfected and Ad-sr39TK-infected spheroids only about 1.5-fold, as also demonstrated in figure 4.19 A. Moreover, the oncolytic activity of Ad-delo-sr39TK-RGD as single treatment induced the strongest reduction of spheroid metabolic activity amongst all oncolytic adenoviruses. Taken together, the analysis of the metabolic activity of spheroids confirmed the data of the spheroid growth monitoring.

Furthermore, detachment of cells from the rim of spheroids, infected with Ad-delo-sr39TK-RGD, Ad-delo3-RGD and Ad-delo-shMGMT-RGD, revealed an enhanced c.p.e. due to the oncolytic effect 10 days post infection (figure 4.19 C). The c.p.e. in additionally TMZ- or GCV-treated spheroids was not as prominent as the c.p.e. elicited in untreated spheroids, probably due to the fact that most of the infected cells had been already lysed or that their growth had been suppressed by the combination of oncolysis and drug treatment. No c.p.e. was induced in Ad-sr39TK-infected spheroids, but their growth was retarded by TMZ, similar to uninfected spheroids. The combination of oncolytic cell killing, TMZ and HSV1-sr39TK/GCV-mediated cytotoxicity (Ad-delo-sr39TK-RGD + GCV/TMZ + GCV) was superior to HSV1-sr39TK/GCV-mediated cytotoxicity alone (Ad-sr39TK + GCV) (figure 4.19 A-C).

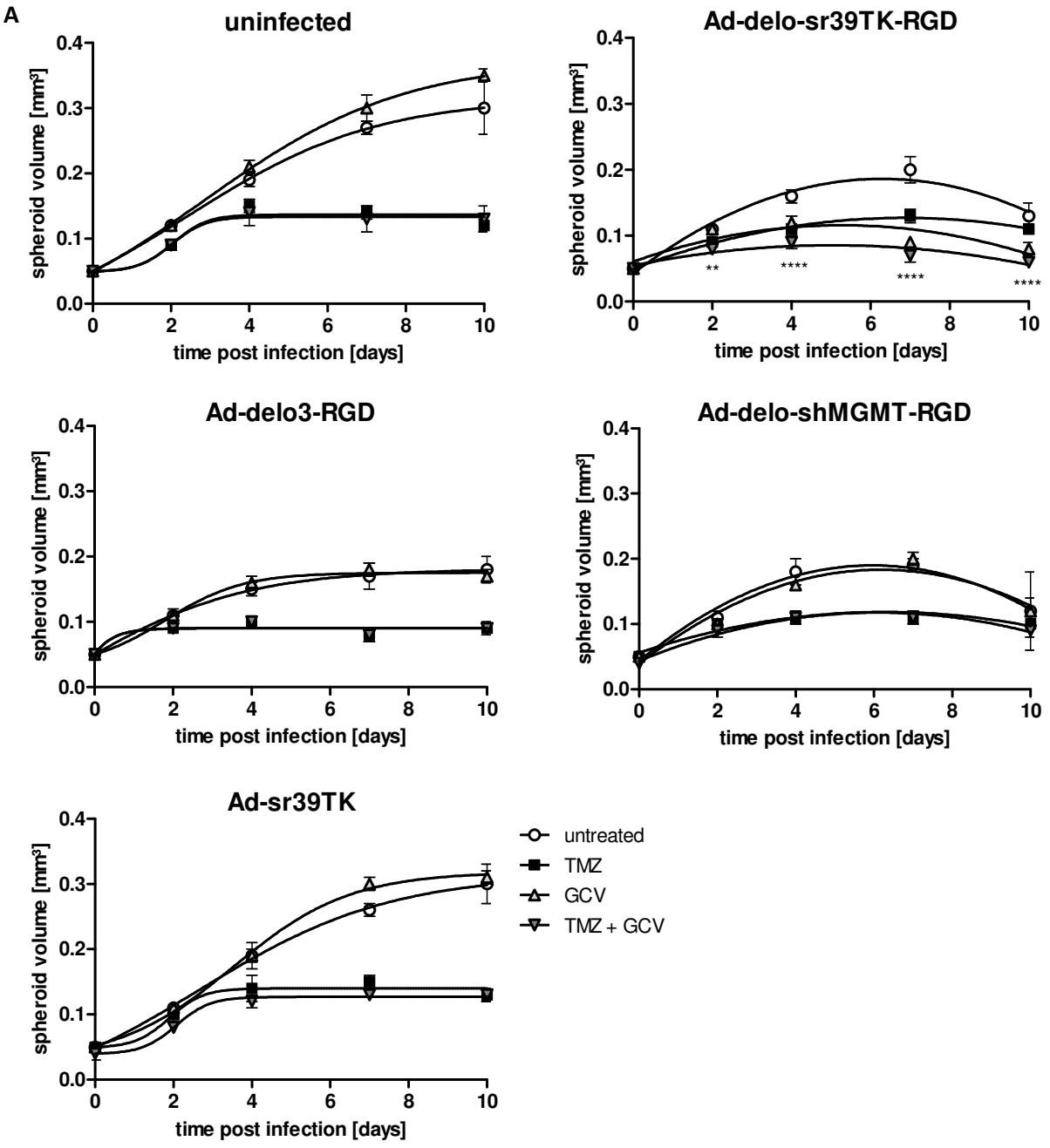

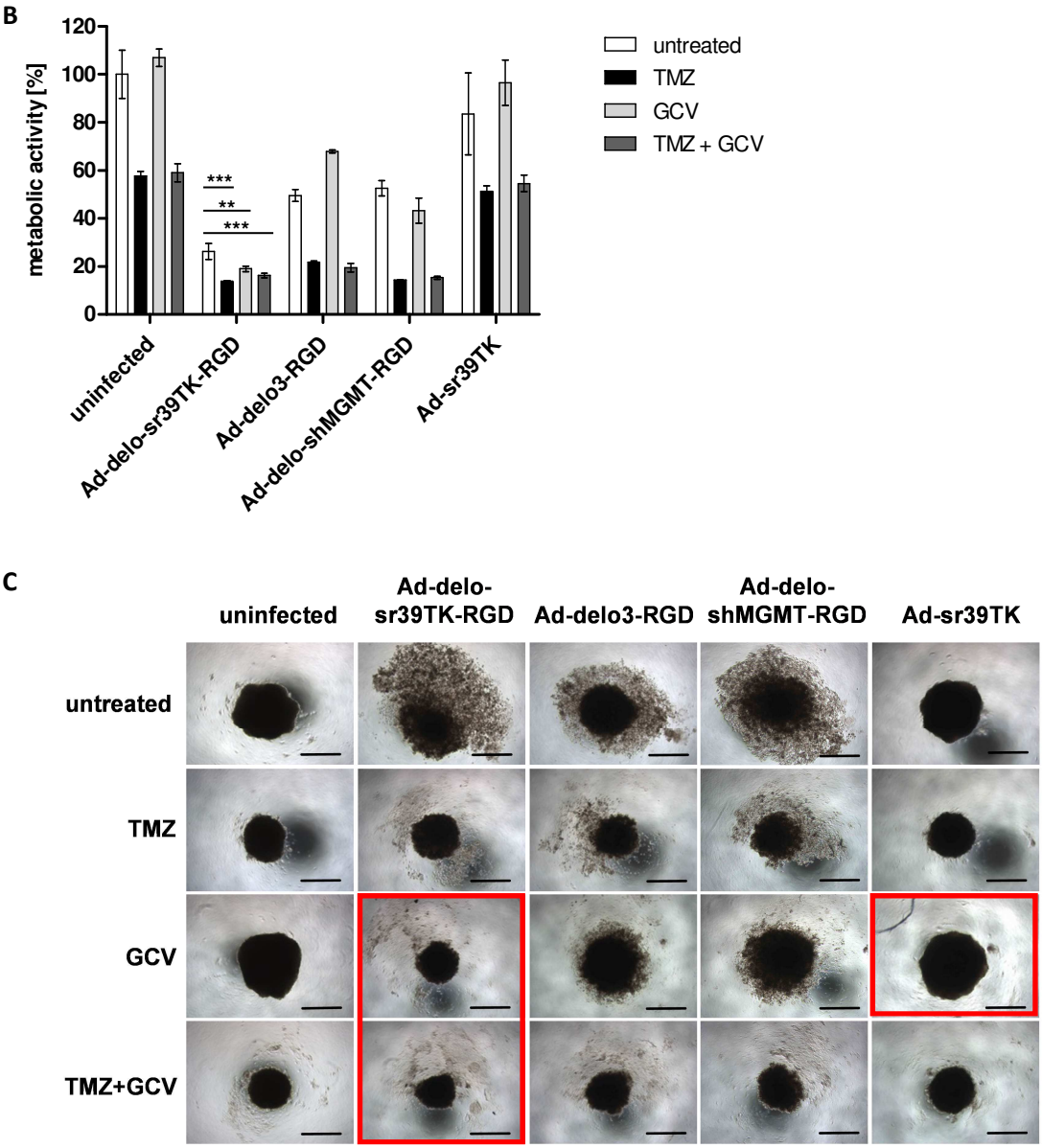

Figure 4.19: Improved cell killing by the combination of oncolytic effect, TMZ and HSV1-sr39TK/GCV-mediated cytotoxicity in 3D glioma spheroids. U87-MG-derived spheroids, consisting of about 1 x 10^5 cells, were treated with 100 µM TMZ 24 h before and immediately after infection with the indicated adenoviruses at MOI of 50 ifu/cell, and/or treated every three days with GCV [0.5 µg/ml] starting 24 h after infection. **A:** Spheroid growth was monitored on an inverted microscope by diameter measurement and volume calculation (mean±SD) 0, 2, 4, 7 and 10 days after infection; n=3. Asterisks indicate significant differences of Ad-delo-sr39TK-RGD, TMZ+GCV vs. untreated: **p=0.001-0.01 (day 2), ****p < 0.0001 (days 4-10), as calculated using two-way ANOVA with Tukey's multiple comparison test. **B:** XTT assay was performed with spheroids, which were infected and treated as described above, 10 days after infection. Asterisks indicate significant differences of Ad-delo-sr39TK-RGD, TMZ and TMZ+GCV vs. untreated: ***p=0.0001-0.001; Ad-delo-sr39TK-RGD, GCV vs. untreated: **p=0.001-0.01, as calculated using one-way ANOVA with Tukey's multiple comparison test. **C:** Representative images of infected and treated spheroids at day 10 after infection reveal c.p.e. caused by the oncolytic viruses. Significant differences between treatment combinations are marked (squares; Ad-delo-sr39TK-RGD, GCV and TMZ+GCV vs. Ad-sr39TK, GCV: ****p<0.0001). Scale bar: 500 µm.

It was thus demonstrated that the combination of oncolytic cell killing, HSV1-sr39TK/GCV-mediated cytotoxicity and TMZ-mediated enhancement of viral oncolysis potentiated the action of the single

treatments. The combined approach was efficient for eradication of glioma cells and 3D spheroids. Furthermore, it is suggested that glioma cells, subjected to the combined action of HSV1-sr39TK/GCV-mediated cytotoxicity and enhancement of oncolysis by TMZ, underwent probably a mixed type of cell death.

4.10. Enhancement of replication of YB-1 dependent adenoviruses by TMZ

As described previously, YB-1, which is accumulated into the nucleus as a result of treatment with cytostatic drugs, augments the replication of YB-1 dependent oncolytic adenoviruses [291, 292]. It was therefore investigated if TMZ was able to boost the replication of YB-1 dependent oncolytic adenoviruses in glioma cells and whether the augmented viral replication was responsible for the enhanced oncolytic activity of these viruses. Moreover, the influence of GCV and combined TMZ and GCV treatment upon adenoviral replication was analysed. Similar to the analyses of cell and spheroid survival after different treatment combinations (figures 4.18 and 4.19), a low concentration of GCV [0.5 µg/ml] was chosen in order to be able to detect subtle effects. A TMZ concentration of 50 µM, which enhanced adenoviral oncolysis of glioma cells substantially (figure 4.16), was applied to 2D cell culture. As for the analysis of spheroid growth (figure 4.19), 100 µM TMZ was applied to spheroids also in this experiment. Adenoviral replication analyses were performed by absolute real-time qPCR with DNA isolated from infected 2D glioma culture and 3D glioma spheroids.

4.10.1. Enhancement of replication in 2D glioma culture

In 2D glioma culture, continuous TMZ treatment induced a highly significant 8-fold increase of Ad-delo-sr39TK-RGD DNA copy number 72 h post infection, compared to a 5-fold and 2-fold replication enhancement of Ad-delo3-RGD and Ad-delo-shMGMT-RGD, respectively, related to untreated infected samples (figure 4.20). Because of its replication-deficient character, no increase in DNA amount of Ad-sr39TK was induced by TMZ. Simultaneous TMZ and GCV treatment resulted in an only 1.7-fold replication augmentation of Ad-delo-sr39TK-RGD, related to Ad-delo-sr39TK-RGD and GCV treatment only. Moreover, GCV reduced the DNA amount of Ad-delo-sr39TK-RGD 3000-fold, as compared to virus infection alone, and 13,700-fold in combination with TMZ, as compared to virus plus TMZ treatment. There is strong evidence that the reduction of the DNA copy number of Ad-delo-sr39TK-RGD by GCV and TMZ plus GCV was caused by attenuation of viral DNA replication by the HSV1-sr39TK/GCV-mediated cytotoxicity (figures 4.18 A and 4.18 B), acting on the DNA of replicating HSV1-TK-bearing adenoviruses. GCV addition did not alter the replication kinetics of the GCV-insensitive adenoviruses Ad-delo3-RGD and Ad-delo-shMGMT-RGD, consequently TMZ and combined TMZ plus GCV treatment caused a similar increase in DNA replication. Single or double treatment did not influence the replication of Ad-sr39TK.

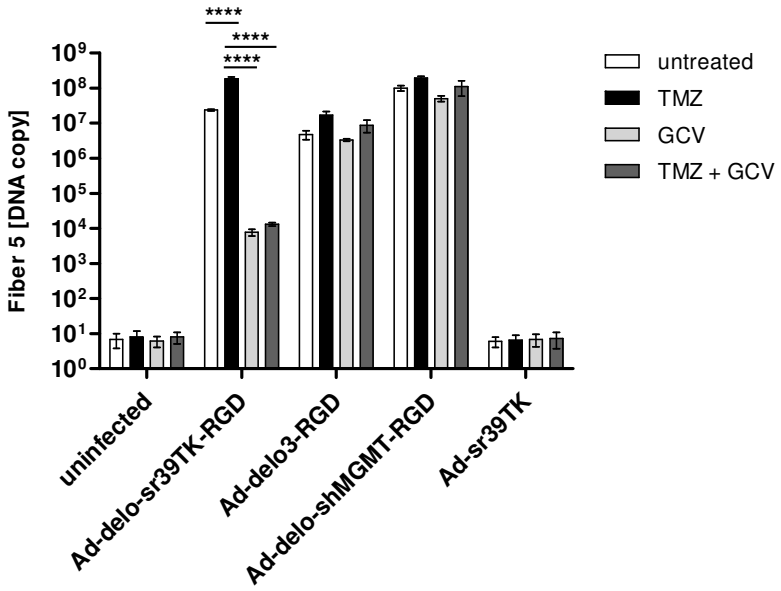

Figure 4.20: Enhancement of oncolytic adenoviral replication by TMZ in 2D culture of glioma cells. U87-MG cells (5 x 10^4) were treated with 50 µM TMZ 24 h before and immediately after infection with the indicated adenoviruses. Infections were performed at MOI of 10 ifu/cell. GCV [0.5 µg/ml] was added 24 h post infection and incubated for 48 h. DNA was isolated from infected cells by phenol-chloroform extraction. *Fiber 5* gene copy number was detected by absolute real-time qPCR of 2 ng DNA (mean±SD); n=3. Asterisks indicate significant differences between treatment approaches (only shown for Ad-delo-sr39TK-RGD in terms of simplification): ****$p < 0.0001$, as calculated using one-way ANOVA with Tukey's multiple comparison test.

4.10.2. Enhancement of replication in 3D glioma spheroids

The enhancement of replication of the oncolytic adenoviruses by TMZ was further investigated in infected 3D glioma spheroids 48 h after infection (figure 4.21). Continuous TMZ application induced a 27-fold replication increase of Ad-delo-sr39TK-RGD DNA, compared to an 11.4-fold and 18.9-fold increase of Ad-delo3-RGD and Ad-delo-shMGMT-RGD DNA, respectively, related to untreated spheroids (figure 4.21 A). As expected, TMZ did not enhance the replication of Ad-sr39TK. Similar to 2D culture, but to a lesser extent, GCV addition to TMZ-untreated or TMZ-treated spheroids 24 h after infection attenuated the replication of Ad-delo-sr39TK-RGD significantly, compared to infected TMZ-/GCV-untreated spheroids. As observed in 2D culture, GCV did not affect Ad-delo3-RGD and Ad-delo-shMGMT-RGD replication negatively.

In parallel with *Fiber 5* replication, the replication of the *HSV1-sr39TK* transgene in Ad-delo-sr39TK-RGD-infected spheroids was enhanced 1.7-fold by TMZ (figure 4.21 B). As for *Fiber 5*, the replication of *HSV1-sr39TK* was attenuated 10- to 25-fold by GCV and combined TMZ plus GCV treatment, as compared to untreated or TMZ-treated Ad-delo-sr39TK-RGD-infected spheroids. The lower level of replication enhancement of *HSV1-sr39TK* than that of *Fiber 5* by TMZ could be due to the different efficiency of the detection chemistries used for detecting *HSV1-sr39TK* and *Fiber 5*, as also described in chapter 4.3. The replication of the transgene in Ad-sr39TK was not augmented by TMZ.

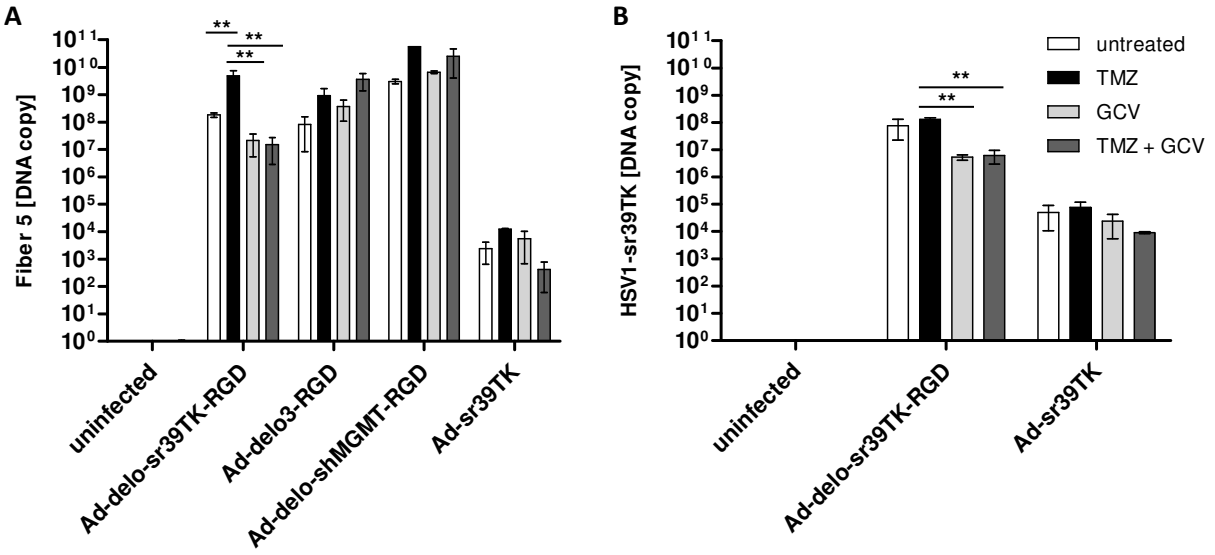

Figure 4.21: Enhancement of oncolytic adenoviral replication by TMZ in 3D glioma spheroids. U87-MG spheroids with volumes of 0.1-0.18 mm³ and consisting of about 1 x 10^5 cells were treated with 100 µM TMZ 24 h before and immediately after infection with the indicated adenoviruses. Infections were performed at MOI of 50 ifu/cell. GCV [0.5 µg/ml] was added 24 h post infection and incubated for additional 24 h. DNA was isolated from infected spheroids by phenol-chloroform extraction. *Fiber 5* **(A)** and *HSV1-sr39TK* **(B)** gene copy number was detected by absolute real-time qPCR of 2 ng DNA (mean±SD); n=3. Asterisks indicate significant differences between treatment approaches (only shown for Ad-delo-sr39TK-RGD in terms of simplification): **p=0.001-0.01, as calculated using one-way ANOVA with Tukey's multiple comparison test.

TMZ caused an efficient augmentation of oncolytic adenoviral replication and transgene DNA accumulation in 2D glioma culture and in 3D glioma spheroids. The enhancement of viral replication by TMZ verified the concept of YB-1 dependent oncolysis in the presence of cytotoxic stress. The augmented replication of the oncolytic adenoviruses resulted in enhancement of both oncolysis and combined oncolytic and HSV1-sr39TK/GCV-mediated cytotoxicity in 2D culture and 3D spheroids, as described in chapter 4.8. and chapter 4.9. However, the HSV1-sr39TK/GCV-mediated cytotoxicity inhibited the DNA replication of Ad-delo-sr39TK-RGD.

4.11. Release and infectivity of newly synthesised viral particles from infected and drug-treated 3D glioma spheroids

The infectivity of newly synthesised and released oncolytic adenoviral particles from infected spheroids was determined by titration of the viral particles using End-point dilution assay. It was also analysed whether the viral titre changed upon TMZ, GCV or combined TMZ plus GCV treatment. Ad-delo-sr39TK-RGD was compared to an oncolytic (Ad-delo3-RGD) and replication-deficient (Ad-sr39TK) adenovirus in respect of infectivity of released particles.

The infectious titre of newly synthesised and released adenoviral particles from infected non-treated spheroids was 1.42 x 10^6 pfu/ml for Ad-delo-sr39TK-RGD and 7.04 x 10^5 pfu/ml for Ad-delo3-RGD two

days post infection, and was not further enhanced by TMZ treatment at that time point (figure 4.22). GCV and combined TMZ plus GCV addition did not result in markedly reduced viral release. The infectious progeny increased to 2.94 x 10^{11} pfu/ml for Ad-delo-sr39TK-RGD and 3.01 x 10^{7} pfu/ml for Ad-delo3-RGD 4 days post infection. TMZ treatment augmented the release of Ad-delo-sr39TK-RGD particles 68-fold, compared to only 1.4-fold for Ad-delo3-RGD. Therefore, the enhancement of viral replication by TMZ (figure 4.21) correlated with an increase of the release of new infectious viral particles. Following GCV addition and combined TMZ and GCV treatment, the amount of released Ad-delo-sr39TK-RGD particles was decreased over 1000-fold in relation to untreated spheroids. GCV treatment did not alter Ad-delo3-RGD viral release. 10 days after infection, TMZ enhanced the viral release of Ad-delo-sr39TK-RGD 36-fold compared to virus infection alone, although the overall viral titre decreased significantly, probably because of pronounced cell killing. A decrease was also observed for the titre of released Ad-delo3-RGD particles upon single and combined treatment. According to its replication-deficiency, Ad-sr39TK did not show increase of the titre of its progeny over time.

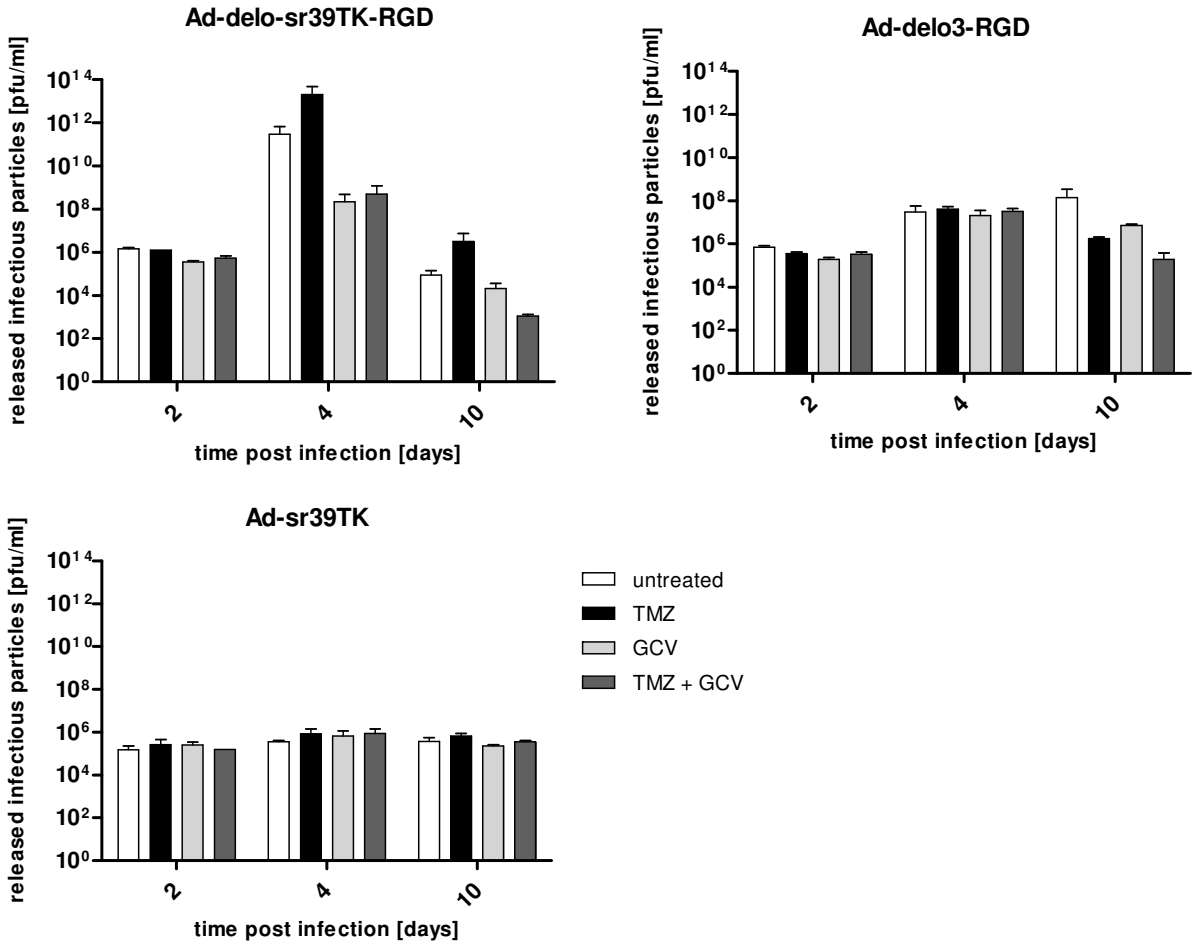

Figure 4.22: Release and infectivity of newly synthesised viral particles from infected 3D glioma spheroids. U87-MG spheroids with volumes of 0.1-0.18 mm³, consisting of about 1 x 10^{5} cells, were infected with MOI of 50 ifu/cell of the indicated adenoviruses after pre-treatment with 100 µM TMZ for 24 h. Following an anew

treatment with 100 µM TMZ directly after infection, GCV [0.5 µg/ml] was added 24 h post infection. Supernatants containing released viral particles were collected 2, 4 and 10 days after infection. Titres of released viral particles, defined as plaque forming units per ml (pfu/ml), were determined in supernatants by End-point dilution assay in HEK293 cells (mean±SD); n=2.

As in 2D culture, YB-1 dependent oncolytic adenoviruses showed successful viral release and infectivity of newly synthesised viral particles in 3D glioma spheroids. The release of Ad-delo-sr39TK-RGD particles was enhanced by TMZ as predicted by viral replication. Moreover, the combined oncolytic effect and HSV1-sr39TK/GCV-mediated cytotoxicity diminished the production of infectious progeny in spheroids, infected with the armed oncolytic adenovirus.

4.12. Adenovirus dissemination and HSV1-sr39TK expression in 3D glioma spheroids

In the following, viral dissemination and transgene expression in spheroids, transduced with oncolytic adenoviruses and treated with TMZ, GCV or a combination of TMZ and GCV, was explored. For this purpose, viral hexon protein and HSV1-sr39TK expression was analysed by simultaneous immunodetection on cryosections of spheroids.

The spread of Ad-delo-sr39TK-RGD, Ad-delo3-RGD and Ad-delo-shMGMT-RGD, as visualised by hexon staining, was mainly restricted to several outer layers of non-drug treated and TMZ-treated spheroids 48 h after infection, but progression to the inner layers was also observed (figure 4.23). The oncolytic adenoviruses were evenly distributed throughout the spheroid layers. A co-localisation of hexon and HSV1-sr39TK expression was observed in Ad-delo-sr39TK-RGD-infected spheroids. Upon GCV and combined TMZ and GCV treatment, adenoviral localisation and transgene expression were focused to only few cells of the outer spheroid layer. Regardless of treatment approach, the oncolytic adenoviruses displayed a prominent lateral spread within a single cell layer of some spheroids, rather than a medial spread, as indicated most distinctively for Ad-delo-sr39TK-RGD (untreated), Ad-delo3-RGD (TMZ + GCV) and Ad-delo-shMGMT-RGD (GCV). This phenomenon was not observed in Ad-sr39TK-infected spheroids, where the overall adenoviral distribution was hampered by the replication-deficient character of the virus. HSV1-sr39TK expression was restricted only to the outer layers of Ad-delo-sr39TK-RGD- and Ad-sr39TK-infected spheroids, regardless of treatment approach. Considering the replication of oncolytic adenoviruses, an enhanced viral spread was observed both in untreated and TMZ-treated spheroids. In contrast, GCV or combined TMZ and GCV treatment impaired intercellular viral dissemination, but not viral replication within spheroid cells, as indicated by the strong localised hexon expression, which resulted in decrease of overall particle amount. These data are consistent with the adenoviral DNA replication pattern as described in chapter 4.10.2.

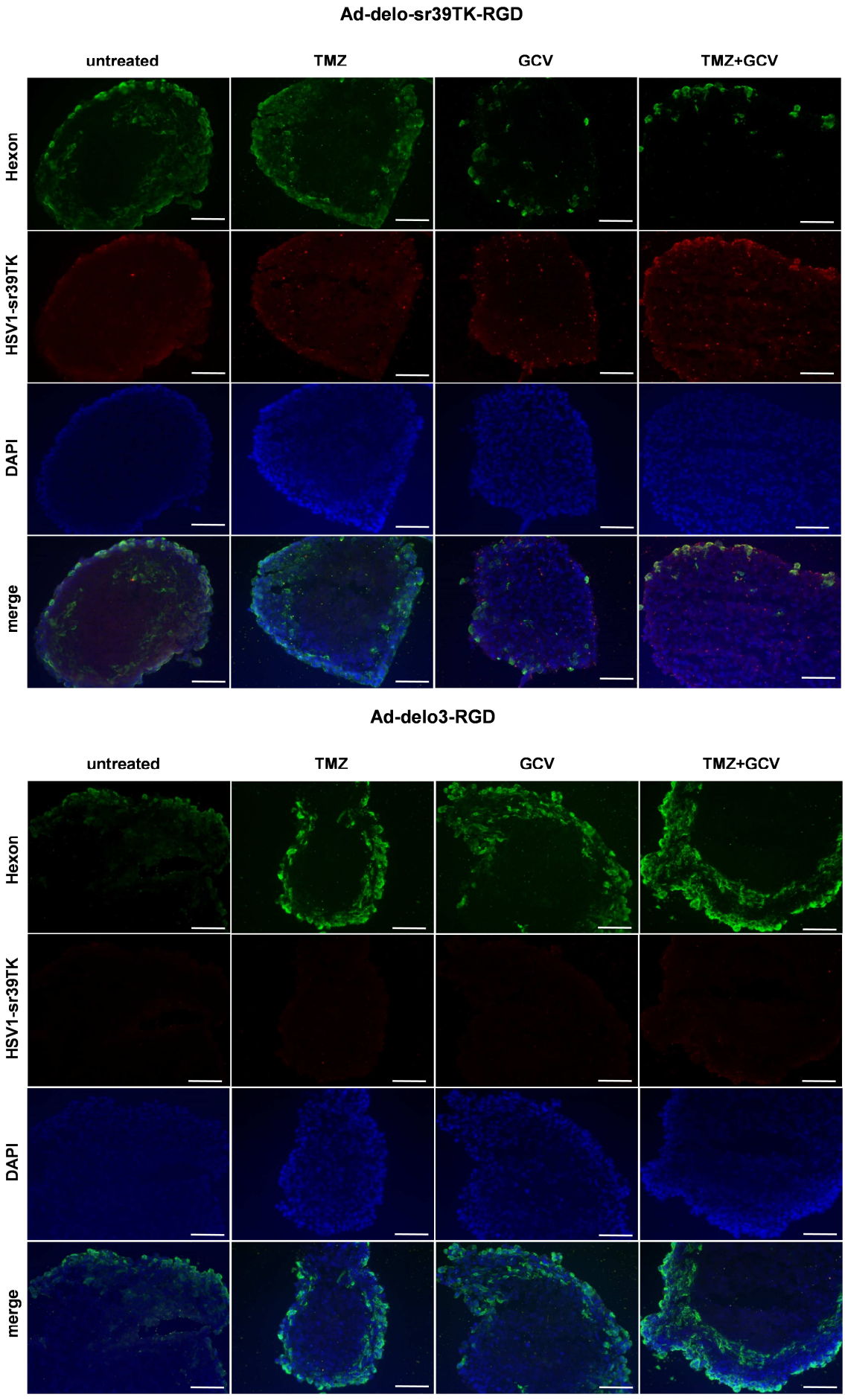
Ad-delo-sr39TK-RGD
untreated
TMZ
GCV
TMZ+GCV
Hexon
HSV1-sr39TK
DAPI
merge
Ad-delo3-RGD
untreated
TMZ
GCV
TMZ+GCV
Hexon
HSV1-sr39TK
DAPI
merge

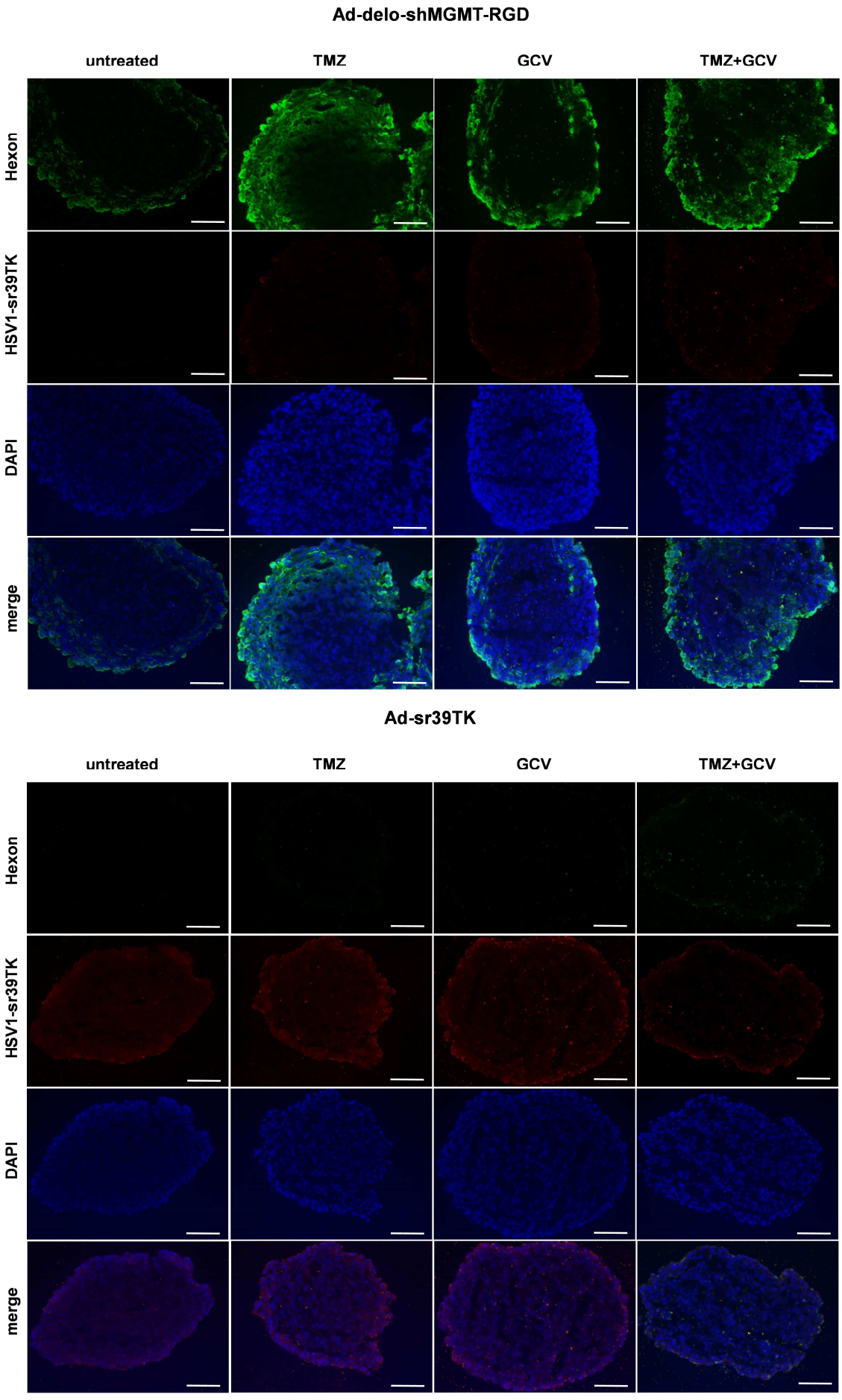
Ad-delo-shMGMT-RGD
untreated
TMZ
GCV
TMZ+GCV
Hexon
HSV1-sr39TK
DAPI
merge
Ad-sr39TK
untreated
TMZ
GCV
TMZ+GCV
Hexon
HSV1-sr39TK
DAPI
merge

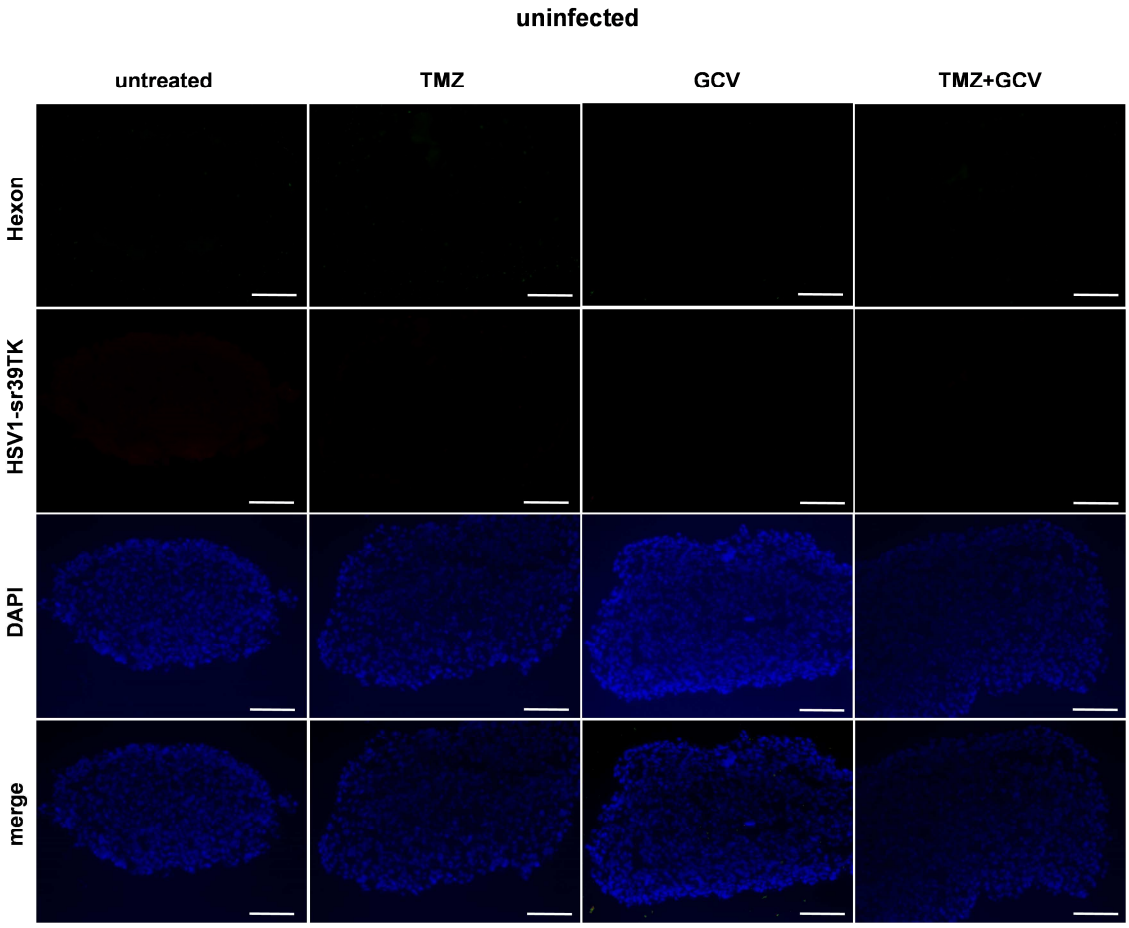

Figure 4.23: Adenovirus dissemination and HSV1-sr39TK expression in 3D spheroid culture model. U87-MG spheroids with volumes of 0.1-0.18 mm³ and consisting of about 1 x 10^5 cells were infected with MOI of 50 ifu/cell of the indicated adenoviruses after pre-treatment with 100 µM TMZ for 24 h. TMZ treatment was repeated again directly after infection and GCV [0.5 µg/ml] was added once 24 h post infection. Immunodetection of adenoviral hexon protein and HSV1-sr39TK was performed on cryosections of infected and treated spheroids 48 h post infection. Cell nuclei were visualized using DAPI staining. Representative sections show the widest diameter of spheroids. Scale bar: 100 µm.

Thus, as a prerequisite for cell killing, the YB-1 dependent oncolytic adenoviruses displayed successful infectivity and spread within glioma spheroids due to their replication competence. In addition, Ad-delo-sr39TK-RGD was able to trigger HSV1-sr39TK expression in parallel with adenoviral replication. However, adenoviral spread was attenuated by the inhibition of viral replication by the HSV1-sr39TK/GCV-mediated suicide system.

4.13. Uptake of [^{18}F]-FHBG by HSV1-sr39TK-expressing glioma cells

In order to evaluate the potential of the armed oncolytic adenovirus for non-invasive imaging using *HSV1-sr39TK* as a reporter gene, *in vitro* uptake studies using the enzymatic activity of HSV1-sr39TK for metabolising the radiotracer [^{18}F]-FHBG were performed by gamma-counting and PET imaging.

4.13.1. [^{18}F]-FHBG accumulation in 2D glioma culture

Regarding the radiotracer uptake in 2D glioma culture, a 2.8-fold lower radiotracer accumulation was mediated by HSV1-sr39TK, when expressed by Ad-delo-sr39TK-RGD, than when delivered by Ad-sr39TK, two days post infection (figure 4.24 A). Thus, these data suggest that the enzyme level of HSV1-sr39TK was attenuated by the progressive oncolytic potential of Ad-delo-sr39TK-RGD. As expected, only background radiotracer accumulation was detected in uninfected and Ad-delo3-RGD-infected glioma cells. The replication-competent adenovirus Ad-delo-sr39TK-RGD was analysed for alteration of its ability to induce radiotracer accumulation over time due to an influence of the viral oncolytic potential and HSV1-sr39TK/GCV-mediated cytotoxicity on transgene expression (figure 4.24 B). The highest uptake was detected three days after infection, when HSV1-sr39TK gave rise to a significant 5.4-fold increase of accumulated radiotracer, compared to the uptake on day 1. GCV addition 24 h prior to the uptake study led to a 2-fold decrease in radiotracer accumulation, compared to the respective approach without GCV, indicating HSV1-sr39TK/GCV-mediated cytotoxicity. Thus, the uptake of radiotracer was positively influenced by the adenoviral replication competence, but was attenuated by HSV1-sr39TK/GCV-mediated cell killing, as demonstrated previously. However, cytotoxicity was not as excessive as to abolish radiotracer accumulation completely. Background levels of radiotracer accumulation were detected in uninfected cells.

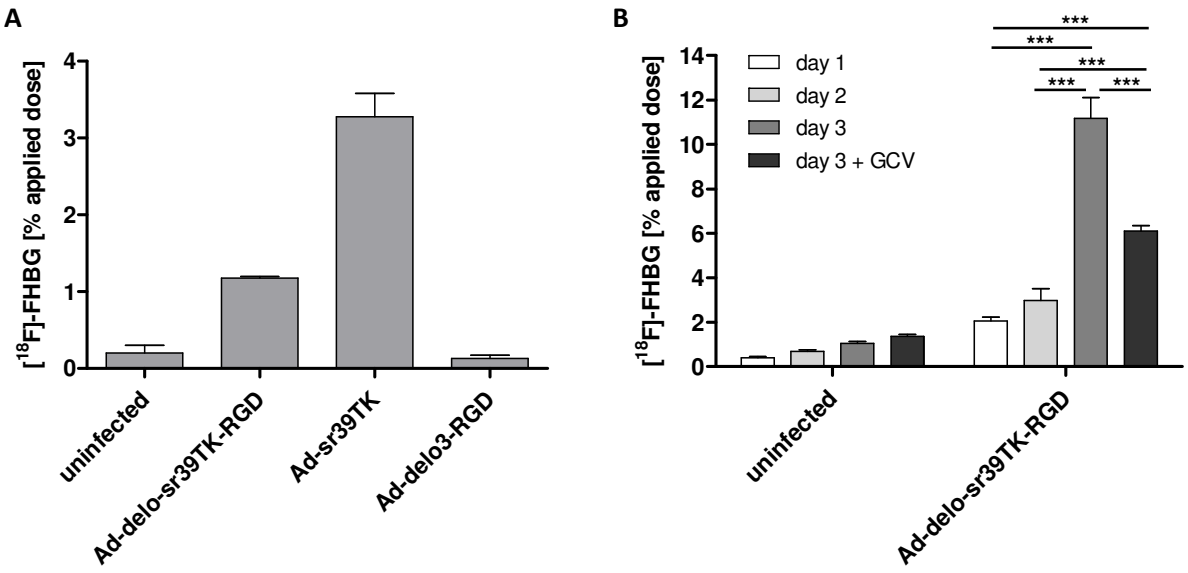

Figure 4.24: Accumulation of [^{18}F]-FHBG in HSV1-sr39TK-expressing glioma cells. 2D culture of U87-MG cells (1 x 10^5) were infected with the indicated adenoviruses at MOI of 10 ifu/cell. [^{18}F]-FHBG uptake was performed

using 1 x 10^5 cells 2 days post infection **(A)** or 1-3 days post infection with GCV [0.5 µg/ml] addition 24 h prior to performing the uptake study on day 3 **(B)**. After labelling with 0.1 MBq [^{18}F]-FHBG per 1 x 10^5 cells, the accumulated radiotracer due to HSV1-sr39TK activity was released from the cells using 1M NaOH and measured by gamma-counting. Accumulated radiotracer dose was calculated as % of total applied (100 %) [^{18}F]-FHBG dose (mean±SD); n=3. Asterisks indicate significant differences between treatment approaches. ***p=0.0001-0.001, as calculated using one-way ANOVA with Tukey's multiple comparison test.

4.13.2. [^{18}F]-FHBG accumulation in 3D glioma spheroids

Measurement of the uptake activity of the enzyme HSV1-sr39TK in 3D spheroids by gamma-counting revealed a slight decrease in radiotracer accumulation upon TMZ treatment of Ad-delo-sr39TK-RGD-infected spheroids, compared to untreated Ad-delo-sr39TK-RGD-infected spheroids (figure 4.25). Radiotracer accumulation was further reduced by GCV treatment and combined TMZ plus GCV application in Ad-delo-sr39TK-RGD-infected spheroids, compared to untreated virus-infected spheroids, indicating an effect of the HSV1-sr39TK/GCV-mediated cytotoxicity in combination with the oncolytic activity of the virus. However, the overall radiotracer accumulation levels in Ad-delo-sr39TK-RGD-infected spheroids were about 10-fold lower than the respective accumulation levels in 2D cell culture three days post infection (figure 4.24), suggesting an influence of the spheroidal geometry on the uptake capacity. Accumulation of metabolised [^{18}F]-FHBG in untreated Ad-sr39TK-infected spheroids was lower than in untreated Ad-delo-sr39TK-RGD-infected spheroids and was not markedly influenced by treatment with TMZ, GCV or by combined TMZ and GCV treatment.

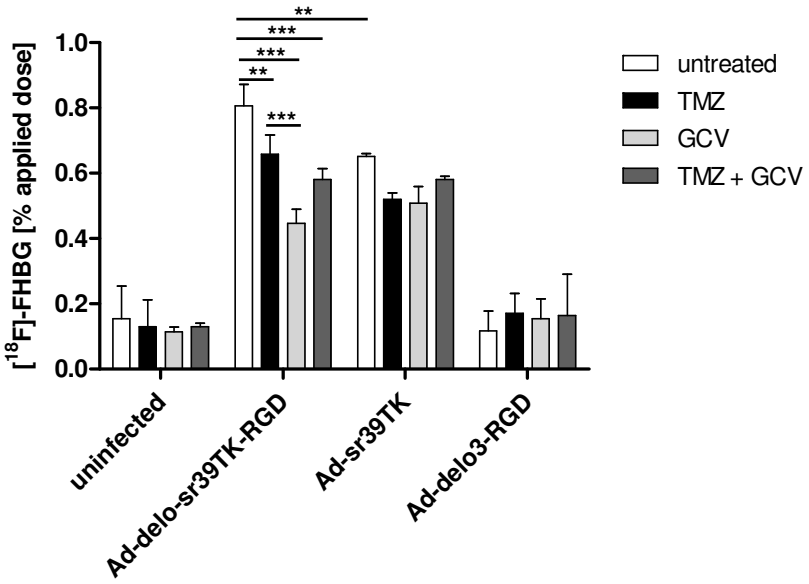

Figure 4.25: Accumulation of [^{18}F]-FHBG in HSV1-sr39TK-expressing 3D glioma spheroids. U87-MG-derived spheroids, containing about 1 x 10^5 cells, were infected at MOI of 50 ifu/cell with the indicated adenoviruses. Spheroids were treated with 100 µM TMZ 24 h before and directly after infection and/or treated with 0.5 µg/ml GCV 24 h after infection. Uptake was performed with 0.1 MBq [^{18}F]-FHBG per spheroid 4 days after infection. Accumulated radiotracer was released from spheroids using 1M NaOH measured by gamma-counting. Radiotracer dose was calculated as % of total applied (100 %) [^{18}F]-FHBG dose (mean±SD); n=3.

Asterisks indicate significant differences between treatment approaches. **p=0.001-0.01, ***p=0.0001-0.001, as calculated using one-way ANOVA with Tukey's multiple comparison test.

The feasibility of HSV1-sr39TK for nuclear non-invasive imaging as well as the spatial distribution of Ad-delo-sr39TK-RGD and Ad-sr39TK were additionally examined by PET measurement of [^{18}F]-FHBG accumulation in virus-infected spheroids (figure 4.26). The accumulated radiotracer activity into representative infected and/or drug-treated spheroids is displayed in figure 4.26 A, showing a single spheroid per well and no overlap between the signals in the wells. Each region of interest (ROI) analysed (circle) had an average volume of 7 mm^3, which corresponded to the actual mean spheroid volume (data not shown). ROI analysis of the single spheroids allowed the calculation of the mean signal intensity of the samples (figure 4.26 B). In addition, the accumulated radiotracer dose [% applied dose] (figure 4.26 C) was determined by means of a standard, consisting of serial dilutions of [^{18}F]-FHBG with indicated absolute intensities (figure 4.26 D).

Accordingly, the spheroids had incorporated 2 to 3 % of the applied radiotracer dose, depending on virus and treatment approach (figure 4.26 C). PET imaging detected about 3- to 5-fold higher levels of accumulated [^{18}F]-FHBG than detected by gamma-counting (figure 4.25). This fact was due to the 4-fold higher cell number in spheroids applied for PET analysis than for gamma-counting, resulting in an enhanced uptake. The data derived by PET imaging revealed no large variations in HSV1-sr39TK-mediated radiotracer incorporation amongst untreated and TMZ-treated Ad-delo-sr39TK-RGD-infected spheroids. As also shown by gamma-counting (figure 4.25), radiotracer incorporation was reduced in GCV-treated and especially in combined TMZ- and GCV-treated Ad-delo-sr39TK-RGD-infected spheroids, indicating activity of the HSV1-sr39TK/GCV-mediated system in cooperation with TMZ-enhanced viral oncolysis. No significant variations in radiotracer accumulation amongst Ad-sr39TK-infected spheroids were detected in respect of treatment approach. The overall [^{18}F]-FHBG accumulation in spheroids, resulting from the use of Ad-sr39TK, was comparable to that in Ad-delo-sr39TK-RGD-infected and combined virus-infected and TMZ-treated spheroids, which was in accordance with the results shown in figure 4.25.

A

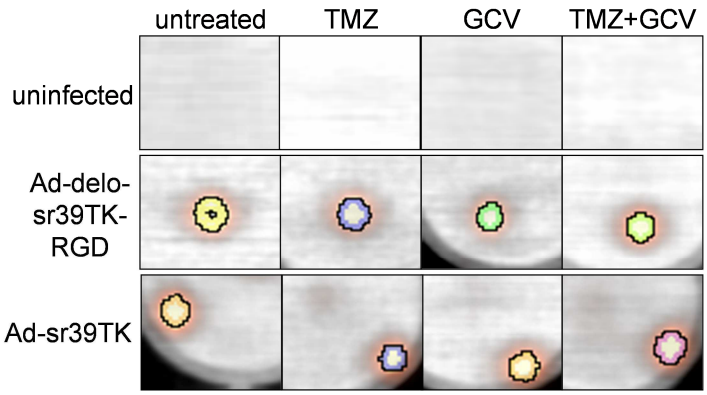

B

Mean intensity of ROI [Bq]

Sample	untreated	TMZ	GCV	TMZ+GCV
uninfected	0	0	0	0
Ad-delo-sr39TK-RGD	2774 ± 14	3015 ± 250	2312 ± 116	1913 ± 88
Ad-sr39TK	3269 ± 260	3379 ± 102	3186 ± 121	3278 ± 115

C

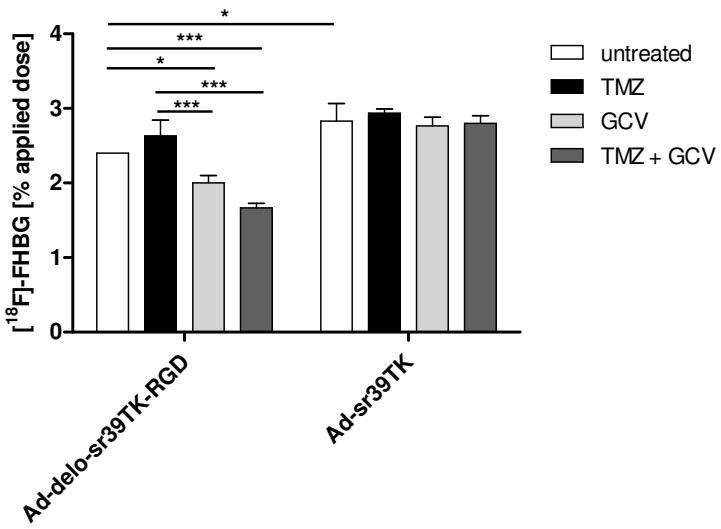

D

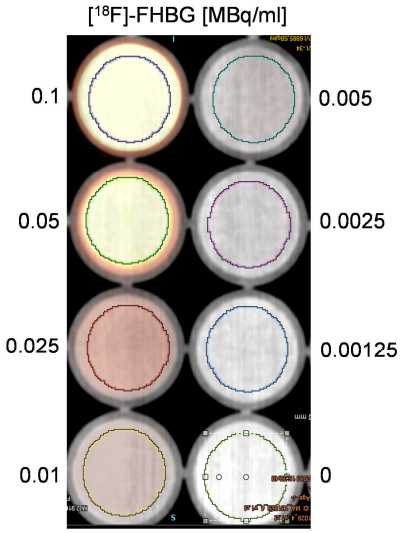

Figure 4.26: Accumulation of [^{18}F]-FHBG in HSV1-sr39TK-expressing 3D glioma spheroids. U87-MG-derived spheroids were infected at MOI of 50 ifu/cell with the indicated adenoviruses. Spheroids containing about 4 x 10^5 cells were treated with 100 µM TMZ 24 h before and directly after infection and/or treated with 0.5 µg/ml GCV 24 h after infection. Uptake was performed with 0.1 MBq [^{18}F]-FHBG per spheroid 4 days after infection. Radiotracer accumulation was measured by PET/CT imaging and mean intensity of ROIs was analysed using OSEM 3D reconstruction algorithm with attenuation correction. One representative ROI is displayed for each data set **(A)**. The average of n=3 ROIs per data set was calculated as mean intensity after decay and volume correction **(B)** and [^{18}F]-FHBG accumulation was calculated as % of total applied [^{18}F]-FHBG dose (mean±SD) **(C)** according to a [^{18}F]-FHBG standard **(D)**. Asterisks indicate significant differences between treatment approaches. *p=0.01-0.05, ***p=0.0001-0.001, as calculated using one-way ANOVA with Tukey's multiple comparison test.

The data above demonstrate the successful radiotracer accumulation in both 2D and 3D glioma cell models infected with HSV1-sr39TK-expressing oncolytic adenovirus, using HSV1-sr39TK as a reporter

gene. The radiotracer uptake rate was facilitated by the replication competence of the virus. However, the radiotracer accumulation was not augmented by enhancement of viral replication through TMZ, presuming that the potentiated oncolytic effect of Ad-delo-sr39TK-RGD by TMZ or the combination of TMZ-mediated enhancement of replication and HSV1-sr39TK/GCV-mediated cytotoxicity resulted in decrease of uptake, compared to Ad-sr39TK-infected glioma cells.

5. DISCUSSION

5.1. Application of YB-1 dependent oncolytic adenoviruses to address limitations of GBM therapy

Despite promising advances in GBM therapy [16, 17], the search for a treatment with sustained efficacy is still a challenge. Major limitations for the success of anti-GBM therapy are the highly aggressive character of the tumour, leading to heterogeneous response to therapy from one GBM case to the other [321], and an acquired drug resistance. Gene therapy with single gene-replacement approaches is often insufficient, because of the accumulation of mutations during cancer progression [37]. Hence, novel targeted experimental approaches are urgently needed. Since conditionally replicating adenoviruses have limited success in clinical trials, combined experimental approaches like YB-1 dependent virotherapy plus chemotherapy [292] or a three-pronged strategy [289] are gaining more interest. Suicide gene therapy is also a potent approach to eradicate tumour cells. However, cell killing is often hampered by impaired diffusion of the prodrug GCV into the cells, by insufficient gene transfer and limited distribution within the tumour mass [54]. The issue of inefficient biodistribution of therapeutic vectors and limited treatment success can be circumvented by introducing a suicide gene into replication-competent adenoviruses. Hence, the objective of this study was to investigate whether the oncolytic effect could be augmented by HSV1-sr39TK/GCV-mediated cytotoxicity and classical TMZ therapy, using the background of YB-1 dependent oncolysis and the finding that YB-1 is upregulated in recurrent glioma [284]. To the author's knowledge, YB-1 dependent oncolytic adenoviruses have so far not been combined with suicide genes. In addition, the suitability of the HSV1-sr39TK-armed oncolytic adenovirus for non-invasive imaging was explored, in order to provide an insight into the viral biodistribution in future preclinical trials.

5.2. Genetic stability and quality of adenoviruses is crucial for their application as anti-tumour agents

The YB-1 dependency of oncolytic adenoviruses is ensured by a deletion in the CR3 of *E1A*, resulting in lack of the transactivating *E1A13S* splice variant [259, 288]. In addition, the YB-1 dependent oncolytic adenoviruses Ad-delo-sr39TK-RGD and Ad-delo3-RGD contain a deletion of *E1B19K*, which increases the cell killing potential of the viruses [201]. The presence of the crucial mutations in the *E1A* and *E3* regions of the adenoviral vectors applied in this thesis, as well as the insertion of the transgene *HSV1-sr39TK* in Ad-delo-sr39TK-RGD and Ad-sr39TK, was verified (table 4.1, figure 4.1), proving the genetic stability of the adenoviruses after CsCl-purification. Thus, the adenoviruses contained the desired modifications in order to be applied as virotherapeutic agents.

A major obstacle in the production of qualitative adenoviral vectors for gene therapy is the potential contamination of adenoviral preparations for clinical application with recombinant RCA. Although there is a safety guideline allowing the presence of not more than 1 RCA per 3 x 10^{10} viral particles in replication-deficient adenovirus preparations for human use, no corresponding guideline for the permissive amount of wild-type-like or non-selective recombinants for oncolytic adenovirus preparations exists [322, 323]. As recombination between residual *E1* sequences in *E1A*-mutated conditionally replicating oncolytic adenoviruses and the *E1* region in HEK293 cells can result in loss of the tumour specificity of oncolytic adenoviruses, RCA generation in large-scale oncolytic adenovirus preparations should be avoided. The lack of contamination of the adenoviruses applied in this thesis with wild-type RCA could not be definitely verified by the applied PCR analysis. Due to the *E1A* deletion of only 11 bp in the oncolytic vectors, the *E1A* PCR products of the oncolytic vectors and of the Ad5-wt-derived reference vector pXC1 were not clearly distinguishable from each other by this standard method for RCA detection (table 4.2, figure 4.2). The *E1A* PCR signals derived from the oncolytic vectors may therefore indicate a false-positive RCA contamination. However, the PCR products derived by *E1*- and *E3*-specific amplification of the oncolytic vectors (table 4.1, figure 4.1), confirmed the lack of wild-type RCA contamination.

In order to discriminate between *E1A*-mutated oncolytic vectors and wild-type RCA contaminations more accurately, PCR analysis can be performed by using primers that amplify only wild-type adenovirus *E1* sequences or DNA fragments of a size of less than 1 kb, which allow the detection of the 11 bp *E1A*-deletion in YB-1 dependent oncolytic vectors [291].

An alternative method for the detection of RCA in preparations of oncolytic adenoviruses represents a bioamplification assay, which amplifies non-selective adenoviruses through multiple passages in order to assess the biological activity of wild-type and non-selective recombinants by a panel of analytical methods [323]. This assay is based on the use of cell lines, permissive only for non-selective RCA and not for conditionally replicating adenoviruses. However, despite of being highly sensitive, this bioamplification assay does not eliminate the need of a specific PCR for detection of potential RCA contaminations, but moreover supports the design of appropriate qPCR assays for detecting RCA. Furthermore, the generation of wild-type RCA can be avoided by the use of alternative virus packaging cell lines for large-scale and clinical applications, such as Per.C6 cells, which contain a truncated *E1* sequence with limited homology to many *E1*-deficient adenoviral vectors [324]. Alternative packaging cell lines with improved safety compared to Per.C6 cells could be the *E1*-transcomplementing cell lines Ac51 and Ac139, derived by stable retrovirus transfection, which contain the *E1A* and *E1B* genes located on separate genomic loci and thus minimising the risk of RCA production [324].

5.3. Efficient replication and oncolytic potential of YB-1 dependent adenoviruses

The localisation of YB-1 in the nucleus of tumour cells is a prerequisite for successful replication of YB-1 dependent oncolytic adenoviruses [259, 265]. The nuclear YB-1 status of U87-MG cells and the multidrug-resistant EPP85-181RDB cell line has been already verified as sufficient to activate adenoviral replication [288, 290, 292]. It is of importance to examine the targeting of multidrug resistance by YB-1 dependent oncolytic adenoviruses, as YB-1 is associated with overexpression of *MDR1* [258]. Moreover, GBM cells often develop multiple resistance against chemotherapy, arising from cancer stem cells [40] or from the overexpression of ABC-transporter proteins in some subsets of stem cells [325].

Indeed, the YB-1 dependent adenoviruses induced c.p.e. and thus oncolytic effect in the YB-1-positive cell lines U87-MG and EPP85-181RDB, confirming the YB-1-based mechanism of activating adenoviral replication (figure 4.3). The strong replication competence of the YB-1 dependent adenoviruses in both tumour cell lines was confirmed by Southern blot (figure 4.4 A) and real-time qPCR analyses (figure 4.5). The results indicate that a threshold amount of produced viral DNA is needed for the virus to be able to induce oncolytic cell killing. The improved replication potency of Ad-delo-sr39TK-RGD over the *E3*-deleted vector Ad-delo3-RGD, despite the identical genetic background of the *E1* region, may be caused by the function of the HSV1-sr39TK enzyme in Ad-delo-sr39TK-RGD. The enzyme is part of the thymidine salvage pathway, catalysing the transfer of the γ-phosphate from ATP to the 5'-hydroxyl of deoxythymidine to form deoxythymidine-5'-monophosphate [326]. Furthermore, as an alphaherpesvirus enzyme, HSV1-TK is in fact a polynucleoside kinase that can phosphorylate all four nucleosides [327]. Therefore, it can be hypothesised that the synthesis of adenoviral DNA can be potentiated by increasing the availability of phosphorylated endogenous nucleosides by HSV1-sr39TK. The incorporation of nucleosides into viral DNA during replication can be analysed by incubation with radiolabelled nucleosides, e.g. [^{3}H]-thymidine [328].

The increasing release of newly synthesised viral particles (figure 4.6) and the high infectivity of the viral progeny (figure 4.7, figure 4.22) proved the disseminating character of the oncolytic adenoviruses and were especially important for enhancing the oncolytic potential. The higher release of newly synthesised Ad-delo-sr39TK-RGD viral particles in comparison to Ad-delo3-RGD release might be explained by the expression of the ADP protein by the armed vector. ADP is required for efficient lysis of adenovirus-infected cells and for release of adenoviral progeny [165]. The attenuated release of Ad-delo-shMGMT-RGD particles compared to Ad-delo-sr39TK-RGD, despite functional ADP, could be due to the anti-apoptotic action of the E1B19K protein, which prevents sufficient viral release, and is therefore deleted in many oncolytic adenoviruses [201, 329]. With its

strong replication capacity, oncolytic potential and successful production of functional progeny, Ad-delo-sr39TK-RGD meets first requirements of efficient oncolytic virotherapy. The tumour-specific replication of the virus, which is comparable in its strength to that of other armed oncolytic adenoviruses used in some preclinical [244, 248] or clinical trials [247], could be therefore beneficial for achieving potent anti-tumour effects in future preclinical studies with Ad-delo-sr39TK-RGD. The viremic threshold of 3 x 10^7 pfu/kg for yielding efficient delivery of oncolytic viruses to tumours [175, 330] could be reached by Ad-delo-sr39TK-RGD.

The correlation between YB-1 and multidrug resistance is controversial [331]. Moreover, it is suggested that YB-1 is necessary for the initiation rather than for the maintenance of drug resistance [332]. These findings could explain the delayed induction of cytopathic effect and attenuated replication of YB-1 dependent oncolytic adenoviruses in the multidrug-resistant cell line EPP85-181RDB 48 h to 72 h post infection in comparison to the U87-MG cell line, as the abundance of cells with nuclear localised YB-1 is probably diminished at late stages of multidrug resistance development.

Malignant glioma cells have been characterised by low to intermediate CAR expression [236, 289, 290, 333-335]. Therefore, the modification of the oncolytic adenoviruses with a RGD motif is crucial for targeting the rather CAR-deficient cell line U87-MG [236, 290, 334]. This cell line exhibits also a moderate expression level of receptor CD46, necessary for binding of adenoviruses of the serotype B [334, 335]. In contrast, U87-MG cells express high levels of $\alpha_v\beta_3/\alpha_v\beta_5$ integrins [334], which interact with the RGD motif and enhance the CAR-independent infectivity of adenoviruses. In addition to their replication competence, the RGD-modified oncolytic adenoviruses have an advantage over the non-RGD-modified replication-deficient Ad-sr39TK in their improved tumour transduction. Though the cell line EPP85-181RGD is also CAR-deficient [336], there is evidence that low viral replication did not result from low infectivity, as the RGD-modified adenoviruses induced c.p.e. in these cells. However, the integrin status of the multidrug-resistant cell line has to be verified.

5.4. Stable expression of HSV1-sr39TK from replication-competent adenoviral vectors

In contrast to the constant transcription of the HSV1-sr39TK transgene into mRNA from the replication-deficient vector Ad-sr39TK as an indication of protein expression, the cumulative production of HSV1-sr39TK mRNA transcripts from Ad-delo-sr39TK-RGD correlated with the replication capacity of the virus in U87-MG and EPP85-181RDB cells (figure 4.8). Consequently, the replication of Ad-delo-sr39TK-RGD was not impaired by the constitutive expression of the transgene. Contrariwise, the HSV1-sr39TK expression level was not attenuated by the induction of c.p.e. in Ad-delo-sr39TK-RGD-infected tumour cells (figure 4.3). The difference in HSV1-sr39TK protein expression

level between Ad-delo-sr39TK-RGD and Ad-sr39TK was marginal (figure 4.9 A), in contrast to mRNA transcription. This finding was due to the fact that all configurations of the protein are detected by Western blotting, including inactivated or degraded forms, making variations in protein expression difficult to recognise. The attenuated expression kinetics of HSV1-sr39TK from Ad-delo-sr39TK-RGD in EPP85-181RDB cells compared to U87-MG cells reflects the attenuated YB-1 dependent replication, as described above. A hypothesis for the decreased expression is that the downregulation of cellular protein biosynthesis in favour of virus replication [161] could be more prominent during maintenance of multidrug resistance.

Taken together, these data prove that propagation of a transgene with viral replication is one of the benefits of applying replication-competent adenoviruses in gene therapy. An alternative method for arming oncolytic adenoviruses is the insertion of a transgene into the *L3* region of the vectors [337]. This method links transgene expression to late viral gene expression and leads to high levels of tumour-specific expression of the transgene. On the contrary, the regulation of a transgene by constitutive promoters or its insertion into *E3* locations may exhibit low levels of off-target gene expression, a critical issue when arming oncolytic adenoviruses with cytotoxic genes [337].

5.5. Multicellular 3D glioma spheroids as a feasible model to explore anti-tumour treatment

Due to their resemblance to tumour tissue *in vivo* in respect of multicellular architecture, growth kinetics and metabolism [205, 209], 3D glioma spheroids were developed in order to explore the efficacy of YB-1 dependent oncolytic adenoviruses in combination with TMZ and the HSV1-sr39TK/GCV suicide system *in vitro*. The 3D spheroids displayed classical tumour characteristics, such as proliferative growth and migration of cells from the tumour focus [8] (figure 4.10, figure 4.11), the latter being a prerequisite for tumour invasion and recurrence [338]. Consistent with this fact, formation of clusters of outgrowing cells were observed with progression of cellular migration (figure 4.11, day 7), giving an indication of the highly invasive character of GBM [8]. These data support the use of spheroids as tumour-mimicking models to study the response of tumour growth to therapy *in vitro* [209]. The tumour characteristics of spheroids can be utilised to explore tumour angiogenesis in a 3D model [339]. Moreover, neurospheres formed by single $CD133^+$ cancer stem cells *in vitro* can be applied to analyse chemoresistance in GBM [340]. The MOI-dependent transduction efficiency of the glioma spheroids indicated their suitability for adenoviral gene transfer (figure 4.12), which was in line with previous observations [210]. It was expected that the introduction of a RGD motif and the use of replicating adenoviruses would enhance viral transduction [341]. The infectivity of spheroids can also predict the transduction efficiency and viral effects in tumours *in vivo* [211].

The dissemination of oncolytic adenoviruses and the combined effect of oncolysis, TMZ and HSV1-sr39TK/GCV-mediated cytotoxicity were investigated in 3D spheroids, because they are more representative than 2D culture as *in vitro* model for solid tumours, where the penetration of large molecules, such as viruses or drugs, is attenuated by the complexity of tumour geometry and the presence of extracellular matrix. In tumour spheroids, cells are clustered together by surface membrane microprojections and a plethora of intercellular junctions [205, 212]. These properties of spheroids reproduce the treatment-related effects *in vivo* more precisely than 2D culture.

5.6. Mutual potentiation of adenoviral oncolysis and HSV1-sr39TK/GCV-mediated effect

The analysis of the HSV1-sr39TK/GCV-mediated cytotoxicity was first carried out in 2D cell culture to optimise the cell killing conditions by variation of dose and timing of pro-drug application. U87-MG glioma cells are susceptible to the suicide gene approach, as indicated by the strong HSV1-sr39TK/GCV-mediated cytotoxicity in Ad-sr39TK-infected cells (figure 4.13 A). Cell killing was induced by the combination of overlapping HSV1-sr39TK/GCV-mediated cytotoxicity and oncolytic activity of Ad-delo-sr39TK-RGD. The E1A12S protein of Ad-delo-sr39TK-RGD might also contribute to the HSV1-sr39TK/GCV-killing, for it is known that E1A as an S-phase inducer enhances the HSV1-TK/GCV activity [342]. Although the oncolytic effect alone was strong enough to induce cell killing, the cells were still metabolically active after c.p.e. (data not shown in figure 4.13 B), in contrast to infected and concomitantly GCV-treated cells (figure 4.13 B). This observation indicated that the HSV1-sr39TK/GCV-mediated cytotoxicity contributes to eradicate tumour cells completely. Important for the successful cell killing were the concentration of GCV and the timing of GCV application. The cell survival was drastically reduced at GCV concentrations of even less than 0.01 µg/ml, indicating that the high sensitivity of HSV1-sr39TK to GCV overlapped with the oncolytic effect of the adenovirus. It was previously reported that HSV1-sr39TK displays a 14-fold decrease in the K_m value for GCV and an 80-fold higher kinetics with GCV when compared with wild-type TK, which enables the use of GCV at lower, less immunosuppressive doses [343]. A recent study demonstrated a strong therapeutic efficacy of the HSV1-sr39TK/GCV system against rat C6 glioma both *in vitro* and *in vivo*, by applying GCV to HSV1-sr39TK-transduced cells at a lower concentration as compared to wild-type TK-transduced cells [317]. Thus, the mutant HSV1-sr39TK is a potent suicide gene for inhibition of tumour growth and favours the application of low GCV doses for mediating cytotoxic effects, which can result in less unspecific toxicity of the prodrug.

The eradication of tumour cells was more successful when GCV was applied one to three days after infection than when applied directly after infection (figure 4.13). This observation was consistent with a previously described study of an HSV1-TK armed oncolytic adenovirus with potent anti-tumour

effects in glioma [240]. The reduced response of cells infected with replicating adenoviruses to GCV when added immediately after infection than when added at later time points could be due to the ability of GCV-triphosphate to extenuate adenoviral replication, as it incorporates into the DNA of dividing cells as well as into replicating viral DNA [61]. This finding is in accordance with the replication analyses shown in this thesis (figure 4.4 B, figure 4.21) and is also supported by the observation of HSV1-TK/GCV-triphosphate-mediated inhibition of replication-competent adenoviruses in other studies [243, 344, 345]. By adding GCV one day post infection, the progressive cytotoxicity mediated by HSV1-sr39TK/GCV exerted a deleterious effect on Ad-delo-sr39TK-RGD DNA, as it abolishes the proliferation of virus-infected cells and thus viral replication and spread (figure 4.22). The attenuated replication of Ad-delo-sr39TK-RGD by GCV, added immediately after infection, was the most probable explanation for the cell survival at 0.1 µg/ml GCV (figure 4.13 A). This dose was insufficient to induce HSV1-sr39TK/GCV-mediated cytotoxicity and to counteract the repressed oncolysis. The deleterious effect of GCV upon viral replication was not dependent on viral dose, as a pronounced cell survival could also be observed with MOI of 10 ifu/cell (data not shown). The finding that the level of HSV1-sr39TK/GCV-mediated cell killing of Ad-sr39TK remained constant regardless of the time point of GCV addition confirmed the inhibitory action of GCV against HSV-TK1-armed replicating adenoviruses. When GCV was applied at later time points, the accumulated Ad-delo-sr39TK-RGD viral particles were able to overcome the initial inhibitory effect of GCV. The oncolysis could be promoted successfully, as already small amounts of *E1A* gene products are sufficient to initiate adenoviral replication [346]. However, the predominating oncolytic effect of Ad-delo-sr39TK-RGD led to decrease in HSV1-sr39TK expression due to cell killing, when GCV was added 48 h to 72 h post infection (figure 4.9 B). This observation suggests that a strong oncolytic potential may lead to an increased risk of uncontrolled viral spread. Inhibition of adenoviral replication by HSV1-TK/GCV at early stages of the viral life cycle presents therefore an important safety regard and a fail-safe means to control viral dissemination, which is crucial for a safe *in vivo* application. In order to maintain a balance between the strength of the oncolytic effect and the activity of the HSV1-sr39TK/GCV system, as well as to control viral spread, the optimal time point of GCV application *in vitro* was determined to be one day after infection.

The weak oncolytic effect of Ad-delo-sr39TK-RGD in EPP85-181RDB cells could not be substantially enhanced by the HSV1-sr39TK/GCV-mediated cytotoxicity, even at a high viral dose (figure 4.14). The high IC_{50} value of HSV1-sr39TK/GCV in EPP85-181RDB cells (50 µg/ml as compared to 0.35 µg/ml in U87-MG cells) and the thus resulting attenuated HSV1-sr39TK/GCV-mediated cell killing could be explained by a low susceptibility of the cell line to GCV as a result of its multidrug-resistant phenotype. Considering the broad spectrum of drug substrates transported by P-gp [50], a developed

cross-resistance towards the guanosine analogue GCV after long-term exposure could be possible. Optimisation of the HSV1-sr39TK/GCV-mediated bystander effect could be considered as a method to increase the GCV-sensitivity of multidrug-resistant cells, as described in the following.

5.7. Potentiation of viral oncolysis by HSV1-sr39TK/GCV-mediated bystander effect

The bystander effect contributed successfully to the HSV1-sr39TK/GCV-mediated cytotoxicity and enabled the eradication of tumour cells containing a small fraction of infected cells (figure 4.15). This observation was in line with previous findings that the mutant sr39TK could induce a strong bystander effect at lower GCV concentrations than the wild-type enzyme *in vitro* as well as *in vivo* [90, 347]. Through the replication-competence of Ad-delo-sr39TK-RGD and the resulting increase in HSV1-sr39TK expression, the oncolytic potential of the virus was enhanced by the bystander effect of HSV1-sr39TK/GCV. Although the bystander effect alone, elicited by Ad-sr39TK, was sufficient to induce almost complete cell eradication due to the high sensitivity of HSV1-sr39TK for GCV, this effect cannot be always translated into an *in vivo* situation. In this context, U87-MG glioma cells have been shown to be susceptible to bystander killing *in vitro* by GCV-mediated apoptosis, but this effect is insufficient *in vivo* [80]. Therefore, the use of replicating adenoviruses has a benefit over replication-deficient adenoviruses in enhancing the bystander effect *in vivo*. Moreover, the use of high viral and prodrug doses, which can compromise the safety of adenovirus-mediated suicide gene therapy [348], can be circumvented by a bystander effect. Regarding the mode of action of the bystander effect, it was demonstrated that TK from a replication-competent HSV-1 was able to enhance connexin 43 subunit (Cx43) expression in the presence of GCV and thus to induce bystander effect in a tumour cell line, suggesting augmented intercellular transport of active GCV through gap junctions [349]. If the enhancement of Cx43 expression by the HSV1-TK/GCV suicide system as a bystander mechanism is also valid in the context of HSV1-TK-armed oncolytic adenoviruses, remains to be shown.

No bystander effect of HSV1-sr39TK/GCV was observed in the multidrug-resistant cell line EPP85-181RDB under the same conditions as for U87-MG cells (figure 4.15). In contrast, a strong bystander cell killing with only 17 % infected cells was induced by applying a 5-fold higher GCV concentration that increased the sensitivity of EPP85-181RDB cells for the prodrug (data not shown). However, an increase of GCV concentration alone may not be sufficient for preventing resistance against HSV1-TK/GCV-mediated killing *in vivo*. Considering the low HSV1-sr39TK expression from Ad-delo-sr39TK-RGD (figure 4.9 A) and the attenuated viral oncolytic effect plus HSV1-sr39TK/GCV-mediated cytotoxicity (figure 4.14, figure 4.15) in EPP85-181RDB cells, it can be assumed that unarmed

conditionally replicating adenoviruses could be more efficient in eradication of multidrug-resistant tumour cells [265, 288, 291] than armed replicating adenoviruses.

A promising approach to target multidrug resistance and to enhance the HSV1-TK/GCV suicide system *in vivo* could be the silencing of *MDR1* by shRNA-targeting [350]. Another consideration for *in vivo* studies is the finding that overexpression of the proto-oncogene *Bcl-2* in GBM is associated with resistance against HSV1-TK/GCV suicide gene therapy [351]. This issue could be addressed by an inhibitor of Bcl-2 [352].

In order to increase the safety and efficacy of the HSV1-TK/GCV suicide system, potent bystander tumour cell eradication in *in vivo* glioma models can be induced through gap junction-mediated transport of toxic metabolites between HSV1-TK expressing bone marrow-derived cells or normal brain cells and glioma cells [353, 354]. These strategies demonstrate that normal brain cells may contribute to the HSV1-TK/GCV therapy by long-term delivery of therapeutic genes and through induction of a bystander effect.

5.8. Potentiation of YB-1 dependent viral oncolysis by TMZ and benefit of viral dissemination in 3D

The oncolytic potency of Ad-delo-sr39TK-RGD was augmented by TMZ treatment of glioma cells in both 2D and 3D culture, as shown by the decrease in cell survival (figure 4.16) and enhancement of viral replication (figure 4.20 and 4.21) and viral release (figure 4.22) by TMZ. Treatment of glioma cells and spheroids with TMZ once before and after infection achieved a higher level of replication enhancement than pre-treatment only (data not shown). This level was also higher than the replication enhancement of Ad-delo3-RGD within an *in vivo* study [292], indicating that the continuous TMZ treatment schedule could be beneficial for improving the oncolytic potential of YB-1 virotherapy *in vivo*. In respect of *in vivo* use, it is noteworthy that the half-life of TMZ in human plasma is only 1.8 h [318, 319], corroborating the need of repeated TMZ addition in order to increase the virotherapeutic performance. These results indicate that sensitisation of glioma cells to adenoviral infection by TMZ could be a promising virotherapeutic approach. As the IC_{50} of TMZ for U87-MG cells was stated to range between < 100 µM [355] and 20.2 mM [103], the IC_{50} of TMZ of > 500 µM for this cell line (figure 4.16) lies within the published range. The discrepancy of IC_{50} of TMZ for U87-MG cells in the literature probably arises from the different incubation periods of the drug on cells: 72 h [355] and 96 h [103]. Here, TMZ was incubated on cells for 24 h (figure 4.16). Thus, the combinatorial approach of virotherapy and TMZ raises the susceptibility of GBM cells to TMZ and allows the use of low virus and TMZ doses (e.g. MOI 10 and 25 µM TMZ, or MOI 20 and 10 µM TMZ) to reach the same level of cell killing as high doses of single treatment (e.g. MOI 50/100 or > 500 µM

TMZ). The combined treatment is therefore beneficial for reducing potential toxic effects in future systemic applications *in vivo*.

The enhancement of oncolysis is based on the nuclear translocation of the transcription factor YB-1 as a result of TMZ-mediated cytostatic stress and thus stimulation of adenoviral replication, as shown previously for Ad-delo3-RGD [292]. The mechanisms of YB-1 nuclear translocation as a result of stress response are not clear yet. There is strong evidence that several concurrent signalling pathways, activated as a result of DNA-damaging agents, are involved in this process [262, 356]. Phosphorylation of YB-1 at Ser102 by the serine/threonine kinase Akt has been shown to trigger the transition of YB-1 to the nucleus [357]. However, the dependence of YB-1 nuclear transport on Akt could not be reproduced for some tumour cell lines [358]. Another regulatory mechanism for nuclear translocation of YB-1 is associated with the C-terminal cleavage of the protein by the 20S proteasome, induced by DNA-damaging agents [359], but the molecular mechanism of YB-1 nuclear transport mediated by proteolysis needs to be re-assessed [360].

The improved oncolytic effect of Ad-delo-sr39TK-RGD over Ad-delo3-RGD in combination with TMZ (figure 4.16) was likely to be caused by the improved viral release of the armed oncolytic adenovirus due to the expression of ADP, as described previously. Ad-delo-sr39TK-RGD demonstrated a similar to slightly stronger oncolytic effect depending on viral MOI and TMZ concentration than Ad-delo-shMGMT-RGD. It was expected that the double function of Ad-delo-shMGMT-RGD in inducing oncolysis and simultaneously potentiating the cytostatic effect of TMZ by silencing of the DNA repair gene *MGMT* [320] could achieve stronger glioma cell killing than YB-1 dependent virotherapy with Ad-delo-sr39TK-RGD alone. A synergistic therapeutic efficacy of oncolytic virotherapy, TMZ and down-modulation of MGMT expression against GBM has been already demonstrated [361], but not in the context of YB-1 dependent oncolysis. However, the use of U87-MG cells to assess the benefit of adding *MGMT*-silencing to YB-1 dependent oncolysis is equivocal, as these cells exhibit *MGMT*-promoter hypermethylation and thus low MGMT expression [355]. The use of TMZ-resistant glioma cells with an unmethylated *MGMT*-promoter reflects the clinical scenario more accurately. Moreover, the lack of the anti-apoptotic protein E1B19K in Ad-delo-sr39TK-RGD contributed to the enhanced TMZ-mediated oncolytic effect of Ad-delo-sr39TK-RGD at low MOIs in comparison to Ad-delo-shMGMT-RGD. Ad-delo-sr39TK-RGD has therefore the potential for eliminating of GBM cells regardless of their MGMT status.

In contrast to the high oncolytic potential of the YB-1 dependent adenoviruses upon TMZ treatment in GBM cells, a 20-fold higher viral MOI and 50- to 200-fold higher TMZ doses than applied in U87-MG cells were needed for the oncolytic viruses to achieve an almost complete eradication of EPP85-181RDB cells (figure 4.17). The multidrug-resistant phenotype of the pancreatic carcinoma cells was most likely to be responsible for the worse response to TMZ and thus low oncolytic potential,

considering also the controversial role of YB-1 in multidrug resistance [331, 332]. Explanations for this worse effect could be on the one hand a cross-resistance towards TMZ. On the other hand, no additional stress stimuli like TMZ could further enhance the nuclear accumulation of YB-1, due to a selection pressure over TMZ, since EPP85-181RDB cells are maintained in the presence of daunorubicin [290].

The role of multidrug resistance-mediating ABC-transporter proteins in GBM is controversial. Although expressed in GBM cells, it is still unknown whether TMZ is actually transported by these proteins [362]. However, evidence exist that MDR1 is associated with TMZ resistance and the protein is therefore an independent predictive factor for the outcome of TMZ therapy [363].

The level of DNA replication enhancement of the oncolytic adenoviruses by TMZ was stronger in spheroids than in 2D culture (figure 4.20, figure 4.21), indicating that the 3D cell structure facilitated the viral spread and confirming the 3D model as the more relevant one for replication analyses. This statement was supported by the finding that Ad-delo-sr39TK-RGD invaded not only the outer layers, but also several inner layers of the spheroids, in contrast to the replication-deficient Ad-sr39TK (figure 4.23). The adenoviral distribution in spheroids shown here was in accordance with the finding of Grill et al. that spread of a replication-deficient adenovirus is restricted to the outer layers of glioma spheroids, but replication-competent and oncolytic adenoviruses invade also the inner layers [210]. The reasons for the restriction of adenoviral replication to the outer replicating layers of spheroids may be the increasing proportion of nonproliferating cells during growth and the occurrence of necrotic regions in the spheroid core as a result of a hypoxic environment and glucose deprivation, similar to cancers *in vivo* [205]. Hypoxia usually exists in sections within solid tumours and can attenuate adenoviral replication by downregulation of viral protein expression [364, 365]. Necrotic regions in the core of tumour spheroids with diameters larger than 400-500 µm, as in the case of the glioma spheroids generated in this thesis, may occur at a distance of 50-300 µm from the spheroid periphery and the thickness of the proliferating layers, surrounding the necrotic centre, may range between 100-220 µm [205, 209].

Spheroids can give also an insight into the mode of viral dissemination within a solid tumour. Regarding viral dissemination, it was shown that oncolytic adenoviruses seemed to favour lateral rather than medial spread within spheroids (figure 4.23). This could be due to a tight lateral clustering of cells or an uneven distribution of the adenovirus-binding integrins $\alpha_v\beta_3$ and $\alpha_v\beta_5$ on the cell surface, as these integrins are known to be overexpressed in the periphery of high-grade gliomas [366].

5.9. Relevance of 3D spheroids for exploring potential *in vivo* effects of the HSV1-sr39TK/GCV suicide system

Although the spread of Ad-delo-sr39TK-RGD (figure 4.23) and the release of infectious Ad-delo-sr39TK-RGD-particles (figure 4.22) was impaired by the inhibitory action of GCV upon viral replication (figure 4.20, figure 4.21), the combined viral and HSV1-sr39TK/GCV approach efficiently induced HSV1-sr39TK/GCV-mediated cytotoxicity in 3D spheroids and was stronger than both oncolytic effect and HSV1-sr39TK/GCV-mediated cytotoxicity alone (figure 4.19). The cell killing was therefore augmented by the bystander effect of GCV and not by adenoviral replication alone. However, evidence exist that HSV1-TK-expressing spheroids display lower GCV-bystander effect than monolayer culture [367]. Here, this finding was in accordance with the lower cytotoxicity of the replication-deficient Ad-sr39TK in spheroids than in 2D culture, presuming a role of the attenuated bystander effect. The potential bystander effect of GCV in spheroids was however enhanced by replication of the oncolytic adenoviruses at late time points and the difference in cell survival after the single viral approach and the combined viral and HSV1-sr39TK/GCV-approach was more prominent in 3D than in 2D. Due to the similarity of the 3D structure to tumour tissue, the results in 3D are assumed to be more relevant for predicting the therapeutic efficacy of the suicide gene system *in vivo*.

There are conflicting data in the literature regarding the efficacy of oncolytic adenoviruses combined with HSV1-TK/GCV suicide therapy. Some studies show that the HSV1-TK/GCV system enhances the oncolytic activity of replication-competent *E1B55K*-deleted adenoviruses [237, 238] or of replication-competent adenoviruses with a deletion of the M_r 19.000 glycoprotein (gp19K) coding sequence in the *E3* region [240], whereas other studies demonstrate no further enhancement of *E1B*-positive oncolytic adenoviruses, especially when the E1B55K protein is functional [368-371]. However, GCV was applied in the latter studies not earlier than two days after infection.

It is suggested that the HSV1-TK/GCV system might still be suitable to enhance the cytoreductive effect of highly potent oncolytic vectors in clinical settings, because immune responses often limit viral spread [369]. Moreover, HSV1-TK/GCV administration might potentiate the oncolytic activity by immune-mediated mechanisms [372]. In this thesis it was demonstrated that the E1B55K-expressing HSV1-sr39TK-armed oncolytic adenovirus had a potent anti-tumour effect by oncolysis alone, especially in 2D glioma culture. Additionally, there was an enhancement of the oncolytic effect by the combination of oncolytic and HSV1-sr39TK/GCV activity, which was more distinctive in 3D spheroids than in 2D cell culture. It can be presumed that the impaired accessibility of cells within spheroids, even by replicating adenoviruses, leading to a delayed oncolytic effect compared to 2D culture, resembles the *in vivo* situation more precisely and can be substantially enhanced by the suicide gene system.

5.10. Combined effect of YB-1 dependent virotherapy, TMZ and HSV1-sr39TK/GCV suicide system against GBM

It was shown that TMZ, by enhancing the replication and thus oncolytic effect of Ad-delo-sr39TK-RGD via triggering the nuclear translocation of YB-1 [292] , acted in combination with the HSV1-sr39TK-/GCV-system to potentiate the decrease of glioma cell survival both in 2D culture (figure 4.18) and 3D spheroids (figure 4.19). Compared to the sole combination of oncolysis and HSV1-sr39TK/GCV-mediated cytotoxicity, additional TMZ-stimulation induced an earlier onset of cell killing and allowed the application of less viral load. In contrast, TMZ exerted rather cytostatic than cytotoxic effects in uninfected spheroids.

The type of cell death, mediated by the combined experimental approach, and the mode of action of this treatment have to be elucidated in more detail. Replicating adenoviruses induce more than one type of cell death or a mixed type of cell death, according to the heterogeneous functions of the adenoviral gene products and the time point of their activation during the adenoviral life cycle [373, 374]. The most commonly observed adenovirus-mediated cell death modes include apoptosis [375], necrosis-like cell death [376], cell lysis [165] and autophagy [377]. As shown in figure 4.18 C, YB-1 dependent oncolytic adenoviruses induced probably an apoptotic cell death after c.p.e., which is in line with previous findings that Ad-delo3-RGD induces apoptosis *in vivo* [292]. The hypothesis that *E1B19K*-deleted adenoviruses, such as Ad-delo-sr39TK-RGD and Ad-delo3-RGD, induce apoptosis, at least in early stages of the viral life cycle, is corroborated by the finding that cells infected with an *E1B19K* mutant undergo apoptosis, because DNA damage caused by viral infection activates the proteosomal degradation of the anti-apoptotic Bcl-2 family member Myeloid Cell Leukemia 1. The Bcl-2 homologue E1B19K is then not at disposal to block this pathway and to counteract apoptosis mediated by E1A [378].

The suggested apoptotic cell death upon TMZ treatment and infection with YB-1 dependent oncolytic adenoviruses (figure 4.18 C) needs to be analysed more thoroughly, since it has been shown that the combination of TMZ and conditionally-replicating adenoviruses elicits autophagic cell death *in vitro* in U87-MG cells, whereas both autophagy and apoptosis are observed *in vivo* in glioma models [379]. Moreover, TMZ induces apoptosis and senescence in GBM spheroids [380], but doses up to 100 µM TMZ do not lead to strong apoptosis [208]. Thus, it can be concluded that tumour cell eradication (figure 4.18, figure 4.19) resulted predominantly from the potentiation of the oncolytic effect by TMZ and the HSV1-sr39TK-/GCV-mediated cytotoxicity, and probably to a lower extent from induction of apoptosis by TMZ. As indicated by the difference in cellular morphology (figure 4.18 C), it can be assumed that the oncolytic effect elicited a different type of cell death than the HSV1-sr39TK/GCV system alone. The HSV1-TK/GCV suicide system has been shown to mediate apoptosis in U87-MG cells [70]. On the contrary, combined TMZ and GCV treatment of Ad-delo-sr39TK-RGD-infected GBM

cells resulted most likely in a mixed apoptotic and necrosis-like mode of cell death. More detailed examinations are necessary to determine the exact type of cell death induced by this triple combinatorial approach.

It has been shown that inhibition of YB-1 sensitizes GBM cells to TMZ [381]. This finding could be one of the mechanisms underlying the additive effect of YB-1 dependent oncolysis and TMZ treatment, as YB-1 is not at disposal because of its function in activating viral replication.

The mechanism of action of the HSV1-sr39TK/GCV-mediated cytotoxicity in potentiating viral oncolysis requires a more detailed elucidation. It has been shown that infection with oncolytic adenoviruses induces a profound overreplication of genomic DNA in permissive cell lines. The overreplication results from the transactivation of cdc25a phosphatase by E1A and the promotion of E1A-induced S phase entry by activated cdc25a [382]. Deregulated cdc25a activity during adenoviral infection induces uncontrolled genomic DNA replication via activation of cdc2. Consequently, DNA overreplication is associated with the occurrence of genomic DNA damage. As a result, the DNA homologous recombination repair pathway, involving the key kinase ataxia telangiectasia and Rad3-related (ATR) and checkpoint kinase 1 (Chk1), is activated in order to maintain the integrity of the genome. Inhibition of the ATR-Chk1 pathway impairs DNA damage repair, which results in accumulation of cytotoxic lesions and consequently leads to cell death [382].

The HSV1-TK/GCV system may interfere in the above described model in a dual mode. First, the incorporation rate of GCV-triphosphate into genomic DNA may be increased due to genomic DNA overreplication in adenovirus-infected cells, since GCV-triphosphate exerts its cytotoxicity upon rapidly dividing DNA. Second, GCV-triphosphate induces an irreversible arrest in late S-G2 phase through activation of the G2-M DNA damage checkpoint and inhibition of the activity of cdc2 [383]. During this irreversible late S-G2 phase arrest, unrepairable DNA double strand breaks may accumulate due to blocked Chk1-mediated homologous recombination repair [384], which adds to the deleterious effect of virus-induced DNA damage. Hence, through the incorporation of GCV-triphosphate during virus-induced DNA overreplication and by interfering with the virus-mediated cell cycle progression and with DNA repair pathways, the HSV1-sr39TK/GCV system exerts additive effects in combination with viral replication for mediation of cell death.

Rainov et al. already assessed the synergy between TMZ and GCV in mediating cytotoxicity in HSV1-TK-expressing malignant glioma cells and elucidated the possible mechanism underlying this synergy [103]. Accordingly, GCV-triphosphate is supposed to inhibit the repair of TMZ-induced DNA-crosslinks by MGMT. According to a model of mutual synergism between chemotherapy and YB-1, defined as Mutually Synergistic Therapy (MUST), chemotherapy leads to increased levels of nuclear YB-1 and consequently enhances adenoviral replication, while viral-mediated nuclear translocation of YB-1 leads to enhanced susceptibility of cells to chemotherapy [265]. Thus, there is strong evidence that

the combined effect of TMZ, YB-1 dependent oncolysis and HSV1-sr39TK/GCV-mediated cytotoxicity is based on the mutual synergism between these three components. In addition, the results of this thesis confirm the increased efficacy of YB-1 dependent virotherapy in multimodal over single-mode approaches against GBM in previous studies [289, 292].

5.11. Suitability of HSV1-sr39TK-armed YB-1 dependent oncolytic adenoviruses for non-invasive reporter gene imaging

Multicellular spheroids had been already used as a relevant *in vitro* model to assess changes in cell viability after treatment with oncolytic adenoviruses by means of a PET scan using [^{18}F]-labelled deoxyglucose [214]. To the author's knowledge, no PET imaging of multicellular spheroids using HSV1-sr39TK has been performed by now. In this thesis, 3D glioma spheroids were used - along with 2D cell culture - as a feasible model for the analysis of the cellular uptake and spatial distribution of PET radiotracer, specific for HSV1-sr39TK. The data demonstrate that Ad-delo-sr39TK-RGD mediated accumulation of radiotracer by the enzymatic activity of HSV1-sr39TK in 2D culture (figure 4.24) and in 3D spheroids (figure 4.25, figure 4.26). The activity of HSV1-sr39TK correlated positively with the amplification of the transgene by viral replication (figure 4.24 B). Although the replication-deficient vector Ad-sr39TK has been successfully applied for non-invasive radiotracer imaging *in vivo* [113, 115], replication-competent adenoviruses may have an advantage over replication-deficient viruses in allowing the use of lower and non-toxic viral doses for *in vivo* imaging, which can be further amplified by replication.

In future *in vivo* studies, progression of tumour cell killing as a result of oncolytic virotherapy in combination with cytostatic agents and the HSV1-sr39TK/GCV-mediated system could be monitored by non-invasive PET radiotracer imaging, having in mind that the accumulation rate correlates with cell viability. The use of the disseminating oncolytic adenovirus Ad-delo-sr39TK-RGD facilitates nuclear reporter gene delivery, as well as biodistribution, and provides first evidence that the therapeutic efficacy of the HSV1-sr39TK/GCV system could be easily monitored *in vivo*. Nevertheless, the radiotracer application should be well timed in order to achieve an equilibrium between the HSV1-sr39TK/GCV-mediated cytotoxicity, oncolytic killing and tracer accumulation. An optimal time point for uptake analysis would be three days post infection (figure 4.24 B), when the amount of oncolytic viral particles is significantly increased due to replication burst. In addition, imaging might be most successful if the radiotracer is applied before GCV treatment [126], because cell depletion by the HSV1-TK/GCV system would thus be circumvented.

Regarding the issue of oncolytic toxicity, which could hamper imaging success, the replication-deficient Ad-sr39TK has an advantage over Ad-delo-sr39TK-RGD for imaging, because of its non-lytic properties (figure 4.24 A). To circumvent the problem of off-target toxicity due to the action of

armed oncolytic adenoviruses and as a safety regard, GCV can be applied in appropriate doses in order to abort the proliferation of HSV1-TK-expressing cells and thus attenuate adenoviral replication when necessary, but maintaining the therapeutic effect. The decrease in [^{18}F]-FHBG accumulation upon dual and triple treatment approaches (figure 4.25, figure 4.26) reflected the enhanced cytoreduction by viral oncolysis in combination with TMZ and upon TMZ plus GCV treatment. These results point out the feasibility and sensitivity of HSV1-sr39TK/[^{18}F]-FHBG reporter gene imaging for monitoring of minor differences in the viability of tumour cells after subjecting them to treatment.

In respect of the technique for radiotracer detection in spheroids, gamma-counting allows a more precise quantification of absolute radiotracer amount on cellular level than PET imaging. Therefore, the determination of radiotracer accumulation by gamma-counting was more sensitive than PET measurement and was able to detect alterations between each of the TMZ, GCV or combined TMZ and GCV treatment approaches in Ad-delo-sr39TK-RGD-infected spheroids more accurately than PET (figure 4.25). Nevertheless, the ability of PET imaging to detect radiotracer accumulation in small tumour spheroids of size about 7 mm³ and consisting of about 4 x 10^5 cells (figure 4.26) proved the feasibility and the high sensitivity of this technique in combination with HSV1-sr39TK and [^{18}F]-FHBG. The high imaging sensitivity when using this reporter gene and probe pair was in accordance with a previously estimated detection limit of 1 x 10^5 HSV1-sr39TK-transduced cells for tumours of size about 3 mm³ [385]. The preliminary results in 3D spheroids provide a first indication of the suitability of HSV1-sr39TK, delivered by an YB-1 dependent replicating adenovirus, in combination with [^{18}F]-FHBG for non-invasive *in vivo* PET imaging.

5.12. Outlook and future perspectives of combined YB-1 dependent virotherapy and HSV1-sr39TK/GCV suicide gene system

The combined approach of YB-1 dependent oncolytic virotherapy, HSV1-sr39TK/GCV suicide system and TMZ therapy proves to be promising, though some improvements are necessary for future application in preclinical studies. There is often a discrepancy between results obtained by *in vitro* and *in vivo* investigations, because monolayer cell culture does not reflect the tumour microenvironment [236]. Even 3D spheroid models, consisting of one cell type, are not able to constitute the complex interplay between tumours, vascularisation, tumour microenvironment and the immune system. Hence, a xenograft GBM *in vivo* model is needed to address the efficacy of the described therapeutic strategy, using the time- and dose-dependent treatment conditions, which were optimised in this study. Moreover, repetitive non-invasive microPET imaging can be performed after intratumoural injection of replicating HSV1-sr39TK-bearing adenoviruses and radiotracer application in order to explore the kinetics of viral replication, biodistribution and the tracer detection limits in respect of time and dosage *in vivo*. The tumour growth or regression after GCV

and TMZ addition, as well as possible toxicity of the combined treatment, can also be monitored by means of microPET imaging. Subtle differences in viral replication during GCV and TMZ treatment can be analysed by immunohistology and the correlation to biodistribution of radiotracer can be assessed. Considering that [^{18}F]-FHBG has background leakage preferentially in the liver [115, 116], analysis of the biodistribution of the radiotracer in tumours and organs can be performed.

An orthotopic GBM xenograft model can be used to examine the correlation between uptake of [^{18}F]-FHBG by HSV1-sr39TK-expressing GBM cells and 3'-deoxy-3'-[^{18}F]-fluorothymidine uptake as a proliferation biomarker [386], in order to assess the effect of combined adenoviral, TMZ and HSV1-sr39TK/GCV treatment on tumour growth and to predict survival outcome. Furthermore, the implantation of Ad-delo-sr39TK-RGD-infected GBM spheroids into established GBM models could result in a bystander effect of HSV1-sr39TK/GCV, induced from infected spheroids on uninfected GBM cells. This bystander effect can facilitate the application of low virus and GCV doses, and could help to avoid potential off-target effects. For all future *in vivo* studies, a GCV application at late time points of viral replication and a systemic TMZ addition should be preferred for enhancing the treatment efficacy and allowing control of virus spread.

Future refinements of the current triple treatment approach may concern vector modifications, strategies for immune evasion, targeted delivery and improvement of the therapeutic efficacy. In order to target tumour cells with a low expression level or insufficient nuclear localisation of YB-1 and in order to expand the application field of YB-1 dependent virotherapy and suicide gene therapy beyond the treatment of malignant gliomas, YB-1 can be cloned into a largely deleted *E1* region of HSV1-sr39TK-armed oncolytic adenoviruses to ensure YB-1 overexpression. It has been demonstrated that YB-1 overexpression from an adenoviral vector can trigger the replication and oncolytic potential of *E1*-deficient adenoviruses [387]. The YB-1 gene can be inserted in place of *E1B55K*, as evidence exist that expression of this gene constitutes no further improvement of viral oncolysis by the HSV1-TK/GCV system. A critical issue hampering the success of virotherapy and suicide gene therapy *in vivo* is the presence of immune responses against the therapeutic vectors [175]. Therefore, virus shielding with polymers [388] or coupling of polymer-coated adenoviruses to therapeutic antibodies that bind to receptors on tumour cells, e.g. EGFR [389], can be considered as future mechanisms to improve systemic tumour transduction *in vivo* and to evade the immune system of the host. In addition, the targeted delivery and the potency of oncolytic adenoviruses *in vivo* can be improved by associating them with magnetic nanoparticles and a magnetic-field-guided infection [390]. Furthermore, the combined oncolytic- and suicide gene strategy can be improved in respect of efficacy and toxicity by the use of sustained intratumoural prodrug delivery systems, e.g. GCV-containing silicone formulations [391] or long-circulating PEGylated liposomes with encapsulated GCV [392]. The addition of immunostimulatory factors like interleukin-12 [393] or the

human soluble Fms-like tyrosine kinase 3 ligand [394] may help to improve the efficacy of combined oncolytic- and suicide gene therapy via stimulating an anti-tumour immunity.
Regarding future preclinical or clinical application of RGD-modified oncolytic adenoviruses, it could be rather of disadvantage for the treatment efficacy when combining them with anti-angiogenic agents as the inhibitor of $\alpha_v\beta_3/\alpha_v\beta_5$ integrins cilentigide [395], because the inhibition of adenovirus-binding integrins may attenuate adenoviral tumour targeting.

Concluding the results of this thesis, the combination between low oncolytic virus, GCV and TMZ doses is as efficient as high doses of the single components for inducing glioma cell eradication. This combined approach might thus reduce the occurrence of potential treatment-induced side effects *in vivo*. Hence, combining YB-1 dependent oncolytic adenoviruses with suicide and reporter gene therapy, and classical anti-glioma chemotherapy, is promising in paving the way to an optimized therapeutic approach against solid cancers, which can be applied *in vivo*.

6. SUMMARY

Glioblastoma multiforme (GBM) is the most common primary brain tumour, characterised with infiltrative growth, high recurrence rate and a fatal outcome. Suicide gene therapy, using the suicide and reporter gene Herpes simplex virus 1 thymidine kinase (*HSV1-TK*) with its prodrug Ganciclovir (GCV), and oncolytic virotherapy are promising tools to address the limitations of current anti-GBM treatment, arising from the aggressive nature of GBM and its resistance to therapy. Conditionally replicating oncolytic adenoviruses are gaining considerable influence in tumour gene therapy. Among them, adenoviruses, dependent in their replication on the oncogenic factor Y-box binding protein 1 (YB-1), contain a manipulation of the essential *E1A* gene, which allows them to replicate in tumour cells with stress-induced nuclear accumulation of YB-1. Despite the success of the HSV1-TK/GCV suicide gene therapy and YB-1 dependent oncolytic virotherapy in the combat of GBM, single-mode approaches are often not as efficient as combined treatments to achieve a sustained therapeutic outcome.

Therefore, based on the finding that YB-1 is overexpressed in GBM, it was of interest to characterise the therapeutic potential of an YB-1 dependent oncolytic adenovirus, armed with the HSV1-TK-mutant *HSV1-sr39TK*, in combination with GCV and the standard anti-GBM chemotherapeutic agent Temozolomide (TMZ) in glioma cells *in vitro*, including a 3D multicellular spheroid model with tumour characteristics. The virus demonstrated strong replication competence, oncolytic potential and ability to produce infectious viral progeny. HSV1-sr39TK transgene expression correlated positively with viral replication, indicating a stable transgene expression despite oncolytic effect. Arming YB-1 dependent oncolytic adenoviruses with a suicide gene was able to eradicate glioma cells more efficiently than oncolysis and HSV1-sr39TK/GCV-mediated cytotoxicity alone in the 3D spheroid model. In 2D culture, oncolysis was potentiated by the HSV1-sr39TK/GCV-mediated cytotoxicity only when GCV was applied at early time points post infection. The potent bystander effect of the suicide gene system in combination with viral replication contributed to the efficacy of the therapeutic approach and allowed for application of low viral load in order to minimise off-target toxicity in non-malignant tissue. In addition, the inhibitory potential of GCV on viral replication at early stages of the viral life cycle represents a fail-safe means to control viral dissemination. Enhancement of YB-1 dependent oncolysis by TMZ and combining this approach with HSV1-sr39TK/GCV-mediated cytotoxicity resulted in a potentiation of glioma cell killing, probably through a combined mode of cell death. In comparison to the oncolytic effect and the HSV1-sr39TK/GCV-mediated cytotoxicity alone, the triple treatment induced significant reduction of 3D spheroid growth. In contrast, viral oncolysis and the HSV1-sr39TK/GCV system exerted a diminished efficacy in the context of multidrug-resistance. Furthermore, HSV1-sr39TK-expressing oncolytic adenoviruses allowed for

radiotracer [^{18}F]-FHBG accumulation in both 2D and 3D glioma models and thus proved to be suitable for non-invasive PET imaging of the therapeutic efficacy within a limited time frame. In conclusion, the results obtained in this thesis highlight the importance of combining YB-1-based virotherapy with conventional cancer treatment and suicide gene therapy for enhancing the therapeutic efficacy of anti-cancer approaches. The problem of impaired efficacy of the suicide gene therapy in many *in vivo* applications, caused by a low transduction efficiency of replication-deficient vectors, can be circumvented by applying replication-competent oncolytic adenoviruses.

7. ZUSAMMENFASSUNG

Glioblastoma multiforme (GBM) ist der häufigste primäre Hirntumor, der sich durch infiltrierendes Wachstum, eine hohe Rezidivrate und eine schlechte Prognose auszeichnet. Die Suizidgentherapie mit dem Herpes simplex virus 1 Thymidinkinase (*HSV1-TK*)/Ganciclovir (GCV)-System, sowie onkolytische Virotherapie, sind vielversprechende Ansätze, um häufig auftretende Einschränkungen der gegenwärtigen Therapiemöglichkeiten für GBM aufzuheben. Diese Einschränkungen resultieren aus dem aggressiven Charakter und der Therapieresistenz von GBM. Tumorzellspezifische onkolytische Adenoviren gewinnen beträchtlich an Einfluss auf die Gentherapie von Tumoren. Unter ihnen befindet sich die Gruppe der Adenoviren, welche in ihrer Replikation von dem onkogenen Faktor Y-Box-bindendes Protein 1 (YB-1) abhängig sind und eine Mutation des essentiellen *E1A*-Gens enthalten. Diese *E1A*-Mutation ermöglicht den Viren die Replikation in Zellen, die eine Stress-induzierte Kernlokalisation von YB-1 aufweisen. Trotz des Erfolges der HSV1-TK/GCV-Suizidgentherapie und der Therapie mit YB-1-abhängigen onkolytischen Adenoviren gegen GBM, sind kombinierte Ansätze meistens effizienter als Monotherapien, um einen nachhaltigen Therapieerfolg zu erzielen.

Basierend auf der Erkenntnis, dass YB-1 in GBM überexprimiert wird, war es daher von Interesse das therapeutische Potential eines *HSV1-sr39TK*-tragenden, YB-1-abhängigen onkolytischen Adenovirus in Kombination mit GCV und dem klassischen anti-GBM-Chemotherapeutikum Temozolomid (TMZ) zu charakterisieren. Die *in vitro* Analyse erfolgte in Gliomzellen, einschließlich eines 3D multizellulären Sphäroid-Modells mit Tumoreigenschaften. Das Virus zeichnete sich durch seine starke Replikationskompetenz, onkolytischen Potential und Fähigkeit zur Produktion von infektiösen viralen Nachkommen aus. Die Expression des Transgens HSV1-sr39TK korrelierte positiv mit der viralen Replikation, was auf eine stabile Expression trotz onkolytischen Effekts hindeutet. Die Kombination aus YB-1-abhängigen onkolytischen Adenoviren und einem Suizidgen ermöglichte ein effizienteres Abtöten von Gliomzellen im 3D Sphäroid-Modell als die Onkolyse und die HSV1-sr39TK/GCV-vermittelte Zytotoxizität allein. Der onkolytische Effekt in 2D Zellkultur wurde durch die HSV1-sr39TK/GCV-vermittelte Zytotoxizität nur unter Zugabe von GCV zu frühen Zeitpunkten nach der Infektion verstärkt. Der starke Bystander-Effekt, induziert durch das Suizidgen-System in Kombination mit viraler Replikation, steuerte zur Wirksamkeit des Therapieansatzes bei und ermöglicht den Einsatz von niedriger Virusdosis, um „Off-target"-Toxizität in nicht-malignes Gewebe zu verhindern. Die Hemmung der viralen Replikation durch GCV in frühen Stadien des viralen Entwicklungszyklus stellt zusätzlich eine zuverlässige Methode dar, um die Ausbreitung des Virus zu kontrollieren. Die Steigerung des YB-1-abhängigen onkolytischen Effektes durch TMZ und die Kombination dieses Ansatzes mit der HSV1-sr39TK/GCV-vermittelten Zytotoxizität führte zu

verstärktem Abtöten von Gliomzellen. Dieses Abtöten kam möglicherweise durch eine kombinierte Art von Zelltod zustande. Im Vergleich zum onkolytischen Effekt und der HSV1-sr39TK/GCV-vermittelten Zytotoxizität allein, erzeugte die dreifache Behandlung eine signifikante Reduktion des Wachstums von 3D Sphäroiden. Im Gegensatz dazu übten die virale Onkolyse und das HSV1-sr39TK/GCV-System einen schwächeren Effekt auf multiresistente Zellen aus. Des Weiteren ermöglichten die HSV1-sr39TK-exprimierenden onkolytischen Adenoviren die Akkumulation des radioaktiven Tracers [^{18}F]-FHBG sowohl in 2D, als auch in 3D Gliom-Modellen und zeigten dadurch ihre Eignung zum nicht-invasiven Imaging der therapeutischen Wirksamkeit im PET-System innerhalb eines begrenzten Zeitfensters. Die Ergebnisse dieser Arbeit heben die Bedeutung der Kombination aus YB-1-abhängiger Virotherapie, konventioneller Krebstherapie und Suizidgentherapie zur Verstärkung der Wirksamkeit von Krebstherapien hervor. Mögliche Beeinträchtigung der Wirksamkeit von Suizidgentherapie *in vivo*, verursacht durch eine niedrige Transduktionseffizienz mit replikationsdefizienten Vektoren, könnte durch den Einsatz von replikationskompetenten onkolytischen Adenoviren umgangen werden.

8. REFERENCES

1. Van Meir, E.G., et al., *Exciting new advances in neuro-oncology: the avenue to a cure for malignant glioma.* CA Cancer J Clin, 2010. **60**(3): p. 166-93.
2. Hadjipanayis, C.G. and E.G. Van Meir, *Brain cancer propagating cells: biology, genetics and targeted therapies.* Trends Mol Med, 2009. **15**(11): p. 519-30.
3. Hadjipanayis, C.G. and E.G. Van Meir, *Tumor initiating cells in malignant gliomas: biology and implications for therapy.* J Mol Med (Berl), 2009. **87**(4): p. 363-74.
4. Bachoo, R.M., et al., *Epidermal growth factor receptor and Ink4a/Arf: convergent mechanisms governing terminal differentiation and transformation along the neural stem cell to astrocyte axis.* Cancer Cell, 2002. **1**(3): p. 269-77.
5. Louis, D.N., et al., *The 2007 WHO classification of tumours of the central nervous system.* Acta Neuropathol, 2007. **114**(2): p. 97-109.
6. Arko, L., et al., *Experimental approaches for the treatment of malignant gliomas.* Pharmacol Ther, 2010. **128**(1): p. 1-36.
7. Ostrom, Q.T., et al., *CBTRUS statistical report: Primary brain and central nervous system tumors diagnosed in the United States in 2006-2010.* Neuro Oncol, 2013. **15 Suppl 2**: p. ii1-56.
8. Adamson, C., et al., *Glioblastoma multiforme: a review of where we have been and where we are going.* Expert Opin Investig Drugs, 2009. **18**(8): p. 1061-83.
9. *US National Institutes of Health. Index of clinical trials.* [last accessed 01.08.2014]; Available from: http://clinicaltrials.gov.
10. Lefranc, F., J. Brotchi, and R. Kiss, *Possible future issues in the treatment of glioblastomas: special emphasis on cell migration and the resistance of migrating glioblastoma cells to apoptosis.* J Clin Oncol, 2005. **23**(10): p. 2411-22.
11. Pulkkanen, K.J. and S. Yla-Herttuala, *Gene therapy for malignant glioma: current clinical status.* Mol Ther, 2005. **12**(4): p. 585-98.
12. Johnson, D.R. and B.P. O'Neill, *Glioblastoma survival in the United States before and during the temozolomide era.* J Neurooncol, 2012. **107**(2): p. 359-64.
13. Tisdale, M.J., *Antitumor imidazotetrazines--XV. Role of guanine O6 alkylation in the mechanism of cytotoxicity of imidazotetrazinones.* Biochem Pharmacol, 1987. **36**(4): p. 457-62.
14. Denny, B.J., et al., *NMR and molecular modeling investigation of the mechanism of activation of the antitumor drug temozolomide and its interaction with DNA.* Biochemistry, 1994. **33**(31): p. 9045-51.
15. Newlands, E.S., et al., *Temozolomide: a review of its discovery, chemical properties, pre-clinical development and clinical trials.* Cancer Treat Rev, 1997. **23**(1): p. 35-61.
16. Stupp, R., et al., *Radiotherapy plus concomitant and adjuvant temozolomide for glioblastoma.* N Engl J Med, 2005. **352**(10): p. 987-96.
17. Stupp, R., et al., *Effects of radiotherapy with concomitant and adjuvant temozolomide versus radiotherapy alone on survival in glioblastoma in a randomised phase III study: 5-year analysis of the EORTC-NCIC trial.* Lancet Oncol, 2009. **10**(5): p. 459-66.
18. Back, M.F., et al., *Improved median survival for glioblastoma multiforme following introduction of adjuvant temozolomide chemotherapy.* Ann Acad Med Singapore, 2007. **36**(5): p. 338-42.
19. Grossman, S.A., et al., *Survival of patients with newly diagnosed glioblastoma treated with radiation and temozolomide in research studies in the United States.* Clin Cancer Res, 2010. **16**(8): p. 2443-9.
20. Beal, K., L.E. Abrey, and P.H. Gutin, *Antiangiogenic agents in the treatment of recurrent or newly diagnosed glioblastoma: analysis of single-agent and combined modality approaches.* Radiat Oncol, 2011. **6**: p. 2.
21. Seystahl, K. and M. Weller, *Is there a world beyond bevacizumab in targeting angiogenesis in glioblastoma?* Expert Opin Investig Drugs, 2012. **21**(5): p. 605-17.
22. Friedman, H.S., et al., *Bevacizumab alone and in combination with irinotecan in recurrent glioblastoma.* J Clin Oncol, 2009. **27**(28): p. 4733-40.
23. Kreisl, T.N., et al., *Phase II trial of single-agent bevacizumab followed by bevacizumab plus irinotecan at tumor progression in recurrent glioblastoma.* J Clin Oncol, 2009. **27**(5): p. 740-5.
24. Weller, M., et al., *Standards of care for treatment of recurrent glioblastoma--are we there yet?* Neuro Oncol, 2013. **15**(1): p. 4-27.
25. Desjardins, A., et al., *Bevacizumab and daily temozolomide for recurrent glioblastoma.* Cancer, 2012. **118**(5): p. 1302-12.

26. Gutin, P.H., et al., *Safety and efficacy of bevacizumab with hypofractionated stereotactic irradiation for recurrent malignant gliomas.* Int J Radiat Oncol Biol Phys, 2009. **75**(1): p. 156-63.
27. Rao, S.K., et al., *A survey of glioblastoma genomic amplifications and deletions.* J Neurooncol, 2010. **96**(2): p. 169-79.
28. Rich, J.N., et al., *Phase II trial of gefitinib in recurrent glioblastoma.* J Clin Oncol, 2004. **22**(1): p. 133-42.
29. Raizer, J.J., et al., *A phase II trial of erlotinib in patients with recurrent malignant gliomas and nonprogressive glioblastoma multiforme postradiation therapy.* Neuro Oncol, 2010. **12**(1): p. 95-103.
30. Akhavan, D., T.F. Cloughesy, and P.S. Mischel, *mTOR signaling in glioblastoma: lessons learned from bench to bedside.* Neuro Oncol, 2010. **12**(8): p. 882-9.
31. Reardon, D.A., et al., *Phase 2 trial of erlotinib plus sirolimus in adults with recurrent glioblastoma.* J Neurooncol, 2010. **96**(2): p. 219-30.
32. Lassen, U., et al., *Phase II study of bevacizumab and temsirolimus combination therapy for recurrent glioblastoma multiforme.* Anticancer Res, 2013. **33**(4): p. 1657-60.
33. Brandes, A.A., et al., *Procarbazine and high-dose tamoxifen as a second-line regimen in recurrent high-grade gliomas: a phase II study.* J Clin Oncol, 1999. **17**(2): p. 645-50.
34. Spence, A.M., et al., *Phase II study of concurrent continuous Temozolomide (TMZ) and Tamoxifen (TMX) for recurrent malignant astrocytic gliomas.* J Neurooncol, 2004. **70**(1): p. 91-5.
35. Kreisl, T.N., et al., *A phase I trial of enzastaurin in patients with recurrent gliomas.* Clin Cancer Res, 2009. **15**(10): p. 3617-23.
36. Louis, D.N., *Molecular pathology of malignant gliomas.* Annu Rev Pathol, 2006. **1**: p. 97-117.
37. Kwiatkowska, A., et al., *Strategies in gene therapy for glioblastoma.* Cancers (Basel), 2013. **5**(4): p. 1271-305.
38. Vega, E.A., M.W. Graner, and J.H. Sampson, *Combating immunosuppression in glioma.* Future Oncol, 2008. **4**(3): p. 433-42.
39. Candolfi, M., et al., *Gene therapy for brain cancer: combination therapies provide enhanced efficacy and safety.* Curr Gene Ther, 2009. **9**(5): p. 409-21.
40. Nduom, E.K., C.G. Hadjipanayis, and E.G. Van Meir, *Glioblastoma cancer stem-like cells: implications for pathogenesis and treatment.* Cancer J, 2012. **18**(1): p. 100-6.
41. Hoeijmakers, J.H., *Genome maintenance mechanisms for preventing cancer.* Nature, 2001. **411**(6835): p. 366-74.
42. Dumenco, L.L., et al., *Increase in nitrosourea resistance in mammalian cells by retrovirally mediated gene transfer of bacterial O6-alkylguanine-DNA alkyltransferase.* Cancer Res, 1989. **49**(21): p. 6044-51.
43. Hegi, M.E., et al., *MGMT gene silencing and benefit from temozolomide in glioblastoma.* N Engl J Med, 2005. **352**(10): p. 997-1003.
44. Belanich, M., et al., *Retrospective study of the correlation between the DNA repair protein alkyltransferase and survival of brain tumor patients treated with carmustine.* Cancer Res, 1996. **56**(4): p. 783-8.
45. Friedman, H.S., et al., *DNA mismatch repair and O6-alkylguanine-DNA alkyltransferase analysis and response to Temodal in newly diagnosed malignant glioma.* J Clin Oncol, 1998. **16**(12): p. 3851-7.
46. Quinn, J.A., et al., *Phase I trial of temozolomide plus O6-benzylguanine for patients with recurrent or progressive malignant glioma.* J Clin Oncol, 2005. **23**(28): p. 7178-87.
47. Quinn, J.A., et al., *Phase II trial of Gliadel plus O6-benzylguanine in adults with recurrent glioblastoma multiforme.* Clin Cancer Res, 2009. **15**(3): p. 1064-8.
48. Quinn, J.A., et al., *Phase 1 trial of temozolomide plus irinotecan plus O6-benzylguanine in adults with recurrent malignant glioma.* Cancer, 2009. **115**(13): p. 2964-70.
49. Gottesman, M.M., T. Fojo, and S.E. Bates, *Multidrug resistance in cancer: role of ATP-dependent transporters.* Nat Rev Cancer, 2002. **2**(1): p. 48-58.
50. Choudhuri, S. and C.D. Klaassen, *Structure, function, expression, genomic organization, and single nucleotide polymorphisms of human ABCB1 (MDR1), ABCC (MRP), and ABCG2 (BCRP) efflux transporters.* Int J Toxicol, 2006. **25**(4): p. 231-59.
51. Lage, H., et al., *Thermosensitivity of multidrug-resistant human gastric and pancreatic carcinoma cells.* Int J Hyperthermia, 2000. **16**(4): p. 291-303.
52. Lage, H. and M. Dietel, *Multiple mechanisms confer different drug-resistant phenotypes in pancreatic carcinoma cells.* J Cancer Res Clin Oncol, 2002. **128**(7): p. 349-57.
53. Gyorffy, B., et al., *Prediction of doxorubicin sensitivity in breast tumors based on gene expression profiles of drug-resistant cell lines correlates with patient survival.* Oncogene, 2005. **24**(51): p. 7542-51.

54. Greco, O. and G.U. Dachs, *Gene directed enzyme/prodrug therapy of cancer: historical appraisal and future prospectives.* J Cell Physiol, 2001. **187**(1): p. 22-36.
55. Moolten, F.L., *Tumor chemosensitivity conferred by inserted herpes thymidine kinase genes: paradigm for a prospective cancer control strategy.* Cancer Res, 1986. **46**(10): p. 5276-81.
56. Ardiani, A., et al., *Enzymes to die for: exploiting nucleotide metabolizing enzymes for cancer gene therapy.* Curr Gene Ther, 2012. **12**(2): p. 77-91.
57. Portsmouth, D., J. Hlavaty, and M. Renner, *Suicide genes for cancer therapy.* Mol Aspects Med, 2007. **28**(1): p. 4-41.
58. Chen, S.H., et al., *Failure of thymidine kinase-negative herpes simplex virus to reactivate from latency following efficient establishment.* J Virol, 2004. **78**(1): p. 520-3.
59. Elion, G.B., et al., *Selectivity of action of an antiherpetic agent, 9-(2-hydroxyethoxymethyl) guanine.* Proc Natl Acad Sci U S A, 1977. **74**(12): p. 5716-20.
60. Balzarini, J., C. Bohman, and E. De Clercq, *Differential mechanism of cytostatic effect of (E)-5-(2-bromovinyl)-2'-deoxyuridine, 9-(1,3-dihydroxy-2-propoxymethyl)guanine, and other antiherpetic drugs on tumor cells transfected by the thymidine kinase gene of herpes simplex virus type 1 or type 2.* J Biol Chem, 1993. **268**(9): p. 6332-7.
61. Field, A.K., et al., *9-([2-hydroxy-1-(hydroxymethyl)ethoxy]methyl)guanine: a selective inhibitor of herpes group virus replication.* Proc Natl Acad Sci U S A, 1983. **80**(13): p. 4139-43.
62. Cheng, Y.C., et al., *Metabolism of 9-(1,3-dihydroxy-2-propoxymethyl)guanine, a new anti-herpes virus compound, in herpes simplex virus-infected cells.* J Biol Chem, 1983. **258**(20): p. 12460-4.
63. Boehme, R.E., *Phosphorylation of the antiviral precursor 9-(1,3-dihydroxy-2-propoxymethyl)guanine monophosphate by guanylate kinase isozymes.* J Biol Chem, 1984. **259**(20): p. 12346-9.
64. Mar, E.C., et al., *Inhibition of cellular DNA polymerase alpha and human cytomegalovirus-induced DNA polymerase by the triphosphates of 9-(2-hydroxyethoxymethyl)guanine and 9-(1,3-dihydroxy-2-propoxymethyl)guanine.* J Virol, 1985. **53**(3): p. 776-80.
65. Cannon, J.S., et al., *Human herpesvirus 8-encoded thymidine kinase and phosphotransferase homologues confer sensitivity to ganciclovir.* J Virol, 1999. **73**(6): p. 4786-93.
66. Oon, C.J., et al., *Hepatitis B virus variants with lamivudine-related mutations in the DNA polymerase and the 'a' epitope of the surface antigen are sensitive to ganciclovir.* Antiviral Res, 1999. **41**(3): p. 113-8.
67. Beltinger, C., et al., *Mitochondrial amplification of death signals determines thymidine kinase/ganciclovir-triggered activation of apoptosis.* Cancer Res, 2000. **60**(12): p. 3212-7.
68. Glaser, T., et al., *Death receptor-independent cytochrome c release and caspase activation mediate thymidine kinase plus ganciclovir-mediated cytotoxicity in LN-18 and LN-229 human malignant glioma cells.* Gene Ther, 2001. **8**(6): p. 469-76.
69. Tomicic, M.T., R. Thust, and B. Kaina, *Ganciclovir-induced apoptosis in HSV-1 thymidine kinase expressing cells: critical role of DNA breaks, Bcl-2 decline and caspase-9 activation.* Oncogene, 2002. **21**(14): p. 2141-53.
70. Fischer, U., et al., *Mechanisms of thymidine kinase/ganciclovir and cytosine deaminase/ 5-fluorocytosine suicide gene therapy-induced cell death in glioma cells.* Oncogene, 2005. **24**(7): p. 1231-43.
71. Kaneko, Y. and A. Tsukamoto, *Gene therapy of hepatoma: bystander effects and non-apoptotic cell death induced by thymidine kinase and ganciclovir.* Cancer Lett, 1995. **96**(1): p. 105-10.
72. Vile, R.G., et al., *Generation of an anti-tumour immune response in a non-immunogenic tumour: HSVtk killing in vivo stimulates a mononuclear cell infiltrate and a Th1-like profile of intratumoural cytokine expression.* Int J Cancer, 1997. **71**(2): p. 267-74.
73. Todryk, S., et al., *Cell death associated with genetic prodrug activation therapy of colorectal cancer.* Cancer Lett, 2001. **174**(1): p. 25-33.
74. Rubsam, L.Z., et al., *Cytotoxicity and accumulation of ganciclovir triphosphate in bystander cells cocultured with herpes simplex virus type 1 thymidine kinase-expressing human glioblastoma cells.* Cancer Res, 1999. **59**(3): p. 669-75.
75. van Dillen, I.J., et al., *Influence of the bystander effect on HSV-tk/GCV gene therapy. A review.* Curr Gene Ther, 2002. **2**(3): p. 307-22.
76. Culver, K.W., et al., *In vivo gene transfer with retroviral vector-producer cells for treatment of experimental brain tumors.* Science, 1992. **256**(5063): p. 1550-2.
77. Freeman, S.M., et al., *The "bystander effect": tumor regression when a fraction of the tumor mass is genetically modified.* Cancer Res, 1993. **53**(21): p. 5274-83.

78. Takamiya, Y., et al., *An experimental model of retrovirus gene therapy for malignant brain tumors.* J Neurosurg, 1993. **79**(1): p. 104-10.
79. Ram, Z., et al., *In situ retroviral-mediated gene transfer for the treatment of brain tumors in rats.* Cancer Res, 1993. **53**(1): p. 83-8.
80. Colombo, B.M., et al., *The "bystander effect": association of U-87 cell death with ganciclovir-mediated apoptosis of nearby cells and lack of effect in athymic mice.* Hum Gene Ther, 1995. **6**(6): p. 763-72.
81. Bi, W.L., et al., *In vitro evidence that metabolic cooperation is responsible for the bystander effect observed with HSV tk retroviral gene therapy.* Hum Gene Ther, 1993. **4**(6): p. 725-31.
82. Elshami, A.A., et al., *Gap junctions play a role in the 'bystander effect' of the herpes simplex virus thymidine kinase/ganciclovir system in vitro.* Gene Ther, 1996. **3**(1): p. 85-92.
83. Asklund, T., et al., *Gap junction-mediated bystander effect in primary cultures of human malignant gliomas with recombinant expression of the HSVtk gene.* Exp Cell Res, 2003. **284**(2): p. 185-95.
84. Munir, K.M., et al., *Herpes thymidine kinase mutants with altered catalytic efficiencies obtained by random sequence selection.* Protein Eng, 1994. **7**(1): p. 83-9.
85. Black, M.E., et al., *Creation of drug-specific herpes simplex virus type 1 thymidine kinase mutants for gene therapy.* Proc Natl Acad Sci U S A, 1996. **93**(8): p. 3525-9.
86. Black, M.E., M.S. Kokoris, and P. Sabo, *Herpes simplex virus-1 thymidine kinase mutants created by semi-random sequence mutagenesis improve prodrug-mediated tumor cell killing.* Cancer Res, 2001. **61**(7): p. 3022-6.
87. Preuss, E., et al., *TK.007: A novel, codon-optimized HSVtk(A168H) mutant for suicide gene therapy.* Hum Gene Ther, 2010. **21**(8): p. 929-41.
88. Preuss, E., et al., *Cancer suicide gene therapy with TK.007: superior killing efficiency and bystander effect.* J Mol Med (Berl), 2011. **89**(11): p. 1113-24.
89. Pantuck, A.J., et al., *Optimizing prostate cancer suicide gene therapy using herpes simplex virus thymidine kinase active site variants.* Hum Gene Ther, 2002. **13**(7): p. 777-89.
90. Wiewrodt, R., et al., *Adenovirus-mediated gene transfer of enhanced Herpes simplex virus thymidine kinase mutants improves prodrug-mediated tumor cell killing.* Cancer Gene Ther, 2003. **10**(5): p. 353-64.
91. Hasenburg, A., et al., *Adenovirus-mediated thymidine kinase gene therapy in combination with topotecan for patients with recurrent ovarian cancer: 2.5-year follow-up.* Gynecol Oncol, 2001. **83**(3): p. 549-54.
92. Hasenburg, A., et al., *Histologic and immunohistochemical analysis of tissue response to adenovirus-mediated herpes simplex thymidine kinase gene therapy of ovarian cancer.* Int J Gynecol Cancer, 2002. **12**(1): p. 66-73.
93. Klatzmann, D., et al., *A phase I/II dose-escalation study of herpes simplex virus type 1 thymidine kinase "suicide" gene therapy for metastatic melanoma. Study Group on Gene Therapy of Metastatic Melanoma.* Hum Gene Ther, 1998. **9**(17): p. 2585-94.
94. Ayala, G., et al., *Biological response determinants in HSV-tk + ganciclovir gene therapy for prostate cancer.* Mol Ther, 2006. **13**(4): p. 716-28.
95. Nasu, Y., et al., *Suicide gene therapy with adenoviral delivery of HSV-tK gene for patients with local recurrence of prostate cancer after hormonal therapy.* Mol Ther, 2007. **15**(4): p. 834-40.
96. Immonen, A., et al., *AdvHSV-tk gene therapy with intravenous ganciclovir improves survival in human malignant glioma: a randomised, controlled study.* Mol Ther, 2004. **10**(5): p. 967-72.
97. Klatzmann, D., et al., *A phase I/II study of herpes simplex virus type 1 thymidine kinase "suicide" gene therapy for recurrent glioblastoma. Study Group on Gene Therapy for Glioblastoma.* Hum Gene Ther, 1998. **9**(17): p. 2595-604.
98. Prados, M.D., et al., *Treatment of progressive or recurrent glioblastoma multiforme in adults with herpes simplex virus thymidine kinase gene vector-producer cells followed by intravenous ganciclovir administration: a phase I/II multi-institutional trial.* J Neurooncol, 2003. **65**(3): p. 269-78.
99. Chiocca, E.A., et al., *Phase IB study of gene-mediated cytotoxic immunotherapy adjuvant to up-front surgery and intensive timing radiation for malignant glioma.* J Clin Oncol, 2011. **29**(27): p. 3611-9.
100. Rainov, N.G., *A phase III clinical evaluation of herpes simplex virus type 1 thymidine kinase and ganciclovir gene therapy as an adjuvant to surgical resection and radiation in adults with previously untreated glioblastoma multiforme.* Hum Gene Ther, 2000. **11**(17): p. 2389-401.
101. Westphal, M., et al., *Adenovirus-mediated gene therapy with sitimagene ceradenovec followed by intravenous ganciclovir for patients with operable high-grade glioma (ASPECT): a randomised, open-label, phase 3 trial.* Lancet Oncol, 2013. **14**(9): p. 823-33.

102. Wahlfors, T., et al., *In vivo enhancement of herpes simplex virus thymidine kinase/ganciclovir cancer gene therapy with polyamine biosynthesis inhibition.* Int J Cancer, 2006. **118**(11): p. 2907-10.
103. Rainov, N.G., et al., *Temozolomide enhances herpes simplex virus thymidine kinase/ganciclovir therapy of malignant glioma.* Cancer Gene Ther, 2001. **8**(9): p. 662-8.
104. Mullen, C.A., M. Kilstrup, and R.M. Blaese, *Transfer of the bacterial gene for cytosine deaminase to mammalian cells confers lethal sensitivity to 5-fluorocytosine: a negative selection system.* Proc Natl Acad Sci U S A, 1992. **89**(1): p. 33-7.
105. Chang, T.K., et al., *Differential activation of cyclophosphamide and ifosphamide by cytochromes P-450 2B and 3A in human liver microsomes.* Cancer Res, 1993. **53**(23): p. 5629-37.
106. Nemunaitis, J., et al., *Pilot trial of genetically modified, attenuated Salmonella expressing the E. coli cytosine deaminase gene in refractory cancer patients.* Cancer Gene Ther, 2003. **10**(10): p. 737-44.
107. Salmons, B., M. Lohr, and W.H. Gunzburg, *Treatment of inoperable pancreatic carcinoma using a cell-based local chemotherapy: results of a phase I/II clinical trial.* J Gastroenterol, 2003. **38 Suppl 15**: p. 78-84.
108. Gambhir, S.S., et al., *Imaging transgene expression with radionuclide imaging technologies.* Neoplasia, 2000. **2**(1-2): p. 118-38.
109. Gambhir, S.S., et al., *Assays for noninvasive imaging of reporter gene expression.* Nucl Med Biol, 1999. **26**(5): p. 481-90.
110. Blasberg, R.G. and J.G. Tjuvajev, *Molecular-genetic imaging: current and future perspectives.* J Clin Invest, 2003. **111**(11): p. 1620-9.
111. Gambhir, S.S., et al., *Imaging of adenoviral-directed herpes simplex virus type 1 thymidine kinase reporter gene expression in mice with radiolabeled ganciclovir.* J Nucl Med, 1998. **39**(11): p. 2003-11.
112. Gambhir, S.S., et al., *Imaging adenoviral-directed reporter gene expression in living animals with positron emission tomography.* Proc Natl Acad Sci U S A, 1999. **96**(5): p. 2333-8.
113. Gambhir, S.S., et al., *A mutant herpes simplex virus type 1 thymidine kinase reporter gene shows improved sensitivity for imaging reporter gene expression with positron emission tomography.* Proc Natl Acad Sci U S A, 2000. **97**(6): p. 2785-90.
114. Anton, M., et al., *Coexpression of herpesviral thymidine kinase reporter gene and VEGF gene for noninvasive monitoring of therapeutic gene transfer: an in vitro evaluation.* J Nucl Med, 2004. **45**(10): p. 1743-6.
115. Miyagawa, M., et al., *PET of cardiac transgene expression: comparison of 2 approaches based on herpesviral thymidine kinase reporter gene.* J Nucl Med, 2004. **45**(11): p. 1917-23.
116. Miyagawa, M., et al., *Non-invasive imaging of cardiac transgene expression with PET: comparison of the human sodium/iodide symporter gene and HSV1-tk as the reporter gene.* Eur J Nucl Med Mol Imaging, 2005. **32**(9): p. 1108-14.
117. Brust, P., et al., *Comparison of [18F]FHPG and [124/125I]FIAU for imaging herpes simplex virus type 1 thymidine kinase gene expression.* Eur J Nucl Med, 2001. **28**(6): p. 721-9.
118. Tjuvajev, J.G., et al., *Comparison of radiolabeled nucleoside probes (FIAU, FHBG, and FHPG) for PET imaging of HSV1-tk gene expression.* J Nucl Med, 2002. **43**(8): p. 1072-83.
119. Min, J.J., M. Iyer, and S.S. Gambhir, *Comparison of [18F]FHBG and [14C]FIAU for imaging of HSV1-tk reporter gene expression: adenoviral infection vs stable transfection.* Eur J Nucl Med Mol Imaging, 2003. **30**(11): p. 1547-60.
120. Pantuck, A.J., et al., *CL1-SR39: A noninvasive molecular imaging model of prostate cancer suicide gene therapy using positron emission tomography.* J Urol, 2002. **168**(3): p. 1193-8.
121. Yang, H., et al., *MicroPET imaging of prostate cancer in LNCAP-SR39TK-GFP mouse xenografts.* Prostate, 2003. **55**(1): p. 39-47.
122. Yaghoubi, S.S., et al., *Imaging progress of herpes simplex virus type 1 thymidine kinase suicide gene therapy in living subjects with positron emission tomography.* Cancer Gene Ther, 2005. **12**(3): p. 329-39.
123. Jacobs, A.H., et al., *Imaging-guided gene therapy of experimental gliomas.* Cancer Res, 2007. **67**(4): p. 1706-15.
124. Jacobs, A., et al., *Positron-emission tomography of vector-mediated gene expression in gene therapy for gliomas.* Lancet, 2001. **358**(9283): p. 727-9.
125. Voges, J., et al., *Imaging-guided convection-enhanced delivery and gene therapy of glioblastoma.* Ann Neurol, 2003. **54**(4): p. 479-87.
126. Penuelas, I., et al., *Positron emission tomography imaging of adenoviral-mediated transgene expression in liver cancer patients.* Gastroenterology, 2005. **128**(7): p. 1787-95.

127. Sangro, B., et al., *A phase I clinical trial of thymidine kinase-based gene therapy in advanced hepatocellular carcinoma.* Cancer Gene Ther, 2010. **17**(12): p. 837-43.
128. Serganova, I., V. Ponomarev, and R. Blasberg, *Human reporter genes: potential use in clinical studies.* Nucl Med Biol, 2007. **34**(7): p. 791-807.
129. Spitzweg, C., et al., *Treatment of prostate cancer by radioiodine therapy after tissue-specific expression of the sodium iodide symporter.* Cancer Res, 2000. **60**(22): p. 6526-30.
130. Jun, K.H., et al., *A novel oncolytic viral therapy and imaging technique for gastric cancer using a genetically engineered vaccinia virus carrying the human sodium iodide symporter.* J Exp Clin Cancer Res, 2014. **33**: p. 2.
131. Wang, Z., et al., *Imaging and therapy of hSSTR2-transfected tumors using radiolabeled somatostatin analogs.* Tumour Biol, 2013. **34**(4): p. 2451-7.
132. van Wieringen, J.P., et al., *Synthesis and characterization of a novel series of agonist compounds as potential radiopharmaceuticals for imaging dopamine D(2)/(3) receptors in their high-affinity state.* J Med Chem, 2014. **57**(2): p. 391-410.
133. Rowe, W.P., et al., *Isolation of a cytopathogenic agent from human adenoids undergoing spontaneous degeneration in tissue culture.* Proc Soc Exp Biol Med, 1953. **84**(3): p. 570-3.
134. Walsh, M.P., et al., *Computational analysis identifies human adenovirus type 55 as a re-emergent acute respiratory disease pathogen.* J Clin Microbiol, 2010. **48**(3): p. 991-3.
135. Robinson, C.M., et al., *Computational analysis and identification of an emergent human adenovirus pathogen implicated in a respiratory fatality.* Virology, 2011. **409**(2): p. 141-7.
136. Hierholzer, J.C., *Adenoviruses in the immunocompromised host.* Clin Microbiol Rev, 1992. **5**(3): p. 262-74.
137. Robinson, C.M., et al., *Molecular evolution of human adenoviruses.* Sci Rep, 2013. **3**: p. 1812.
138. Smith, J.G., et al., *Adenovirus.* Curr Top Microbiol Immunol, 2010. **343**: p. 195-224.
139. Nemerow, G.R., P.L. Stewart, and V.S. Reddy, *Structure of human adenovirus.* Curr Opin Virol, 2012. **2**(2): p. 115-21.
140. Reddy, V.S., et al., *Crystal structure of human adenovirus at 3.5 A resolution.* Science, 2010. **329**(5995): p. 1071-5.
141. Liu, H., et al., *Atomic structure of human adenovirus by cryo-EM reveals interactions among protein networks.* Science, 2010. **329**(5995): p. 1038-43.
142. Burnett, R.M., *The structure of the adenovirus capsid. II. The packing symmetry of hexon and its implications for viral architecture.* J Mol Biol, 1985. **185**(1): p. 125-43.
143. Saban, S.D., et al., *Visualization of alpha-helices in a 6-angstrom resolution cryoelectron microscopy structure of adenovirus allows refinement of capsid protein assignments.* J Virol, 2006. **80**(24): p. 12049-59.
144. Russell, W.C., *Adenoviruses: update on structure and function.* J Gen Virol, 2009. **90**(Pt 1): p. 1-20.
145. Vellinga, J., S. Van der Heijdt, and R.C. Hoeben, *The adenovirus capsid: major progress in minor proteins.* J Gen Virol, 2005. **86**(Pt 6): p. 1581-8.
146. Bergelson, J.M., et al., *Isolation of a common receptor for Coxsackie B viruses and adenoviruses 2 and 5.* Science, 1997. **275**(5304): p. 1320-3.
147. Mathias, P., et al., *Multiple adenovirus serotypes use alpha v integrins for infection.* J Virol, 1994. **68**(10): p. 6811-4.
148. Meier, O. and U.F. Greber, *Adenovirus endocytosis.* J Gene Med, 2004. **6 Suppl 1**: p. S152-63.
149. Leopold, P.L., et al., *Dynein- and microtubule-mediated translocation of adenovirus serotype 5 occurs after endosomal lysis.* Hum Gene Ther, 2000. **11**(1): p. 151-65.
150. Trotman, L.C., et al., *Import of adenovirus DNA involves the nuclear pore complex receptor CAN/Nup214 and histone H1.* Nat Cell Biol, 2001. **3**(12): p. 1092-100.
151. Hearing, P., et al., *Identification of a repeated sequence element required for efficient encapsidation of the adenovirus type 5 chromosome.* J Virol, 1987. **61**(8): p. 2555-8.
152. de Jong, R.N. and P.C. van der Vliet, *Mechanism of DNA replication in eukaryotic cells: cellular host factors stimulating adenovirus DNA replication.* Gene, 1999. **236**(1): p. 1-12.
153. Russell, W.C., *Update on adenovirus and its vectors.* J Gen Virol, 2000. **81**(Pt 11): p. 2573-604.
154. Berk, A.J., et al., *Pre-early adenovirus 5 gene product regulates synthesis of early viral messenger RNAs.* Cell, 1979. **17**(4): p. 935-44.
155. Jones, N. and T. Shenk, *An adenovirus type 5 early gene function regulates expression of other early viral genes.* Proc Natl Acad Sci U S A, 1979. **76**(8): p. 3665-9.

156. Frisch, S.M. and J.S. Mymryk, *Adenovirus-5 E1A: paradox and paradigm.* Nat Rev Mol Cell Biol, 2002. **3**(6): p. 441-52.
157. Pelka, P., et al., *Intrinsic structural disorder in adenovirus E1A: a viral molecular hub linking multiple diverse processes.* J Virol, 2008. **82**(15): p. 7252-63.
158. Fattaey, A.R., E. Harlow, and K. Helin, *Independent regions of adenovirus E1A are required for binding to and dissociation of E2F-protein complexes.* Mol Cell Biol, 1993. **13**(12): p. 7267-77.
159. Spitkovsky, D., et al., *S-phase induction by adenovirus E1A requires activation of cdc25a tyrosine phosphatase.* Oncogene, 1996. **12**(12): p. 2549-54.
160. Querido, E., et al., *Degradation of p53 by adenovirus E4orf6 and E1B55K proteins occurs via a novel mechanism involving a Cullin-containing complex.* Genes Dev, 2001. **15**(23): p. 3104-17.
161. Flint, S.J. and R.A. Gonzalez, *Regulation of mRNA production by the adenoviral E1B 55-kDa and E4 Orf6 proteins.* Curr Top Microbiol Immunol, 2003. **272**: p. 287-330.
162. Han, J., et al., *The E1B 19K protein blocks apoptosis by interacting with and inhibiting the p53-inducible and death-promoting Bax protein.* Genes Dev, 1996. **10**(4): p. 461-77.
163. Hay, R.T., et al., *Molecular interactions during adenovirus DNA replication.* Curr Top Microbiol Immunol, 1995. **199 (Pt 2)**: p. 31-48.
164. de Jong, R.N., P.C. van der Vliet, and A.B. Brenkman, *Adenovirus DNA replication: protein priming, jumping back and the role of the DNA binding protein DBP.* Curr Top Microbiol Immunol, 2003. **272**: p. 187-211.
165. Tollefson, A.E., et al., *The adenovirus death protein (E3-11.6K) is required at very late stages of infection for efficient cell lysis and release of adenovirus from infected cells.* J Virol, 1996. **70**(4): p. 2296-306.
166. Lichtenstein, D.L., et al., *Functions and mechanisms of action of the adenovirus E3 proteins.* Int Rev Immunol, 2004. **23**(1-2): p. 75-111.
167. Weitzman, M.D., *Functions of the adenovirus E4 proteins and their impact on viral vectors.* Front Biosci, 2005. **10**: p. 1106-17.
168. Lai, C.M., Y.K. Lai, and P.E. Rakoczy, *Adenovirus and adeno-associated virus vectors.* DNA Cell Biol, 2002. **21**(12): p. 895-913.
169. Chen, P.H., D.A. Ornelles, and T. Shenk, *The adenovirus L3 23-kilodalton proteinase cleaves the amino-terminal head domain from cytokeratin 18 and disrupts the cytokeratin network of HeLa cells.* J Virol, 1993. **67**(6): p. 3507-14.
170. Kasel, J.A., *Diagnostic procedures for viral, rickettsial and chlamydial infections*. Adenoviruses, ed. E.H. Lennette and N.J. Schmidt. 1979, Washington, DC: American Public Health Association.
171. Kanerva, A. and A. Hemminki, *Modified adenoviruses for cancer gene therapy.* Int J Cancer, 2004. **110**(4): p. 475-80.
172. Bett, A.J., L. Prevec, and F.L. Graham, *Packaging capacity and stability of human adenovirus type 5 vectors.* J Virol, 1993. **67**(10): p. 5911-21.
173. Bett, A.J., et al., *An efficient and flexible system for construction of adenovirus vectors with insertions or deletions in early regions 1 and 3.* Proc Natl Acad Sci U S A, 1994. **91**(19): p. 8802-6.
174. Alemany, R., C. Balague, and D.T. Curiel, *Replicative adenoviruses for cancer therapy.* Nat Biotechnol, 2000. **18**(7): p. 723-7.
175. Russell, S.J., K.W. Peng, and J.C. Bell, *Oncolytic virotherapy.* Nat Biotechnol, 2012. **30**(7): p. 658-70.
176. Lal, R., et al., *Reovirus: Rationale and clinical trial update.* Curr Opin Mol Ther, 2009. **11**(5): p. 532-9.
177. Haag, A., et al., *Highly efficient transduction and expression of cytokine genes in human tumor cells by means of autonomous parvovirus vectors; generation of antitumor responses in recipient mice.* Hum Gene Ther, 2000. **11**(4): p. 597-609.
178. Altomonte, J., et al., *Engineered newcastle disease virus as an improved oncolytic agent against hepatocellular carcinoma.* Mol Ther, 2010. **18**(2): p. 275-84.
179. Zamarin, D. and P. Palese, *Oncolytic Newcastle disease virus for cancer therapy: old challenges and new directions.* Future Microbiol, 2012. **7**(3): p. 347-67.
180. Myers, R., et al., *Oncolytic activities of approved mumps and measles vaccines for therapy of ovarian cancer.* Cancer Gene Ther, 2005. **12**(7): p. 593-9.
181. Tai, C.K. and N. Kasahara, *Replication-competent retrovirus vectors for cancer gene therapy.* Front Biosci, 2008. **13**: p. 3083-95.
182. Yamamoto, M. and D.T. Curiel, *Current issues and future directions of oncolytic adenoviruses.* Mol Ther, 2010. **18**(2): p. 243-50.

183. Nettelbeck, D.M., *Virotherapeutics: conditionally replicative adenoviruses for viral oncolysis.* Anticancer Drugs, 2003. **14**(8): p. 577-84.
184. Jiang, H., et al., *Examination of the therapeutic potential of Delta-24-RGD in brain tumor stem cells: role of autophagic cell death.* J Natl Cancer Inst, 2007. **99**(18): p. 1410-4.
185. Nandi, S., et al., *Low-dose radiation enhances survivin-mediated virotherapy against malignant glioma stem cells.* Cancer Res, 2008. **68**(14): p. 5778-84.
186. Wu, C.L., et al., *Tumor-selective replication of an oncolytic adenovirus carrying oct-3/4 response elements in murine metastatic bladder cancer models.* Clin Cancer Res, 2008. **14**(4): p. 1228-38.
187. Bischoff, J.R., et al., *An adenovirus mutant that replicates selectively in p53-deficient human tumor cells.* Science, 1996. **274**(5286): p. 373-6.
188. Heise, C., et al., *ONYX-015, an E1B gene-attenuated adenovirus, causes tumor-specific cytolysis and antitumoral efficacy that can be augmented by standard chemotherapeutic agents.* Nat Med, 1997. **3**(6): p. 639-45.
189. Yang, C.T., et al., *p14(ARF) modulates the cytolytic effect of ONYX-015 in mesothelioma cells with wild-type p53.* Cancer Res, 2001. **61**(16): p. 5959-63.
190. Edwards, S.J., et al., *Evidence that replication of the antitumor adenovirus ONYX-015 is not controlled by the p53 and p14(ARF) tumor suppressor genes.* J Virol, 2002. **76**(24): p. 12483-90.
191. Fueyo, J., et al., *A mutant oncolytic adenovirus targeting the Rb pathway produces anti-glioma effect in vivo.* Oncogene, 2000. **19**(1): p. 2-12.
192. Rodriguez, R., et al., *Prostate attenuated replication competent adenovirus (ARCA) CN706: a selective cytotoxic for prostate-specific antigen-positive prostate cancer cells.* Cancer Res, 1997. **57**(13): p. 2559-63.
193. Li, Y., et al., *A hepatocellular carcinoma-specific adenovirus variant, CV890, eliminates distant human liver tumors in combination with doxorubicin.* Cancer Res, 2001. **61**(17): p. 6428-36.
194. Huang, T.G., et al., *Telomerase-dependent oncolytic adenovirus for cancer treatment.* Gene Ther, 2003. **10**(15): p. 1241-7.
195. Duncan, S.J., et al., *Infection of mouse liver by human adenovirus type 5.* J Gen Virol, 1978. **40**(1): p. 45-61.
196. Kim, M., et al., *The therapeutic efficacy of adenoviral vectors for cancer gene therapy is limited by a low level of primary adenovirus receptors on tumour cells.* Eur J Cancer, 2002. **38**(14): p. 1917-26.
197. Dmitriev, I., et al., *An adenovirus vector with genetically modified fibers demonstrates expanded tropism via utilization of a coxsackievirus and adenovirus receptor-independent cell entry mechanism.* J Virol, 1998. **72**(12): p. 9706-13.
198. Ulasov, I.V., et al., *Survivin-driven and fiber-modified oncolytic adenovirus exhibits potent antitumor activity in established intracranial glioma.* Hum Gene Ther, 2007. **18**(7): p. 589-602.
199. Kimball, K.J., et al., *A phase I study of a tropism-modified conditionally replicative adenovirus for recurrent malignant gynecologic diseases.* Clin Cancer Res, 2010. **16**(21): p. 5277-87.
200. Pesonen, S., et al., *Integrin targeted oncolytic adenoviruses Ad5-D24-RGD and Ad5-RGD-D24-GMCSF for treatment of patients with advanced chemotherapy refractory solid tumors.* Int J Cancer, 2012. **130**(8): p. 1937-47.
201. Sauthoff, H., et al., *Deletion of the adenoviral E1b-19kD gene enhances tumor cell killing of a replicating adenoviral vector.* Hum Gene Ther, 2000. **11**(3): p. 379-88.
202. Sova, P., et al., *A tumor-targeted and conditionally replicating oncolytic adenovirus vector expressing TRAIL for treatment of liver metastases.* Mol Ther, 2004. **9**(4): p. 496-509.
203. Lamfers, M.L., et al., *Tissue inhibitor of metalloproteinase-3 expression from an oncolytic adenovirus inhibits matrix metalloproteinase activity in vivo without affecting antitumor efficacy in malignant glioma.* Cancer Res, 2005. **65**(20): p. 9398-405.
204. Kanerva, A., et al., *Antiviral and antitumor T-cell immunity in patients treated with GM-CSF-coding oncolytic adenovirus.* Clin Cancer Res, 2013. **19**(10): p. 2734-44.
205. Sutherland, R.M., *Cell and environment interactions in tumor microregions: the multicell spheroid model.* Science, 1988. **240**(4849): p. 177-84.
206. Monazzam, A., et al., *Multicellular tumour spheroid as a model for evaluation of [18F]FDG as biomarker for breast cancer treatment monitoring.* Cancer Cell Int, 2006. **6**: p. 6.
207. Monazzam, A., et al., *Application of the multicellular tumour spheroid model to screen PET tracers for analysis of early response of chemotherapy in breast cancer.* Breast Cancer Res, 2007. **9**(4): p. R45.
208. Herrmann, R., et al., *Screening for compounds that induce apoptosis of cancer cells grown as multicellular spheroids.* J Biomol Screen, 2008. **13**(1): p. 1-8.

209. Mehta, G., et al., *Opportunities and challenges for use of tumor spheroids as models to test drug delivery and efficacy.* J Control Release, 2012. **164**(2): p. 192-204.
210. Grill, J., et al., *The organotypic multicellular spheroid is a relevant three-dimensional model to study adenovirus replication and penetration in human tumors in vitro.* Mol Ther, 2002. **6**(5): p. 609-14.
211. Lamfers, M.L., et al., *Potential of the conditionally replicative adenovirus Ad5-Delta24RGD in the treatment of malignant gliomas and its enhanced effect with radiotherapy.* Cancer Res, 2002. **62**(20): p. 5736-42.
212. van Beusechem, V.W., et al., *Conditionally replicative adenovirus expressing a targeting adapter molecule exhibits enhanced oncolytic potency on CAR-deficient tumors.* Gene Ther, 2003. **10**(23): p. 1982-91.
213. Lam, J.T., et al., *A three-dimensional assay for measurement of viral-induced oncolysis.* Cancer Gene Ther, 2007. **14**(4): p. 421-30.
214. Idema, S., et al., *Evaluation of adenoviral oncolytic effect on glioma spheroids by 18F-DG positron-emission tomography.* Oncol Res, 2007. **16**(10): p. 471-7.
215. Garber, K., *China approves world's first oncolytic virus therapy for cancer treatment.* J Natl Cancer Inst, 2006. **98**(5): p. 298-300.
216. Frew, S.E., et al., *Chinese health biotech and the billion-patient market.* Nat Biotechnol, 2008. **26**(1): p. 37-53.
217. Kaufman, H.L. and S.D. Bines, *OPTIM trial: a Phase III trial of an oncolytic herpes virus encoding GM-CSF for unresectable stage III or IV melanoma.* Future Oncol, 2010. **6**(6): p. 941-9.
218. Harrington, K.J., et al., *Phase I/II study of oncolytic HSV GM-CSF in combination with radiotherapy and cisplatin in untreated stage III/IV squamous cell cancer of the head and neck.* Clin Cancer Res, 2010. **16**(15): p. 4005-15.
219. Hwang, T.H., et al., *A mechanistic proof-of-concept clinical trial with JX-594, a targeted multi-mechanistic oncolytic poxvirus, in patients with metastatic melanoma.* Mol Ther, 2011. **19**(10): p. 1913-22.
220. Heo, J., et al., *Randomized dose-finding clinical trial of oncolytic immunotherapeutic vaccinia JX-594 in liver cancer.* Nat Med, 2013. **19**(3): p. 329-36.
221. Khuri, F.R., et al., *a controlled trial of intratumoral ONYX-015, a selectively-replicating adenovirus, in combination with cisplatin and 5-fluorouracil in patients with recurrent head and neck cancer.* Nat Med, 2000. **6**(8): p. 879-85.
222. Nemunaitis, J., et al., *Phase II trial of intratumoral administration of ONYX-015, a replication-selective adenovirus, in patients with refractory head and neck cancer.* J Clin Oncol, 2001. **19**(2): p. 289-98.
223. Vasey, P.A., et al., *Phase I trial of intraperitoneal injection of the E1B-55-kd-gene-deleted adenovirus ONYX-015 (dl1520) given on days 1 through 5 every 3 weeks in patients with recurrent/refractory epithelial ovarian cancer.* J Clin Oncol, 2002. **20**(6): p. 1562-9.
224. Nemunaitis, J., et al., *A phase I trial of intravenous infusion of ONYX-015 and enbrel in solid tumor patients.* Cancer Gene Ther, 2007. **14**(11): p. 885-93.
225. Hecht, J.R., et al., *A phase I/II trial of intratumoral endoscopic ultrasound injection of ONYX-015 with intravenous gemcitabine in unresectable pancreatic carcinoma.* Clin Cancer Res, 2003. **9**(2): p. 555-61.
226. Hamid, O., et al., *Phase II trial of intravenous CI-1042 in patients with metastatic colorectal cancer.* J Clin Oncol, 2003. **21**(8): p. 1498-504.
227. Reid, T.R., et al., *Effects of Onyx-015 among metastatic colorectal cancer patients that have failed prior treatment with 5-FU/leucovorin.* Cancer Gene Ther, 2005. **12**(8): p. 673-81.
228. Chiocca, E.A., et al., *A phase I open-label, dose-escalation, multi-institutional trial of injection with an E1B-Attenuated adenovirus, ONYX-015, into the peritumoral region of recurrent malignant gliomas, in the adjuvant setting.* Mol Ther, 2004. **10**(5): p. 958-66.
229. Nemunaitis, J., et al., *A phase I study of telomerase-specific replication competent oncolytic adenovirus (telomelysin) for various solid tumors.* Mol Ther, 2010. **18**(2): p. 429-34.
230. Nandi, S. and M.S. Lesniak, *Adenoviral virotherapy for malignant brain tumors.* Expert Opin Biol Ther, 2009. **9**(6): p. 737-47.
231. Papanastassiou, V., et al., *The potential for efficacy of the modified (ICP 34.5(-)) herpes simplex virus HSV1716 following intratumoural injection into human malignant glioma: a proof of principle study.* Gene Ther, 2002. **9**(6): p. 398-406.
232. Harrow, S., et al., *HSV1716 injection into the brain adjacent to tumour following surgical resection of high-grade glioma: safety data and long-term survival.* Gene Ther, 2004. **11**(22): p. 1648-58.

233. Kanai, R., et al., *Effect of gamma34.5 deletions on oncolytic herpes simplex virus activity in brain tumors.* J Virol, 2012. **86**(8): p. 4420-31.
234. Galea, I., I. Bechmann, and V.H. Perry, *What is immune privilege (not)?* Trends Immunol, 2007. **28**(1): p. 12-8.
235. Jiang, H., et al., *Oncolytic adenovirus: preclinical and clinical studies in patients with human malignant gliomas.* Curr Gene Ther, 2009. **9**(5): p. 422-7.
236. Van Houdt, W.J., et al., *Gene delivery into malignant glioma by infectivity-enhanced adenovirus: in vivo versus in vitro models.* Neuro Oncol, 2007. **9**(3): p. 280-90.
237. Wildner, O., et al., *Adenoviral vectors capable of replication improve the efficacy of HSVtk/GCV suicide gene therapy of cancer.* Gene Ther, 1999. **6**(1): p. 57-62.
238. Wildner, O., R.M. Blaese, and J.C. Morris, *Therapy of colon cancer with oncolytic adenovirus is enhanced by the addition of herpes simplex virus-thymidine kinase.* Cancer Res, 1999. **59**(2): p. 410-3.
239. Ahn, M., et al., *Enhanced combined tumor-specific oncolysis and suicide gene therapy for prostate cancer using M6 promoter.* Cancer Gene Ther, 2009. **16**(1): p. 73-82.
240. Nanda, D., et al., *Treatment of malignant gliomas with a replicating adenoviral vector expressing herpes simplex virus-thymidine kinase.* Cancer Res, 2001. **61**(24): p. 8743-50.
241. Ji, X., et al., *Oncolytic adenovirus delivering herpes simplex virus thymidine kinase suicide gene reduces the growth of human retinoblastoma in an in vivo mouse model.* Exp Eye Res, 2009. **89**(2): p. 193-9.
242. Zhang, J.F., et al., *Potent anti-tumor activity of telomerase-dependent and HSV-TK armed oncolytic adenovirus for non-small cell lung cancer in vitro and in vivo.* J Exp Clin Cancer Res, 2010. **29**: p. 52.
243. Freytag, S.O., et al., *A novel three-pronged approach to kill cancer cells selectively: concomitant viral, double suicide gene, and radiotherapy.* Hum Gene Ther, 1998. **9**(9): p. 1323-33.
244. Freytag, S.O., et al., *Replication-competent adenovirus-mediated suicide gene therapy with radiation in a preclinical model of pancreatic cancer.* Mol Ther, 2007. **15**(9): p. 1600-6.
245. Freytag, S.O., et al., *Phase I study of replication-competent adenovirus-mediated double-suicide gene therapy in combination with conventional-dose three-dimensional conformal radiation therapy for the treatment of newly diagnosed, intermediate- to high-risk prostate cancer.* Cancer Res, 2003. **63**(21): p. 7497-506.
246. Freytag, S.O., et al., *Phase I trial of replication-competent adenovirus-mediated suicide gene therapy combined with IMRT for prostate cancer.* Mol Ther, 2007. **15**(5): p. 1016-23.
247. Freytag, S.O., et al., *Five-year follow-up of trial of replication-competent adenovirus-mediated suicide gene therapy for treatment of prostate cancer.* Mol Ther, 2007. **15**(3): p. 636-42.
248. Abate-Daga, D., et al., *Oncolytic adenoviruses armed with thymidine kinase can be traced by PET imaging and show potent antitumoural effects by ganciclovir dosing.* PLoS One, 2011. **6**(10): p. e26142.
249. Rajecki, M., et al., *SPECT/CT imaging of hNIS-expression after intravenous delivery of an oncolytic adenovirus and 131I.* PLoS One, 2012. **7**(3): p. e32871.
250. Grunwald, G.K., et al., *Sodium iodide symporter (NIS)-mediated radiovirotherapy of hepatocellular cancer using a conditionally replicating adenovirus.* Gene Ther, 2013. **20**(6): p. 625-33.
251. Oneal, M.J., et al., *Effect of increased viral replication and infectivity enhancement on radioiodide uptake and oncolytic activity of adenovirus vectors expressing the sodium iodide symporter.* Cancer Gene Ther, 2013. **20**(3): p. 195-200.
252. Grunwald, G.K., et al., *Systemic image-guided liver cancer radiovirotherapy using dendrimer-coated adenovirus encoding the sodium iodide symporter as theranostic gene.* J Nucl Med, 2013. **54**(8): p. 1450-7.
253. Grunwald, G.K., et al., *EGFR-Targeted Adenovirus Dendrimer Coating for Improved Systemic Delivery of the Theranostic NIS Gene.* Mol Ther Nucleic Acids, 2013. **2**: p. e131.
254. Dias, J.D., et al., *Targeted chemotherapy for head and neck cancer with a chimeric oncolytic adenovirus coding for bifunctional suicide protein FCU1.* Clin Cancer Res, 2010. **16**(9): p. 2540-9.
255. Dong, X., et al., *Potent antitumoral effects of targeted promoter-driven oncolytic adenovirus armed with Dm-dNK for breast cancer in vitro and in vivo.* Cancer Lett, 2013. **328**(1): p. 95-103.
256. Kohno, K., et al., *The pleiotropic functions of the Y-box-binding protein, YB-1.* Bioessays, 2003. **25**(7): p. 691-8.
257. Spitkovsky, D.D., et al., *Tissue restricted expression and chromosomal localization of the YB-1 gene encoding a 42 kD nuclear CCAAT binding protein.* Nucleic Acids Res, 1992. **20**(4): p. 797-803.
258. Bargou, R.C., et al., *Nuclear localization and increased levels of transcription factor YB-1 in primary human breast cancers are associated with intrinsic MDR1 gene expression.* Nat Med, 1997. **3**(4): p. 447-50.

259. Holm, P.S., et al., *YB-1 relocates to the nucleus in adenovirus-infected cells and facilitates viral replication by inducing E2 gene expression through the E2 late promoter.* J Biol Chem, 2002. **277**(12): p. 10427-34.
260. Evdokimova, V., L.P. Ovchinnikov, and P.H. Sorensen, *Y-box binding protein 1: providing a new angle on translational regulation.* Cell Cycle, 2006. **5**(11): p. 1143-7.
261. Soop, T., et al., *A p50-like Y-box protein with a putative translational role becomes associated with pre-mRNA concomitant with transcription.* J Cell Sci, 2003. **116**(Pt 8): p. 1493-503.
262. Koike, K., et al., *Nuclear translocation of the Y-box binding protein by ultraviolet irradiation.* FEBS Lett, 1997. **417**(3): p. 390-4.
263. Stein, U., et al., *Hyperthermia-induced nuclear translocation of transcription factor YB-1 leads to enhanced expression of multidrug resistance-related ABC transporters.* J Biol Chem, 2001. **276**(30): p. 28562-9.
264. Jurchott, K., et al., *YB-1 as a cell cycle-regulated transcription factor facilitating cyclin A and cyclin B1 gene expression.* J Biol Chem, 2003. **278**(30): p. 27988-96.
265. Mantwill, K., et al., *Inhibition of the multidrug-resistant phenotype by targeting YB-1 with a conditionally oncolytic adenovirus: implications for combinatorial treatment regimen with chemotherapeutic agents.* Cancer Res, 2006. **66**(14): p. 7195-202.
266. Goldsmith, M.E., et al., *A Y-box consensus sequence is required for basal expression of the human multidrug resistance (mdr1) gene.* J Biol Chem, 1993. **268**(8): p. 5856-60.
267. Mertens, P.R., et al., *Glomerular mesangial cell-specific transactivation of matrix metalloproteinase 2 transcription is mediated by YB-1.* J Biol Chem, 1997. **272**(36): p. 22905-12.
268. Norman, J.T., et al., *The Y-box binding protein YB-1 suppresses collagen alpha 1(I) gene transcription via an evolutionarily conserved regulatory element in the proximal promoter.* J Biol Chem, 2001. **276**(32): p. 29880-90.
269. Oda, Y., et al., *Nuclear expression of Y-box-binding protein-1 correlates with P-glycoprotein and topoisomerase II alpha expression, and with poor prognosis in synovial sarcoma.* J Pathol, 2003. **199**(2): p. 251-8.
270. En-Nia, A., et al., *Transcription factor YB-1 mediates DNA polymerase alpha gene expression.* J Biol Chem, 2005. **280**(9): p. 7702-11.
271. Wu, J., et al., *Disruption of the Y-box binding protein-1 results in suppression of the epidermal growth factor receptor and HER-2.* Cancer Res, 2006. **66**(9): p. 4872-9.
272. Samuel, S., K.K. Beifuss, and L.R. Bernstein, *YB-1 binds to the MMP-13 promoter sequence and represses MMP-13 transactivation via the AP-1 site.* Biochim Biophys Acta, 2007. **1769**(9-10): p. 525-31.
273. Evdokimova, V., et al., *Translational activation of snail1 and other developmentally regulated transcription factors by YB-1 promotes an epithelial-mesenchymal transition.* Cancer Cell, 2009. **15**(5): p. 402-15.
274. To, K., et al., *Y-box binding protein-1 induces the expression of CD44 and CD49f leading to enhanced self-renewal, mammosphere growth, and drug resistance.* Cancer Res, 2010. **70**(7): p. 2840-51.
275. Fotovati, A., et al., *YB-1 bridges neural stem cells and brain tumor-initiating cells via its roles in differentiation and cell growth.* Cancer Res, 2011. **71**(16): p. 5569-78.
276. Okamoto, T., et al., *Direct interaction of p53 with the Y-box binding protein, YB-1: a mechanism for regulation of human gene expression.* Oncogene, 2000. **19**(54): p. 6194-202.
277. Lasham, A., et al., *The Y-box-binding protein, YB1, is a potential negative regulator of the p53 tumor suppressor.* J Biol Chem, 2003. **278**(37): p. 35516-23.
278. Ohga, T., et al., *Direct involvement of the Y-box binding protein YB-1 in genotoxic stress-induced activation of the human multidrug resistance 1 gene.* J Biol Chem, 1998. **273**(11): p. 5997-6000.
279. Faury, D., et al., *Molecular profiling identifies prognostic subgroups of pediatric glioblastoma and shows increased YB-1 expression in tumors.* J Clin Oncol, 2007. **25**(10): p. 1196-208.
280. Maciejczyk, A., et al., *Elevated nuclear YB1 expression is associated with poor survival of patients with early breast cancer.* Anticancer Res, 2012. **32**(8): p. 3177-84.
281. Oda, Y., et al., *Prognostic implications of the nuclear localization of Y-box-binding protein-1 and CXCR4 expression in ovarian cancer: their correlation with activated Akt, LRP/MVP and P-glycoprotein expression.* Cancer Sci, 2007. **98**(7): p. 1020-6.
282. Hyogotani, A., et al., *Association of nuclear YB-1 localization with lung resistance-related protein and epidermal growth factor receptor expression in lung cancer.* Clin Lung Cancer, 2012. **13**(5): p. 375-84.

283. Kolk, A., et al., *Expression of Y-box-binding protein YB-1 allows stratification into long- and short-term survivors of head and neck cancer patients.* Br J Cancer, 2011. **105**(12): p. 1864-73.
284. Del Valle, L., et al., *Reactivation of human neurotropic JC virus expressing oncogenic protein in a recurrent glioblastoma multiforme.* Ann Neurol, 2000. **48**(6): p. 932-6.
285. Wu, J., et al., *YB-1 is a Transcription/Translation Factor that Orchestrates the Oncogenome by Hardwiring Signal Transduction to Gene Expression.* Transl Oncogenomics, 2007. **2**: p. 49-65.
286. Swaminathan, S. and B. Thimmapaya, *Regulation of adenovirus E2 transcription unit.* Curr Top Microbiol Immunol, 1995. **199 (Pt 3)**: p. 177-94.
287. Kovesdi, I., R. Reichel, and J.R. Nevins, *Role of an adenovirus E2 promoter binding factor in E1A-mediated coordinate gene control.* Proc Natl Acad Sci U S A, 1987. **84**(8): p. 2180-4.
288. Holm, P.S., et al., *Multidrug-resistant cancer cells facilitate E1-independent adenoviral replication: impact for cancer gene therapy.* Cancer Res, 2004. **64**(1): p. 322-8.
289. Bieler, A., et al., *Novel three-pronged strategy to enhance cancer cell killing in glioblastoma cell lines: histone deacetylase inhibitor, chemotherapy, and oncolytic adenovirus dl520.* Hum Gene Ther, 2006. **17**(1): p. 55-70.
290. Bieler, A., et al., *Impact of radiation therapy on the oncolytic adenovirus dl520: implications on the treatment of glioblastoma.* Radiother Oncol, 2008. **86**(3): p. 419-27.
291. Rognoni, E., et al., *Adenovirus-based virotherapy enabled by cellular YB-1 expression in vitro and in vivo.* Cancer Gene Ther, 2009. **16**(10): p. 753-63.
292. Holzmuller, R., et al., *YB-1 dependent virotherapy in combination with temozolomide as a multimodal therapy approach to eradicate malignant glioma.* Int J Cancer, 2011. **129**(5): p. 1265-76.
293. Haley, K.P., et al., *Transformation properties of type 5 adenovirus mutants that differentially express the E1A gene products.* Proc Natl Acad Sci U S A, 1984. **81**(18): p. 5734-8.
294. Mantwill, K., et al., *YB-1 dependent oncolytic adenovirus efficiently inhibits tumor growth of glioma cancer stem like cells.* J Transl Med, 2013. **11**: p. 216.
295. Ebeling, S.B., et al., *Development and application of quantitative real time PCR and RT-PCR assays that discriminate between the full-length and truncated herpes simplex virus thymidine kinase gene.* J Virol Methods, 2003. **109**(2): p. 177-86.
296. McKinnon, R.D., S. Bacchetti, and F.L. Graham, *Tn5 mutagenesis of the transforming genes of human adenovirus type 5.* Gene, 1982. **19**(1): p. 33-42.
297. Ng, P., et al., *An enhanced system for construction of adenoviral vectors by the two-plasmid rescue method.* Hum Gene Ther, 2000. **11**(5): p. 693-9.
298. Mizuno, N.S., B. Zakis, and R.W. Decker, *Binding of daunomycin to DNA and the inhibition of RNA and DNA synthesis.* Cancer Res, 1975. **35**(6): p. 1542-6.
299. Alauddin, M.M. and P.S. Conti, *Synthesis and preliminary evaluation of 9-(4-[18F]-fluoro-3-hydroxymethylbutyl)guanine ([18F]FHBG): a new potential imaging agent for viral infection and gene therapy using PET.* Nucl Med Biol, 1998. **25**(3): p. 175-80.
300. Graham, F.L., et al., *Characteristics of a human cell line transformed by DNA from human adenovirus type 5.* J Gen Virol, 1977. **36**(1): p. 59-74.
301. Ponten, J. and E.H. Macintyre, *Long term culture of normal and neoplastic human glia.* Acta Pathol Microbiol Scand, 1968. **74**(4): p. 465-86.
302. Leske, H., et al., *Varicella zoster virus infection of malignant glioma cell cultures: a new candidate for oncolytic virotherapy?* Anticancer Res, 2012. **32**(4): p. 1137-44.
303. Maizel, J.V., Jr., D.O. White, and M.D. Scharff, *The polypeptides of adenovirus. I. Evidence for multiple protein components in the virion and a comparison of types 2, 7A, and 12.* Virology, 1968. **36**(1): p. 115-25.
304. Southern, E.M., *Detection of specific sequences among DNA fragments separated by gel electrophoresis.* J Mol Biol, 1975. **98**(3): p. 503-17.
305. Sambrook, J., E.F. Fritsch, and T. Maniatis, *Molecular Cloning. A Laboratory Manual*. 1989, Cold Spring Harbor Laboratory Press
306. Heid, C.A., et al., *Real time quantitative PCR.* Genome Res, 1996. **6**(10): p. 986-94.
307. Livak, K.J. and T.D. Schmittgen, *Analysis of relative gene expression data using real-time quantitative PCR and the 2(-Delta Delta C(T)) Method.* Methods, 2001. **25**(4): p. 402-8.
308. Zipper, H., et al., *Investigations on DNA intercalation and surface binding by SYBR Green I, its structure determination and methodological implications.* Nucleic Acids Res, 2004. **32**(12): p. e103.
309. Clegg, R.M., *Fluorescence resonance energy transfer and nucleic acids.* Methods Enzymol, 1992. **211**: p. 353-88.

310. Holland, P.M., et al., *Detection of specific polymerase chain reaction product by utilizing the 5'----3' exonuclease activity of Thermus aquaticus DNA polymerase.* Proc Natl Acad Sci U S A, 1991. **88**(16): p. 7276-80.
311. Bradford, M.M., *A rapid and sensitive method for the quantitation of microgram quantities of protein utilizing the principle of protein-dye binding.* Anal Biochem, 1976. **72**: p. 248-54.
312. Laemmli, U.K., *Cleavage of structural proteins during the assembly of the head of bacteriophage T4.* Nature, 1970. **227**(5259): p. 680-5.
313. Skehan, P., et al., *New colorimetric cytotoxicity assay for anticancer-drug screening.* J Natl Cancer Inst, 1990. **82**(13): p. 1107-12.
314. Gerlier, D. and N. Thomasset, *Use of MTT colorimetric assay to measure cell activation.* J Immunol Methods, 1986. **94**(1-2): p. 57-63.
315. Scudiero, D.A., et al., *Evaluation of a soluble tetrazolium/formazan assay for cell growth and drug sensitivity in culture using human and other tumor cell lines.* Cancer Res, 1988. **48**(17): p. 4827-33.
316. Hehir, K.M., et al., *Molecular characterization of replication-competent variants of adenovirus vectors and genome modifications to prevent their occurrence.* J Virol, 1996. **70**(12): p. 8459-67.
317. Li, L.Q., et al., *Gene Therapy with HSV1-sr39TK/GCV Exhibits a Stronger Therapeutic Efficacy Than HSV1-TK/GCV in Rat C6 Glioma Cells.* ScientificWorldJournal, 2013. **2013**: p. 951343.
318. Newlands, E.S., et al., *Phase I trial of temozolomide (CCRG 81045: M&B 39831: NSC 362856).* Br J Cancer, 1992. **65**(2): p. 287-91.
319. Brada, M., et al., *Phase I dose-escalation and pharmacokinetic study of temozolomide (SCH 52365) for refractory or relapsing malignancies.* Br J Cancer, 1999. **81**(6): p. 1022-30.
320. Kato, T., et al., *Efficient delivery of liposome-mediated MGMT-siRNA reinforces the cytotoxity of temozolomide in GBM-initiating cells.* Gene Ther, 2010. **17**(11): p. 1363-71.
321. Carson, K.A., et al., *Prognostic factors for survival in adult patients with recurrent glioma enrolled onto the new approaches to brain tumor therapy CNS consortium phase I and II clinical trials.* J Clin Oncol, 2007. **25**(18): p. 2601-6.
322. Health, U.S.D.o., et al., *Guidance for human somatic cell therapy and gene therapy.* Hum Gene Ther, 2001. **12**(3): p. 303-14.
323. Shih, S.J., et al., *Use of a bioamplification assay to detect nonselective recombinants and assess the genetic stability of oncolytic adenoviruses.* Hum Gene Ther, 2010. **21**(12): p. 1707-21.
324. Farson, D., et al., *Development of novel E1-complementary cells for adenoviral production free of replication-competent adenovirus.* Mol Ther, 2006. **14**(2): p. 305-11.
325. Hirschmann-Jax, C., et al., *A distinct "side population" of cells with high drug efflux capacity in human tumor cells.* Proc Natl Acad Sci U S A, 2004. **101**(39): p. 14228-33.
326. Wild, K., et al., *The structures of thymidine kinase from herpes simplex virus type 1 in complex with substrates and a substrate analogue.* Protein Sci, 1997. **6**(10): p. 2097-106.
327. Gill, M.B., J.E. Murphy, and J.D. Fingeroth, *Functional divergence of Kaposi's sarcoma-associated herpesvirus and related gamma-2 herpesvirus thymidine kinases: novel cytoplasmic phosphoproteins that alter cellular morphology and disrupt adhesion.* J Virol, 2005. **79**(23): p. 14647-59.
328. Hodson, J.A., J.M. Bailis, and S.L. Forsburg, *Efficient labeling of fission yeast Schizosaccharomyces pombe with thymidine and BUdR.* Nucleic Acids Res, 2003. **31**(21): p. e134.
329. Liu, T.C., et al., *Functional interactions of antiapoptotic proteins and tumor necrosis factor in the context of a replication-competent adenovirus.* Gene Ther, 2005. **12**(17): p. 1333-46.
330. Breitbach, C.J., et al., *Intravenous delivery of a multi-mechanistic cancer-targeted oncolytic poxvirus in humans.* Nature, 2011. **477**(7362): p. 99-102.
331. Kaszubiak, A., et al., *Regulation of MDR1 gene expression in multidrug-resistant cancer cells is independent from YB-1.* Biochem Biophys Res Commun, 2007. **357**(1): p. 295-301.
332. Vaiman, A.V., et al., *Intracellular localization and content of YB-1 protein in multidrug resistant tumor cells.* Biochemistry (Mosc), 2006. **71**(2): p. 146-54.
333. Fuxe, J., et al., *Expression of the coxsackie and adenovirus receptor in human astrocytic tumors and xenografts.* Int J Cancer, 2003. **103**(6): p. 723-9.
334. Zheng, S., et al., *Fiber-knob modifications enhance adenoviral tropism and gene transfer in malignant glioma.* J Gene Med, 2007. **9**(3): p. 151-60.
335. Paul, C.P., et al., *Characterization of infectivity of knob-modified adenoviral vectors in glioma.* Cancer Biol Ther, 2008. **7**(5): p. 786-93.
336. Kaszubiak, A., *Adenoviraler Transfer von anti-MDR1 shRNAs. Implikationen für die Gentherapie multidrug-resistenter Tumoren.* 2007, Dissertation an der Humboldt-Universität zu Berlin.

337. Robinson, M., et al., *Comparison of the E3 and L3 regions for arming oncolytic adenoviruses to achieve a high level of tumor-specific transgene expression.* Cancer Gene Ther, 2008. **15**(1): p. 9-17.
338. Hanahan, D. and R.A. Weinberg, *Hallmarks of cancer: the next generation.* Cell, 2011. **144**(5): p. 646-74.
339. Seano, G., et al., *Modeling human tumor angiogenesis in a three-dimensional culture system.* Blood, 2013. **121**(21): p. e129-37.
340. Liu, G., et al., *Analysis of gene expression and chemoresistance of CD133+ cancer stem cells in glioblastoma.* Mol Cancer, 2006. **5**: p. 67.
341. Grill, J., et al., *Combined targeting of adenoviruses to integrins and epidermal growth factor receptors increases gene transfer into primary glioma cells and spheroids.* Clin Cancer Res, 2001. **7**(3): p. 641-50.
342. Parada, C., et al., *Adenovirus E1a protein enhances the cytotoxic effects of the herpes thymidine kinase-ganciclovir system.* Cancer Gene Ther, 2003. **10**(2): p. 152-60.
343. Kokoris, M.S. and M.E. Black, *Characterization of herpes simplex virus type 1 thymidine kinase mutants engineered for improved ganciclovir or acyclovir activity.* Protein Sci, 2002. **11**(9): p. 2267-72.
344. Wildner, O., et al., *Comparison of HSV-1 thymidine kinase-dependent and -independent inhibition of replication-competent adenoviral vectors by a panel of drugs.* Cancer Gene Ther, 2003. **10**(10): p. 791-802.
345. Ibrisimovic, M., et al., *Targeted expression of herpes simplex virus thymidine kinase in adenovirus-infected cells reduces virus titers upon treatment with ganciclovir in vitro.* J Gene Med, 2012. **14**(1): p. 3-19.
346. Hitt, M.M. and F.L. Graham, *Adenovirus E1A under the control of heterologous promoters: wide variation in E1A expression levels has little effect on virus replication.* Virology, 1990. **179**(2): p. 667-78.
347. Ardiani, A., M. Sanchez-Bonilla, and M.E. Black, *Fusion enzymes containing HSV-1 thymidine kinase mutants and guanylate kinase enhance prodrug sensitivity in vitro and in vivo.* Cancer Gene Ther, 2010. **17**(2): p. 86-96.
348. Trask, T.W., et al., *Phase I study of adenoviral delivery of the HSV-tk gene and ganciclovir administration in patients with current malignant brain tumors.* Mol Ther, 2000. **1**(2): p. 195-203.
349. Luo, C., et al., *Replication-competent, oncolytic herpes simplex virus type 1 mutants induce a bystander effect following ganciclovir treatment.* J Gene Med, 2007. **9**(10): p. 875-83.
350. Park, S.Y., et al., *Combination gene therapy using multidrug resistance (MDR1) gene shRNA and herpes simplex virus-thymidine kinase.* Cancer Lett, 2008. **261**(2): p. 205-14.
351. Fels, C., et al., *Bcl-2 expression in higher-grade human glioma: a clinical and experimental study.* J Neurooncol, 2000. **48**(3): p. 207-16.
352. Pareja, F., et al., *PI3K and Bcl-2 Inhibition Primes Glioblastoma Cells to Apoptosis through Downregulation of Mcl-1 and Phospho-BAD.* Mol Cancer Res, 2014. **12**(7): p. 987-1001.
353. Huang, Q., et al., *The anti-glioma effect of suicide gene therapy using BMSC expressing HSV/TK combined with overexpression of Cx43 in glioma cells.* Cancer Gene Ther, 2010. **17**(3): p. 192-202.
354. Miletic, H., et al., *Normal brain cells contribute to the bystander effect in suicide gene therapy of malignant glioma.* Clin Cancer Res, 2007. **13**(22 Pt 1): p. 6761-8.
355. Yoshino, A., et al., *Gene expression profiling predicts response to temozolomide in malignant gliomas.* Int J Oncol, 2010. **36**(6): p. 1367-77.
356. Shiota, M., et al., *Twist promotes tumor cell growth through YB-1 expression.* Cancer Res, 2008. **68**(1): p. 98-105.
357. Sutherland, B.W., et al., *Akt phosphorylates the Y-box binding protein 1 at Ser102 located in the cold shock domain and affects the anchorage-independent growth of breast cancer cells.* Oncogene, 2005. **24**(26): p. 4281-92.
358. Evdokimova, V., et al., *Akt-mediated YB-1 phosphorylation activates translation of silent mRNA species.* Mol Cell Biol, 2006. **26**(1): p. 277-92.
359. Sorokin, A.V., et al., *Proteasome-mediated cleavage of the Y-box-binding protein 1 is linked to DNA-damage stress response.* EMBO J, 2005. **24**(20): p. 3602-12.
360. Cohen, S.B., et al., *Genotoxic stress-induced nuclear localization of oncoprotein YB-1 in the absence of proteolytic processing.* Oncogene, 2010. **29**(3): p. 403-10.
361. Alonso, M.M., et al., *Adenovirus-based strategies overcome temozolomide resistance by silencing the O6-methylguanine-DNA methyltransferase promoter.* Cancer Res, 2007. **67**(24): p. 11499-504.
362. Beier, D., J.B. Schulz, and C.P. Beier, *Chemoresistance of glioblastoma cancer stem cells--much more complex than expected.* Mol Cancer, 2011. **10**: p. 128.

363. Schaich, M., et al., *A MDR1 (ABCB1) gene single nucleotide polymorphism predicts outcome of temozolomide treatment in glioblastoma patients.* Ann Oncol, 2009. **20**(1): p. 175-81.
364. Pipiya, T., et al., *Hypoxia reduces adenoviral replication in cancer cells by downregulation of viral protein expression.* Gene Ther, 2005. **12**(11): p. 911-7.
365. Shen, B.H. and T.W. Hermiston, *Effect of hypoxia on Ad5 infection, transgene expression and replication.* Gene Ther, 2005. **12**(11): p. 902-10.
366. Bello, L., et al., *Alpha(v)beta3 and alpha(v)beta5 integrin expression in glioma periphery.* Neurosurgery, 2001. **49**(2): p. 380-9; discussion 390.
367. Finocchiaro, L.M., et al., *Herpes simplex virus thymidine kinase/ganciclovir system in multicellular tumor spheroids.* Cancer Gene Ther, 2004. **11**(5): p. 333-45.
368. Wildner, O. and J.C. Morris, *The role of the E1B 55 kDa gene product in oncolytic adenoviral vectors expressing herpes simplex virus-tk: assessment of antitumor efficacy and toxicity.* Cancer Res, 2000. **60**(15): p. 4167-74.
369. Morris, J.C. and O. Wildner, *Therapy of head and neck squamous cell carcinoma with an oncolytic adenovirus expressing HSV-tk.* Mol Ther, 2000. **1**(1): p. 56-62.
370. Lambright, E.S., et al., *Inclusion of the herpes simplex thymidine kinase gene in a replicating adenovirus does not augment antitumor efficacy.* Gene Ther, 2001. **8**(12): p. 946-53.
371. Raki, M., et al., *Utility of TK/GCV in the context of highly effective oncolysis mediated by a serotype 3 receptor targeted oncolytic adenovirus.* Gene Ther, 2007. **14**(19): p. 1380-8.
372. Barba, D., et al., *Development of anti-tumor immunity following thymidine kinase-mediated killing of experimental brain tumors.* Proc Natl Acad Sci U S A, 1994. **91**(10): p. 4348-52.
373. Braithwaite, A.W. and I.A. Russell, *Induction of cell death by adenoviruses.* Apoptosis, 2001. **6**(5): p. 359-70.
374. Baird, S.K., et al., *Oncolytic adenoviral mutants induce a novel mode of programmed cell death in ovarian cancer.* Oncogene, 2008. **27**(22): p. 3081-90.
375. Hong, S., Q.X. Paulson, and D.G. Johnson, *E2F1 and E2F3 activate ATM through distinct mechanisms to promote E1A-induced apoptosis.* Cell Cycle, 2008. **7**(3): p. 391-400.
376. Abou El Hassan, M.A., et al., *Conditionally replicating adenoviruses kill tumor cells via a basic apoptotic machinery-independent mechanism that resembles necrosis-like programmed cell death.* J Virol, 2004. **78**(22): p. 12243-51.
377. Jiang, H., et al., *Human adenovirus type 5 induces cell lysis through autophagy and autophagy-triggered caspase activity.* J Virol, 2011. **85**(10): p. 4720-9.
378. Cuconati, A., et al., *DNA damage response and MCL-1 destruction initiate apoptosis in adenovirus-infected cells.* Genes Dev, 2003. **17**(23): p. 2922-32.
379. Ulasov, I.V., et al., *Combination of adenoviral virotherapy and temozolomide chemotherapy eradicates malignant glioma through autophagic and apoptotic cell death in vivo.* Br J Cancer, 2009. **100**(7): p. 1154-64.
380. Gunther, W., et al., *Temozolomide induces apoptosis and senescence in glioma cells cultured as multicellular spheroids.* Br J Cancer, 2003. **88**(3): p. 463-9.
381. Gao, Y., et al., *Inhibition of Y-box binding protein-1 slows the growth of glioblastoma multiforme and sensitizes to temozolomide independent O6-methylguanine-DNA methyltransferase.* Mol Cancer Ther, 2009. **8**(12): p. 3276-84.
382. Connell, C.M., et al., *Genomic DNA damage and ATR-Chk1 signaling determine oncolytic adenoviral efficacy in human ovarian cancer cells.* J Clin Invest, 2011. **121**(4): p. 1283-97.
383. Halloran, P.J. and R.G. Fenton, *Irreversible G2-M arrest and cytoskeletal reorganization induced by cytotoxic nucleoside analogues.* Cancer Res, 1998. **58**(17): p. 3855-65.
384. Ladd, B., et al., *Unrepairable DNA double-strand breaks initiate cytotoxicity with HSV-TK/ganciclovir.* Cancer Gene Ther, 2011. **18**(10): p. 751-9.
385. Johnson, M., et al., *Titration of variant HSV1-tk gene expression to determine the sensitivity of 18F-FHBG PET imaging in a prostate tumor.* J Nucl Med, 2009. **50**(5): p. 757-64.
386. Viel, T., et al., *Early assessment of the efficacy of temozolomide chemotherapy in experimental glioblastoma using [18F]FLT-PET imaging.* PLoS One, 2013. **8**(7): p. e67911.
387. Glockzin, G., et al., *Characterization of the recombinant adenovirus vector AdYB-1: implications for oncolytic vector development.* J Virol, 2006. **80**(8): p. 3904-11.
388. Cattaneo, R., et al., *Reprogrammed viruses as cancer therapeutics: targeted, armed and shielded.* Nat Rev Microbiol, 2008. **6**(7): p. 529-40.

389. Morrison, J., et al., *Cetuximab retargeting of adenovirus via the epidermal growth factor receptor for treatment of intraperitoneal ovarian cancer.* Hum Gene Ther, 2009. **20**(3): p. 239-51.
390. Tresilwised, N., et al., *Boosting oncolytic adenovirus potency with magnetic nanoparticles and magnetic force.* Mol Pharm, 2010. **7**(4): p. 1069-89.
391. Maeda, M., et al., *New drug delivery system for water-soluble drugs using silicone and its usefulness for local treatment: application of GCV-silicone to GCV/HSV-tk gene therapy for brain tumor.* J Control Release, 2002. **84**(1-2): p. 15-25.
392. Kajiwara, E., et al., *Long-circulating liposome-encapsulated ganciclovir enhances the efficacy of HSV-TK suicide gene therapy.* J Control Release, 2007. **120**(1-2): p. 104-10.
393. Freytag, S.O., K.N. Barton, and Y. Zhang, *Efficacy of oncolytic adenovirus expressing suicide genes and interleukin-12 in preclinical model of prostate cancer.* Gene Ther, 2013. **20**(12): p. 1131-9.
394. Puntel, M., et al., *A novel bicistronic high-capacity gutless adenovirus vector that drives constitutive expression of herpes simplex virus type 1 thymidine kinase and tet-inducible expression of Flt3L for glioma therapeutics.* J Virol, 2010. **84**(12): p. 6007-17.
395. Reardon, D.A., et al., *Randomized phase II study of cilengitide, an integrin-targeting arginine-glycine-aspartic acid peptide, in recurrent glioblastoma multiforme.* J Clin Oncol, 2008. **26**(34): p. 5610-7.

9. APPENDIX

9.1. Abbreviations

”	Inch
°C	Degree Celsius
Δ	Deletion
ρ	Volumetric mass density
aa	Amino acid
ABC	ATP-binding cassette
ACV	Acyclovir
Ad5	Human adenovirus type 5
ADP	Adenovirus death protein
Akt	Protein kinase B
ATCC	American Type Culture Collection
ATP	Adenosine triphosphate
ATR	Ataxia telangiectasia and Rad3-related
Bcl-2	B cell lymphoma-2
bp	Base pair
Bq	Becquerel
BSA	Bovine Serum Albumin
$CaCl_2$	Calcium chloride
CAR	Coxsackie and adenovirus receptor
CD	Cluster of differentiation
CD (b/y)	Cytosine deaminase (from bacteria or yeast)
Cdc(x)	Cell division cycle (x=number)
cDNA	Complementary DNA
Chk1	Checkpoint kinase 1
$C_2H_3NaO_2$	Sodium acetate
cm	Centimetre
cm^3	Cubic centimetre
CMV	Cytomegalovirus
CNS	Central nervous system
CO_2	Carbon dioxide
CR	Conserved region
Cre	Cyclization recombinase
CsCl	Cesium chloride
C_t	Cycle threshold
CT	Computed tomography
c.p.e.	Cytopathic effect
cpm	Counts per minute
Cx43	Connexin 43 subunit
Da	Dalton
DAPI	4´,6´-diamidino-2-phenylindole
delo2/3	Deletion on 2/3 locations
dH_2O	Distilled water
DIG	Digoxigenin
DMEM	Dulbecco's Modified Eagle’s Medium
DMSO	Dimethyl sulfoxide
DNA	Deoxyribonucleic acid
DNase	Deoxyribonuclease

dNTP	Deoxynucleoside triphosphate
ds	Double-stranded
dUTP	2´-deoxyuridine 5´-triphosphate
EDTA	Ethylenediamine-tetraacetic acid
E2F	E2 promoter binding factor
e.g.	For example
eGFP	Enhanced green fluorescent protein
EGFR	Epidermal growth factor receptor
FAM	6-carboxyfluorescein
FBS	Fetal bovine serum
5-FC	5-fluorocytosine
FHBG	9-[4-fluoro-3-(hydroxymethyl)butyl]guanine
FIAU	2'-fluoro-2'-deoxy-5-iodo-1-β-D-arabinofuranosyl
FITC	Fluorescein isothiocyanate
5-FU	5-fluorouracil
g	Gravitational field strength
g	Gramme
G	Gauge
G	Giga
GBM	Glioblastoma multiforme
GCV	Ganciclovir
h	Hour
HCl	Hydrochloric acid
HEK	Human embryonic kidney
HEPES	4-(2-Hydroxyethyl)piperazine-1-ethanesulfonic acid
hNIS	Human sodium-iodide symporter gene
HNSCC	Head and neck squamous cell carcinoma
HRP	Horseradish peroxidase
HS	Horse serum
HSV	Herpes simplex virus
HSV1-TK	Herpes simplex virus 1 thymidine kinase
hTERT	Human telomerase reverse transcriptase
IC_{50}	Half maximal inhibitory concentration
IF	Immunofluorescence
ifu	Infectious units
Ig	Immunoglobulin
kb	1000 base pairs
KCl	Potassium chloride
KH_2PO_4	Potassium dihydrogen phosphate
kIU	Kallikrein Inhibitor Units
K_m	Michaelis constant
l	Litre
loxP	Locus of X-over of P1
M	Mega
M	Molarity
mA	Milliampere
mAU	Milli-arbitrary unit
mCMV	Murine cytomegalovirus
MDR1	Multidrug resistance gene 1
MEM	Minimum Essential Medium
mg	Milligramme
$MgCl_2$	Magnesium chloride

MGMT	O^6-methylguanine-DNA methyltransferase
min	Minute
mJ	Millijoule
ml	Millilitre
mm	Millimetre
mM	Millimolar (mmol/l)
MOI	Multiplicity of infection
M_r	Relative molecular mass
mRNA	Messenger RNA
MTIC	5-(3-methyltriazen-1-yl)-imidazole-4-carboxamide
mTOR	Mammalian target of rapamycin
µg	Microgramme
µl	Microlitre
µm	Micrometre
µM	Micromolar (µmol/l)
NaCl	Sodium chloride
$NaHCO_3$	Sodium hydrogen carbonate
Na_2HPO_4	Sodium phosphate
NaOH	Sodium hydroxide
NEAA	Non-essential amino acids
ng	Nanogramme
$NH_4C_2H_3O_2$	Ammonium acetate
$(NH_4)_2SO_4$	Ammonium sulfate
nm	Nanometre
nM	Nanomolar (nmol/l)
nt	Nucleotide
OD	Optical density
pIX	Minor capsid protein IX
PAGE	Polyacrylamide gel electrophoresis
PBS	Phosphate buffered saline
PCR	Polymerase chain reaction
PEG	Polyethyleneglycol
PET	Positron emission tomography
pfu	Plaque forming units
pg	Picogramme
P-gp	P-glycoprotein
PI3K	Phosphatidylinositide 3-kinase
PKC	Protein kinase C
poly(A)	Polyadenylation
pRB	Retinoblastoma protein
PS	Penicillin and streptomycin
PVDF	Polyvinylidene fluoride
qPCR	Quantitative PCR
r	Radius
RCA	Replication-competent adenoviruses
RDB	Resistant to daunoblastin
RGD	Arginine-glycine-aspartic acid
rGFP	recombinant green fluorescent protein
RIPA	Radio-Immunoprecipitation Assay
RNA	Ribonucleic acid
rRNA	Ribosomal RNA
RNase	Ribonuclease

ROI	Region of interest
rpm	Revolution per minute
RT	Room temperature
SD	Standard deviation
SDS	Sodium dodecyl sulfate
sec	Second
shRNA	Short hairpin RNA
siRNA	Small interfering RNA
SPECT	Single photon emission computed tomography
SRB	Sulforhodamine B
ss	Single-stranded
SSC	Sodium chloride-sodium citrate buffer
SV40	Simian virus 40
TAE	Tris-acetate-EDTA
TAMRA	6-carboxytertramethylrhodamine
Taq	*Thermus aquaticus*
TCA	Trichloroacetic acid
T_m	Melting temperature
TMZ	Temozolomide
U	Unit
UV	Ultraviolet
V	Volt
V	Volume
VEGF	Vascular endothelial growth factor
VP	Viral particles
WB	Western blot
wt	Wild-type
w/v	Weight/volume
XTT	Sodium 3´-[1-(phenylaminocarbonyl)- 3,4-tetrazolium]-bis (4-methoxy-6-nitro) benzene sulfonic acid hydrate
YB-1	Y-box binding protein 1

9.2. Publications

9.2.1. Original articles

Kostova Y, Mantwill K, Holm PS, Anton M: *An armed, YB-1 dependent oncolytic adenovirus as a candidate for a combinatorial anti-glioma approach of virotherapy, suicide gene therapy and chemotherapeutic treatment*. Cancer Gene Therapy 2015 Jan; 22 (1): 30-43. doi: 10.1038/cgt.2014.67. Epub 2014 Dec 12.

Kostova Y, Schillinger U, Wolf A, Koch C, Plank C, Anton M: *Spatio-temporal control of growth factor gene expression in 2D and 3D rat mesenchymal stem cell cultures and its influence on differentiation potential*. In preparation

Anton M, Kostova Y, Wolf A, Mykhaylyk O, Ogris M, Plank C: *Imaging of spatio-temporal control by TNFalpha-inducible cox-2 promoter dependent luciferase gene expression*. In preparation

9.2.2. Posters

Kostova Y*, Mantwill K, Dumler K, Wolf A, Wester HJ, Gänsbacher B, Holm PS, Anton M: *Functional analysis of armed oncolytic adenoviruses for nuclear reporter gene imaging*. 17th Annual Meeting of the German Society for Gene Therapy (DG-GT e.V.), Munich, Germany (October 2010).

Kostova Y*, Mantwill K, Dumler K, Wolf A, Gänsbacher B, Holm PS, Anton M: *A YB-1-dependent, armed oncolytic adenovirus as a candidate for nuclear reporter gene imaging and suicide tumour gene therapy*. Collaborative Congress of the European Society of Gene and Cell Therapy and British Society for Gene Therapy, Brighton, UK (October 2011).

Anton M*, Hillreiner M, Kostova Y, Koch C, Eglin D, Zelphati O, Borget P, Daculsi G, Alini M, Plank C: *Development of gene activated matrices for tissue regeneration in osteoarthritis*. Collaborative Congress of the European Society of Gene and Cell Therapy and French Society of Cell and Gene Therapy, Versailles, France (October 2012).

9.2.3. Oral presentations

Anton M*, Kostova Y, Schillinger U, Eglin D, Sapet C, Borget P, Daculsi G, Alini M, Plank C: *Development of gene activated matrices for tissue regeneration in osteoarthritis*. Tissue Engineering and Regenerative Medicine International Society – EU Meeting, Genova, Italy (June 2014).

* Presenting author

10. ACKNOWLEDGEMENTS

At the end of my PhD I would like to acknowledge all the people, who contributed to the accomplishment of this work.

First of all, I would like to express my gratitude to Prof. Dr. Ernst Wagner for the supervision of my PhD thesis, for his constant support and valuable discussions.

I would like to thank Prof. Dr. Christian Plank for his supervision, help and guidance, especially in the last phase of my thesis.

I would like to express my special gratitude to Dr. Martina Anton for giving me the opportunity to conduct my thesis in her group and for introducing me to this exciting research field. I appreciate her for all fruitful scientific discussions, for her faith in me and for filling me with enthusiasm for scientific work, and I thank her for the pleasant work environment.

Many thanks to the former and present directors of the Institute of Experimental Oncology and Therapy Research, Klinikum rechts der Isar, Prof. Dr. Bernd Gänsbacher and Prof. Dr. Percy Knolle, for the possibility to perform my work in their institute.

I would like to thank my colleagues Katja Dumler, Dr. Daniela Hirsch, Eva Schmalzl and Anja Wolf of the Anton group for the friendly lab atmosphere and for always lending a hand when something went wrong.

PD Dr. Per Sonne Holm and Klaus Mantwill are acknowledged for their contribution in terms of providing materials, for all helpful discussions of emerging issues regarding oncolytic adenoviruses and for their support in manuscript preparation.

I would like to thank all the members of the Institute of Experimental Oncology and Therapy Research for their support, material supply and the numerous great social events. Special thanks to Dr. Susanne Schaten for assistance in cryosectioning, to Dr. Vroni Girbinger and Dirk Weinspach for our friendship and for always being ready to help. Thank you all very much.

I am grateful to Dr. Iina Laitinen for her support in performing PET analysis, to Sybille Reder, Dr. Hans-Jürgen Wester, Michael Herz and the other members of the imaging facility in the Department of Nuclear Medicine for their assistance and for providing radiotracer.

Many thanks to my friends, especially to Viktoriya, for always being there for me.

I would like to thank my parents, who always encouraged me and supported me throughout my whole education. Благодаря Ви.

Last but not least, I thank my boyfriend Andreas. Thank you for your patience, your encouraging words and for being by my side in all situations.